Remediation of Lead-acid Battery Wastewater and Sludge: Synthesis of Functionalized Sorbents and Manufacturing of Fired Clay Bricks

A Thesis Submitted in

Partial Fulfillment of the Requirement for the Degree of

Doctor of Philosophy

by

Vihangraj V. Kulkarni

DEPARTMENT OF CIVIL ENGINEERING

INDIAN INSTITUTE OF TECHNOLOGY GUWAHATI

GUWAHATI – 781039 (INDIA)

August 2018

DEDICATED TO MY

PARENTS' PATIENCE

Declaration of Originality

I certify that the work presented here in the thesis has not been accepted/submitted in substance for any degree, and is not concurrently submitted for any degree other than Ph.D in the Department of Civil Engineering, being studied at Indian Institute of Technology Guwahati, India. I also declare that the work presented is my original research, result of my own investigations, and that I have not plagiarized somebody else's work.

Date:

Vihangraj V. Kulkarni
Roll No. 126104003
Research Scholar
Department of Civil Engineering
Indian Institute of Technology Guwahati, Guwahati

CERTIFICATE

*This is to certify that the thesis entitled "**Remediation of Lead-acid Battery Wastewater and Sludge: Synthesis of Functionalized Sorbents and Manufacturing of Fired Clay Bricks**" being submitted by **Mr. Vihangraj V. Kulkarni (126104003),** to the Indian Institute of Technology Guwahati, India, for the award of Doctor of Philosophy, is a record of bonafide research work carried out by him under our guidance and supervision. The work embodied in this thesis has not been submitted for any other degree or diploma. In our opinion, the thesis is up to the standard of fulfilling the requirements of the doctoral degree as prescribed by the regulations of this Institute.*

Date:

Prof. Pranab Kumar Ghosh
Department of Civil Engineering
Indian Institute of Technology Guwahati,
Guwahati-781039. India

Dr. Animes Kumar Golder
Chemical Engineering Department
Indian Institute of Technology Guwahati,
Guwahati-781039. India

Acknowledgements

To me Ph.D. was not the destination but a journey; I take this opportunity to thank everyone who made this journey a successful and beautiful one. First and the foremost, I would like to express my deepest gratitude to thesis supervisors Prof. Pranab Kumar Ghosh and Dr. Animes Kumar Golder for believing in me; without their guidance, persistent help, comments, and valuable suggestions I would not have reached my destination. I thank Dr. Pranab Kumar Ghosh for initiating and shaping the work in early stages of Ph.D. and constantly shepherding throughout. I would like to thank him also for providing every possible help from the institute, may it be regarding work/sample analysis permissions or any other monetary affair. Many thanks must go to Dr. Animes Kumar Golder for his dedication, concern, warm relationship, constant encouragement, and being a thrust whenever I was despondent with my Ph.D. I thank him for his invaluable comments, diligent profound discussions from chemical engineering perspectives that improved my work and widened its reach enormously. Besides this, I thank my doctoral committee members Prof. Chandan Mahanta, Prof. Bishnupada Mandal, and Dr. Ajay Kalamdhad for their time and valuable suggestions those improved quality of work in various engineering facets. I am indebted indeed to Dr. Hemant Kaushik for sharing knowledge in brick manufacturing and testing.

I thank the head of the civil and chemical engineering departments (former and present), Faculty In-charge of environmental engineering laboratory (former and present) and staff members viz. scientific officer Jonali Saikia, junior technical superintendent Chittaranjan Medhi , and Pathak Da for providing uninterrupted help accomplishing the Ph.D. work. I acknowledge Central Instrument Facility, all departments of IIT Guwahati, and Guwahati University for allowing usage of sophisticated instruments. I would be happy to mention names of few staff members from different departments apart from mentioned above for their help; Harshraj da, Dr. Luku da, Deepak Da, Mr. N. K. Das sir, Amjad bhai, Minesh Medhi Da, Bojal Da, Rajib Gogoi Da, Upadhyay Ji, Tapan Da.

I am grateful to my senior friends Dr. Ravindra Patil, Dr. M. Gagrai, Dr. Bharti, Dr. A.S. Giri, Dr. Sushant Padhi, Mr. Sachin Tomar, Dr. K. Damodharan, Dr. V. Sudharsan Varma and Dr. Arvind Shakya for their co-operative assistance and suggestions in performing experiments. I also thank my present and past lab members and my juniors for

their help in during my Ph.D. I have no words to thank all my friends who have made the stay at IIT Guwahati a memorable one.

I thank my friend and a companion Ms. Rakhee Das for her belief in me and unconditional love that kept me alive inside to be a better human being. I feel lucky to be in a family that I am in and take this opportunity to thank parents for their patience during my Ph.D. I thank my brother and cousins for their unconditional support and more importantly moral and emotional support.

Above all, I believe that everything happens for a good reason, so I thank almighty for giving me exposure to such a life changing experience of Ph.D.

Vihangraj V. Kulkarni

Abbreviations

AAS: Atomic Absorption Spectroscopy
AC: Activated Carbon
ASTM: American Society for Testing and Materials International
BCR: Bureau of Community Reference
BET: Brunauer-Emmett-Teller
BIS: Bureau of Indian Standards
BMHR: Batteries (Management and Handling) Rules
BOD: Biochemical Oxygen Demand
CAC: Commercial Activated Carbon
CEC: Cation Exchange Capacity
CEDTA: Concentration of EDTA Moiety
CHNS: Carbon, Hydrogen, Nitrogen and Sulphur
CI: Crystallinity Index
COD: Chemical Oxygen Demand
DSPA: Dual-Site Proton Adsorption
DTG: Differential Thermogravimetry
DTPA: Diethylenetriaminepentaacetic Acid
EC: Electrical Conductivity
EDTAD: EDTA Dianhydride
EDX: Energy Dispersive X-ray
ETP: Effluent Treatment Plant
E-waste: Electronics Waste
FESEM: Field emission scanning electron microscopy
FFA: Functionalized Fibrous Adsorbent
FMH: Functionalized Mercerized Husk
FMMH: Functionalized double Mercerized Husk
FRH: Functionalized Raw Husk
FTIR: Fourier transform infrared
KM: Binding Constant
LAB: Lead Acid Battery
LABS: Lead Acid Battery Sludge
LABW: Lead Acid Battery Wastewater
LoI: Loss on Ignition
LPSA: Laser Particle Size Analysis
MC: Moisture Content
MH: Mercerized Husk
OPC: Ordinary Portland Cement
PAM: Proton Adsorption Model
PBDEs: Polybrominated Diphenyl Ethers
PBS: Pulverized LABS
PCB: Printed Circuit Board
PCDD/Fs: Polychlorinated Dibenzo-p-Dioxins and Polychlorinated Dibenzofurans
PCS: Pulverized Clay Soil
PER: Potential Ecological Risk
pHzpc: Point of Zero Charge
pKa: Dissociation Constant
PLI: Pollution Load Index

PPC: Pozzolana Portland Cement
RH: Raw Husk
RMSE: Root Mean Squire Error
SCE: Sequential Chemical Extraction
TCLP: Toxicity Characteristic Leaching Procedure
TDS: Total dissolved Solids
TGA: Thermogravimetric Analysis
TSS: Total Suspended Solids
ULAB: Used Lead Acid Battery
USEPA: United States Environmental Protection Agency
UTM: Universal Testing Machine
VS: Volatile Solids
XRD: X-ray Diffractogram
XRF: X-ray Fluorescence

TABLE OF CONTENTS

List of Tables

List of Figures

ABSTRACT

On account of growing automobiles demand, constant expansion of telecommunication infrastructure, increasing number of solar power projects, growing IT industry, and more importantly explosion in production of battery-driven e-bikes/cars the lead-acid batteries (LABs) market in India is expected to grow at a compound annual growth rate of over 8%, in value terms, between 2017 and 2022. The LAB industry is one of the most polluted industries that generate highly contaminated heavy metal laden wastewater (LABW) as well as sludge (LABS). In this dissertation, attempts have been made to prepare new adsorbents and resins for LABW decontamination and valorization of LABS as a potential building material is explored in order to achieve simultaneous environmental and monetary benefits.

A new functionalized fibrous adsorbent (FFA) and bio-resin was synthesized using arecanut husk, an agriculture waste material as the precursor for the decontamination of LABW through sulfuric acid treatment. It was characterized using proximate & ultimate, spectroscopic, and thermogravimetric analyses. A simple dual-site proton adsorption model (PAM) was developed on the basis of mass balance and applied for equilibrium Pb(II) uptake. The results of potentiometric titrations were fitted to PAM to determine the acid dissociation constants (pK_a) and the concentration of functional groups, which were mostly involved in metals uptake. The FTIR spectra and the pK_a values of 3.21 and 1.62, respectively, confirmed the presence of surface carboxylic and sulfonic groups onto FFA. It exhibited significant Pb(II) uptake and the Pb(II) ions predominantly attached to the carboxylic group even though the concentration was about 25% lower than the sulfonic group. The Pb(II) binding constant for carboxylic and sulfonic groups were found to be 5.2×10^6 and 28.11 L/mol respectively. FFA with a dose of 1 g/L showed around 98.3% Pb(II) removal at pH 5 from an initial concentration of 32 mg/L (0.157 mM). It showed the exhaustion capacity of 194.94 mg/g, which was about 3.4 times higher than the commercial activated carbon. Comparison of FFA with commercial resin showed Langmuir capacity of 1.1 times than that of IR120 for Pb(II) removal with the regeneration efficiency of 92%. Application of FFA for LABW treatment removed Pb completely and the removal efficiencies of Fe, Cd, and Mg were 85, 84, and 56%, respectively, at 5 g/L FFA complying the discharge standards adopted in India.

The functionalized bio-resin was synthesized from arecanut husk through mercerization and ethylenediaminetetraacetic dianhydride (EDTAD) carboxylation reactions. Mercerization extracted lignin from the vesicles on the husk and EDTAD was ridged into through an acylation reaction in dimethylformamide media. The reaction induced carboxylic groups as high as 0.735 mM/g and a cation exchange capacity of 2.01 meq/g of functionalized mercerized husk (FMH). Potentiometric titration data were fitted to the modified single-site PAM that gave pKa of 3.29 and carboxylic groups concentration of 0.741 mM/g. FMH showed 99% efficiency in Pb(II) removal from synthetic wastewater (initial concentration 0.157 mM), for which the Pb(II) binding constant was 1.73×10^3 L/mol as estimated from the modified PAM. The exhaustion capacity was estimated to be 18.7 mg/g of FMH. Desorption efficiency of Pb(II) from exhausted FMH was found to be about

97% with 0.1 N HCl. The FMH simultaneously removed Pb and Cd below the detection limits from LABW along with the removal of accompanying Fe, Mg, Ni, and Co.

An effective handling solution to LABW along with the generation of revenue is a long standing interest of the LAB industries. For this purpose, potential metal recovery from LABS and its utilization as a potential building material are demonstrated. LABS was found to be highly contaminated with Pb, Fe, Zn, Cu, and Cd with a concentration of 8322±11, 15721±21, 310±2, 175±4, and 1215±7 mg/kg, respectively, those were mostly concentrated in the finer fractions and, only 5% in coarser fraction (>75 microns). BCR sequential chemical extraction studies revealed that the Al and Ca were prominent in exchangeable, Fe, Mn, and Zn reducible, Pb (67%) and Cu (55%) in oxidizable and, Mg and Cd were mostly in the residual fraction. TCLP (toxicity characteristic leaching procedure) concentrations for Pb and Cd exceeded the prescribed standards and toxicity indices classified LABS as a hazardous waste with very high-risk for direct land disposal. Valorization through progressive acidification showed a metal recovery potential of 47, 77, 60, 19, 58, 59, 67, 41, and 51% for Pb, Fe, Cu, Cd, Ni, Mn, Al, Co, and Zn using citric acid. The utilization of LABS in fired brick manufacturing was fortified by spectroscopic studies, and LABS could be used as a partial replacement of fertile clay. The B5 bricks (5% LABS by w/w) showed the highest compressive strength of 74 N/mm^2 against the water absorption of 2.1% at a firing temperature of 1050°C. The bricks were also tested for linear shrinkage behavior, the volume of open pores, apparent porosity, bulk density, and loss on ignition. LABS added bricks showed higher porosity compared to pure clay bricks that restrained deformation and distortion of bricks during firing. The addition of LABS improved the ductile behavior of bricks avoiding catastrophic failure and imparted yellow coloration due to high CaO content. Furthermore, the TCLP test confirmed an effective fixation of Pb, Cd Ni, and Zn, and B20 bricks complied IS:1077:1992 class 12.5 and ASTM International.

In summary, two numbers of new adsorbents/bio-resins have been synthesized using agricultural waste material (arecanut husk) which were found to be efficient enough to remove Pb(II) not only from synthetically prepared wastewater (mono and binary metal systems) but also from real LAB wastewater to meet discharge standards in India. Critical analysis of LABS revealed its hazardous nature and valorization potential by recovering heavy metals or utilizing as construction material. Furthermore, LABS could be used in fired brick production to improve brick properties such as compressive strength and ductility along with effective heavy metal fixation. Finally, the bricks thus prepared complied Indian Standards as well as ASTM International.

Keywords: Lignocellulose material; Functionalized adsorbent; Potentiometric titration; Proton adsorption model; Pb(II) removal; Carboxylic bio-resin; Lead acid battery industry; BCR extraction; Heavy metal speciation; TCLP; Pollution indices; Fired clay brick; Non-hazardous bricks; Brick standards compliance

CHAPTER 1

Introduction and Literature Review Framing Objectives

1.1 Introduction

Many a times, the rapid industrial development, and urbanization adversely affect environment as well as human life as it leads to the generation of hazardous wastewater and solid waste. Water is a vital natural resource and will continue to be renewable as long as it is well managed. The management of water resource also includes regulating industrial discharges as per standard norms. Undoubtedly, the water pollution control efforts have been underway in many countries and, have already achieved some successes. Besides the success stories, pollution problems particularly in the developing countries like India have intensified to an alarming scale with a huge complexity. The current (unlawful) practice of discharging untreated or inadequately treated industrial wastewater and sludge is only worsening the situation [2, 3]

The industries generating highly contaminated wastewater includes chemical, pharmaceutical, electrochemical, electronics, petrochemical, metal plating, metal finishing, storage battery, and food processing. The lead-acid battery (LAB) industry is one of the most polluting industrial sectors and generates LAB wastewater (LABW) containing an extremely high concentration of Pb, Cd, Ni, Fe, and Zn along with a low pH and high total suspended solids (TSS) [4-6]. Adsorption and ion exchange are the techniques that could remove heavy metals from LABW; however, its industrial application is limited due to a high operational cost and complexity in the regeneration of spent adsorbents and resins [6, 7]. Therefore, the development of low cost adsorbent using biomaterials has gained the attention of researchers. Most of the lignicellulosic biomaterials carry various unexposed functional groups bound in the lignicellulosic matrix [8]. The physicochemical treatments such as chemical activation, thermal activation, and thermochemical activation could induce and expose functional groups. In addition, the functionalization of biomaterials also

can be carried out through crosslinking and grafting that could improve the leaching resistance, swelling properties as well as thermal stability [9]. Therefore, there are huge scopes of researches for the development of functionalized adsorbent and bio-resin using lignocellulosic biomasses, which is in particular not suitable for the bio-fuel production.

On the other hand, lead-acid battery sludge (LABS) arising from the alkali treatment of LABW contains high amounts of Pb, Cd, Ni, and Zn and, it is categorized as a hazardous solid waste [4, 10]. The typical treatment of LABS includes operations such as thickening, conditioning, dewatering, and drying. The possible disposal options of LABS are incineration, landfilling, ocean dumping, stabilization/solidification, and lagooning. However, incineration causes the release of toxic gases, landfilling and solidification may leach out the heavy metals in due course of time. The most effective way of LABS disposal could be its utilization in agricultural and nonagricultural lands by minimizing the metal loading along with the recovery of heavy metals. At the same time, the land application of LABS needs an extensive assessment of sludge toxicity to living organisms and plants with a proper knowledge of metal speciation [11-13]. Besides, the ecological risk assessment of LABS could be useful in deciding a suitable disposal options, proposing metal recovery potential, and/or its reuse along with an effective heavy metal fixation, which is mostly neglected for LABS. The solidification of heavy metallic sludge (LABS) with an appropriate binder results in heavy metal immobilization, however, the value addition of the immobilized materials is not usually considered. A study reports compressive strength improvement of soft clay soil with the addition of recycled basanite as an admixture [14]. A value added utilization of heavy metallic hazardous sludge (such as LABS) as a bricking material with a partial replacement of fertile clay could be a promising alternative to take care of its disposal problems. More explicitly, the use of LABS in fired brick manufacturing not only benefits with sludge disposal but also has many advantages:

i) Utilization of waste that needs a proper treatment
ii) Fixation of toxic metals
iii) Improvement of brick properties such as compressive strength and porosity
iv) Reduction in depletion of highly fertile clay
v) Generation of combustive energy from waste reducing energy consumption by increasing local temperature of the kiln
vi) Reduction in freshwater requirement for brick manufacturing utilizing high water content of sludge

1.2 Heavy metal pollution and toxicity

Metals can be categorised in three class viz. metals, metalloids, and heavy metals. Heavy metal is any metallic element having a relatively high atomic density (> 5 g/cm^3) and atomic weights between 63.5 and 200.6 [15]. In the context of environmental engineering, the term heavy metal has a little relation with density or weight but largely concerns about its chemical properties and toxicity. Hence, the heavy metals are the metals or metalloids whose concentration exceeding prescribed limit can cause acute or chronic toxicity to humans. However, not all heavy metals are toxic at low concentrations. Depending upon its chemical properties and impact on health effects, heavy metals can be subdivided in to three category viz. essential (nutritionally essential), beneficial (metals with possible beneficial effects), and detrimental (metals with no known beneficial effects). Fe, Cu, Zn, Cr-III, and Co are essential, Si, B, V, and Ni are beneficial, and Pb, Cd, As, Cr-VI, and Hg are considered as detrimental heavy metals [16, 17]. Zn is important in physiological tissue activities and regulating various biological processes in the human body. However, the excess concentrations may cause skin irritations, stomach cramps, vomiting, nausea, neurologic degeneration, and anaemia [18]. High concentrations of Ni may cause acute toxicity in terms of dermatitis; nickel carbonyl, and encephalopathy. Whereas, prolonged exposure to Ni result in pulmonary fibrosis, reduced sperm count, and nasopharyngeal tumour [19]. Cd is declared as a carcinogen by the U.S. Environmental Protection Agency (USEPA). Chronic exposure of Cd results in kidney dysfunction, hypertension, hepatic injury, renal dysfunction, teratogenic effects, and lung damage; high levels of exposure may result in death [20]. Pb is one of the toxic heavy metals and categorised as a carcinogen by the USEPA. Pb attacks nervous system resulting in reduced work efficiency. Pb exposure may cause weakness in fingers, wrists, or ankles and increases blood pressure particularly in middle-aged and older people. Higher levels of exposure severely affects kidney and brain ultimately causing death [21].

1.3 Sources of heavy metals in environment

Heavy metals are distributed in the earth crust over a larger area and harmoniously exist in the environment. However, anthropogenic activities such as industrialization concentrate heavy metals at one point, resulting in heavy metal pollution (Fig. 1.1). Heavy metals are found in environment in various forms and in various mediums, that decides the

toxicity of heavy metals. In general, the sources of heavy metals in environment include agricultural, domestic, air-borne, and industrial or anthropogenic.

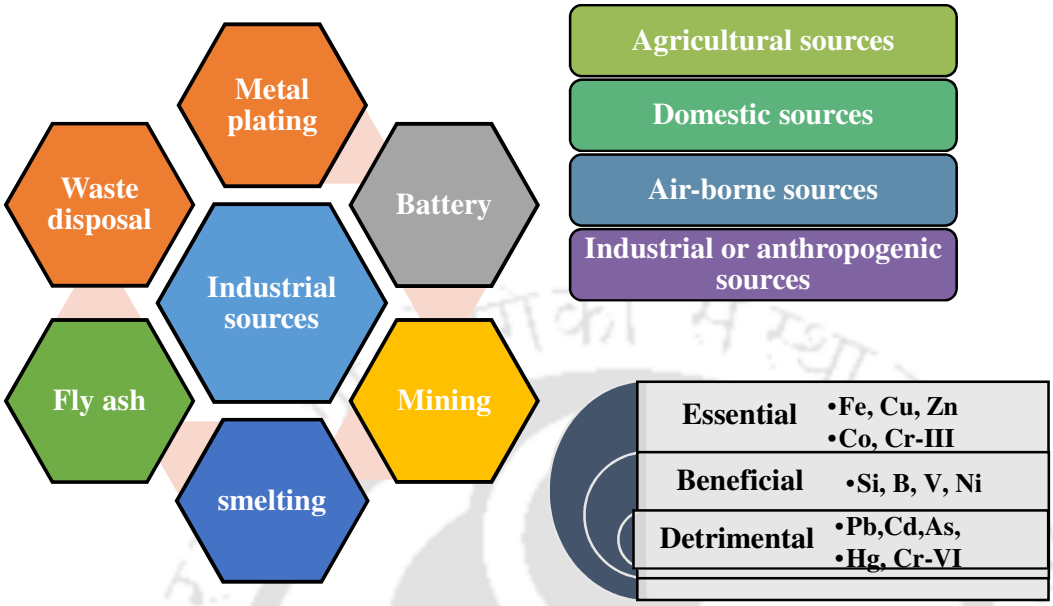

Figure 1.1: Pictorial representation of sources and nature of heavy metals.

Agricultural sources of heavy metals primarily include fertilizer, fungicides, herbicides, phosphate, decaying plant, animal manures, bio-solids (sewage sludge), compost, and pesticides [22]. Such sources primarily affect soil, leading to heavy metal concentration higher than the desired value [23]. The water seeping through soil or runoff water over the soil carries these heavy metals and joins water body, causing water pollution. The urbanised lifestyle has resulted in the usage of actual goods that may contain heavy metals. Hence, heavy metals are also found in domestic wastewater. A study has reported that sources of heavy metals can be actual goods, e.g. runoff from roofs, wear of tires, food, or activities, e.g. large enterprises, car washes etc. [24]. Airborne sources of metals include industrial stack or duct emissions of air, gas, or vapour streams, and fugitive emissions such as dust from storage areas or waste piles. Metals from airborne sources are generally released as particulates contained in the gas stream. Some metals or metalloids such as As, Cd, and Pb can also volatilize at high-temperature [22]. Fugitive emissions are often distributed over a much smaller area because emissions are made near the ground. In general, contaminant concentrations are lower in fugitive emissions compared to stack emissions. The type and concentration of metals emitted from both types of sources is dependent to site conditions. Pb, Cd as well as solid particles in stack emissions are deposited in soil, water, and oceans contributing to heavy metal pollution [22, 25].

Industrial sources of heavy metals include those arising from chemical, pharmaceutical, electrochemical, electronics, petrochemical, metal plating, metal finishing, and food processing industries. Discharge of potential heavy metals from industrial point sources is the major sources of urban water pollution. The contributory industries can be metallurgical, glassware and ceramic, tannery, dyestuff, pesticides, synthetic chemicals, petroleum, explosives, electroplating, photographic, pigments, steel manufacturing, chrome plating, and LAB industry. [26-30]. Concentration of heavy metals in industrial discharge are varying and differs with industry, manufacturing process adopted, and raw material used. For this reason, industrial wastewater is treated individually rather than in combination with domestic sewage.

1.4 Industrial heavy metal pollution: The insights

The industrialization has increased immensely in the last century to meet the demand of rapid urbanization. This has raised concerns of heavy meal pollution to an alarming level. The heavy metals have become an integral part of urban life those help humans in various phases and ultimately end up in landfill or wastewater, creating pollution.

1.4.1 Heavy metal flow in environment

Some of the heavy metals are severely poisonous and naturally occur in soil, surface water, and plants at low concentrations. Anthropogenic activities such as mining and dumping from industries has resulted in increased concentration of heavy metals in natural habitats such as forests, rivers, lakes, and ocean [31]. Industries are the major stakeholder for the heavy metal pollution arising from industrial discharges [32] and from ores and mines [33]. The heavy metals in environment, beginning from its ore throughout its utility period meet wastewater or end up in the landfill. The flow of heavy metals is shown here with a flow chart (Fig. 1.2). A report states that 80–90% of industrial wastewater in developing countries is discharged over soil/land or into surface water bodies without any treatment [2]. Wastewater discharged by numerous industries contains high concentrations of heavy metals, thus its treatment is of high priority in the context of human health as well as a threat to the environment and biodiversity [34]. The soil pollution may result in entry of heavy metals in the food chain. There are several reports on the presence of heavy metals viz. Cd, Pb, Ni, and Zn above WHO permissible limits in a vegetable *Beta vulgaris* (palak

in India) that was cultivated on a land irrigated with treated, partially treated, or untreated industrial wastewater [35-37].

Mining is the first operation to avail heavy metals for anthropogenic usage. The prime pollution concerns of mining are dumping of mining wastes, acid mine drainage (AMD), management and treatment of mine tailings/effluents, deforestation, and land degradation. The mining operation pollutes water, air, and soil by producing AMD, metallic dust, and mine tailings, respectively [38]. AMD have generated a widespread environmental pollution problem. During mining, the sulphide minerals are exposed to the atmosphere that causes its weathering, when it meets water, the heavy metals are dissolved imparting acidity to water. The AMD from mines is not limited till its operational period but it continues to generate AMD for hundreds of years, even after closure [39]. A study reported that Japan recorded 5487 number of closed mines by year 2000 [33], where the concentration of Fe, Al, Cu, Zn, As, and Si were 715, 45, 13, 15, 862, and 22.9 mg/L in AMD from a closed mine. The mine tailings contains heavy metals such as Pb, Zn, and Cd, those are difficult to recover due to technological process constraints. The heavy metallic dust generated in mining operation severely affects human, animal, flora, and fauna [40]. A study on treatment technologies at 108 active and passive mines in Canada and other countries showed that they produce about 9500 tons of dry sludge per year. The concentration of Al, Cu, Fe, Mg, Mn, and Zn were reported to be 627, 398, 223, 1824, 881, and 2074 mg/L respectively. These figures are indicative of huge production of sludge from AMD neutralization and expected to grow in upcoming years [38].

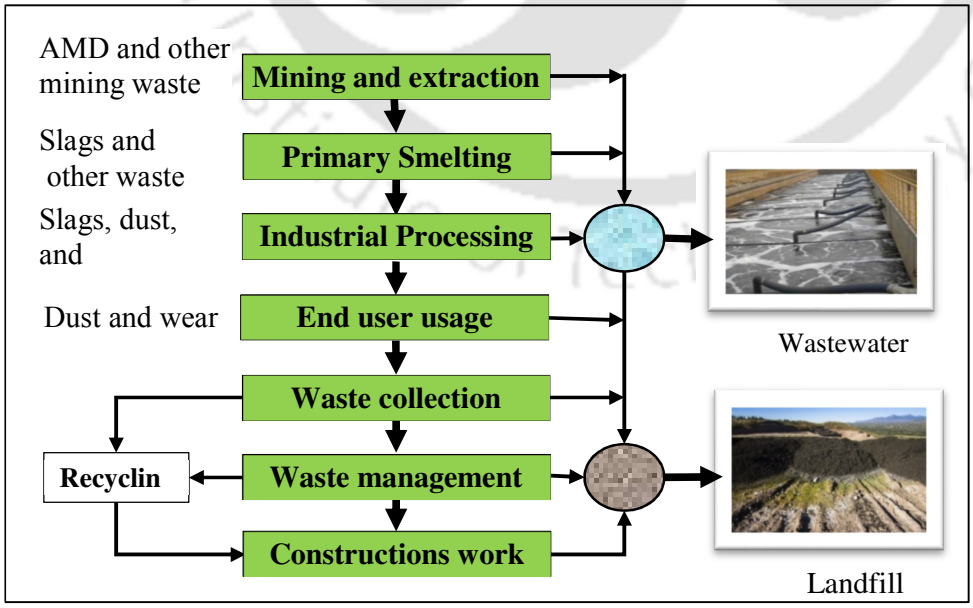

Figure 1.2: Material flow of heavy metals in environment.

1.4.2 Metal processing industries

Many metal processing industries are the cause of the cumulative injury to the environment through water, soil, and air pollution. The steel plants contributes to heavy metal pollution from various units such as coal washery, coke ovens, blast furnace, steel melting shop, and rolling mills. The waste generated from each unit differs in type and volume of contaminants; coal washery wastes contain high solids (dissolved and suspended), calcite, gypsum, kaolite, pyrite, and other impurities such as clay and shale; this imparts alkalinity as well as hardness to water [41]. An ammoniacal liquor is the concern from coke oven unit and contains ammonia, phenols, and toxic chemicals. Blast furnace essentially emits hot flue gas that is loaded with flue dust, Fe, Zn, and C [42]. Higher concentrations of Zn (>120 g/ton of pig iron) generates high amounts of dusts or slag due to a sudden fall of the furnace load [43]. The waste generated from this unit is a hazardous metallurgical solid waste i.e. blast furnace slag. The slag is stored in ponds until suitable disposal methods are available; leaching of Zn, Fe, and Pb from slag causes serious surface and groundwater pollution. A study reported that the blast furnace slag contained 41, 2, and 0.06% (by weight) of Fe, Zn, and Pb respectively [42]. Wastewater from blast furnace unit is alkaline whereas the pickling waste is acidic: neutralization is usually adopted mixing both wastes judiciously [44]. The characteristics of wastewater generated from electroplating, electroless plating, anodizing, coating (chromating, phosphating and coloring), chemical etching, milling, and printed circuit board manufacturing (PCB) are more or less same, a subject variant is raw material used and the manufacturing process followed [40]. Effluents of these primarily contain heavy metals, waste solvent, and heavy metal-containing debris. Specifically, it contains highly unacceptable concentrations of Cr, Cu, Cd, and Zn [45]. The lime treatment of wastewater generates hazardous sludge as solid waste. A study reported that the PCB wastewater treatment sludge contained Fe, Cu, Zn, Ni, Cr, and Cd in concentrations of 233, 169, 1, 0.7, 0.19, and 0.007 mg/g, respectively [46]. A metal plating wastewater was reported to be contaminated with complexed metals originating from Ni and Zn plating process in concentrations of 282 & 236 mg/L respectively [47]. Effluent of a metal plating plant was characterized for Cu, Cr, and Ni and found to contain 45, 45, and 394 mg/L, respectively [48]. Cleaning, pickling, and processing operations in electroplating industries generate toxic chemical compounds, cyanides, chromates, and heavy metals [40].

1.4.3 Electronics industry

Advances in electronics technology have boosted electronic industry resulting in e-waste generation. It is estimated that the global annual e-waste generation in the year of 2014 was 42 million tons [49]. The e-waste usually contains Cd, Cr, Pb, Hg, Cu, Se, Zn, Ag, Au, and Pt in varying amounts. The recovery of these useful and precious metals is possible, however the crude and unsupervised recovery practices in developing countries result in heavy metal pollution [50].

Heavy metal contamination of water, soil, and plants around an electronic waste dumpsite in Nigeria found to contain Pb, Cd, Zn, Cr, and Ni in concentrations of 2.7, 0.012, 0.95, 0.52, and 1.45 mg/L in wells situated in a market. The concentrations of the same in soil samples (depth 0-15 cm) at e-waste dumpsite were recoded, and were 630, 10, 55, 47, and 85 mg/kg. The heavy metal concentration uptaken by plants were analyzed separately in root, stem, and leaf; it was the highest in roots with 86, 1, 29, 3, and 16 mg/kg for Pb, Cd, Zn, Cr, and Ni, respectively [51].

1.4.4 Industrial heavy metal pollution: Indian scenario

People near the industrial areas are the most affected due to industrial pollution. The Katedan industrial development area, Hyderabad, India has around 300 industries; those include dyeing, edible oil production, battery manufacturing, metal plating, chemicals, etc. These industries were reported to dispose untreated effluents and solid wastes, i.e., sludge in the ditches or open land [52]. A study analyzed soil samples from the area and found that the heavy metals concentration of Pb, Cr, Ni, Zn, As, Cd, and Cu was in the range of 65–2000, 62–433, 19–90, 180–1213, 12–100, 0.7-19, and 63–71 mg/kg respectively. It is reported that the mobility of metals is low in soils as compared to water. But the mobility of these metals is found higher in the rainy season expecting to contaminate groundwater in the vicinity [52]. Hence, the dumping of industrial waste can spread heavy metal pollution and is dependent on rainfall patterns. The fly ash deposits in the industrial region of Chhattisgarh, India, reported higher concentrations of Mn and Cr than the prescribed WHO drinking standards throughout the year; Fe also reached the threshold after monsoon [53]. The heavy metal pollution not only harms humans but all the living organisms. In Cochin estuary, India, heavy metal pollution has brought reduction/adaptation in the distribution, diversity, and enzyme expression profile of bacteria. This will ultimately impart adverse impacts on ecosystem functioning [54].

Table 1.1: Heavy metals occurrences in Indian rivers [55].

Heavy metal	Number of locations	Number of samples	Maximum concentration occurred, µg/L	No. of noncompliance instances (IS: 10500:2012)
As	387	1921	9.47	0
Cd	NA	1934	4	7
Cr	14	1917	366	21
Cu	387	1924	180	68
Fe	NA	1918	6.65*	492
Pb	NA	NA	48.92*	67
Hg	387	872	NA	0
Ni	NA	1637	80.51	107
Zn	387	1913	NA	0

* Concentration in mg/L
NA: Not available

The illegal industrial effluent discharge ultimately joins nearby rivers in due course of time, majorly through surface runoff. Hence, the heavy metal pollution of rivers may present an idea of the extent of industrial pollution. The heavy metals concentration in 16 river basins of India at 396 locations was analyzed by Central Water Commission, Ministry of Water Resources, Government of India [55]: the statistics is presented in Table 1.1. It was reported that the heavy metal concentrations were the highest in nearby major cities of India as a result of treated, untreated, and/or partially treated industrial discharge/disposal. The stretch of Damodar river near Durgapur industrial complex, West Bengal, India had heavy metals enrichment in the river sediment expressed as enrichment factor (a dimensionless quantity) was found to be 39.90, 33.15, 0.16, and 0.013 for Cd, Pb, Mn, and Fe respectively. The geoaccumulation index for Cd and Pb varied from moderate to high and was 4.73 and 4.466 respectively with the pollution load index of 1.05 [56]. A study on heavy metal pollution of Yamuna and associated drains used for irrigation in rural and peri-urban settings of Delhi NCR was carried out. The concentrations of heavy metals viz. Cu, Cr, Zn, Pb, Cd, and Ni were in the range of 0.02–0.64, 0–0.42, 0.13–2.22, 0.03–0.27, 0–0.07, and 0.01–0.13 mg/L respectively. The high levels of the heavy metals were found to be the result of rampant discharge from industries such as battery, electrical appliances manufacturing, printing, electroplating, steel processing, dyeing, etc. [57].

Many a times the treated or untreated industrial discharges are used for irrigation due to lack of other source. However, the practice is unhealthy as may result in entry of heavy metals in the food chain. An investigation on Pb pollution in soils and plants irrigated with untreated sewage water in some industrialized cities of Punjab, India was undertaken.

Table 1.2: Industrial metal pollution of different medium.

Industry and waste	Medium	Cr(VI)	Ni(II)	Cu(II)	Fe(II)	Zn(II)	Pb(II)	Cd(II)	Reference
Blast furnace slag	Soil*	NA	NA	NA	41	2	0.06	NA	[42]
PCB sludge	Soil*	0.19	0.7	169	233	1	NA	0.007	[46]
Metal plating wastewater	Water#	45	282–394	45	NA	236	NA	NA	[47, 48]
E-waste dumpsite	Well# Soil* Plant*	0.52 47 3	1.45 85 16	NA	NA	0.95 55 29	2.7 630 86	0.012 10 1	[51]
Near industrial area	Soil*	62–433	19–90	63–71	NA	180–1213	65–2000	0.7–19	[52]

*concentration of heavy metals in mg/kg
#concentration of heavy metals in mg/L

The study revealed that the sewage irrigated soils and cultivated vegetation showed Pb concentrations 4.61 and 548 times than that of the tube well irrigated sites. The analysis of Pb concentrations in vegetable and average per capita consumption showed that the Pb consumption of an individual was far exceeding the WHO limits [58]. In another study, the maximum concentrations of As, Si, Pb, Cr, Cd, and Ni in soils tested at 4 places were 117, 249, 79.4, 138, 163, and 36.5 mg/kg respectively [59]. A few instances of heavy metal contamination by industries are enlisted in Table 1.2.

1.5 LAB industry and heavy metal pollution

The LAB industries find its roots long back in the 18th century, and it was first discovered by Siemens in 1850, which later was commercialized and patented in 1859 by Plante [60]. Since then, the LABs never looked back in terms of demand and growth. As of today, even with the introduction of Lithium ion, Nickel batteries, and fuel cells, the LABs are predominantly used in the automobile sector, electric powered vehicles, computer and telecommunication systems, and sometimes for the purpose of emergency battery backup. The LABs are the most economical, manufactured with well-established technology, and researched enough to understand capabilities and limitations. These advantages overcome its drawback of being heavy and attract industries to use in every possible sector. It possesses high recyclable capacity and is dependent upon lead that owe 50% of its manufacturing cost [61]. Most of the lead mined every year is used in batteries, it was 28% in 1960, 74% in 1999, and 85% in 2015 [60-62]. The lead used in battery is either primary i.e. mined or secondary i.e. recycled. It is estimated that a recycling rate of 90–100% is achieved in developed countries, whereas it varies from 60–90% in developing countries

[63, 64]. The LAB manufacturing as well as recycling process generates wastewater that is highly contaminated with heavy metals such as Pb, Cd, Ni, Zn, and is highly acidic due to the use of sulphuric acid. The instances of pollution caused by LAB industry and its effects on human, animals, and environment are copious. Pb is lost at various stages beginning from mining to LAB manufacturing. It is estimated that the loss of Pb during mining and concentrating, primary smelting, recycling, and battery manufacturing process are 16.2, 7.2, 13.6, and 4.4% (% by weight) respectively. These figures are huge and indicative of the extent of air, water, and soil pollution that can be caused by LAB industries [65].

1.5.1 Reports of LAB pollution

The human habitat is severely affected by LAB pollution through various exposure pathways. The Pb levels in children's blood residing nearby LAB manufacturing plant were found to be as high as 120 µg/L, through exposure of soil/dust [66]. The literature on blood lead levels was reviewed by Gottesfeld and Pokhrel (2011) [67] and reported that the highest blood Pb levels of children in developing countries was 470 µg/L near LAB manufacturing plants, whereas it was 640 µg/L nearby used LAB (ULAB) recycling plants. The topsoil (at depth 90−5 cm) and house dust concentrations of Pb near a LAB manufacturing plant were tested. The concentration of Pb was significant up to 500 m distance from the manufacturing plant with the highest (12.65 µg/g) near fencing [68]. Increased LAB manufacturing plants are increasing the level and the extent of Pb pollution in developing countries. A statistical analysis recorded 50 cases of Pb poisoning in China during 2004−2012, out of them 19, 17, and 6 were caused by lead smelting, LAB manufacturing, and LAB recycling [69]. There is no safe blood lead level threshold for children as per ASTDR 2017; however, Centre for Disease Control, USA considers 100 µg/L as a level of concern.

1.5.2 Reports of ULAB pollution

In the case of ULAB pollution, the technical process of recycling is of great importance as the advanced techniques provide a check to trap pollution. The technical process, efficiency, and pollution caused in ULAB recycling in Delhi were studied. It was found that the recycling is carried out by authorized and unauthorized small-scale industries, the earlier being well organized, and the later fully unorganized. The public preferred to sale used lead acid batteries to unauthorized sector as they get higher selling price than authorized ones [61]. In India, around 88.5% of the lead acid batteries are

recycled by unauthorized sector [70]. The unauthorized sector is unskilled or semiskilled; as a result the recovery of lead is achieved in a crude manner leading to noise, air, soil, and water pollution affecting health of workers as well as public in nearby areas. Similar results for lead smelting units in Kolkata are reported [71]. The authors reported the boundaries of the government in order to tackle pollution from lead smelting pants in Kolkata. It was found that the pollution control devices were ineffective to meet desired standards. Lead smelting was the prime reason of air pollution in this area, which was also responsible for soil and water pollution. Such crude and informal/unorganized practices of Pb recovery from ULABs result in low recovery rate and high levels of Pb pollution [72]. Though there are no reports on LAB pollution in many other places in India, it is no exception for ULAB pollution [3]. The images of crude lead recovery practices, lack of skilled workers, safety essentials for workers, and resulting pollution in a LAB processing industry in India are shown in Fig. 1.3

Figure 1.3: Crude, unhealthy, and illegal practices of ULAB recycling: (a) separation of lead grids, (b) and (c) breaking of batteries for lead recovery, (d) spillage of acid around in the battery, (e) lead fumes and spurt in trolley filing, (f) lead recovery furnace and (g) lead fumes during the rotary operation. (Pictures courtesy: (a) and (b) self-captured and (c), (d), (e), (f), and (g) are adopted from Trivedi (2017) [3]).

A technical report on the current status of recycling of LABs in China reported that LAB industry have created severe environmental pollution problems in China [73]. A study from Dakar, Senegal reported that Pb pollution by ULAB recycling caused death of 18 children due to inhalation of dust and soil contaminated with Pb [74]. The instances of higher Pb content in vegetables, soil, fruits, or plants are copious in literature [12, 35, 36].

Although there are various instances that prove LAB industry causes serious heavy metal pollution, it can be minimized through stringent laws, substitution of raw materials, and reforms in manufacturing process. To understand the scenario of Pb pollution one should possess overview of LAB manufacturing and recycling.

1.6 Manufacturing/recycling process of LAB/ULABs

The lead contaminated wastewater as well as sludge is generated during the manufacture as well as recycling of LABs. Hence, it is of great importance to understand the process that involves waste generation.

1.6.1 LABs manufacturing process

The LABs are made up of positive and negative electrodes and an electrolyte. Pure Pb is used as a negative electrode i.e. cathode, Pb oxide is used as a positive electrode i.e. anode, and dilute sulphuric acid as an electrolyte. The reactions involving charging and discharging of the LABs are presented in following equations (Eq. 1.1 to 1.2).

Negative plate reaction:

$$Pb(s) + HSO_4^-(aq) \rightarrow PbSO_4(s) + H^+(aq) + 2e^- \quad (1.1)$$

Positive plate reaction:

$$PbO_2(s) + HSO_4^-(aq) + 3H^+(aq) + 2e^- \rightarrow PbSO_4(s) + 2H_2O(l) \quad (1.2)$$

The manufacturing process of the LABs involves various unit operations such as lead oxide preparation by milling, lead grid casting, paste manufacturing, grid pasting, plate curing, plate parting, and battery assembling. The batteries are then finally boxed, welded, sealed, tested for air leakage, and then charged. The fully charged batteries are then shipped for trade. A typical process flow chart for manufacturing of LABs is presented in Fig. 1.4.

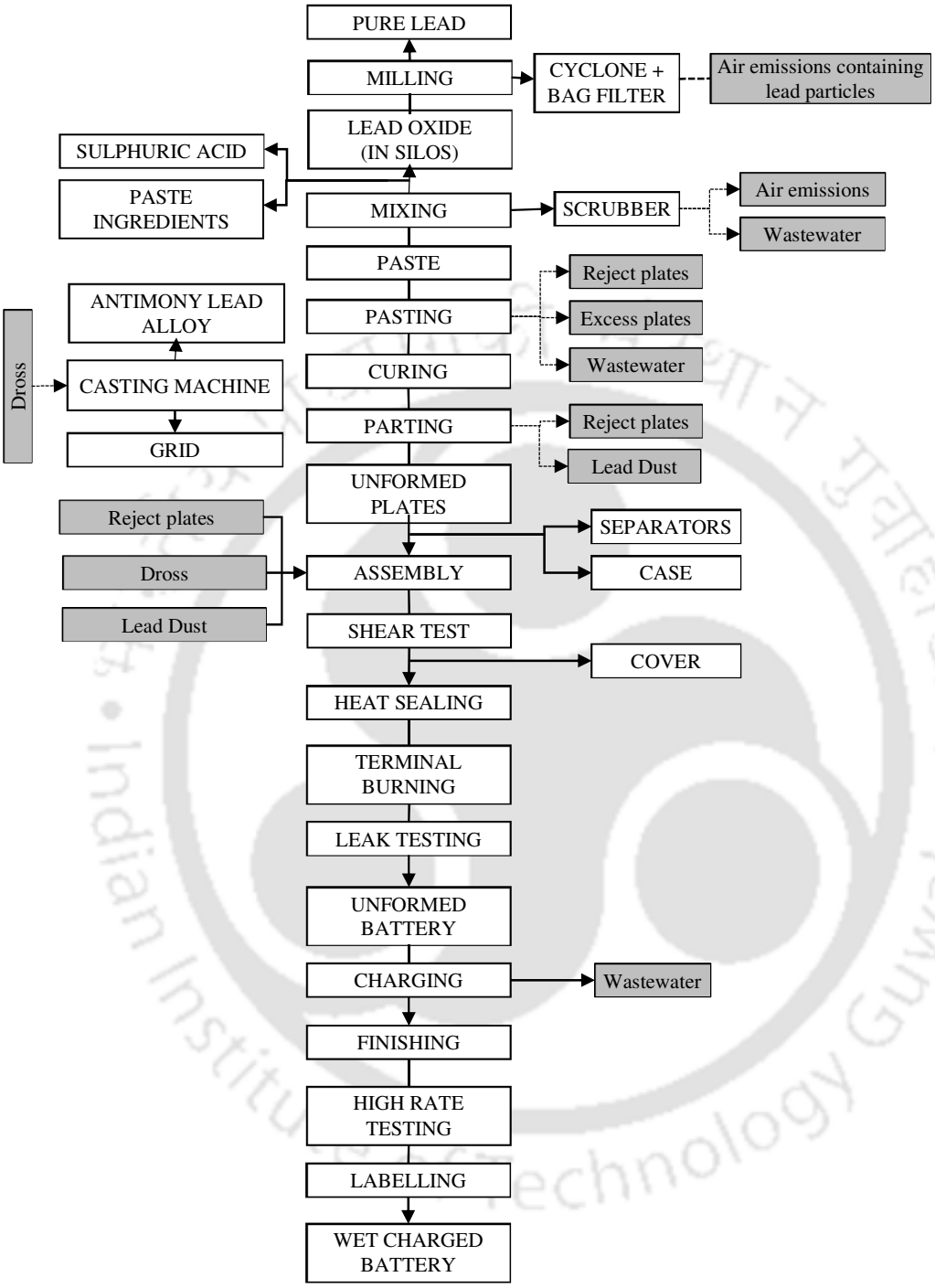

Figure 1.4: A typical process flow diagram for LAB manufacturing industry [1].

1.6.2 LABs: effluent characteristics and sources

The effluent of LAB industry usually contain Pb (2-50 mg/L), high TDS (up to 10000 mg/L), Ni (up to 2 mg/L), Cu (up to 2 mg/L) with pH between 1-2 [27, 75] . In manufacturing of LAB, lead oxide is prepared from pure Pb. This lead oxide, dilute sulphuric acid, Milli-Q water, and other additives (different for positive and negative paste) are mixed proportionately to form a paste. It is then pasted on lead grid prepared by using lead alloy to make battery plates. Thereafter, the plates are cured, dried, and cut in to single to assemble in battery. The single plates are then stacked and fused to form positive and negative using lead straps and burning strips and separators are placed appropriately. After proper assembling of batteries, these are filled with dilute sulphuric acid and charged with DC supply. Every unit operation in manufacturing generates different type of waste. The unit operation, process involved, and waste generated during is tabulated in Table 1.3.

Table 1.3: Unit operation, process involved and waste generated from each process in LAB manufacturing [76].

Process	**Operation involved**	**Waste generated**
Oxide milling	Pure lead to lead oxide by melting and oxidizing.	Lead emissions
Lead grid casting	Lead alloy bars melted and poured in grid moulds. On cooling, grid is trimmed and excess lead is recycled.	Dross (lead waste) and solid wastes
Paste manufacturing	Positive and negative pastes are prepared using lead oxide and additives in paste mixer.	Pb Vapours
Grid pasting	Plates are prepared by pasting on grids. Process is completed in sequence of paste feeding, pasting, drying, and collection with the help of the belt conveyor system.	Reject plates, spillage as sludge, Pb wash water
Plate curing	Plates are exposed to air at temperature <60°C with 90% humidity for minimum 32h. Exposure to air converts free lead to lead oxide.	Lead dust, wash water
Plate parting	After curing, the plates are parted into two by an automated machine and collected manually. Plates are then stacked and assembled in battery case.	Lead dust, reject plates, machine washed oily water
Battery assembly	Assembling of battery primarily include enveloping stacked plates. Plates are connected as per layout and inter-cell connections are made.	Reject plates, dross, wash water
Finishing and quality checks	Finishing operations include a shear test, heat sealing, terminal burning, and leak testing.	Reject batteries, straps, tags
Charging	Charging includes filling batteries with sulphuric acid and passing electricity. After full charging, the batteries are emptied, washed with water, and filled with fresh sulphuric acid. Batteries are tested labelled, and packed for dispatch.	Acidic wastewater from battery charging and washing

It can be seen from Table 1.3 that the manufacturing of LABs generates solid waste as well as wastewater. The solid waste includes rejected plates, batteries, plastic material, scrapped cases, and sludge. Whereas, wastewater is generated through washing and cleaning machines and area, battery washing operation, use of wet scrubber for dust control, and cooling process. Most of the solid wastes excluding sludge are recycled. Wastewater bearing high concentrations of Pb and sulphate is treated by the lime addition in the effluent treatment plant. This further generates heavy metallic sludge.

1.6.3 ULABs recycling process

The ULABs are recycled through the breaking of the battery case manually or in a hammer mill according to the size of recycling unit. In this process, lead, polypropylene, lead grids, and slags are separated, and the acid is stored in a pit. From separated materials, lead grids are melted at lower temperatures and the lead is recovered. The recovery of lead from the remaining paste is carried out at higher temperatures. Lead sulphate is the major component of the paste and weights almost 60%, along with lead dioxide of 28%, lead oxide of 9%, and metallic lead 3% by weight [77]. A typical Pb recovery method is illustrated in Fig. 1.5.

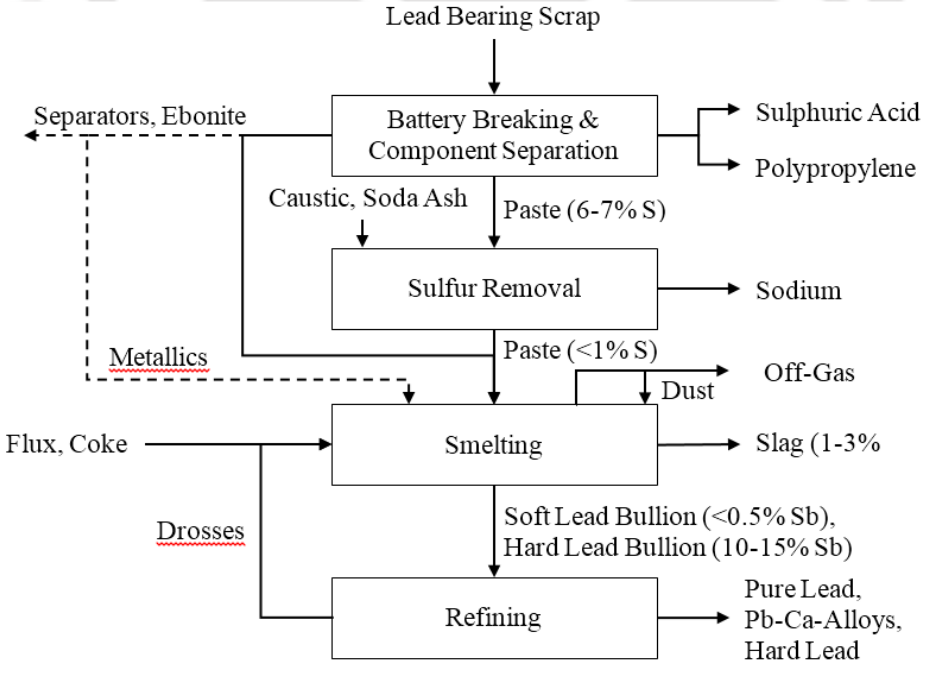

Figure 1.5: A typical process flow diagram for recycling of LABs [62].

In ULAB recycling, Na_2CO_3 or NaOH is added as desulphurization agent followed by smelting and sulphur is as a retrieved by-product having a sellable market value. The sludge generated through this comprises of insoluble salts, which is collected and routed to the smelter. This is the typical process of the ULAB recycling, however as mentioned earlier, lack of infrastructure, skilled supervision, and greed of money is driving small-scale industries in developing countries for unorganized recycling. This kind of crude recovery is worsening the water and soil pollution by dumping of slag and acids on soil or in water bodies.

1.7 Stipulated limits of heavy metals discharge/disposal

Table 1.3 shows various unit operations or processes of a typical battery industry (manufacturing and recycling) that generates various wastes. The stringent laws may help reducing pollution, as industries will be asked to pay for the waste disposal/treatment, they tend to adopt reduce waste generation. Considering ill effects of heavy metal, the Indian Standard (IS: 2296-1982) limits heavy metal concentration in surface waters. It also disallows the heavy metal discharge from industrial sources beyond the prescribed limit (Table 1.4). However, the standards for sludge disposal on soil are not provided as per Indian Standards.

Table 1.4: Surface water quality and discharge standards of various metallic pollutants.

Heavy metal	**Surface water quality standards (ppm)***			**General Standards for discharge of effluents (ppm)****			
Class/water body	A	B	C	A	B	C	D
Copper	1.5	-	1.5	3	3	NIL	30
Lead	0.1	-	0.1	0.1	1	NIL	1
Zinc	15		15	5	15	NIL	15
Arsenic Total	0.05	0.2	0.2	0.2	0.2	0.2	0.2
Mercury	0.001			0.01	0.01	0.01	0.01
Cadmium	0.01		0.01	2	1	NIL	2
Chromium (VI)	0.05	0.05	0.05	0.1	2	NIL	1

* IS: 2296-1982, Class A – Drinking water without conventional treatment but after disinfection, Class B –Water for outdoor bathing, Class C – Drinking water with conventional treatment followed by disinfection

**As per schedule of the Environment Protection Rules 1989, A– surface water, B– public sewer, C– irrigation water, D–coastal water

1.8 Conventional treatment of heavy metallic wastewater

Various treatment technologies used to remove heavy metals from wastewater include chemical precipitation, ion-exchange, adsorption, membrane filtration, electrochemical treatment technologies, engineered wetland treatment, biosorption etc. [29, 78-85]. Barakat (2011) [86] and Fu and Wang (2011) [87] concluded that lime precipitation is the most effective and economical technique of heavy metals removal from wastewater. However, it generates a large amount of precipitate sludge that requires further treatment. New adsorbents and membrane filtration are the most frequently studied and widely applied [86]. Reverse osmosis, ion-exchange and other membrane separation techniques can effectively reduce metal ions, but their uses are limited due to a number of disadvantages such as high material and operational cost, and their operational problems [29]. General LAB wastewater treatment block diagram is presented in Annexure I [88].

1.8.1 Chemical precipitation

In chemical precipitation, chemicals are added to wastewater to alter the physical state of the dissolved and suspended solids to facilitate their removal by sedimentation [79, 89]. A variety of hydroxides has been used to precipitate metals from wastewater based on cost and ease of handling: lime is the preferred choice in hydroxide precipitation with relative simplicity, low cost, and ease of pH control [79, 87]. A plenty of studies are reported on heavy metal removal by precipitation. However, results of a few relevant are tabulated in Table 1.5.

Table 1.5: Operating parameters and heavy metal removal efficiency of precipitation.

Metal ion	Precipitant	Initial metal, mg/L	Efficiency, %	Optimum pH	Reference
Zn(II)	CaO	32	>99	9 to 10	[78]
Zn(II)	$Ca(OH)_2$	450	>99	11	[90]
Cd(II)	$Ca(OH)_2$	150			
Mn(II)	$Ca(OH)_2$	1085			
Cu(II)	$Ca(OH)_2$	100	>99	7 to 11	[91]
Zn(II)	$Ca(OH)_2$				
Cr(III)	$Ca(OH)_2$				
Pb(II)	$Ca(OH)_2$				
Cd(II)	$Fe(OH)_3$	37	96	11	[92]
Cu(II)	$Mg(OH)_2$	16	80	9.5	
Cu(II)	H_2S	1	100	3	[93]
Zn(II)	H_2S	87	>94		
Pb(II)	H_2S	477	>92		
Cr(III)	CaO, MgO	5563	8	>99	[94]

From Table 1.5, it can be seen that the most metals can be removed with precipitation. A study reported removal of chemical oxygen demand (COD) along with Z(II) with >99% efficiency through a hybrid process of electro-Fenton and chemical precipitation [78]. The precipitation of heavy metals is highly dependent upon pH and every metal possess different solubility at the same pH. Hence, the knowledge of metal speciation is necessary. A study on precipitation of Cu(II), Pb(II), and Ni(II) showed feasibility to control selective precipitation of each metal by controlling the solution pH [30].

1.8.2 Electrocoagulation (EC)

EC is a process consisting of creating metallic hydroxides flocs within the wastewater by electro-dissolution of soluble anodes, usually made of iron or aluminium [95]. The process of EC is a complicated one involving many chemical and physical phenomena that use consumable electrodes (Fe/Al) to supply ions into the water stream. The consumable (sacrificial) metal anodes are used to produce polymeric hydroxides near anode. Coagulation occurs when these metal cations combine with the negative particles carried toward the anode by electrophoretic motion. Contaminants present in the wastewater stream are treated either by chemical reactions and precipitation or by physical and chemical attachment to colloidal materials, being generated by the electrode corrosion. They are then removed by electroflotation, sedimentation, and filtration. In a conventional coagulation process, coagulating chemicals are added, whereas, these coagulating agents are generated in situ in EC process. Brief mechanism of coagulation process is described below (Eq. 1.3 to 1.5)

$$Al \rightleftharpoons Al^{3+} + 3e^{-} \text{(Anode)} \quad (1.3)$$

$$3H_2O + 3e^{-} \rightleftharpoons 0.5H_2 + 3\,OH^{-} \text{ (Cathode)} \quad (1.4)$$

In addition, Al^{3+} and OH^{-} ions generated at electrode surfaces react in the bulk wastewater to form aluminum hydroxide.

$$Al^{3+} + 3OH^{-} \rightleftharpoons Al(OH)_3 \quad (1.5)$$

If the anode potential is sufficiently high, secondary reactions may occur at the anode, such as direct oxidation of organic compounds and of H_2O or Cl^{-} present in wastewater (Eq. 1.6 to 1.7).

$$2Cl^{-} \rightleftharpoons Cl_2 + 2e^{-} \quad (1.6)$$

$$2H_2O \rightleftharpoons O_2 + 4H^+ + 4e^- \quad (1.7)$$

Aluminium hydroxide flocs act as a trap for heavy metals and settles along with heavy metals thereby removing it from wastewater. A similar mechanism is applicable with the iron anode.

1.8.3 Biosorption

The term biosorption, signifies passive sorption and complexation of metal ions by dead biomass e.g. fungus, algae, spirogyras, bacteria, yeast, peat moss, etc. The mechanisms of biosorption involve electrostatic attractions, ion exchange, and metal ion chelation or complexation between metal ions and the surface functional groups [96]. Different materials are being used as bio-sorbents such as fungus, algae, spirogyras, bacteria, bio-sludge, peat moss, yeast, waste materials of industries and agriculture [97-100].

The removal of Cu(II) by green alga *Spirogyra* showed maximum biosorption capacity of 133.3 mg/g (pH 5) at a dose of 20 g/L. The desorption showed 95% efficiency using HCl in 15 min [101]. In a study of Pb(II) biosorption by green algae, the maximum adsorption capacity was 140 mg/g from an initial 200 mg/L concentration at pH 5 [102]. Another study revealed that Pb(II) and Cd(II) were removed by chemisorption onto green alga (*Ulva lactuca*) biomass with a maximum capacity of 34.7 and 29.2 mg/g, respectively. The thermodynamic calculations showed that biosorption of Pb (II) and Cd (II) was feasible, spontaneous, and exothermic in nature [103]. However, the biosorption suffers from disadvantages such as early saturation, necessity of desorption for repetitive use, and it cannot change valency state of metal [104].

1.8.4 Adsorption

Adsorption can be defined as the accumulation of substances at the interface between two phases [105]. For wastewater treatment, it is polishing a technique and is a mass transfer process by which a substance is transferred from the liquid phase to the surface of a solid, and becomes bound by physical and/or chemical interactions [85, 86]. Being a polishing technology, it is not been adopted in wastewater treatment, however, the demands for better quality of effluent, including toxicity reduction, has led use of adsorption for wastewater treatment [106].

Adsorption have gained high popularity and shown reliability for heavy metallic wastewater treatment. The flexibility in design and operation and ability to produce high-quality treated effluent are major advantages of adsorption. In addition, exhausted adsorbents can be regenerated by a suitable desorption process [87]. The adsorption could be physical or chemical, earlier involve binding through Van der Waals forces and later through chemical interactions [107]. The steps involved in adsorption are transport of the adsorbate from bulk solution to adsorbent, mass transfer by pore diffusion and adsorption of adsorbate on the active sites of the pores of adsorbent. AC is the most common adsorbent in water and wastewater treatment due to its high surface area to volume ratio. The efficacy of commercial AC is well documented [108, 109]. Being a tertiary treatment, cost associated with AC adsorption is very high, which led researchers to find low cost adsorbent. Natural biomaterial or certain industrial wastes can be potential precursor in synthesis of low cost adsorbents. Such precursor are locally abundant, hence are inexpensive or possess little economic value [110]. Natural materials such as chitosan, zeolite, clay, red mud or certain waste from industrial operations such as fly ash, coal, and oxides are few commonly used low-cost adsorbents. The advantages and disadvantages of various treatment technologies are tabulated in Table 1.6.

Table 1.6: Advantages and disadvantages of heavy metal removal technologies **[111].**

Treatment	Advantages	Disadvantages
Chemical precipitation	Process simplicity, inexpensive capital cost	Not suitable for mixed metals, large amount of metallic sludge generation of high sludge disposal cost, high maintenance costs
Ion exchange	Withstand shock loading, metal selective, limited pH tolerance, high regeneration	Fouling of bed by organic components, plugging of resin bed by suspended solids, resins requires regeneration or disposal, high initial capital cost, high maintenance costs
Electro-chemical treatment	Rapid process and effective for certain metal ions, can treat effluent > 2000 mg/L, metal recovery possible, less operational cost	High capital costs, low solubility of target pollutants, production of H_2 (in some processes), formation of by-products
Adsorption	Wide variety of target pollutants, high capacity, fast kinetics, possibly selective depending on adsorbent	Performance depends on type of adsorbent, require chemical regeneration to improve its sorption capacity
Coagulation and flocculation	Bacterial inactivation capability, good sludge settling and dewatering characteristics	High chemical consumption, high sludge volume generation

1.9 Heavy metal removal by commercial adsorbents

The commercially available adsorbents for wastewater treatment include activated carbon (AC), silica gel, activated alumina, nanomaterials, and ion exchange resins. The term 'commercial adsorbent' refers to those adsorbents, which are currently produced on a large scale by various industries. The commercial adsorbents usually possess a high specific surface area and remove heavy metals by physical adsorption. AC is highly porous, amorphous solid consisting of micro crystallites with a graphite lattice, available in the form of granules or powder [112]. Activated alumina is a porous granular form of aluminum oxide possessing a larger surface area. It can remove heavy metals from aqueous solutions by physical adsorption especially at low pH and metal concentration. Silica gel is characterized by porous texture with corpuscular structure (three dimensional particle connectivity) and hence used for heavy metal adsorption in virgin or modified form. The modification for introduction of various functional groups is common for removal of specific target pollutant. Nanomaterials also possess high specific surface area, are selective in metal removal, and have high activities due to size quantization effect. Nanomaterials are becoming popular as they can be impregnated into porous adsorbents to synthesize porous and selective composites [113]. The most popular among all commercial adsorbents is AC and is widely used for contaminants (organic and inorganic) removal from industrial and municipal wastewater. The commercial production of AC began in 1900–1901 replacing bone char in the sugar refining industry [114]. Wood or any biomaterial with high carbon content can be used for the production of AC. However, wood-based AC turned out to be expensive as wood being a limited resource. Hence, the research is encouraged to explore utilization of various biomaterials such as apricot stone, hazelnut shell, [28, 115, 116], tamarind wood [117], walnut shells [118], coir pith [119, 120], almond husk [121], beet pulp [122], palm shell [123], and coconut tree sawdust [124] for AC production. A few significant reports on production of AC from biomaterials are discussed below. A coir pith AC showed maximum removal efficiency of 73% for Cu(II), 100% for Hg(II), Pb(II), Cd(II), and 92% for Ni(II) at pH 5.0 for Cu(II), 4.0 for Pb(II), 3.5 for Ni(II) and Hg(II), and 4.0 for Cd(II). Authors reported that adsorption was favoured in pH range 4–5 as a result of partial hydrolysis of metals, whereas it was less in acidic pH due to competitive adsorption [125]. Almond husk AC was synthesized using H_2SO_4 and carbon dioxide activation at elevated temperatures (300–1000°C) under inert an atmosphere. The highest (97%) removal efficiency was achieved at 700°C in Ni(II) removal from an initial

concentration of 25 mg/L and adsorbent dose of 5 g/l [121]. An AC was prepared from apricot stone treating with H_2SO_4 (1:1 by weight) followed by oven heating at 200°C for 24 h. It showed a high surface area (566 m^2/g) and, the maximum adsorption capacity was obtained at pH 1–2 for Cr(VI) and in the pH range of 3–6 for Cd(II), Co(II), Ni(II), Cu(II), and Pb(II). The order of adsorption capacity for metals was found to be Cr(VI) > Cd(II) > Co(II) > Cr(III) > Ni(II) > Cu(II) > Pb(II) [115]. In another study, tamarind wood AC prepared by sulphuric acid activation showed 98% Pb(II) removal from an initial concentration of 40 mg/L, adsorbent dose of 3 g/L, and pH of 6.5. The Langmuir adsorption capacity of 134.22 mg/g was obtained which was comparable to the commercially AC [117]. A palm oil sludge bio-char was used for AC production through KOH treatment that showed a surface area of 87 m^2/g [123].

The laboratory studies of AC synthesis are successful and are plenty, but its scaling up to a commercial scale is not seen very often. Despite of all above materials for AC production, coal since beginning and now a day's coconut shell remains most popular choices as raw material for AC production. An alternative techniques such crosslinking, grafting and/or functionalization of biomaterial to convert biomaterials into adsorbents and/or resin for heavy metal remediation is explored by many researchers.

1.10 Heavy metal removal by functionalized absorbents

The term 'functionalized adsorbents' refers to the adsorbents induced with functional groups possessing affinity for heavy metals. These functional groups include carboxylic, amine, sulfonic, hydroxide, carbonyl, and ester. Among them, carboxylic, amine, and sulfonic groups have the highest affinity to many heavy metals [126]. Biomaterials such as rice husk, areca nut, wheat straw, tree bark, sugarcane bagasse, coconut waste, coir pith, fruit peels, and sawdust, etc. are examples of various lignicellulosic materials. The percentage of lignin, cellulose, hemicellulose, and other constituents of each biomaterial may vary but it has a same bio-origin [127]. The lignicellulosic materials usually carry a lone pair of electron on functional groups such as alcohols, aldehydes, ketones, carboxylic, phenolic, and ether groups. [128]. However, the functional groups are tightly packed within the lignocellulosic mass and are inaccessible in ordinary conditions. Various physicochemical pre-treatments such as ethanol process, boiling, heating, electrochemical, microwave radiation, acid or alkali exposure are practiced to loosen the lignicellulosic packing to make them accessible (Fig. 1.6) [129].

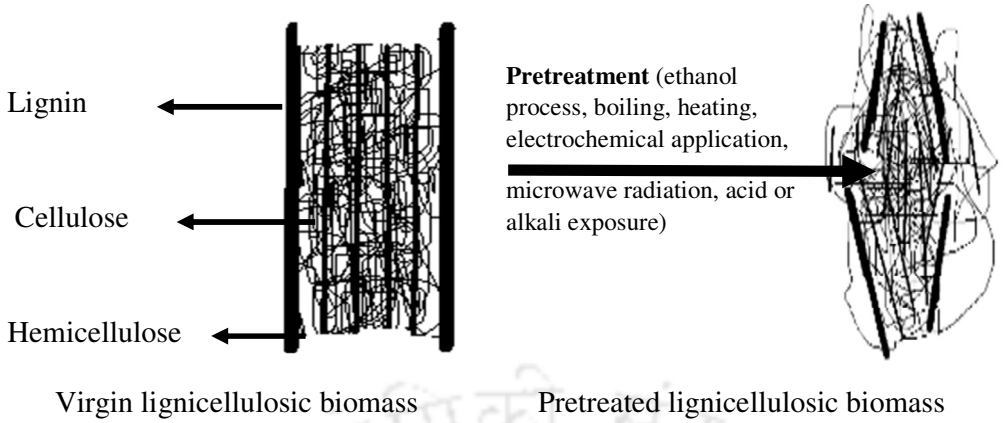

Figure 1.6: Effect of pre-treatment on lignicellulosic packing of biomass [130].

Once the functional groups are exposed, the same material with or without further treatment can be utilized for desired purposes such as biofuel production, heavy metal removal, and fibre softening [130]. The chemical agents such as acids, alkalis, cyclic anhydrides such as succinic, phthalic, EDTA, and maleic can be used to induce one or more functional groups on the pre-treated biomaterial. Once the biomaterials are functionalized, the remaining unreacted chemical agent is washed with appropriate reagent and finally with Milli-Q water. The induction of such groups empowers the functionalized adsorbents to be used for heavy metal remediation.

1.10.1 Functionalization by acid-base treatment

Various acids such as sulphuric, orthophospheric, hydrochloric, nitric, etc. can be used for functionalization of biomaterial. The reaction of acid/base with biomaterial induces functional groups having affinity towards metal. A study reported on sugar beet pulp functionalized with two parts of concentrated sulphuric at 150°C for 6 h. The Langmuir capacity of 24 mg/g was obtained for Cr(VI) removal at 25°C [122]. Treatment of orange peel with 0.1 M HNO_3 resulted in induction of the carboxylic group, that removed 90% of Cd(II), Cu(II), and Pb(II) in 30 min [131]. Similarly, grinded peanut husk (0.5–0.8 mm) functionalized with 0.1 N HCl removed Zn(II) at pH 6 in 2 h and reported to be half the price of the cheapest commercial AC [132]. In another study, treatment of corncob with citric and nitric acids (1 M solution) induced carboxylic groups that increased adsorption capacity for Cd(II) by 10.8 and 3.8 folds, respectively. The mechanism of Cd(II) removal was stated to be ion exchange primarily [133]. A similar study in modification of oak

sawdust by HCl treatment showed maximum removal efficiencies of 93% for Cu(II) at pH 4, 82% for Ni(II) at pH 8, and 84% for Cr(VI) at pH 3. The treatment of oak sawdust with HCl prevented elution of tannin compounds that would stain the treated water, and greatly improved the proportion of active surfaces responsible for metal removal [134].

The poplar sawdust (*Samsun Clone*) treatment with 1 N H_2SO_4 (sawdust/H_2SO_4: 1:2 w/v) followed by heating at 150°C for 24 h resulted in an increased adsorption capacity of sawdust by 2.5 times, to 13.5 mg/g for Cu(II). The maximum removal efficiency of raw and functionalized sawdust was 47.05% and 92.4% at pH 4 and 5, respectively [135]. Kinetic studies of adsorption of Pb(II), Cr(III) and Cu(II) were carried out by sawdust and peanut husk modified with H_2SO_4. The formalin pre-treatment was implicated to reduce organic pigment from peanut husk. The study reported the presence of carboxylic groups on raw peanut husk [136]. Removal of Cr(VI) using Bael fruit (*Aegle marmelos correa*) shells functionalized with phosphoric acid (1:1 w/w) contained amino, and hydroxyl groups which were responsible for removal of Cr(VI). The highest Cr(VI) removal was achieved at pH 2 due to chemisorption and, the capacity of functionalized adsorbent was 17.27 mg/g [137].

Despite of the success of acid-alkali treatment for functionalizing a biomaterial, at many instances the biomaterial do not possess mechanical strength, contains water-soluble compounds, and has higher swelling/shrinkage behaviour. In such cases, the acid alkali treatment cannot be applied to biomaterial. The grafting of the bio-materials with acrylamide (graft polymerization) may improve mechanical resistance and leaching properties of the biomaterial. Therefore, in addition to the acid-base functionalization, graft polymerization using various cyclic anhydrides has gained popularity for functionalization of biomaterials.

1.10.2 Functionalization by graft polymerization

Various chemicals such as epichlorohydrin, hydroxyethylmethanacrylate (HEMA), methylenebisacrylamide (MBA), succinic anhydride, ethylenediamne, ceric ammonium nitrate, dimethyl formamide, EDTA dianhydride (EDTAD), etc. are used for induction of carboxylic functional groups through graft polymerization. Graft polymerization is gaining popularity because it confers mechanical strength, leaching resistance, and decreases swelling/shrinkage behaviour of biomaterials [138]. In 1980, removal of arsenate by hydrous Fe(III) grafted with polyacrylamide was studied using ammonium peroxydisulphate as a polymerization initiator. The study showed that the arsenate could be

removed in pH range 5–8 with an adsorption capacity of 43 mg/g. [139]. Fanta et al. (1987) and co-workers [140] grafted acrylonitrile onto grounded, water-washed wheat straw using Fe(II)/H_2O_2 as an initiator in dimethylformamide (DMF) media. The final product contained 30–35% acrylonitrile. The study reported that hemicellulose was the major contributor for successful grafting [140]. In contrast, a similar study was carried out for graft polymerization of methyl methacrylate on stone ground wood using Fe(II)/H_2O_2 system. The authors reported that the lignin was the major reason for polymer grafting and hydroxyl groups in lignin accelerated graft co polymerization in the presence of ferrous ions [141]. In another approach, EDTA dianhydride was mounted onto soy protein isolate by glutaraldehyde grafting. This study showed that incorporation of ionizable carboxyl groups into soy proteins increased the net negative charge on the surface [142]. For the first time, the polyacrylamide grafting was experimented with biomaterial i.e. sawdust using potassium peroxidisulphate as a polymerization initiator. The carboxylated sawdust showed > 90% removal efficiency for Pb(II), Hg(II), and Cd(II), which was afterwards regenerated using 0.5 N HCl. The carboxylated sawdust was used for 3 cycles and the reduction in removal efficiency was <15% [143]. In another study, polyacrylamide was grafted on hydrous titanium oxide using Fe(II)/H_2O_2 system. The product was then treated with ethylenediamine in tolune to introduce spacer groups. In order to functionalize with carboxylate groups, succinic anhydride was used in 1, 4 dioxane at pH 4 for 6 h. The removal efficiencies of Pb(II), Hg(II), and Cd(II) were found to be 2.3, 2.8, and 2.9 times higher for carboxylated adsorbent than the virgin [144]. Similarly, grafting of acrylamide onto sawdust using potassium peroxydisulphate as an initiator resulted in maximum adsorption of 91% at 30°C from an initial concentration of 100 mg/L Cr(VI) at pH 3 [145]. A study carried out successful functionalization of oil palm trunk, fibre lignin, poplar lignin, maize stem lignin, barley, wheat, and rice straw lignin by esterification with succinic anhydride in aqueous solutions. The study reported improved thermal resistance of the modified fibres when compared to the unmodified ones [9]. The sugarcane bagasse was inducted carboxylic groups using succinic anhydride, that used to anchor amine groups via the formation of amide functions [146].

In a study, a chelating material was synthesized from mercerized (NaOH treated) cellulose through conversion of cellulose I into cellulose II. On succinic anhydride grafting of both material, the mercerized cellulose showed a higher degree of succelylation and carboxylic group concentration. The materials were further treated with bicarbonate solution to release the carboxylate functions. The adsorption capacity of the final

functionalized adsorbent was found to be 30.4, 86, and 205 mg/g for Cu(II), Cd(II), and Pb(II), respectively [147]. In a similar study, sugarcane bagasse was functionalized using succinic anhydride after double mercerization. The study showed that the mercerization decreased crystallinity index and increased the separation of the cellulose chains. These modifications helped for impregnation of succinic anhydride and resulted in a higher concentration of carboxylic groups on the surface [148].

In another approach, EDTAD was used for modification of the baker's yeast using glutaraldehyde as a crosslinking agent. The EDTAD functionalized adsorbent showed maximum adsorption capacity of 92.3 and 65 mg/g for Pb(II) and Cu(II) by metal complexation [149]. In another study, EDTAD functionalized sugarcane bagasse was successfully applied for the removal of malachite green with an adsorption capacity of 157.2 mg/g [150]. Similar functionalization of cellulose and sugarcane bagasse is also reported in literature [147]. The functionalization of wood sawdust and sugarcane bagasse using EDTAD showed Zn(II) adsorption capacities of 80 and 105 mg/g for functionalized sawdust and bagasse from synthetic wastewater. It was also used for the removal of Zn(II) from electroplating wastewater with capacities of 47 and 45 mg/g, respectively [151]. A new polystyrene supported EDTAD resin showed a great affinity for the adsorption of heavy metals in the order of Cu(II) > Zn(II) > Ni(II) > Pb(II) [152].

1.11 Treatment and utilization of heavy metallic sludge

The 'sludge' is a residual, semi-solid material and is concentrated with heavy metals as the result of chemical precipitation. Sludge management is considered as a major challenge for water pollution due to their immediate offensive nature and pollution potential. Treatment and management of heavy metalic sludge is a thrust area of research. A dedicated research is needed for the disposal/management of sludge to encourage the recycling and reuse possibilities. The unfriendly disposal methods such as dumping on grounds or in sea are not legal. The possibilities of valorization and recovery of value added products from sludge have been explored recently [4, 153, 154] as a result of stringent environmental laws, regulatory interventions, and public pressures. The reuse and recycle of sludge are advisable against incineration or landfilling to control emissions of flue gases and possible metal leaching [38]. However, the process of recycling and/or reusing is not possible always due to higher heavy metallic loading. Hence, efforts are made to decontaminate heavy metallic sludge through various treatments such as electrokinetic

migration techniques [153, 155], chemical leaching [38, 156], and bioleaching [157]. Reuse or recycle of sludge include its use as a construction material [158, 159], bricking material or partial replacement of clay in fired clay bricks [160, 161]. Though there are various options for sludge management, choosing a technology is solely dependent upon the characteristics of the sludge and its intended use.

1.11.1 Electrokinetic migration/recovery of heavy metals in sludge

Heavy metals can be removed by applying a significantly high potential difference across sludge through electrokinetic migration. The contaminant transport occurs due to various coupled mechanisms such as electromigration, electroosmosis, and electrophoresis, which take place together with the electrolysis of water at electrodes [162, 163].

Electrokinetic migration of Ni(II) through synthetically prepared sludge was studied. The study showed the feasibility of elecrokinetic migration of heavy metals with the highest Ni(II) concentration near anode (462 mg/kg) and the lowest concentration (64 mg/kg) near cathode [164]. Migration of Cu(II) and Fe(II) from anaerobic granular sludge in an open and a closed cell was studied. The authors reported that conditioning of cathode with acid could enhance heavy metal migration through sludge [165]. A study reported that the addition of chelating agents such as EDTA forms negatively charged compounds with heavy metals in neutral or acidic pH and accelerate heavy metal migration [165, 166]. Another study reported that acidification of sludge increased mobility of metals and followed the order as Ni > Zn > Cu > As > Cr > Pb [167]. Similar results for sewage sludge are also reported in literature [162].

1.11.2 Sludge in brick production

Brick is one of the oldest construction materials known to humans. Presently bricks are of two types' viz. conventional bricks that are prepared with clay followed by kiln firing and cemented bricks using ordinary Portland cement (OPC) concrete or other appropriate binder. The production of fired as well as cemented bricks leaves a large carbon footprints through the emission of gases and other wastes generated in manufacturing [168]. Hence, the developed countries have already started using of sludge for production of bricks in order to conserve limited resources. However, the developing countries are exploring the possible utilization of wastes in bricks production [169]. Sludge from various industries can be utilized for bricking through conventional firing or cementing.

1.11.2.1 Production of cemented bricks

The production of cemented bricks includes manufacturing in different shapes such as cubes, bricks, circular castings, and paver blocks. The usage of the cemented sludge brick depends upon the properties of sludge. The industrial sludge is formed by precipitation of heavy metals as result of lime addition to wastewater. Hence, sludge contains, metal hydroxides, gypsum, basanite, and various minerals. Cementing of bricks involves raw materials such as OPC, Pozzolana Portland cement (PPC), fly ash, silica sand, and sludge. The raw materials show very limited individual cementing property; however, their blends at particular proportions form cementitious substances at ambient temperatures having a low solubility. The contaminant present in sludge is contained in the cementitious matrix by the physical as well as chemical entrapment. Waste materials from industries such as fly ash [170] and blast furnace slag [171] are used as binder to for contaminant of containment in cemented bricks. The use of OPC as a binder in cemented bricks accelerates metal fixation of sludge that also depends on the chemistry of the mix.

The hydration of cement follow a series of chemical reactions involving dissolution of phases, precipitation of low solubility substances such as calcium silicate hydrate gel (C–S–H), portlandite and other reaction products, and formation of equilibrium of hydration products. The hydration reaction series is self-limiting and controlled by the permeability of the coating layer covering cement particles [172]. The presence of external agents or admixtures may alter the colloidal properties i.e. permeability resulting in retardation or acceleration of hydration reaction rates. The typical reactions involved in the hydration of cement and strength development are presented here (Eq. 1.8 to 1.11). The addition of water to dry mix of raw materials results in hydration of aluminate first. The aluminate hydrates confer initial rigidity to the mix through initial setting and evolves a moderate amount of heat (Eq. 1.8). Gypsum present in the cement disallows quick setting of the mix and reacts with aluminate to form ettringite (Eq. 1.9). Thus, the ettringite particles surrounds cement particles that retard quick setting of the cement. The calcium silicates i.e. alite and belite are the binding elements in the cemented bricks that react with water to form C–S–H. The earlier is responsible for the first 28 days strength development (Eq. 1.10); whereas, the later develops major strength over a period of 1 year and continues further (Eq. 1.11).

$$3CaO.Al_2O_3 + 12H_2O + Ca(OH)_2 \rightarrow 3CaO.Al_2O_3.Ca(OH)_2 + 12H_2O \quad (1.8)$$

Aluminate Tricalcium aluminate hydrate

$$3CaO.Al_2O_3 + 12H_2O + 3CaSO_4.2H_2O \rightarrow 3CaO.Al_2O_3 \rightarrow 3CaO.Al_2O_3.3CaSO_4.14H_2O \quad (1.9)$$
Aluminate Ettringite

$$2(3CaO.SiO_2) + 6H_2O \rightarrow 3CaO.2SiO_2.3H_2O + 3Ca(OH)_2 \quad (1.10)$$
Alite Calcium silicate hydrate (C–S–H) gel

$$2CaO.SiO_2 + 4H_2O \rightarrow 3CaO.2SiO_2.3H_2O + 3Ca(OH)_2 \quad (1.11)$$
Belite Calcium silicate hydrate (C–S–H) gel

Addition of wastes affects the hydration reaction and strength development of mix in solidification/stabilisation process. Addition of metal contaminated sludge accelerates the hydration of tricalcium silicate (C_3S) and Portland cement, whereas they tend to retard precipitation of portlandite due to low pH of the mix [173]. H^+ ions generated attack on cement phases and forms calcium metal hydroxides and promoting the decomposition of C_3S [174]. Heavy metallic sludge from various industries is been utilized for cemented brick production and the studies from literatures are summarized in Table 1.7.

Table 1.7: Studies carried out on cemented brick production utilizing industrial waste.

Sl. no.	Waste utilized (% w/w)	Brick size (mm)	Curing condition	Characterizations/Tests undertaken	Reference
1	Blast furnace slag (5–35%)	190×90×90	Cured in humid (95%) atmosphere at 270–272°C for 28 days	Compressive strength, bulk density, water absorption	[175]
2	Class F fly ash (60–90%)	220×110×75	Cured in water filled curing tanks at 23.2°C	Compressive strength, water absorption, density, durability	[176]
3	Plastic fiber, straw, polystyrene fabric (1, 20, 5%)	150×150×150	Wet gunny bags curing for 7 days	Water absorption, compressive strength	[177]
4	Class F fly ash (50–80%)	45 ϕ	Steam curing and autoclaving at pressure 0.5–2 MPa for 3–12 h	Compressive strength, water absorption, unit weight, thermal conductivity	[178]
5	Limestone and sawdust (15%)	105×90×75	Water curing for 28 days	Compressive strength, water absorption, flexural strength, test	[179]
6	Cotton waste –lime powder waste, 10% by volume	105×90×75	Lime saturated water curing at 22°C for 28 days	Water absorption, compressive strength, flexural strength, ultrasonic pulse velocity (UPV) test	[180]
7	Crumb rubber waste (10%)	105×100 ×75	Water curing for 28 days	Compressive strength, water absorption, flexural strength, UPV test, splitting strength test	[181]
8	Low-silicon tailings (83%)	240×115×53	Sealed in plastic bag for 6 h, and then autoclaved	Compressive and bending strengths, freeze–thaw resistance, dry shrinkage	[182]
9	Dyestuff industry sludge (33–50%)	40×40×160	Cured in humid atmosphere (100%) for 24 h, and then cured in water at 20°C for 28 days	Compressive strength, freeze–thaw resistance, leaching	[183]

Sl. no.	Waste utilized (% w/w)	Brick size (mm)	Curing condition	Characterizations/Tests undertaken	Reference
10	Recycle paper mill waste (80–95%)	230×105×80	Solar dried	Compressive strength, water absorption, specific weight, moisture content	[184]
11	Hematite tailings (70%)	50×23 (cylindrical)	Steam and autoclave curing	Compressive strength, flexural strength, freeze–thaw resistance	[185]
12	Waste phosphogypsum (75%)	240×115×53	Wet cured for 1 day, dried at 180°C for 2 h, immersed in water for 1 h, and naturally cured	Compressive strength, bending strength, water absorption, freeze–thaw resistance	[186]
13	Coal combustion residues (70 and 90% by vol.)	140×140×90	Cured with water spraying and covered with plastic sheet	Compressive strength, unit weight	[187]
14	Fly ash, quarry dust, and billet scale (85% and 90%)	200×90×60	Wet jute fabric covering overnight, and then in humid atmosphere (95%)	Compressive strength, water absorption, modulus of rupture, UPV, efflorescence, durability	[188]

1.11.2.2 Production of fired bricks

Brick is one of the oldest, and the principal building material since 3000 BC [169]. The global annual production of fired bricks is about 1391 billion units and it is obvious that it will grow in the near future [168]. India is the second largest producer of fired clay bricks, holding a share of >10% of the global production. In India, there are more than 100,000 registered brick kilns those produce about 150-200 billion bricks annually. The bricks today are utilized for various purposes such as partition walls, thermal insulation, and decoration purpose. The oldest process of brick manufacturing is the firing of clay [169]. In production of fired bricks, the clay is mixed with water in sufficient quantity (20 to 40%) and, the bricks are casted in moulds. The raw bricks are sundried and fired at higher temperatures (900 to 1000°C) [189]. A typical process flow diagram for clay brick production is shown in Fig. 1.7. During the firing of bricks, a mixture i.e. clay minerals, silt, and sand is transformed by heat to form new minerals those are hard, non or less water absorbing, porous, and thermally insulated [190]. The production of fired clay bricks causes depletion of highly fertile clay, thus an extensive research is emerged to search for alternatives or substitutions for clay [189]. The utilization of sludge in fired brick manufacturing has added benefits from saving fertile clay such as metal fixation, value addition to sludge, manufacturing of thermal resistant bricks, and colored bricks. The specific characteristics of brick can be achieved through the addition of various industrial wastes.

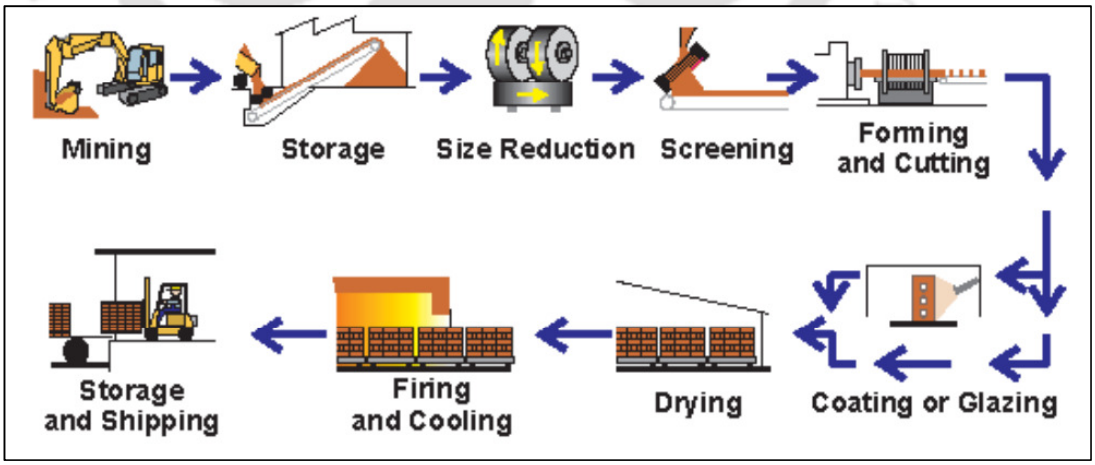

Figure 1.7: Diagrammatic representation of brick manufacturing processes (Brick Industry Association TN9, 2006).

Researchers have utilized waste products from industries for the purpose that include mine tailings [185], fly ash [170], blast furnace slag [171], [191], processed waste tea [192], textile laundry sludge [193], gypsum sludge and Pb/Zn smelting slag [159], degraded municipal solid waste [194], arsenic–iron sludge [195], and calamine processing wastes [196], etc. A few of the studies are discussed here and are summarized in Table 1.8. It can be observed from Table 1.8 that various industrial wastes are utilized for manufacturing of fired bricks. Waste was added as a partial replacement of clay and other processes were same as in Fig. 1.7. Xu et al. (2014) [197] explored the utilization of urban river sediments for production of insulation brick. The pore forming property of the waste was tested adding 50% to 70% waste by mass at different firing temperature of 1000, 1050, and 1100°C. The study showed that the thermal conductivity decreased by 40% on addition of the urban river sediment. The compressive strength was reduced with the increase in waste percentage; however, acceptable properties of brick were achieved with the addition of 50% urban river sediments fired at 1050°C. Taha et.al., (2016) [196] suggested an alternative technique for conservation of fertile clay and reduction in both brick production cost as well as industrial waste volume. Treated calamine processing wastes was added (up to 40%) to clay and fired at various temperatures of 900, 950, 1000, and 1050°C. A similar trend of increased compressive strength, contaminant immobilization, and reduced water absorption was achieved at a higher firing temperature. The flexural strength was increased from 0.6 (900°C) to 7.1 MPa (1050°C) in bricks containing up to 30% of waste. The produced bricks were tested for a number of tests such as compressive strength, water absorption, density, porosity, thermal conductivity, and metal leaching. The most important parameters for fired clay brick are compressive strength and water absorption. The parameters such as porosity and density are interdependent and inversely proportional to each other. An increase in porosity make the brick lighter but at the same time it increases the water absorption and decreases compressive strength [198]. The firing temperature plays a crucial role in strength building in fired clay bricks. Higher temperatures usually result in a higher compressive strength. At higher temperatures, the clay minerals melt to form new glassy minerals those possess high compressive strength and low water absorption. The acceptable compressive strength and water absorption values as per ASTM and Indian standard are given in Table 1.9.

Table 1.8: Details of studies on fired brick production utilizing industrial waste.

Sl. No.	Waste used (% w/w)	Size of brick (mm)	Firing conditions	Tests undertaken	Reference
1	Paper processing residues, (10%)	85×85×10	Fired at 2.5°C/min until 600°C, and then at 10 C/min until 1100°C, for 1 h	Bulk density, apparent porosity, water absorption, compressive strength and thermal conductivity	[199]
2	ETP sludge, (10 %)	230×110×60	Fired in a combustion chamber at 880–1000°C	Water absorption, compressive strength, and leachate test	[200]
3	Waste tea, (5%)	40×70×100	Fired at the rate of 2°C/min until 600°C and then 5°C/min until 900°C for 2 h	Density, water absorption, and compressive strength	[192]
4	Petroleum sludge, (46%)	280×130×170	Fired at 1000°C	Water absorption, compressive strength, and efflorescence	[201]
5	Welding flux slag, (5%)	115×254 (cylindrical)	Fired in a furnace at 950°C for 2 h	Density, water absorption, and flexural strength	[202]
6	Urban river sediments (50–70%)	70×70×70	Fired at 1000, 1050, and 1100°C in muffle furnace	Loss on ignition (LOI), linear shrinkage, bulk density, water absorption, compressive strength, microscopy, and thermal conductivity	[197]
7	Treated calamine processing wastes, (0–50%)	Rectangular 100×20×12 and cylindrical blocks 5.4 Ø and 38 high	Fired at various temperatures: 900, 950, 1000 and 1050°C	Water absorption, firing shrinkage, pore distribution, flexural strength, metal leaching, and efflorescence	[196]
8	Arsenic–iron sludge, (3–12%)	250×125×75	Fired at 500°C for 12 h and then 1000°C for another 12 h	Moisture content, specific gravity, metal leaching, water absorption capacity, and compressive strength	[195]

Sl. No.	Waste used (% w/w)	Size of brick (mm)	Firing conditions	Tests undertaken	Reference
9	Degraded municipal solid waste, (5–20%)	61×29×19	Fired at 850 and 900°C in muffle furnace	Bulk density, linear shrinkage, LOI, water absorption, compressive strength, and modulus of elasticity	[194]
10	Textile laundry sludge, (5–20%)	73×35×55	Fired 100 to 900°C in 3 days with increases at each 24 h	Compressive strength, water absorption	[193]
11	Hot-dip galvanizing sludge, (3–6%)	Tiles 120×50×14, hollow blocks 55.3×36×36, and cubes 30×30×30	Fired at 870, 920, 970, and 1020°C for 2 h: heating rate of 1.4 C/min up to 610 and later 2.5°C/min	compressive strength, Water absorption, porous structure, and heavy metal leaching	[203]
12	Steel Mill Sludge, (0–15%)	NA	NA	Shrinkage, density, initial rate of suction and compressive strength	[160]
13	Paper mill sludge, (0–20%)	61×29×19	Firing at 900°C in muffle furnace	Linear shrinkage, compressive strength, water absorption, LOI, and bulk density	[191]
14	Waste steel slag, (5–30%)	50×50×50	30–500°C in 3 h for 2 h and later designated temperature 800–1100°C in 6 h	Water absorption, LOI, firing shrinkage, and compressive strength	[204]

Table 1.9: Specifications and classification of bricks as per ASTM and Indian Standard (IS 1077:1992) [205].

Standard	**Brick**	**Minimum compressive strength, N/mm^2**		**Maximum water absorption, % (24 h cold water immersion)**	
Type	**designation**	**Average of 5**	**Individual**	**Average of 5**	**Individual**
ASTM	Grade SW	20.7	17.2	17	20
	Grade MW	17.2	15.2	22	25
	Grade NW	10.3	8.6	No limit	No limit
Indian Standard	35	NA	35	NA	Water absorption shall not be more than 20% by weight up to class 12.5 and 15% by weight for higher classes.
	30	NA	30	NA	
	25	NA	25	NA	
	20	NA	20	NA	
	17.5	NA	17.5	NA	
	15	NA	15	NA	
	12.5	NA	12.5	NA	
	10	NA	10	NA	
	7.5	NA	7.5	NA	
	5	NA	5	NA	
	3.5	3.5	3.5		

1.12 Lacunae in literature and research objectives

Various methods practiced for heavy metal removal from wastewater are adsorption, ion exchange, precipitation, and treatment by natural habitat such as biological treatment. Adsorption is considered as one of the best process that is generally used as a polishing unit to reduce heavy metal concentration not only to meet discharge standards but also to meet surface water quality for various purposes. Although, there are several reports on preparation of adsorbents using a wide variety of raw materials, most of those have been tested on pollutant removal only from synthetically prepared wastewater. LAB industry is not only one of the most growing industries in India but also most polluting one. The present practice of LAB wastewater treatment involves addition of lime to raise pH of the wastewater achieving precipitation of lead and other metals, and subsequent formation heavy metals laden lime sludge. Although such sludge appears to hold the heavy metals strong enough preventing its leaching, regular monitoring of sludge stability against leaching are not carried out by the industry. Based on thorough literature review, the following scopes for future research in this area have been identified:

1) Preparation of new low cost adsorbents from locally available lignocellulosic biomaterial for heavy metal removal from synthetic as well as LAB wastewater. Arecanut husk, which is abundant in the state of Assam, India, contain about 44% cellulose, 28% hemicellulose and 11% lignin. However, its use is limited as a biofuel feedstock due to its high ash content and lower susceptibility to enzymatic digestion. Hence, the locally abundant biomaterial i.e. arecanut husk is a potential biomass source for the development of new, cost effective, and re-generable functionalized adsorbent and bio-resin for LABW treatment. The cheaply available arecanut husk as an adsorbent for wastewater treatment remained unexplored and, the reports on other uses such as thick board, plastics, and wrapping paper manufacturing are also fewer [206, 207].
2) Characterization of LABS produced by lime addition to LABW, assessment of its toxicity and stability against leaching of precipitated metals. This will help assessing the suitability of the current practice of lime treatment of LABW and the hazardous nature of the sludge produced. In addition to this, it will help in deciding practicability of heavy metal recovery from lime sludge.
3) Management of already produced heavy metal laden LAB sludge and its valorization as a construction material.

Thus, based on the above literature review and identified research gaps, following objectives of the dissertation are designed.

- **Heavy metals (especially Pb) removal from LABW using functionalized adsorbent and bio-resin**
  - Synthesis of functionalized sorbents from arecanut husk and determination of its physiochemical attributes
  - Studies on potential of functionalized sorbents for heavy metal removal from synthetic as well as LABW and comparison with commercial activated carbon and ion exchange resins
  - Development of a simple proton adsorption model for the determination of metal binding constants and mechanistic investigations
  - Investigations on regeneration of exhausted adsorbent/resin and finding out a suitable eluent for recyclability

- **Toxicity assessment and valorization potential of heavy metallic sludge**
  - Characterizations, toxicity and risk assessment, speciation, and valorization of LABS by progressive acidification
  - Pertinence of heavy metallic sludge for the production of fired clay bricks and effective heavy metal fixation
  - Testing of manufactured fired clay bricks for its suitability as construction material through compressive strength, water absorption capacity, and toxicity characteristics leaching procedure

1.13 Thesis organization

The whole thesis is organized in six chapters. The current **Chapter 1** is framed to present a general overview of the present work including knowledge on industrial heavy metal pollution and toxicity with a special reference to the battery manufacturing industry. It describes manufacturing process and possible waste generations in battery industry. In addition to this, an extensive literature survey is presented to describe the state-of-art literature on the treatment of battery industrial wastes. The summary of literature at the end uncurtains the lacunas in literature to frame the objectives of this work. **Chapter 2** presents the materials used and methodologies followed in this project. **Chapter 3** investigates on synthesis, characterization, and application of functionalized fibrous adsorbent (FFA) using arecanut husk, for heavy metal removal from synthetic as well as LABW. Performance of FFA in metal removal is compared with the commercial cation exchange resins and AC). **Chapter 4** studies on the synthesis, characterization, and application of bio-resin in Pb(II) removal from synthetic as well as LABW. **Chapter 5** focuses on LABS characterization and its valorization through heavy metal recovery by progressive acidification. Further, a detailed study is presented on the utilization of LABS in the fired brick production. **Chapter 6** outlines the major findings, limitations of the present study, and recommendations for further research directions.

CHAPTER 2

Materials and Methods

This chapter provides the details of chemicals, reagents, instruments, analytical techniques, experimental procedures, and characterization techniques used in this study. Any specific change or deviation in methodology from what is mentioned here is detailed in the respective Chapter(s)/Section(s). The methodologies in the study are broadly categorized in to two parts viz., (a) synthesis and characterization of sorbents for LABW remediation and (b) characterization of LABS and bricking clay, and its valorization studies. The earlier includes sorbent precursor selection criterion, synthesis protocol, characterization, and adsorption procedures for Pb(II) removal mostly from synthetic and real LABW. The characterization procedures of LABS and clay and the valorization experiments such as progressive acidification and brick manufacturing are explained in the later part of this Chapter.

2.1 Chemicals and reagents

Milli-Q water (resistivity less than 15 MΩ cm) was used to prepare all standards, stock, and reagent solutions (Millipore S.A.S., Molsheim, France). All the chemicals were either of analytical or laboratory reagent grades. The chemicals were procured from either Loba Chemie India, Merck India or S.D. Fine Chemicals, India (Table 2.1). All plastic wares used were made of polypropylene procured from Tarson Products Pvt. Ltd., Kolkata, India. The glassware having low coefficient of linear expansion (32.5×10^{-7} cm/cm/°C) was supplied by Borosil Glass Works Ltd. (BGWL), India.

Table 2.1: List of chemicals, their purity, and the purpose of use in this study.

Reagent name	**Purity/assay, %**	**CAS number**	**Purpose**	**Provider**
Copper sulfate pentahydrate	Assay 99	7758-99-8	Cu(II) stock solution preparation	S.D. Fine Chemicals, India
Lead nitrate	Assay 99	10099-74-8	Pb(II) stock solution preparation	
Acetone	Assay 99	67-64-1	Washing of bio-resin	Loba Chemie Pvt. Ltd., India
Ammonium ferrous sulphate hexahydrate	Purity 98.5	7783-85-9	Bio-resin synthesis	
Calcium chloride dihydrate	Assay 99	10035-04-8	Source of calcium in metal solution	
Diethyl ether	Assay 98	60-29-7	Washing of bio-resin	
Dimethylformamide	Assay 99.6	68-12-2	Bio-resin synthesis	
EDTA disodium salt	Assay 99.5	6381-92-6	EDTAD synthesis	
Hydrochloric acid	Assay 35.4	7647-01-0	EDTAD synthesis and metal recovery from LABS	
Nitric acid	Assay 68-72	7697-37-2	pH adjustment and metal recovery from LABS	
Potassium bromide	Purity 99	7758-02-3	FTIR analysis	
Sodium bicarbonate	Purity 99	144-55-8	Washing of bio-resin	
Sodium hydroxide	Assay 98	1310-73-2	pH adjustment	
Sodium nitrate	Purity 99	7631-99-4	Source of nitrate in metal solution and for potentiometric titration	
Sulphuric acid	Assay 98	7664-93-9	Adsorbent synthesis, regeneration, and metal recovery from LABS	
Absolute ethanol	Purity 99.5	64-17-5	Washing of bio-resin	Merck India
Cadmium nitrate tetrahydrate	Assay 98	10022-68-1	Cd(II) standard preparation	
Cobalt(II) sulfate heptahydrate	Assay 95	10026-24-1	Preparation of Co(II) standard	
Iron sulfate heptahydrate	Assay 98	7782-63-0	Fe(II) standard preparation	
Magnesium chloride	Purity 95	7786-30-3	Preparation of Mg(II) standard	
Manganese chloride	Assay 97	7773-01-5	Preparation of Mn(II) standard solutions	
Nickel chloride hexahydrate	Assay 98	7791-20-0	Ni(II) standard preparation	
Zinc chloride	Assay 98	7646-85-7	Preparation of Zn(II) standard solution	
Ammonium acetate	Assay 98	631-61-8	BCR sequential chemical extraction	Sigma-Aldrich, India
Citric acid	Purity 99.5	77-92-9	Metal recovery from LABS	

Reagent name	Purity/assay, %	CAS number	Purpose	Provider
Diethylene triamine penta-acetic acid	Assay 98	67-43-6	DTPA test	
Glacial acetic acid		64-19-7	Metal recovery from LABS	
Hydrogen peroxide	Purity 30	7722-84-1	Metal recovery from LABS	
Hydroxylammonium chloride	Assay 98	5470-11-1	BCR sequential chemical extraction	
Oxalic acid	Purity 99	144-62-7	Metal recovery from LABS	
Phosphoric acid	Assay 85	7664-38-2	Metal recovery from LABS	
Sodium sulphate	Assay >99	7757-82-6	Determination of cation exchange capacity	

2.2 Commercial ion exchange resins and instruments used

Two different cation exchange resins viz. IR120 and IRC50 containing either sulfonic or carboxylic groups used in this study were procured from Central Drug House (P) Ltd., India. The resins were used without any pre-treatment or modification for the adsorption experiments. The properties of commercial ion exchange resins provided by the manufacturer are presented in Table 2.2. The list of instruments employed in this study is provided in Table 2.3.

Table 2.2: Properties of commercial cation exchange resins.

Resin	IRC50	IR120
Particle size	20–50 mesh	20–50 mesh
Ionic form	H^+	H^+
Ion exchange capacity	Minimum 10 meq/g	Minimum 4.5 meq/g
Cross-linking	–	8%
Loss on drying (~105°C)	Maximum 45–50%	Maximum 45–50%
Resin type	Weakly acidic	Strong cationic
BET surface area	3 m^2/g	4 m^2/g
Functional groups	–COOH	$-SO_3H$

Table 2.3: List of the instruments/equipment used in this study.

Sl	Instrument	Purpose	Model/Manufacturer
1	Hot air oven	Drying	ICT Kolkata, India
2	Conductivity meter	Conductivity measurement	VSI Electronics Pvt. Ltd., India
3	Muffle furnace	Proximate and solids analysis	RMF 46/14/ Reico, Kolkata, India
4	Flame photometer	Anion analysis	128/ Systronic, Ahmedabad, India

Sl	Instrument	Purpose	Model/Manufacturer
5	Atomic absorption spectrometer	Metal analysis	55B, Spectra AA/ Varian, Australia
6	Incubator shaker	Shaking of samples	1005R/ Lab Tech, New Delhi, India
7	Autotitrator	Potentiometric titrations	DL60/ Mettler Toledo, Switzerland
8	Fourier-transform infrared spectrometer	Acquiring FTIR spectra	PE-RXI/ Perkin-Elmer, USA
9	Field emission scanning electron microscope	Acquiring microscopic images	Sigma/ Zeiss, Germany
10	pH meter	pH measurement	µph-361/ Systronic, Ahmedabad, India
11	Indian Standards sieves	Adsorbent and LABS sieving	Heico, USA
12	Block digestion system	LABS digestion	Pelican Equipments Chennai, India
13	CHNS analyser	Ultimate analysis	EA3000/ Eurovector, Redavalle, Italy
14	Centrifuge	Centrifugation	R-24/ REMI Instruments Ltd., Mumbai, India
15	Water bath shaker	Temperature controlled shaking	IKON Instruments, India
16	Electronic balance	Weighing reagents	WENSAR/ Weighing Scale Ltd., India
17	Thermogravimetric analyser	Thermogravimetric analysis	TG 209/ NETZSCH INDIA, Chennai, India
18	Surface area analyser	Surface area measurement	ASIQM0000-4/Quantachrome, USA
19	X-ray diffractometer	Acquiring XRD spectra	X'Pert Pro/ PANalytical, Netherlands
20	Laser particle size analyser	Particle size distribution analysis	Malvern, United Kingdom
21	Muffle furnace	Brick firing	LHT 02/16/ Nabertherm, Lilienthal, Germany
22	Universal testing machine	Brick testing	UTM Median-250/ BISS, Banglore, India
23	Vernier caliper	Brick dimension measurement	530-312CAL/ Mitutoyo, Japan
24	Mechanical shaker	For shaking of sieves	Heico, USA
25	Millipore water system	For washing, and solution preparation	Millipore S.A.S./ Molsheim, France

2.3 LABW, LABS and clay collection

LABW was collected from one of the effluent treatment plants (ETP) of a leading LAB Industry (name withheld) located in Maharashtra, India. It was characterized for its initial pH and concentration of different heavy metals using an Atomic Absorption Spectrometer (AAS) (55 B, Spectra AA, Varian, Australia). The wastewater generated in LAB indusry is currently treated by the addition of calcium hydroxide (slaked lime) to remove metals as precipitates in the form of mainly metal hydroxides or sulphides. The sludge slurry is then dewatered using 'press mud' and sun dried in drying beds to produce sludge cakes. The dewatered LABS was collected and wrapped in polyethylene sheets to prevent moisture loss, transported to the laboratory in high-density polyethylene trash bags and stored at 4°C. For the manufacturing of fired clay bricks, the bricking clay was collected from the local brick kiln at North Guwahati, Assam, India.

2.4 Synthesis and characterization of sorbents

2.4.1 Selection of precursor for sorbent synthesis

In this study, sorbents (both FFA and bio-resin) were synthesized from arecanut husk, an agricultural waste that was locally available (Fig. 2.1). The fruit of tall palm commonly known as arecanut palm or betel-nut palm (scientific name *Areca catechu)* is included in the tribe Arece of the family, Palmae.

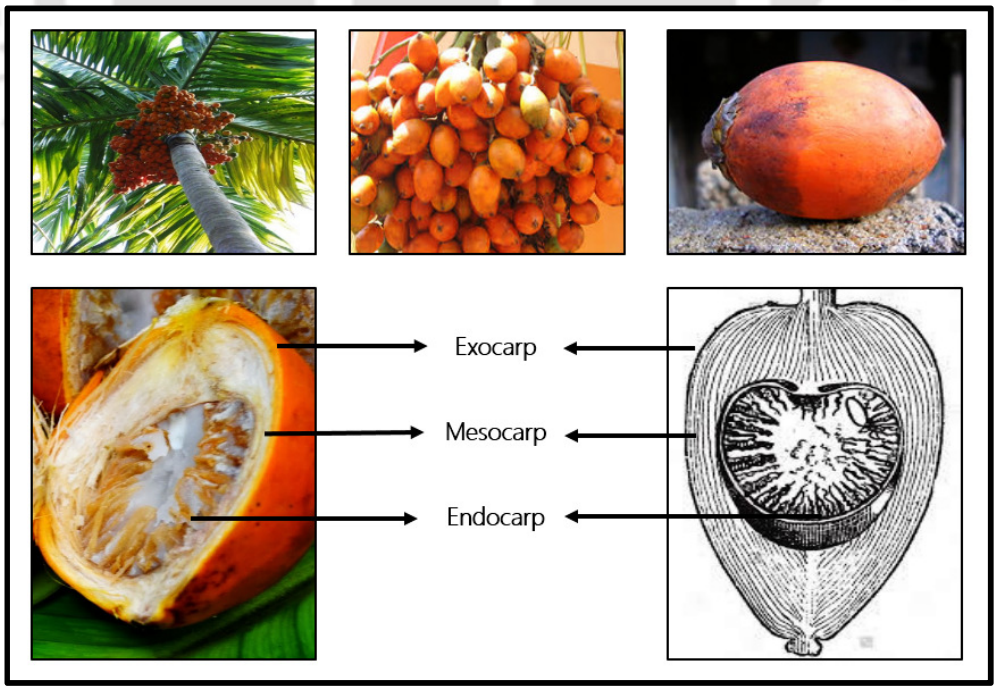

Figure 2.1: Pictorial views of arecanut and schematic showing various parts [208, 209].

The arecanut husk is a principal chewing material in India and in the far eastern countries [210]. The fruit has a smooth, yellowish to orangeish exocarp, a fiber-rich mesocarp and a wooded endocarp, which is the edible nut (Fig. 2.1). Arecanuts are consumed in India either raw or cured as a chewing material. The husk is covering to the edible part and consists of a large number of short staple fibers embedded in a matrix of thin parenehymatous tissue [206]. The husk covering the chewing material i.e. endocarp, is thrown away in the environment and constitutes about 60 to 80% of the total weight of arecanut [211]. India is the largest consumer and producer of *Areca catechu* and covers up to 52.8% of global production [206]. It is estimated that, in India at least 5,35,262 tons of arecanut is produced per annum [212]. In India, Karnataka, Kerala and Assam holds about 83% share in terms of cultivation area and production of arecanut. Assam is the 3rd highest producer among them [206, 210]. Disposal of husk is one of the major problems faced by local trading shops in many parts of India, especially in Assam. There are limited studies on the utilization of arecanut husk such as for the preparation of thick board and wrapping paper [206, 207]. Acid treatment of such lignocellulose is an established procedure in the field of biofuel production and various other uses [130, 213]. Acid breaks the lignin seal and disrupts the hydrogen bonding between cellulose making it more accessible [130]. High temperature (160-220°C) during acid treatment hydrolyses the hemicellulosic part increasing the porosity of biomaterial [214]. Although arecanut husk contain about 44% cellulose, 28% hemicellulose and 11% lignin, [215] its use as a feedstock for biofuel production is limited due to its high ash content and lower susceptibility to enzymatic digestion [215]. Arecanut husk is found to be an efficient adsorbent for Pb(II) removal after its functionalization using Fenton reagent with Fe^{2+}/H_2O_2 molar ratio of 0.01 [216]. Keeping in mind the need of low cost adsorbent for the removal of heavy metals from wastewater, arecanut husk was selected as the precursor for the synthesis of functionalized adsorbent and bio-resin (Section 1.10, Chapter 1).

2.4.2 Synthesis protocol of sorbents

The precursor i.e. the arecanut husk was collected from local trading shops nearby to the Indian Institute of Technology Guwahati. It was thoroughly washed with tap water to wipe out the dirt and stuck particles. It was then dried overnight at 70°C in a hot air oven (ICT Kolkata, India). The dry husk was cut into small pieces (0.2 to 0.5 cm size) to be functionalized and termed as the raw husk (RH). The pictorial images of raw arecanut husk and dried husk are illustrated in Fig. 2.2.

Figure 2.2: The pictorial images of (a1 and a2) collected raw husk, (b1 and b2) washing of raw husk, and (c1 and c2) cut raw husk after drying at 105°C.

2.4.2.1 Synthesis of functionalized fibrous adsorbent (FFA)

In synthesis experiments of FFA, 150 g of dried RH was taken in a 2 L borosilicate glass beaker and required amount of concentrated H_2SO_4 (98%) was added to make a mass to volume ratio (RH: H_2SO_4 acid) of 1:2 (w/v) [115, 116, 122]. It was swirled with the help of a glass rod. The temperature of the content of beaker reached to around 120°C due to an exothermic reaction between acid and RH. The temperature gradually dropped down to 105°C in 20 min, and the beaker was then kept in a hot air oven at the same temperature for 2 h [217, 218]. The acid treated husk thus prepared was washed with Milli-Q water several times until the pH of wash water became 5.00±0.10. It was then dried at 105°C to obtain FFA. The FFA particles were screened using Indian Standard sieves. Particles passing through 1000 µm sieve and retained on 300 µm sieve were collected and stored in a desiccator for further experimentation. The schematic of FFA synthesis process is presented in Fig. 2.3.

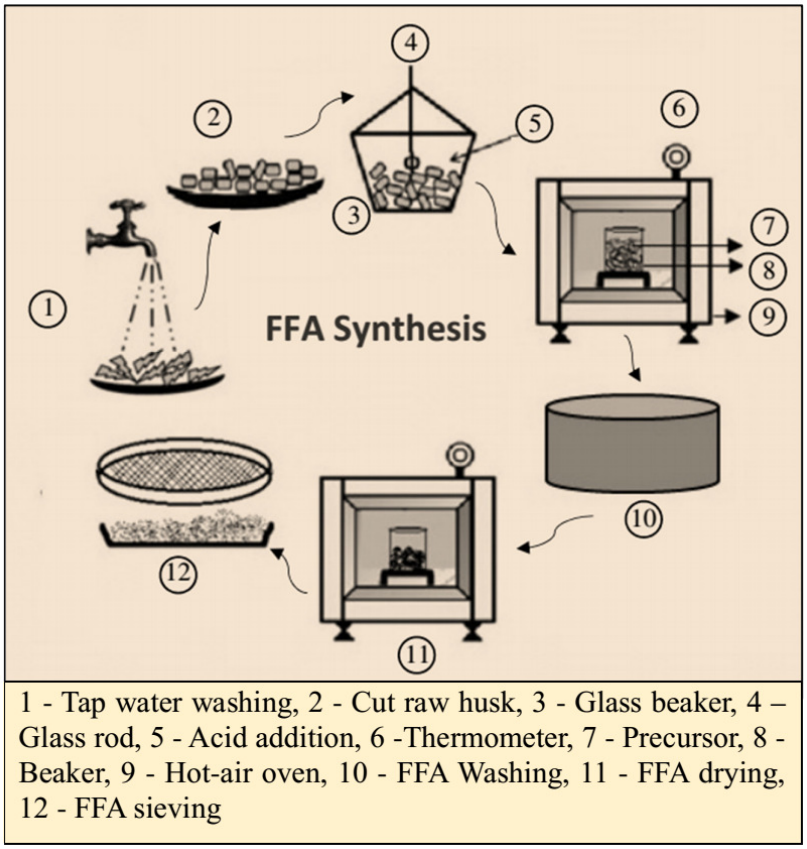

Figure 2.3: A schematic representing synthesis procedure of FFA.

2.4.2.2 Synthesis protocol of bio-resin

Mercerization of RH: RH was treated with 10-30% (w/w) NaOH solution with 20 g RH/L at 25°C for 24 h with continuous stirring at 400 rpm using a magnetic stirrer. The reaction time and temperature was varied from 8 to 40 h and 25 to 75°C, respectively. It was then centrifuged (R-24, REMI Instruments Limited, India) and washed several times with Milli-Q water until pH became 5.00±0.10 (µpH System-361, Systonic, India) followed by ethanol and acetone rinse. Afterwards, it was dried at 105°C for 1 h, left to cool in a desiccator and termed as the mercerized husk (MH). It was then subjected to the similar procedure to obtain the double mercerized husk and is designated as MMH [147].

EDTAD synthesis and functionalization: EDTA disodium salt was added in Milli-Q water (1:10 w/v) followed by the dropwise addition of concentrated HCl until complete precipitation of EDTAD [147]. The precipitate was collected by centrifugation at 5000 rpm for 20 min and washed with 95% ethanol followed by diethyl ether. It was dried for 2 h at 105°C and, finally left to cool in a desiccator [147].

In the functionalization step, 5 g of each specimen (RH, MH or MMH) was refluxed with EDTAD in anhydrous dimethylformamide (DMF) (1:4:42 w/w/v) in a flat bottom round contactor for 20 h at 75°C. It was then washed in a sequence with DMF, Milli-Q water, saturated sodium bicarbonate solution (10%), Milli-Q water, ethanol and finally with acetone followed by hot air oven drying at 80°C for 1 h [147]. Thus, EDTAD functionalized RH, MH and MMH (also combinedly termed as bio-resins) are designated as Functionalized Raw Husk (FRH), Functionalized Mercerized Husk (FMH), and Functionalized double Mercerized Husk (FMMH), respectively.

2.4.3 Sorbents characterization and analytical techniques

2.4.3.1 Proximate and ultimate analysis

In proximate analysis, 5 g of sample (FFA, FMH or LABS) was put into a clean and dry crucible equipped with a lid, and heated up to 575°C in a muffle furnace (RMF 46/14, Reico Equipments and Instruments, Kolkata, India) for 3 h. Moisture content (MC) (Eq. 2.1), volatile solids (VS) (Eq. 2.2), and ash content (Eq. 2.3) were estimated as follows [215].

$$\text{MC}\ (\%) = \left[\frac{m_1 - m_2}{m_1 - m_0}\right] \times 100 \quad (2.1)$$

$$\text{VS}\ (\%) = \left[\frac{m_2 - m_3}{m_1 - m_0}\right] \times 100 \quad (2.2)$$

$$\text{Ash content}\ (\%) = \left[\frac{m_3 - m_0}{m_1 - m_0}\right] \times 100 \quad (2.3)$$

Where, m_0 = weight of empty crucible, m_1 = weight of crucible + sample before drying, m_2= weight of crucible + sample after drying at 105°C, m_3= weight of crucible + sample after drying at 575°C.

The ultimate analysis of sorbents was carried out using CHNS elemental analyzer (EA3000, Eurovector, Italy) by taking 1 mg of the specimen in a tin boat assortment for the determination of percentage composition of carbon, hydrogen, sulphur, and nitrogen. The approximate percentage of oxygen was determined by means of difference [215].

2.4.3.2 Thermogravimetric analyses (TGA) and differential thermogravimetry (DTG)

The mass losses of sorbent specimens with the temperature were studied by TGA (TG 209 F1 Libra, NETZSCH, Germany) under nitrogen gas environment. An amount of

10 mg of sample was loaded in a moisture free crucible and heated in the temperature range of 30–900°C at a heating rate of 10°C/min. The data was obtained by uninterrupted records of weight loss vs. temperature throughout the analysis and plotted using origin software (Origin 8.5.1, Origin Lab) to obtain the profile of weight loss vs. temperature for each sample. The DTG profiles were obtained using inbuilt Star software to identify even the small variations in the weight loss.

2.4.3.3 Brunauer-Emmett-Teller (BET) surface area analysis

The BET surface area of precursor and sorbents was determined using N_2 adsorption–desorption isotherm at -196°C (ASIQM0000-4, Autosorb IQ, Quantachrome Instruments, Boynton Beach, FL, USA). The samples were degassed at a temperature 150°C for 6 h before analysis. The BET surface area, average pore size, and pore volume was estimated for the appropriate samples.

2.4.3.4 Potentiometric titrations

Potentiometric titration was used to identify and quantify the surface functional groups present on sorbents. It is based on the hypothesis that each site is occupied by titratable protons. In a particular procedure, either 0.05 g (FFA) or 0.25 g (FMH) was added to 50 mL 0.1 N sodium nitrate solution in a glass container [219, 220]. The pH of the solution was set at two and agitated overnight in an incubator shaker at 180 rpm, 30°C (LSI-1005R, Lab Tech, India) to reach at equilibrium. Along with the sorbent, it was titrated against 0.5 N NaOH using an automated precision titrator (DL60, Mettler Toledo, Switzerland). A control run without sorbent was also performed to find the difference of hydrogen ions.

2.4.3.5 Fourier transform infrared (FTIR) spectroscopy

The precursor as well as sorbents (FFA, RH, MH, RRH, FMH, and FMMH) was grinded with KBr salt in the ratio of 1:100 (w/w) to prepare a homogenous mixing. The pallets were formed in a casting die by applying pressure of 5 to 7 tons. The background correction was done with pure KBr pallet by scanning from 450 to 4500 1/cm with a resolution of 4 1/cm. The FTIR spectra (PE-RXI, Perkin-Elmer, USA) were recorded for each sample between 400 and 4000 1/cm wavenumber to identify the surface functional groups.

2.4.3.6 Field emission scanning electron microscopy (FESEM) and energy dispersive X-ray (EDX) spectroscopy

FESEM (Sigma, Zeiss, Germany) micrographs were acquired to study the morphological and textural changes in precursor and sorbents during each stage of synthesis. The micrographs of the sorbents were also recorded after the adsorption experiment. Micrographs with different magnifications ranging from 500-50000X were acquired to identify the textural changes. The EDX analysis was employed as a confirmative analysis for heavy metal adsorption through elemental mapping.

2.4.3.7 Cation exchange capacity (CEC)

The CEC of sorbents (FFA, RH, MH, FMH, FMMH, and IR120) was determined by the titration method [221]. In a particular test, FFA/bio-resin was first converted to H^+ form by treating with an excess of 1 N HNO_3; it was then filtered and rinsed with Milli-Q water several times to remove unreacted acid and air dried. The dried FFA/bio-resin (1 g) was added to 300 mL of 0.5 N sodium sulphate solution in a conical flask and agitated overnight at 180 rpm in an incubator shaker (25°C). The sorbent was filtered out, and the filtrate was titrated against 0.1 N NaOH until the phenolphthalein endpoint. The CEC was calculated using Eq. 2.4.

$$\text{CEC (meq/g)} = \frac{(\text{Volume of NaOH, mL} \times \text{Normality of NaOH, mol/L})}{\text{Mass of sorbent/resin, g}} \quad (2.4)$$

2.4.3.8 Mass percent gain (mpg)/loss (mpl)

The mpl for RH after mercerization was estimated as follows (Eq. 2.5),

$$\text{mpl (\%)} = \frac{m_i - m_f}{m_i} \times 100 \quad (2.5)$$

The mpg for bio-resins viz. FRH, FMH, and FMMH was calculated as follows (Eq. 2.6),

$$\text{mpg (\%)} = \frac{m_f - m_i}{m_i} \times 100 \quad (2.6)$$

Where, m_f and m_i represent the mass of the sample before and after EDTAD functionalization.

2.4.3.9 Crystallinity index (CI)

CI is the measure of crystallinity of cellulose I and cellulose II [147]. CI decreases with the exposure of the hydroxyl group mostly from cellulose II during mercerization [222]. CI of sorbents (RH, MH, MMH, and FMH) was calculated from X-ray diffractograms of the samples recorded between 15-90° 2θ value (X'Pert Pro, PANalytical, Netherlands) using Eq. 2.7 [223].

$$\text{CI}\ (\%) = \frac{(I_{002} - I_{AM})}{I_{002}} \times 100 \qquad (2.7)$$

Where, I_{002} is the maximum intensity of the (002) lattice diffraction and, I_{AM} is the intensity of diffraction at 2θ = 18°.

2.4.3.10 Heavy metal analysis

Heavy metals present in solution phase were analyzed in AAS. Pb(II) was analyzed in air-acetylene flame with a lamp current of 5 mA . The standard Pb(II) solutions ranging from 2-50 mg/L were used having a minimum detection limit of 0.05 mg/L. The absorbance for each standard was measured by AAS which is directly proportional to the concentration of Pb(II) in solution. The calibration curve was prepared for every metal and a sample is shown for Pb(II) measurement in Fig. 2.4. The analytical conditions for different heavy metal analysis in AAS are shown in Table 2.4

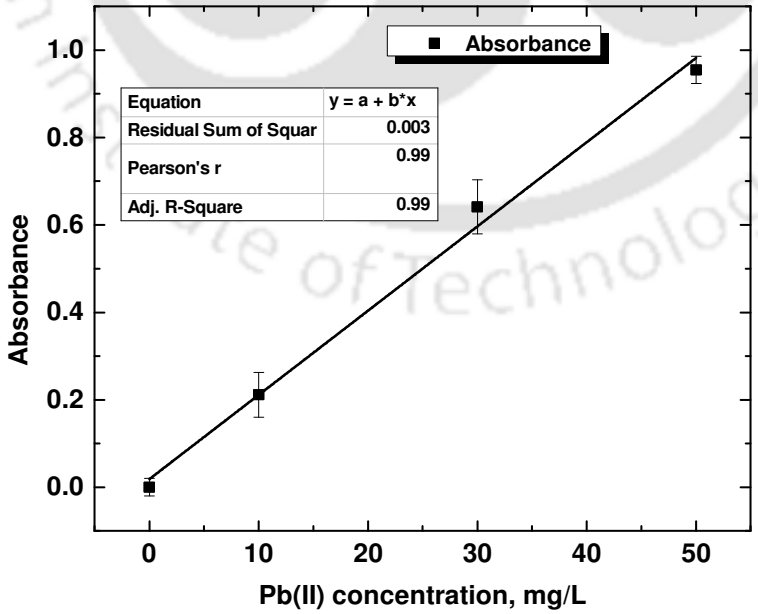

Figure 2.4: The standard calibration curve of Pb(II) analysis in AAS.

Table 2.4: Operating conditions of AAS during analysis of various heavy metals.

Metal	Operating conditions						
	Lamp current, mA	Fuel	Support	Flame stoichio-- metry	Wavelength, nm	Silt width, nm	Working range, mg/L
Al	10	Acetylene	Nitrous oxide	Reducing, red cone	309.3	0.5	0.3-250
Zn	5	Acetylene	Air	Oxidizing	213.9 307.6	1.0 1.0	0.01-2 100-14000
Ca	10	Acetylene	Nitrous oxide	Reducing, red cone	422.7 239.9	0.5 0.2	0.01-3 2-800
Cd	4	Acetylene	Air	Oxidizing	228.8 326.1	0.5 0.5	0.02-3 20-1000
Co	7	Acetylene	Air	Oxidizing	240.7 304.4	0.2 0.5	0.05-15 1-200
Cu	4	Acetylene	Air	Oxidizing	324.7 327.4 217.9	0.5 0.2 0.2	0.03-10 0.1-24 0.2-60
Pb	5	Acetylene	Air	Oxidizing	217.0 283.3	1.0 0.5	0.1-30 0.5-50
Fe	5	Acetylene	Air	Oxidizing	248.3 372.0	0.2 0.2	0.06-15 1-100
Ni	4	Acetylene	Air	Oxidizing	232.0 341.5	0.2 0.2	0.1-20 1-100
Mg	4	Acetylene	Air	Oxidizing	285.2 202.6	0.5 1.0	0.003-1 0.15-20
Mn	5	Acetylene	Air	Oxidizing	279.5 403.1	0.2 0.2	0.02-5 0.5-60

2.5 Adsorption studies and supporting experimentation

The methodologies of heavy metal removal using synthesized sorbents (FFA and bio-resin) are elaborated in two subsections. Firstly, adsorption procedures for heavy metal removal from synthetic as well as LABW using FFA are presented. Performance of FFA in heavy metal removal is compared with commercial resins and AC. Supporting experiments such as precipitation and metal speciation studies are also included in this section. In the next section, the heavy metal adsorption studies using synthesized bio-resin are detailed. The experiments were conducted varying operational parameters such as pH, contact time, FFA/bio-resin dose, and initial metal concentration. Finally, both FFA and bio-resin was tested for heavy metal removal from LABW.

2.5.1 Application of FFA in heavy metal removal

2.5.1.1 Batch adsorption studies

All batch adsorption studies were performed in a series of 250 mL borosilicate conical containers. Pb(II) spiked 100 mL Milli-Q water was agitated at 180 rpm in an incubator shaker with a fixed FFA dosage of 1 g/L. The experiments were conducted at varying initial pH between 1.0 and 5.0 at 30°C. Initial pH of the solution was not raised beyond 5.0 to avoid Pb(II) precipitation at higher pH [224] as well as reduction in active sites of FFA. Sulfuric acid and sodium hydroxide solution of suitable strengths were used to adjust the solution pH. The samples were withdrawn at regular intervals of time, filtered (Whatman # 41), and analyzed for residual Pb(II) concentration in AAS.

In this study, the uptake capacity of the adsorbent refers to the maximum amount of metal uptake in one cycle at a fixed initial metal concentration. The metal uptake capacity, was determined by varying the initial Pb(II) concentration from 25 to 200 mg/L with 1 g/L at an initial pH of 5.0. The exhaustion capacity was calculated by adding uptake capacity of all cycles until exhaustion. In order to determine the exhaustion uptake capacity using Eq. 2.8, the spent FFA was reused for multiple cycles. After each cycle, FFA was filtered out (Whatman # 41), washed with Milli-Q water and oven-dried at 105°C for 2 h. The recovered FFA was then used in the next adsorption cycle with the fresh Pb(II) solution. The performance of FFA in terms of exhaustion capacity for Pb(II) removal was compared with the commercial activated carbon (CAC), as a reference adsorbent.

$$\text{Metal uptake capacity of FFA (mg/g)} = \frac{\sum_{i=1}^{12}[C_o - C_e]_i \times V}{m} \qquad (2.8)$$

Where, i = number of cycles, C_o = initial Pb(II) concentration (mg/L) is same for all the cycles, C_e = final Pb(II) concentration (mg/L) from individual cycle, V = volume of Pb(II) solution treated (L), and m = mass of FFA (g).

2.5.1.2 Batch desorption studies

The desorption studies were carried out using 0.1 N HCl, HNO_3 and H_2SO_4 at a dose of 2 g/L spent FFA (collected after the 1st cycle of synthetic wastewater treatment) [225] at 30°C in a thermostatic incubator shaker with 180 rpm agitation speed. The eluent that desorbed the maximum amount of Pb(II) from the spent FFA was selected for the regeneration study of the exhaust FFA collected after the 12th cycle [129].

2.5.1.3 Comparison of FFA with commercial resins on heavy metal removal

A series of experiments were conducted in batch mode to compare the performance of FFA with two commercial resins namely, IRC50 and IR120 for Pb(II) and Cu(II) removal in the mono and binary metal systems. The total initial metal concentration was 0.157 mM (32 and 10 mg/L for Pb(II) and Cu(II), respectively) in both the systems. In the binary metal removal system, the experiments were performed with equimolar concentration. The adsorption experiments, sample collection, and metal analysis were carried out as described in Section 2.5.1.1.

Sequence of experiments conducted are as follows: The metal solutions containing either Pb(II) or Cu(II) (mono metal system) were prepared at different initial pH of 1.0, 2.0, 3.0, 4.0 and 5.0. The pH of a solution was adjusted using NaOH or HNO_3 solutions. No efforts were made to maintain the initial pH during the experiment. Resin/adsorbent dose of 1 g/L was added to the conical flasks and agitated for 9 h in an incubator shaker [129]. The poor performing resin i.e. IRC50 was discontinued in further experimentation (Section 3.2.3.1, Chapter 3). pH at which the maximum removal of metals achieved in the case of IR120 was selected for further studies viz. the kinetic study, equilibrium study, and effect of common cations on the metal removal efficiency. The kinetic study was carried out for 9 h at the optimum pH and 1 g/L of adsorbent or resin dose to determine the equilibrium time. The performance of FFA and IR120 in Pb(II) and Cu(II) removal was evaluated in a wide range of metal concentrations from 0.157 to 3 mM (at optimal pH and adsorbent dose). The equilibrium study was carried out with IR120 and FFA at optimum pH and 30ºC for an equilibrium time of 5 h, with varying adsorbent doses of 0.2, 0.4, 0.6, 0.8, 1.0, 1.2, 1.4, 1.6, 1.8 and 2 g/L. After the isotherm study, the effects of common water-borne ions viz. Ca^{2+}, Na^{+} and EDTA were investigated in the mono metal system using IR120 and FFA. The concentration of Ca^{2+} and Na^{+} in the range of 0.5–2.5 and 0.2–1 mM/L, respectively, were maintained using $CaCl_2.2H_2O$ and $NaNO_3$. The concentrations of these ions were selected based on field analyses at different locations in and around Guwahati, India. The effect of EDTA on Pb(II) and Cu(II) uptakes was investigated keeping the molar ratio of EDTA: metal ions to 1:100, 1:10, 1:1 and 10:1. The concentration of EDTAD and cations was maintained by adding the required amount from the respective stock solutions. In the binary mixture of Pb(II) and Cu(II) (binary system), the adsorption test was carried out for 7 h at pH 5.0 and a dosage of 1 g/L. The selectivity experiments were carried out with 0.157 mM Pb(II) in the presence of an equal amount of the second metal (M(II)) in the binary system with 100 mL solution, adsorbent dose 1 g/L, pH 5, temperature 30°C, and 180 rpm.

The selectivity factor$\left(\alpha_{M(II)}^{Pb(II)}\right)$, with respect to Pb(II) for each binary system was calculated as follows (Eq. 2.9) [32]

$$\alpha_{M(II)}^{Pb(II)} = \frac{D_{Pb(II)}}{D_{M(II)}} \quad (2.9)$$

D is the ratio of the equilibrium uptake capacity (mM/g) and equilibrium concentration (mM) of the subscript metal ions.

2.5.1.4 Performance of FFA in LABW treatment

The untreated LABW was collected from a leading LAB manufacturing unit as outlined in Section 2.3. The performance of FFA in removal of Pb and other metals from LABW was carried out in batch mode. The experiments were carried out at 30ºC and 180 rpm with the addition of varying dosages of FFA between 0.5 and 6 g/L in a series of conical glass containers containing 100 mL of LABW adjusted to pH 4.0 for a period of 9 h. The sample collection and metal analysis were done as outlined in Section 2.5.1.1.

2.5.1.5 Supporting experiments

Precipitation experiment: Precipitation of Pb(II) if any, with the variation of solution pH was tested. In a typical experiment, 50 mL Pb(II) solution was taken in 100 mL borosilicate glass contactors. The concentration of Pb(II) was 32 mg/L (0.157 mM) and pH of the solution was adjusted between 4.0 and 12.0 by the addition of NaOH solutions with continuous swirling. It was then allowed to settle for about 1 h. The supernatant was decanted and further filtered (Whatman # 42) before the analysis of Pb(II) concentration present in the solution.

Pb(II) and Cu(II) speciation by MINTEQ: Visual MINTEQ software Version 3.0 was used to determine the species concentration of Pb(II) at different solution pH. The speciation of Pb(II) and Cu(II) in presence of EDTA was also carried out to enlighten the variation in metal uptakes with change in concentration of EDTA. The input parameters were the concentrations of EDTA, Pb(II), and the equilibrium solution pH.

2.5.2 Application of bio-resin in heavy metal removal

2.5.2.1 Batch adsorption studies

Pb(II) adsorption using bio-resin, from synthetic wastewater was carried out in the batch mode. Pb(II) solution of 100 mL was taken into the glass contactors of 250 mL and,

pH was adjusted in between 1.0 and 5.0. A dose of 5 g/L bio-resin was employed for both RH and synthesized bio-resins at 30°C, 32 mg/L initial Pb(II), and 180 rpm. The dose of FMH was varied from 0.5 to 10 g/L that gave highest Pb(II) removal among all synthesized bio-resins in the present study. The optimized dose of FMH was used in the kinetic studies of Pb(II) removal up to the contact time of 8 h. The intermediate samples were withdrawn and, FMH was separated from the solution by filtration (Whatman # 41) before analyzed for metal concentration and pH. The exhaustion capacity of the FMH was estimated similar to that of FFA (Section 2.5.1.1).

Pb(II) removal along with other metals present in LABW was carried out using FMH in batch mode. A volume of 100 mL LABW at pH 5.0 was tested in 250 mL capacity glass contactors with a wide dose of FMH in the range of 2–20 g/L. The agitation speed of 180 rpm was maintained at 30°C for 8 h in an incubator shaker.

2.5.2.2 Batch regeneration desorption studies

The regeneration experiments were performed with exhausted FMH using 0.1 N three commonly used reagents viz. EDTA, HCl and absolute ethanol at eluent/bio-resin (E/B) ratio of 1:2, contact time of 30 min, and agitation speed of 180 rpm [149, 226]. Further, the desorption experiments at varying E/B ratio were carried out with the most efficient eluent.

2.6 LABS valorization studies and brick manufacturing

LABS and clay was collected as explained in Section 2.3 and characterized through different techniques viz., laser particle size analyzer (LPSA), electrical conductivity, pH, VS, MC, proximate analysis, CEC, X-ray diffraction, total metal content in various sizes of LABS, toxicity characteristic leaching procedure (TCLP) test, diethylenetriaminepenta-acetic acid (DTPA) test, and sequential heavy metal extraction using Bureau of Community Reference (BCR) scheme. The progressive acidification of LABS was carried out in order to explore heavy metal recovery potential. The potential of the pulverized LABS (PBS) was tested as a partial replacement for pulverized clay soil (PCS) in manufacturing of fired clay bricks. Finally, the fired bricks were tested as per the protocol prescribed in IS: 3495: 1992 [227].

2.6.1 LABS characterization

In this section, the techniques employed for the characterization of LABS are included. The characterization and analytical techniques already explained in Section 2.3 are not repeated further.

2.6.1.1 LPSA, pH and electrical conductivity

The lumps of dried LABS at 105°C were pulverized and the particle size distribution was studied in LPSA (Malvern, UK) using water as the dispersant. Five gram of pulverized LABS (screened through 0.22 mm sieve) was dispersed in Milli-Q water (1:20 w/v solids: liquid) through agitation in a horizontal shaker (Optics Technology, India) for 2 h at 100 rpm. The sample was filtered and, the filtrate was analysed for pH and electrical conductivity (VSI electronics, India)

2.6.1.2 Cation exchange capacity (CEC)

CEC of LABS was determined by ammonium acetate method. In a typical procedure, 25 g of oven dried LABS (passing through 75 µm) was taken in 250 mL conical flasks and 125 mL of NH_4OAc was added. The flask was shaken on a horizontal shaker for 16 h to equilibrate. The contents of conical flasks were filtered through suction filter using 0.45 µm glass filter with addition of 25 mL aliquots at an interval of 3-4 min. till total leachate volume becomes 250 mL [228]. The exchangeable cations in leachate were measured using flame photometer and AAS.

2.6.1.3 Heavy metal analysis

Total metal: The individual total metal concentration in LABS was determined using the acid digestion method. In particular procedure, LABS as a whole was added to a mixture of H_2SO_4 and $HClO_4$ acids (5:1, v/v) at a L/S ratio of 50, in the block digestion system (Pelican equipments, India) for 2 h at 350°C [229]. After digestion, samples were diluted to required volume and analyzed in AAS for the determination of Al, Ca, Cu, Ni, Zn, Mn, Mg, Co, Pb, Cd, and Fe concentration. The concentration of heavy metal was calculated as in Eq. 2.10, and expressed in mg/kg of LABS.

$$\text{Heavy metal concentration (mg/kg)} = \frac{\text{heavy metal (mg/L)} \times \text{volume (L)}}{\text{mass of dry sludge used (kg)}} \qquad (2.10)$$

The individual total concentration in LABS represents the extent of contamination, but provides a little idea about its toxicity and forms in which the metals are present. The potential toxicity of heavy metals depends upon its mobility and bioavailability. The sequential chemical extraction (SCE) is an established experimental procedure to study the mobility, transport, toxicity, and bioavailability of heavy metals in industrial sludge, sediment and soils [230]. The study of different binding states of heavy metals is also important to understand metal fractionation and attachment with different lattices of the solids, which gives important information on environmental contamination risk. There are several methodologies developed for metal extraction using different chemicals. The Tessier 5 step extraction and Kerstin and Fronstier 6 step extraction methods are widely accepted. However, many authors reported flaws in these methods and modified it accordingly [231]. To make uniform comparison of different studies, a group of experts who worked under the European Commission for the framework of BCR, Community Bureau of Reference (now named Standards, Measurement and Testing Program) proposed a standardized sequential extraction procedure named BCR® SEP (a registered trademark of the European Commission), in terms of worldwide acceptance [230]. The sequential extraction procedure followed is presented in Fig. 2.5 and explained below.

Exchangeable metal fraction (F1): A quantity of 1 g of dry LABS was taken into 50 mL polypropylene containers to which 40 mL of 0.11 M acetic acid (solution A) was added and shaken for 16 h at 22±3°C, 30 rpm. The same containers were centrifuged at 6000 rpm for 20 min and supernatant was collected and analysed for heavy metal concentration using AAS. The samples were washed with 20 mL Milli-Q water and centrifuged at 3000 rpm for 10 min. The washed out water was discarded without any loss of solids.

Metals bound to iron and manganese oxides (Reducible fraction, F2): An amount of 40 mL of solution B (0.1 M hydroxylammonium chloride solution adjusted to pH 2 with 2 M nitric acid) was added to the residue collected from F1. The sample containers were again set on the vertical shaker for continuous stirring at 30 rpm and 22±3°C for 16 h. The supernatant collection, metal analysis, and washing procedure were similar to that of F1.

Metals bound to organic matter and sulphides (oxidizable fraction, F3): The residue collected from F2 was digested by adding 10 mL of 30% H_2O_2 (solution C) at room temperature for 1 h. The sample containers were placed in a water bath (IKO-015/ IKON Instruments, India) at 85±5°C and, samples were digested for 1 h until the volume of the

solution in the containers became less than 3-4 mL. After the reduction in volume, a second aliquot of 10 mL H_2O_2 was added and allowed to digest for another hour and, the volume reduction took place to 3-4 mL. The residue was added with 50 mL of solution D (1 M ammonium acetate solution adjusted to pH 2 with concentrated HNO_3) and shaken for 16 h at room temperature. The extract was separated out, analyzed for metal concentration, and the residue was washed as described earlier.

Residual fraction (F4): The residual fraction of heavy metals was estimated by digesting the residue collected from F2 following the method of total metal analysis as depicted earlier in the same Section.

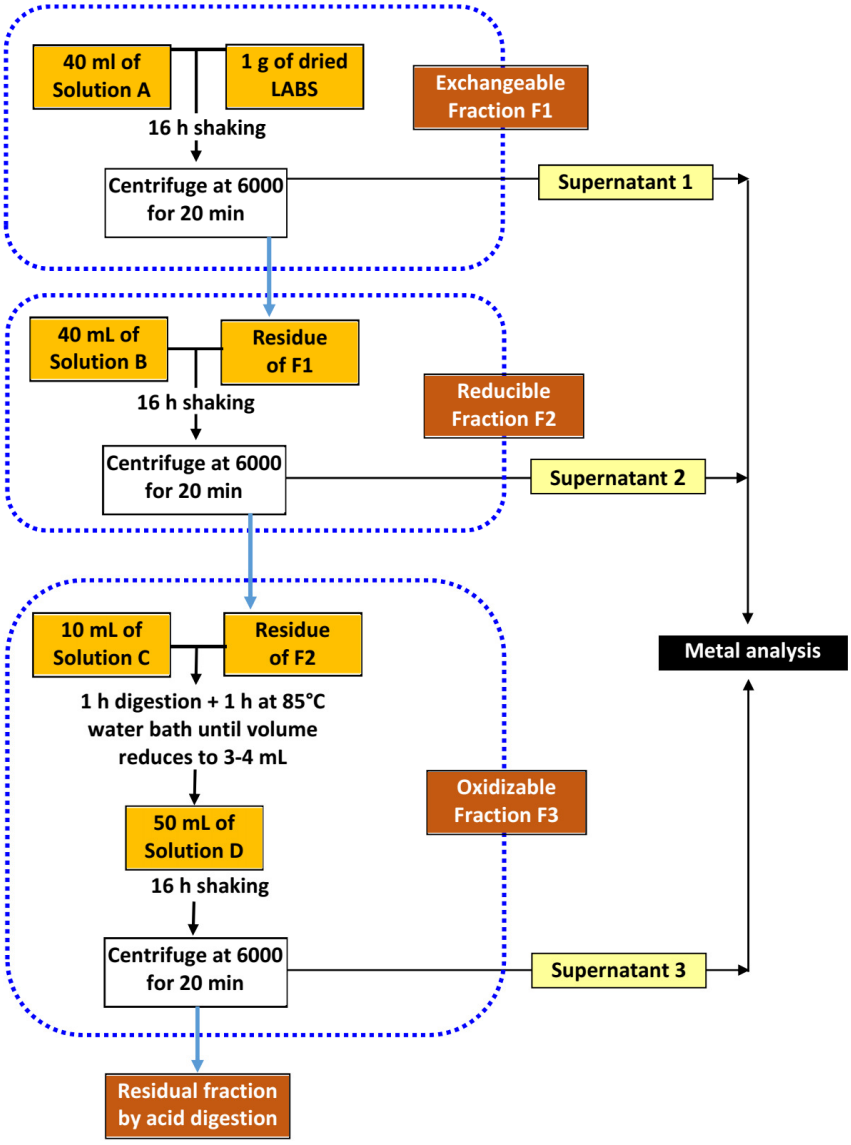

Figure 2.5: BCR three step extraction procedure for speciation of heavy metals present in LABS.

2.6.1.4 Physical segregation of LABS for heavy metal abundance

LABS was graded in different sizes through wet sieving technique using a series of Indian standard (IS) sieves of 1000, 425, 106, 75, 45, 20, and 10 µm sizes as shown in Fig. 2.6 following the procedure explained by Marchioretto, M.M., 2003 [232]. An amount of 100 g of dried LABS was added to 1 L of Milli-Q water, passed through the sieves equipped with a pan mounted on a mechanical shaker (Heico, USA). The amount of solids retained by the sieves and suspension regimented in the pan were separately collected, acid digested, and analyzed for metal content as depicted in Section 2.6.1.3 [229]. It was expressed in mg/kg of each fraction of LABS.

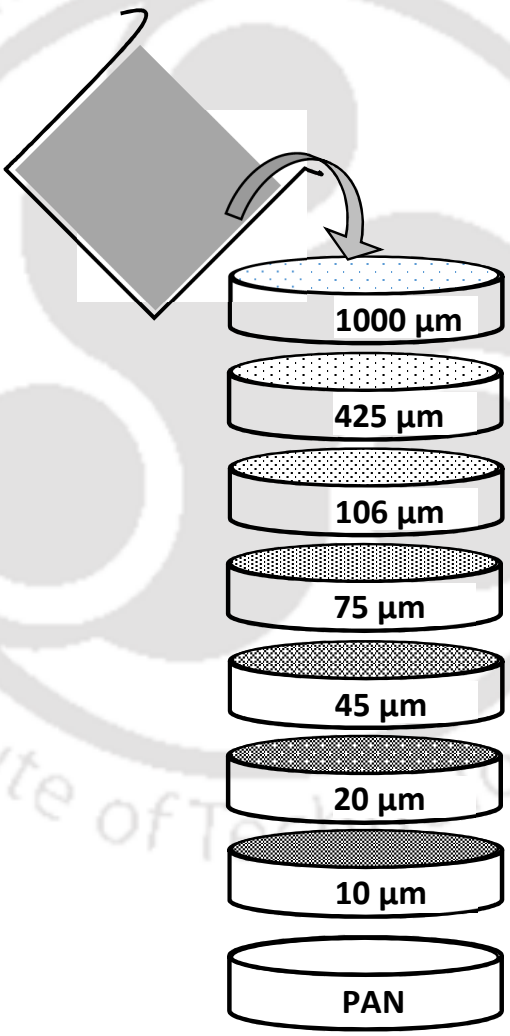

Figure 2.6: Scheme for physical segregation of LABS particles.

2.6.1.5 TCLP and DTPA testing of LABS

Toxicity characteristics of LABS were studied by following the TCLP test procedure as suggested by USEPA method #1311 using a recommended instrument (Millipore, Darmstadt, Germany) [233]. The LABS was extracted using an extraction fluid (pH 4.93) prepared by mixing 5.7 mL of glacial acetic acid and 64.1 mL of 1 N NaOH to a final volume of 1 L in Milli-Q water. The dried LABS sample was added to the sample bottle with a liquid to solid ratio (L/S) of 20:1 and set onto a horizontal shaker at 30±2 rpm (YT31ORAHW Millipore, USA) for 18 h. The sample was then filtered using a pressure filtration assembly (YT30142HW, Millipore, USA) with an increment of 10 psi for 2 min with a maximum pressure of 50 psi (XX6700P05, Millipore, USA). The filtrate collected was analyzed for total metal concentration in AAS. For diethylene triamine penta-acetic acid (DTPA) extractable heavy metals, LABS was added to 0.005 M DTPA, 0.01 M $CaCl_2$ and 0.1 M (triethanolamine) with a L/S (v/v) of 10 at pH 7.3 [234].

2.6.2 Valorization of LABS through progressive acidification

Valorization of LABS recovering metals through progressive acidification was experimented. The scheme of experiments is presented in Fig. 2.7. Citric acid (CA) and oxalic organic acids (OA) of mild acidity and biodegradable nature, and different strong inorganic acids were used in this study [235].

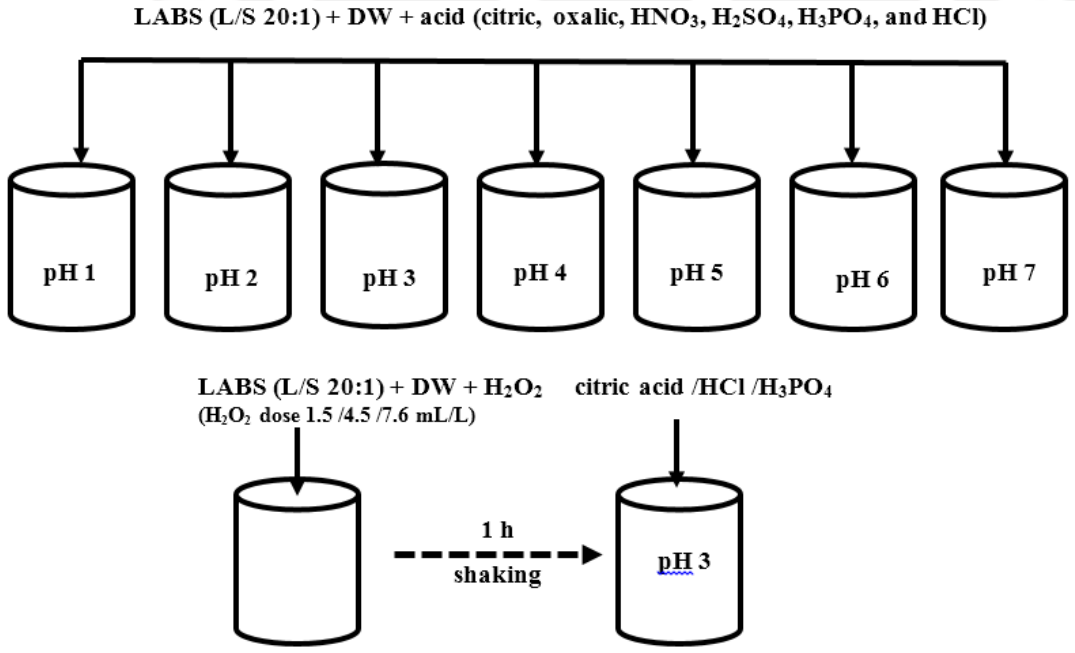

Figure 2.7: Heavy metal recovery through progressive acidification of LABS.

LABS was added with 100 ml of Milli-Q water in conical containers (L/S ratio 20:1) at room temperature, and pH was adjusted in the range of 1-7 using one of the acids. The containers were agitated for 1 h on horizontal shaker at 150 rpm and then centrifuged at 5000 rpm for 10 min and, the treated sludge was digested and analyzed as described earlier. The effect of contact time (0.5, 1, 2, 4, 8, 16, and 24 h) on metal recovery was also studied with citric, H_3PO_4, and HCl acids. The effect of H_2O_2 addition along with effective leaching acids (Citric, HCl, H_3PO_4) on metal recovery was also studied [236]. The dose of H_2O_2 was selected based on Fe concentration in LABS to maintain the necessary ratio of Fe:H_2O_2 for Fenton type reaction in a typical range of Fe:H_2O_2 (1:5 to 1:25) and pH range of 3 to 5. Hence, the dose of H_2O_2 taken for Fe:H_2O_2 of 1:5, 1:15 and 1:25 was 1.52 ml, 4.55 ml and 7.6 ml of 30% H_2O_2. [232]. The metal recovery percentage was estimated as given in (Eq. 2.11).

$$\text{Metal recovery, \%} = \frac{C_i - C_f}{C_i} \times 100 \quad (2.11)$$

Where, c_i and c_f represents concentration of metal or particular fraction of metal in raw and treated LABS.

2.6.3 Risk assessment indices

The risk associated with land disposal of LABS was assessed through the estimation of contamination factor (C_f^i), contamination degree (C_d), pollution load index (PLI), and potential ecological risk (PER). The following equations (Eq. 2.12, 2.13, and 2.14) were used for the estimation of risk indices [237].

$$C_f^i = \frac{C_{individual}}{C_{reference}} \quad (2.12)$$

$$C_d = \sum_{i=1}^{n} C_f^i \quad (2.13)$$

$$PLI = (C_{f1}^i \times C_{f2}^i \times C_{f3}^i \times \ldots\ldots\ldots\ldots \times C_{fn}^i)^{1/n} \quad (2.14)$$

Here, $C_{individual}$ is the concentration of an individual metal examined. $C_{reference}$ is the maximum allowable concentration in sludge for land application set by USEPA [63]. The reference concentration for metals not listed by USEPA was adopted from average metal concentrations of industrial sludge in developing countries [11]. C_f^i of an individual metal is the ratio of metal concentration in LABS to its reference concentration and

estimated accordingly (Eq. 2.12). PLI is the n^{th} root of the multiplication of contamination factors of n contaminants. PER for individual metal can be estimated as (Eq. 2.15).

$$PER = \sum_{i=1}^{n} E_r^i \quad (2.15)$$

The sum of individual E_r^i $[T_r^i \times C_f^i]$ represents PER of the LABS. T_r^i is the toxic response factor (Zn = 1, Cr = 2, Cu = Ni = Pb = 5, As = 10, Cd = 30) assigned by the level of risks associated with LABS was decided on the basis of PER value, as low, moderate, considerable, and very high contamination [238].

2.6.4 LABS for fired clay brick manufacturing

2.6.4.1 Brick manufacturing

The potential of PBS for fired clay brick manufacturing was tested with an incremental addition of PBS to PCS. For laboratory investigation, cuboid bricks were cast manually by molding and pressing as per IS 2117:1991 [239] with a scaled down size of 60 cm × 30 cm × 20 cm in Perspex molds [191]. The bricks were cast with varying PBS amounts of 2.5, 5, 7.5, 10, 12.5, 15, 20, 30, 40, and 50% by weight. The bricks without PBS were also cast to treat as a reference. Dry PCS and PBS were blended homogeneously and added with 35–40% tap water (w/w) to maintain consistency of the binary mix. The molded bricks were air dried for 24 h at ambient temperature and then dried at 105°C for another 24 h in a hot air oven. The oven dried bricks were then fired in the range of 500–1250°C in muffle furnace (LHT 02/16, Nabertherm, Germany) to find the optimum firing temperature. The firing temperature was increased stepwise at a rate of 2°C/min, held at the peak temperature for 2 h, and allowed to cool naturally [240]. The heating curve was designed resembling the industrial brick manufacturing process [189]. The bricks are termed as B5 for 5% PBS content in PCS (w/w) and, a similar notation is used for all bricks with a variant amount of PBS.

2.6.4.2 Brick testing and characterization

The dimensions of the brick before and after firing were measured using Vernier caliper (530-312CAL, Mitutoyo, Japan) with a precision of ±0.01 mm. The bricks were dried at 105°C to attain a constant weight (M1) measured in grams, thereafter stored in a desiccator. In cold water absorption test, completely dried specimen were immersed in Milli-Q water at a temperature of 27±2°C for 24 h. The brick specimens were removed, and

wiped with a damped cloth and weighted (M2). The mass loss/gain on firing/water absorption was determined, and the volume of bricks (V) in cm^3 was determined using water displacement method based on Archimedes principle. The dimensional shrinkage [241], water absorption, volume of open pores, apparent porosity, and bulk density [242] were determined from above measured parameters, as follows (Eq. 2.16 to 2.19).

$$\text{Water absorption } (\%) = \frac{M_2 - M_1}{M_1} \times 100 \quad (2.16)$$

$$\text{Volume of open pores } (cm^3) = M_2 - M_1 \quad (2.17)$$

$$\text{Apparent porosity } (\%) = \frac{M_2 - M_1}{V} \times 100 \quad (2.18)$$

$$\text{Bulk density } (g/cc) = \frac{M_1}{V} \quad (2.19)$$

The compressive strength of the brick specimens was determined using the Universal testing machine (UTM Median-250, BISS, India) following the BIS3495: 1992 procedure [227]. The constant weight dried brick specimens were centrally placed under the plates of UTM and the axial load was applied gradually. The pattern of the brick failure was closely observed and the maximum load a brick can withstand was calculated. The compressive strength (Eq. 2.20) was determined by dividing the maximum load with which the brick can withstand without failure by the area of the brick under compression. Modulus of elasticity (E) was also determined from the load-displacement curve. Finally, toxicity of PCS, PBS, and bricks B5–B50 was evaluated through the TCLP test as per procedure explained in Section 2.6.1.5.

$$\text{Compressive strength } (N/mm^2) = \frac{\text{Maximum load without failure}}{\text{Area under compression}} \quad (2.20)$$

CHAPTER 3

Synthesis of Functionalized Fibrous Adsorbent for LAB and Synthetic Wastewater Treatment

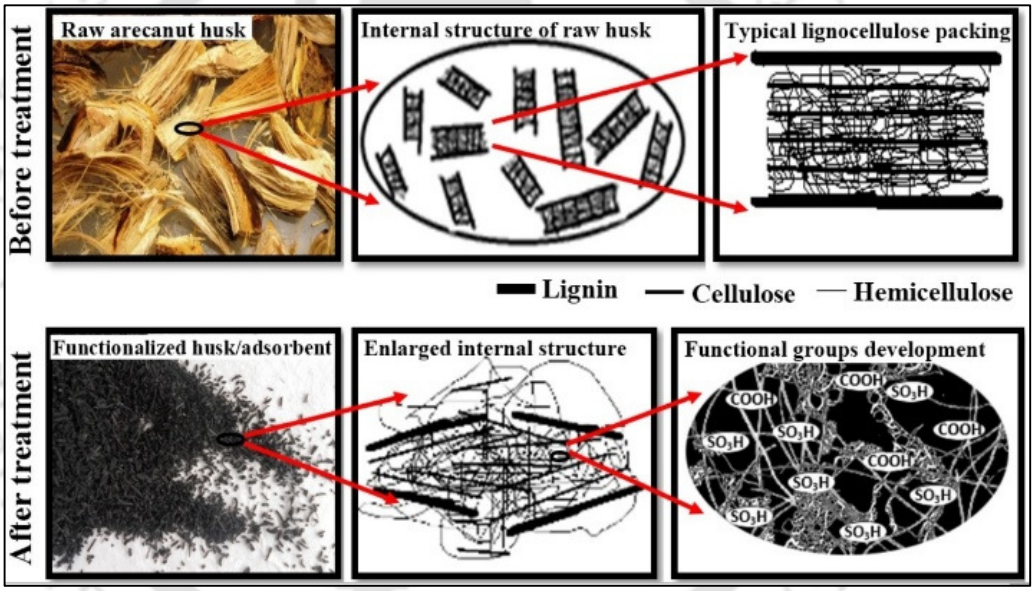

3.1 Specific background

Removal of heavy metals from industrial wastewater is commonly achieved through chemical precipitation and sometimes by adsorption using commercial adsorbents and resins. Each of these techniques has their own merits and limitations in applications (Section 1.8, Table 1.6, Chapter 1). There are several studies reported (Section 1.10, Chapter 1) on synthesis of low-cost adsorbents from lignicellulosic materials as precursor through various physicochemical processes and functionalization techniques. Major lignocellosic materials used for the same includes chitosan [6], zeolites [243], mineral clays [244], coir pith [125], peanut husk [245], jute fibres, sawdust [246], and rice husk [247]. Selection of a precursor is of utmost important for synthesizing high uptake capacity and

easily regenerable adsorbents. Selection criteria include local availability, low-cost, non-hazardous nature, high carbon and low ash content. The application of such adsorbents for the treatment of heavy metal laden industrial wastewater is also scarce due to its complex contaminant combination. Furthermore, the industrial wastewaters are often laden with various backgrounds ions and compounds such as EDTA [248, 249]. They can form the metal complexes and could interfere metal interaction with the functional groups of the adsorbents. The existing studies have indeed developed the protocols of adsorbent synthesis using lignicellulosic materials. However, many potential lignicellulosic materials remain unexplored to be utilized as adsorbent for heavy metal removal in particular when the mechanistic aspects of functional group development and its potential role in metal-binding are considered. Arecanut husk contains about 44% cellulose, 28% hemicellulose and 11% lignin [215]. Its use as a feedstock for biofuel production is limited due to its high ash content and lower susceptibility to enzymatic digestion [215], which makes it appropriate to be used for the synthesis of functional adsorbent (Section 2.4.1, Chapter 1).

In this study, the arecanut husk is selected as the precursor and functionalized through sulphuric acid treatment under the first primary objective 'Heavy metal removal using functionalized adsorbent and bio-resin'. The functionalized fibrous adsorbent (FFA) thus obtained was tested on heavy metals removal from synthetic as well as real LABW. The FFA was characterized through various analytical and instrumental procedures. A simple equilibrium dual-site proton adsorption (DSPA) model was developed, and dissociation constants of acidic sites present onto FFA were determined using potentiometric titration. FFA was used for Pb(II) removal from aqueous solution and DSPA model was applied to uncover the mechanism of Pb(II) binding. The synergistic effects of the functional groups of FFA on heavy metal removal from solutions of mono and binary metal(s) were also explored. The metal uptake capacity was compared with commercial mono-functional sulfonic (IR120) and carboxylic (IRC50) resins in order to assess its applicability in industrial wastewater treatment. Considering the complexity of industrial wastewater, the influence of usually occurring ions such as Ca^{2+} and Na^{+}, and EDTA on the uptake capacity were also investigated and, compared with the low-cost adsorbents and commercial ion exchange resins and activated carbon. The selectivity of FFA was studied for the preferential Pb(II) uptake in a binary system (synthetic) in the presence of Cu(II). The possibility of chemical regeneration of exhausted FFA was also studied in details. Furthermore, FFA was applied for the treatment of an industrial wastewater collected from a LAB manufacturing industry.

3.2 Results and Discussions

In this section, physicochemical characteristics of FFA are outlined at the beginning, after that, the performance of FFA for the removal of Pb(II) was compared with commercial resins and activated carbon. A simple proton adsorption model was developed to understand the mechanism of Pb(II) uptake by FFA in terms of determination of dissociation constants of functional groups and metal (Pb(II)) binding constants. At the end of the Chapter, FFA was applied for the treatment of lead acid battery wastewater (LABW).

3.2.1 Characterizations of FFA

3.2.1.1 Proximate & ultimate analyses, TGA, and BET surface area

The results of proximate and ultimate analyses of RH and FFA are shown in Table 3.1. RH contained about 2.93% ash, 6.4% moisture, and high amount of volatile matter. After acid treatment, ash and volatile matter increased and moisture content decreased. C and S content in FFA increased slightly compared to RH. The increase in S content was attributed to toting of sulfonic functional groups, later confirmed by FTIR and potentiometric titration.

Table 3.1: Proximate & ultimate analyses and BET surface area of RH and FFA.

Sample	Proximate analysis, %			Ultimate analysis, %					BET, m^2/g
	Ash	VS	MC	C	H	O	N	S	
RH	2.93	90.37	6.4	47.6	6.31	45.8	0.18	0.02	1.06
FFA	3.08	93.91	3.01	52.7	3.58	42.4	Nil	1.23	13.69

The similar trend of ash content for both RH and FFA can also be seen from the TGA of RH and FFA at 700°C as shown in Fig. 3.1. It can be seen that the weight loss for FFA was greater when compared to RH up to 280°C. Whereas at higher temperatures (>280°C) the weight loss in RH was higher than that of FFA. Further, the results of differential thermogravimetric (DTG) analysis for RH were analyzed and shown in Fig. 3.2. The DTG curves showed three major grooves at 280, 325, and 500°C, referring to decomposition of hemicellulose, cellulose, and lignin, respectively. Hemicellulose and cellulose degradation usually start at around 206 and 315°C, respectively, while lignin decomposition begins above 330°C [215]. The results obtained in the present study well match with the degradation pattern of lignocellulosic materials such as bonbogori, moz, bagasse, and cashew shell [215, 250].

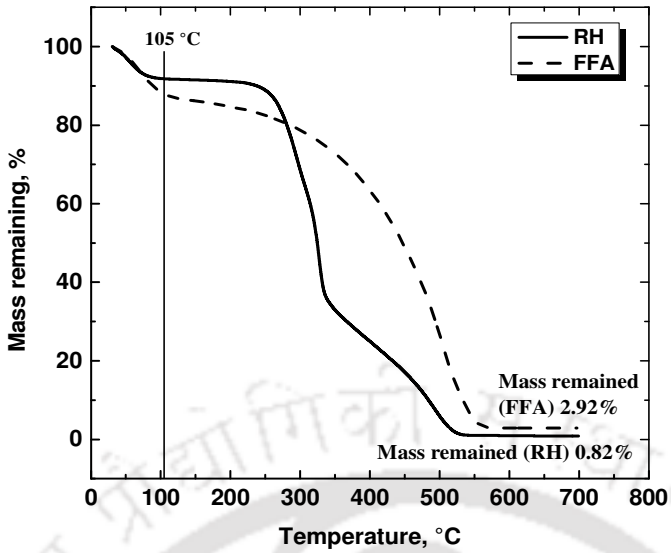

Figure 3.1: Thermogravimetric analysis of RH and FFA showing its degradation as a function of temperature [range 30-700°C].

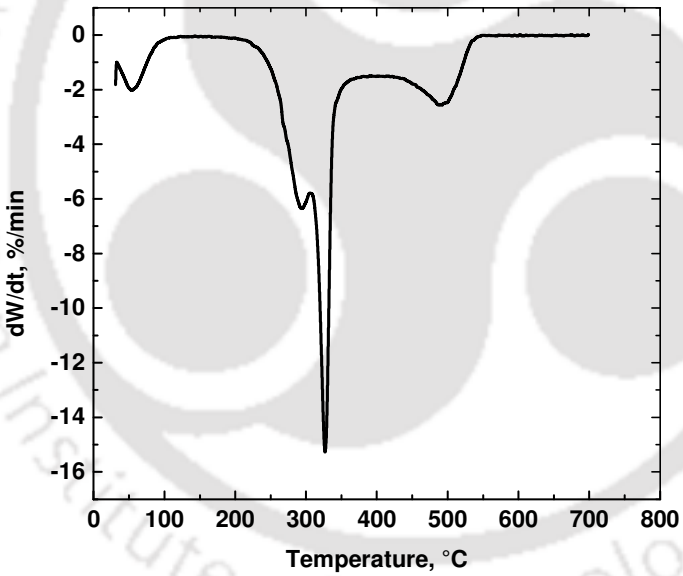

Figure 3.2: Differential thermogravimetric analysis of RH [range 30-700°C].

For FFA, there was only a little increase in BET surface area with acid treatment (Table 3.1). However, both RH and FFA gave notably lower surface area compared to AC and activated alumina [109]. The BET surface area, pore volume and average pore size of the reference adsorbent i.e. commercial activated carbon (CAC) were found as 646.7 m^2/g, 0.442 cm^3/g and 2.158 nm, respectively. The lower temperature attained (max 120°C) during FFA synthesis caused melting of the crystalline part of hemicellulose and removed

it partially. Hence, surface area did not increase much. Higher synthesis temperature was avoided as it could hydrolyze hemicellulose completely but may cause loss of lignin and cellulose content [214, 251] which may in turn reduce a total number of acidic site present.

3.2.1.2 FESEM images and EDX spectra

The surface of RH appeared to be very smooth having no cracks. The small ridges of lignicellulosic materials on the surface of RH were arranged in a regular fashion (Figs. 3.3a1-a3). Whereas, the surface of fresh FFA was highly uneven with a few irregular pores and cracks on its surface owing to acid treatment (Figs. 3.3b1-b3). Acid treatment of RH caused swelling of husk resulting in the formation of pores and cracks due to a destruction of lignicellulosic structure and partial hydrolysis of hemicellulose [130, 214]. Similar results are reported for nitric acid treated bael fruit shell [137]. The surface appeared to be sticky after Pb(II) adsorption, and no pore was visible (Figs. 3.3c1-c3) indicating that all the pores were occupied by Pb(II). Pb(II) loading onto FFA estimated by EDX analysis (Fig. 3.4) and experimentally showed error within ±5%.

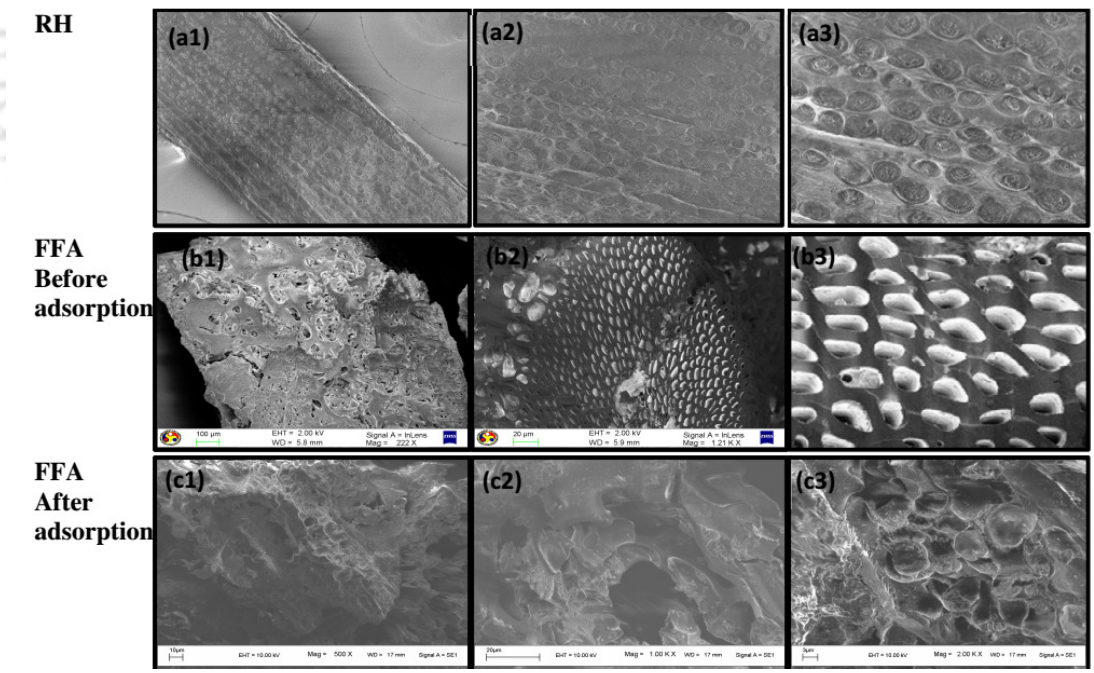

Figure 3.3: FESEM images of RH (a1, a2, and a3), FFA before Pb(II) adsorption (b1, b2, and b3), and FFA after Pb(II) adsorption (c1, c2, and c3) [Pb(II) loading 75 mg/g FFA, temperature 30°C, agitation speed 180 rpm, and contact time 5 h].

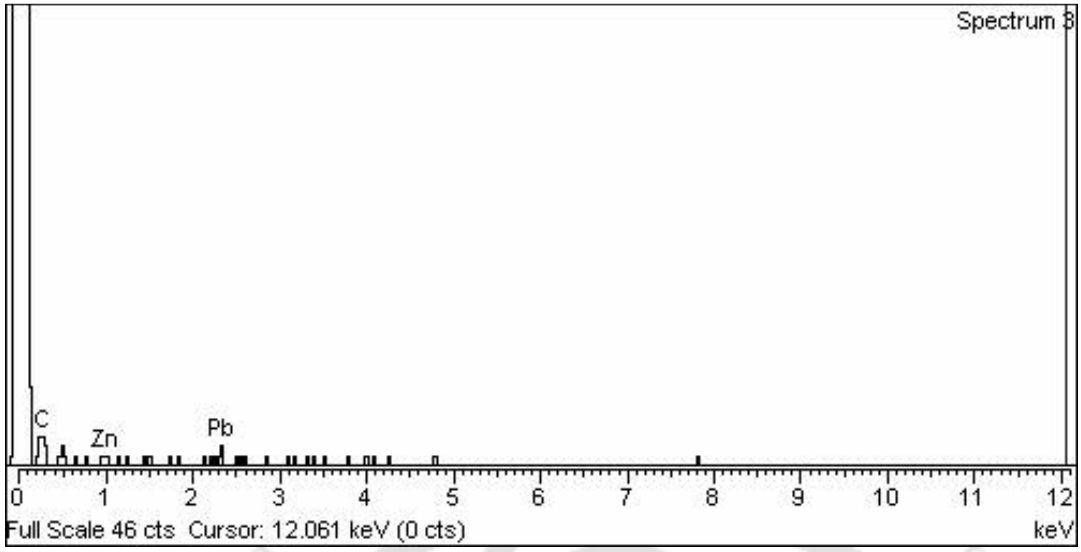

Figure 3.4: EDX spectrum of Pb(II) loaded spent FFA [Pb(II) loading 75 mg/g, 5 h, and 30°C].

3.2.1.3 FTIR spectra

FTIR spectra of FFA before Pb(II) adsorption showed a higher transmittance in the range of 3500 to 3700 1/cm (Fig. 3.5). The peak appearing at 3606 1/cm is likely to be attributed to hydrogen bonded alcohol group over a broader stretch and higher intensity. These groups are supposed to yield from glucoside linkage of cellulose or hydroxyphenyl and syringyl groups of lignin. The similar results for arecanut husk are also reported [215]. The peak near 1700 1/cm for most of the carbonaceous biomass materials possesses C=C stretching absorption frequency [8, 252]. FTIR spectra confirmed the presence of C=O stretch of α, β unsaturated -COOH group originating from deeper oxidation of part of alcoholic hydroxyl groups of lignin present on RH identified from the peak at 1705 1/cm (Fig. 3.5) [127]. The peak at 1400 1/cm can be recognized as C-O stretch of -COOH group. The band due to O-H stretching vibration of hydrated sulfonic acid is very broad having several maxima in the regions between 1650 and 2800 1/cm. The peak at 1168 1/cm can be attributed to SO_3 asymmetric stretching vibrations. The shift of peaks from 3606 to 3620, 2350 to 2357, 1705 to 1731 and 1168 to 1198 1/cm were noticed after Pb(II) adsorption (Fig. 3.5). It clearly demonstrates significant affinity of Pb(II) towards sulfonic and carboxylic groups. However, protonation and deprotonation plays a major role in the affinity behavior of Pb(II) to different acidic groups.

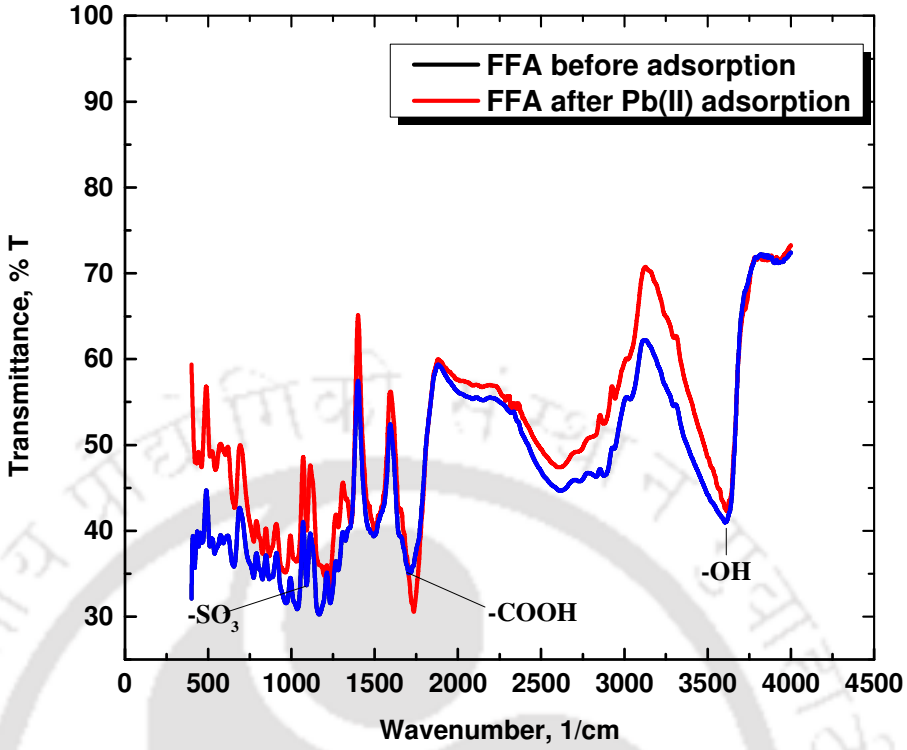

Figure 3.5: FTIR spectra of virgin and Pb(II) loaded FFA [initial Pb(II) 100 mg/L, adsorbent dose 1 g/L, agitation speed 180 rpm, temperature 30°C, contact/ equilibrium time 5 h].

3.2.1.4 Potentiometric titration and buffering capacity of FFA

Fig. 3.6 shows the titration curve for FFA against the cumulative volume of 0.5 N NaOH added. The shift of the titration curve towards right-side with FFA can be seen. It is evident that the solution with FFA showed buffering capacity confirming the release of protons into bulk solution (Fig. 3.7). The progressive dissociation of protonated sites was observed as titration continued. The titration curve of FFA was not so distinguishable to locate the equivalence points referring to neutralization of each acidic groups. It signifies that FFA is composed of many titratable functional groups dissociated with pH elevation [253]. The change in solution pH was referred solely to the exchange of protons between FFA and the bulk solution. Similar results for the characterization of oxidized activated carbon are also reported [254]. However, almost no deflection in the titration curve was observed in the case of RH. Likewise, it overlapped with the titration curve with no adsorbent.

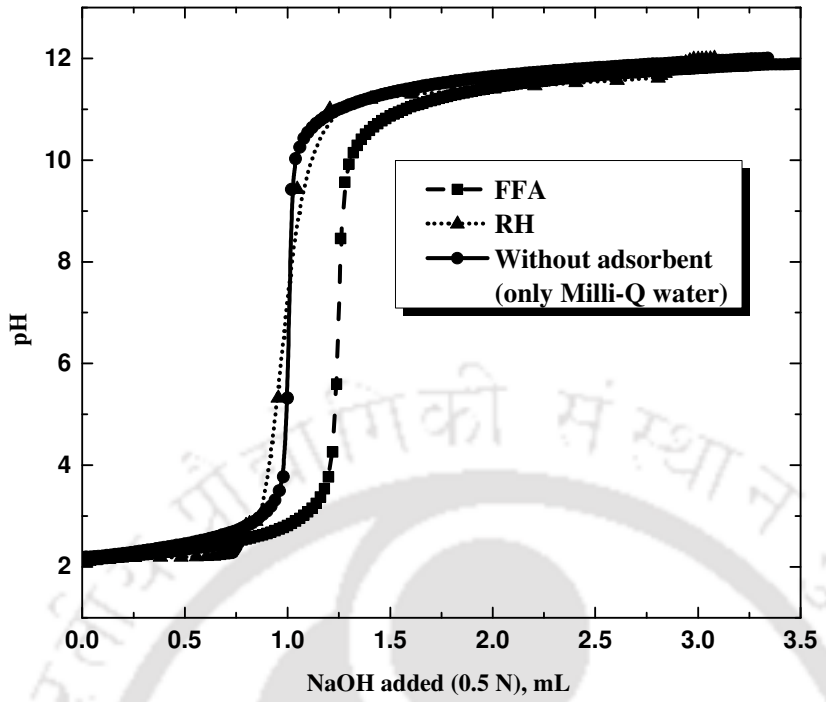

Figure 3.6: Titration curves without and with adsorbents [FFA and RH dosage 1 g/L, temperature 30°C and agitation speed 180 rpm].

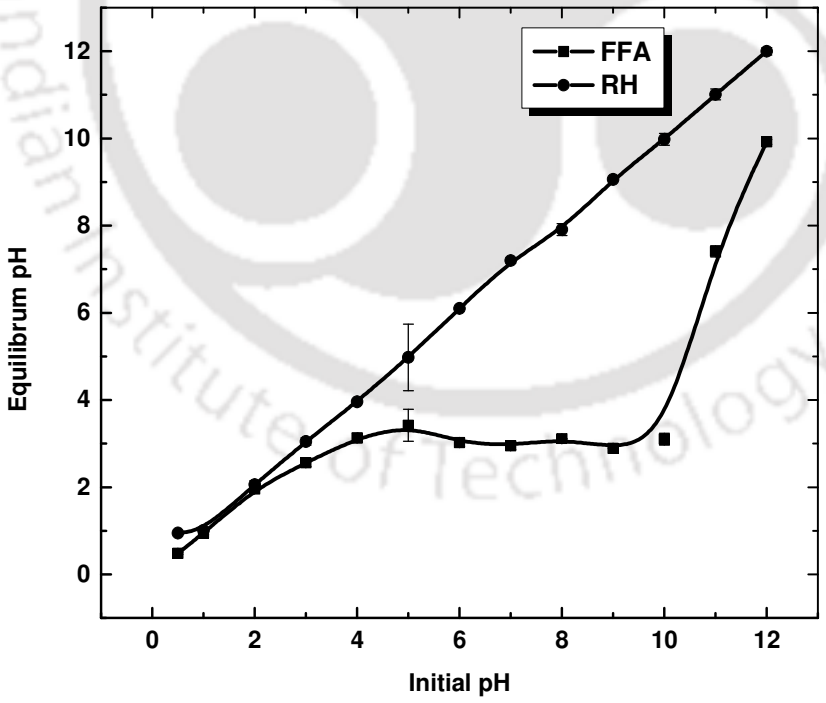

Figure 3.7: Variation of equilibrium pH without Pb(II) but in the presence of adsorbents [FFA and RH dosage 1 g/L, temperature 30°C and agitation speed 180 rpm].

The buffering capacity of the FFA was calculated by the difference in volume of NaOH need to be added to reach pH 12, with and without FFA. The buffering capacity of FFA with 1 g/L dosage was found to be 1.88×10^{-2} mol/g. The functionalized adsorbents prepared using the dead biomass of *B. subtillis* and *S. oneidensis* showed the buffering capacities of 2.8×10^{-4} and 3.1×10^{-4} mol/g with the dosage of 75-150 and 50 g/L, respectively [255]. A higher buffering capacity of FFA in comparison with the dead microorganisms refers to the presence of strongly accessible acidic sites on the surface of FFA, releasing protons. Fig. 3.7 shows the variation of equilibrium pH with respect to initial pH in the absence of Pb(II). FFA displayed an unusual buffering capacity in the pH range of 2.8 to 3.1 for initial pH from 3.0 to 10.0. On the other hand, RH did not show the buffering capacity as in accordance with the titration (Fig. 3.6).

3.2.2 Application of FFA for Pb(II) removal from synthetic solution

In this study, a range of FFA was synthesized by varying the concentration of H_2SO_4. The assortment of adsorbents was based on the performance in Pb(II) removal. FFA prepared with 24, 48, 72 and 98% H_2SO_4 showed Pb(II) removal efficiencies of 28, 36, 42 and 98.3%, respectively, from an initial Pb(II) concentration and pH of 32 mg/L (0.157 mM) and pH 5.0. The diluted H_2SO_4 could only breach the lignin walls partially and, so the lower Pb(II) uptake was noted [122]. Hence, the subsequent studies were carried out with the FFA prepared using the highest strength of acid.

In a detailed study, the initial pH of the solution was varied from 1.0 to 5.0 to study its effects on the kinetics of Pb(II) uptake. The concentration of H^+ ion is a crucial factor for Pb(II) uptake as the dissociation of acidic sites as well as the metal chemistry strongly depends on it [7, 256]. The studies targeting effect of pH on Pb(II) speciation reported that at pH< 6, Pb^{2+} is the predominant species. Above pH 6 Pb exists as $Pb(OH)^+$ and $Pb(OH)^0_2$ hence, removal could also be by precipitation of $Pb(OH)^0_2$ and sorption of $Pb(OH)^+$ [224]. The effect of contact time on Pb(II) uptake is shown in Fig. 3.8. Negligible Pb(II) uptake capacity of 1.39 mg/g was observed for RH; whereas it was 31.47 mg/g for FFA both at pH 4.0 and 5.0 (Fig. 3.8). The rate of Pb(II) binding was faster during first 30 min, reduced afterward and the uptake began to plateau after 5 h. The fall in uptake rates can be explained on the basis of concentration gradient and availability of active acidic sites.

The decrease in Pb(II) removal (Fig. 3.9) at lower pH can be explained with possible two reasons. Firstly, in acidic range there is a competition between Pb(II) and H^+ ions for the same binding sites which inhibits Pb(II) removal. Similar results in the removal of heavy

metals have been reported by various researchers [125, 246, 256]. The second reason is on the basis of surface complexation at lower pH. Protonation of chelating groups reduces complexation with available ligands and hence the percentage uptake decreases [257]. The optimum pH was taken as 5.0 based on experimental results on Pb(II) uptake and literature reported on speciation of Pb(II). Hence, all further experiments were carried out at pH 5.0 to avoid possible precipitation of Pb(II) [224]. It is also necessary to mention that the final pH of the solution was about 3.1 (Fig. 3.9) for all the experiments irrespective to the initial pH. The reduction in solution pH indicates that removal of Pb(II) ions was facilitated by ion exchange i.e. H^+ ion was released from functional groups present on FFA. A similar phenomenon in the removal of Cr(III) using cation exchanger is reported [258]. Removal of Cd(II) by nitric acid modified corncob also confirmed ion exchange as removal mechanism [133]. The FFA gave a very high exhaustion capacity of 194.94 mg/g (calculated using Eq. 2.8) as compared to adsorbents prepared by acid treatment using low-cost biomaterials (Table 3.2).

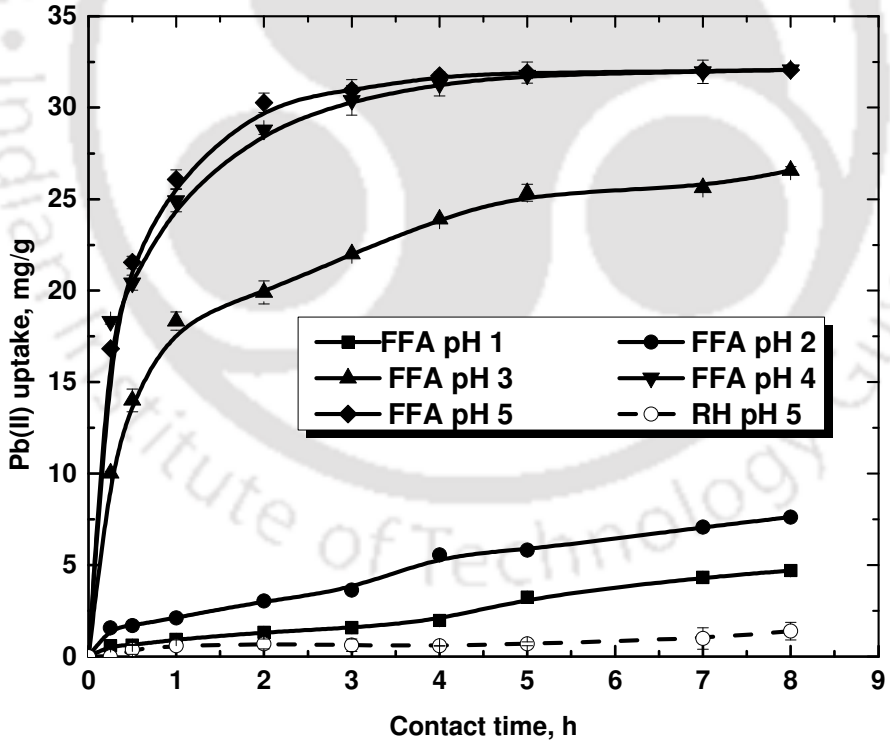

Figure 3.8: Kinetics of Pb(II) using RH and FFA as a function of contact time at different initial pH [contact time 5 h, initial Pb(II) 32 mg/L (0.157 mM), FFA dose 1 g/L, temperature 30°C, and agitation speed 180 rpm].

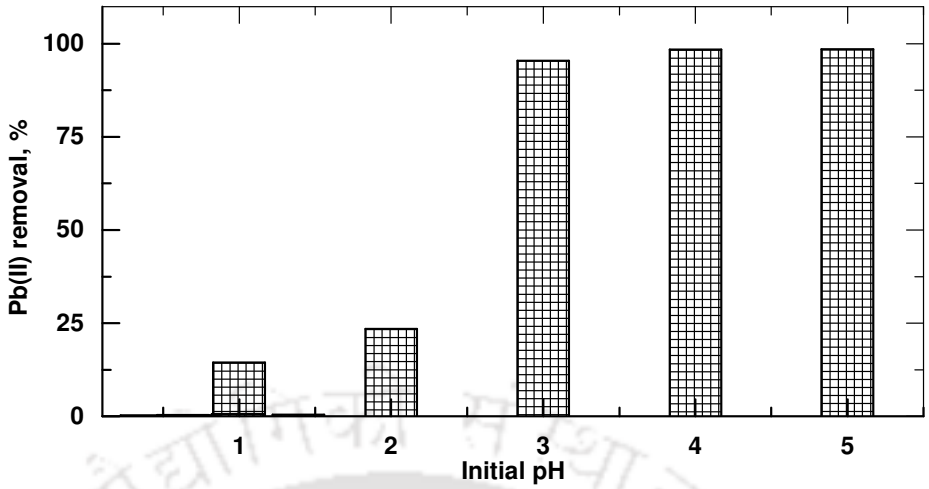

Figure 3.9: Percentage removal of Pb(II) at equilibrium [contact time 5 h, initial Pb(II) 32 mg/L (0.157 mM), FFA dose 1 g/L, temperature 30°C, and agitation speed 180 rpm].

Table 3.2: Comparison of adsorption capacities of adsorbents prepared using different acids with FFA in present study.

Precursor	**Modifying agent**	**Metal**	**Test conditions**	**q_{max}, (mg/g)**	**Reference**
Rice husk	Tartaric acid	Cu(II) Pb(II)	Initial Pb 400-1200 mg/L, Initial Cu 100-450 mg/L, Adsorbent dosage 5 g/L, 150 rpm, 4 h, pH 4, and Langmuir capacity	31.85 120.48	[259]
Sawdust (Poplar tree)	Sulfuric acid	Cu(II)	Initial Cu 30-150 mg/L, Adsorbent dosage 5 g/L, 200 rpm, 1 h, pH 5.5, Langmuir capacity, and 1 N H_2SO_4 1:2 (sawdust/H_2SO_4; w/v)	13.95	[135]
Sawdust (Oak tree)	HCl acid	Cu(II) Ni(II) Cr(VI)	Adsorbent dose 40 g/L, pH 4 Adsorbent dose 30 g/L, pH 8 Adsorbent dose 60 g/L, pH 3 Metal concentration 0.1-100 mg/L, and Langmuir capacity	3.60 3.37 1.74	[134]
Peanut husk	Sulfuric acid	Pb(II) Cr(III) Cu(II)	Metal concentration 5-50 mg/L, pH 4, 200 rpm, adsorbent dose 2 g/L, Langmuir capacity, equilibrium time: Cu and Pb 1 h, Cr 6 h	29.14 7.67 10.15	[136]
Wheat bran	Sulfuric acid	Cu(II)	150 rpm for 2 h, adsorbent dose 1 g/L, initial Cu 25-250 mg/L	51.5	[260]

Precursor	Modifying agent	Metal	Test conditions		q_{max}, (mg/g)	Reference
Banana pith	Nitric acid	Cu(II)	Adsorbent dose 5 g/L, initial Cu 10-100 mg/L, pH 4.4, 200 rpm, and Langmuir isotherm		13.46	[261]
Corncorb	Nitric acid	Cd(II)	Adsorbent dose 0.1-1 g/L, initial Cd 5-120 mg/L, pH 6, and equilibrium time 5 d		19.30	[133]
Arecanut husk	Sulphuric acid	Pb(II)	FFA dose 1 g/L, initial Pb 32 mg/L, pH 5, and 180 rpm	After 1st cycle	31.47	Present study
				After 12th cycle	194.94	

3.2.3 Performance of FFA and commercial resins in Pb(II) and Cu(II) removal

The performance of FFA for the removal of Pb(II) and Cu(II) from mono and binary-metal solutions was compared with commercial resins viz. IR120 and IRC50. The results are presented below.

3.2.3.1 Effects of pH and initial metal concentration

The hydrogen ion concentration in the metal solution is a crucial factor on its uptake [7]. It is not only responsible for the adsorptive site dissociation, but the metal chemistry is also associated with it [256]. It essentially controls metal adsorption at adsorbent–water interfaces [262]. The measured CEC and buffering capacity of FFA was 5.48×10^{-3} and 18.8×10^{-3} mM/g against IR120 were found to be of 4.64 meq/g and 8.96×10^{-3} mM/g against 5.52 and 3.86 meq/g, and 5.48×10^{-3} and 18.8×10^{-3} mM/g for IRC50 and FFA. The surface area of FFA was 13 m^2/g. It was 3 and 4 m^2/g for IRC50 and IR120.

In order to study the effect of pH in non-competitive metal adsorption by FFA, IR120, and IRC50, the test was carried out at pH 1.0, 2.0, 3.0, 4.0 and 5.0 and results are shown in Fig. 3.10. At pH 1.0, Pb(II) and Cu(II) removal efficiencies by IR120, IRC50, FFA were 91, 3, 14% and 69, 5, 19% respectively. However, the removal efficiency was increased with the increase in pH. At pH 5.0, removal efficiencies were 99, 15, 99% and 98, 23, 93%, respectively, for Pb(II) and Cu(II). The variation in metal removal at different pH can be explained by two possible reasons on the basis of metal speciation as shown in Fig. 3.11. In the pH range of 4.0 to 5.0, both the metals (M) present as $M(OH)^+$ and $M(OH)_2$ due to partial hydrolysis. These species have higher tendency to get adsorbed onto the charged surface. Also, in the acidic range, the competition between metal ions and H^+ ions for the same sites inhibits metal removal efficiency at lower pH [125, 246, 256].

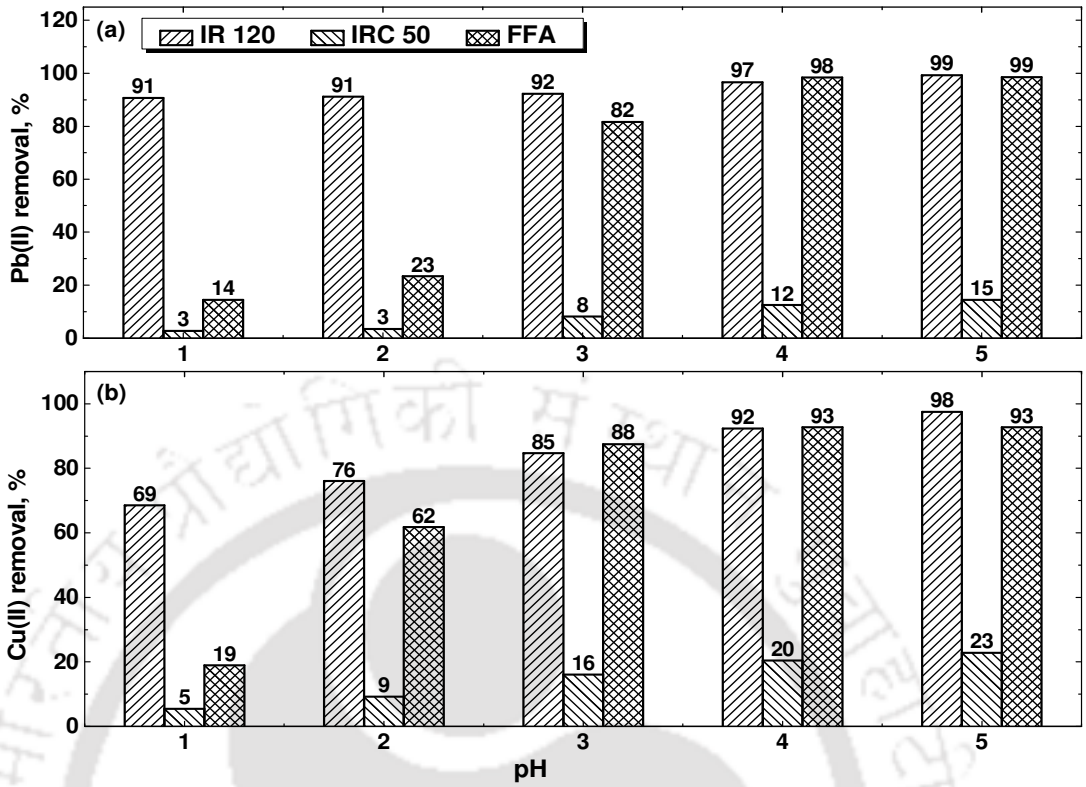

Figure 3.10: Effects of pH on removal of (a) Pb(II) and (b) Cu(II) [Pb(II) or Cu(II) 32 mg/L (0.157 mM), adsorbent dose 1 g/L, contact time 9 h, temperature 30°C, 180 rpm].

The FFA contains both sulfonic and carboxylic functional groups. Relatively, at a lower pH, the sulfonic groups were protonated more than the carboxylic groups. So, the removal of Pb(II) and Cu(II) at lower pH was facilitated by sulfonic groups and at higher pH by carboxylic groups [129]. This observation was also backed by the experimental results with IR120 and IRC50, wherein IR120 removed both Pb(II) and Cu(II), even at lower pH. IRC50 could only remove 23 and 15% of Pb(II) and Cu(II), respectively. IRC50 bears weak acidic carboxylic groups with pK_a value of 5.47 [263] and, hence, it is expected to have a relatively better uptake of metals at higher pH [264]. IRC50 also has a higher affinity for H^+ ions. For this reason, several researchers suggest the modification of its ionic form for the better removal efficiency [265, 266].

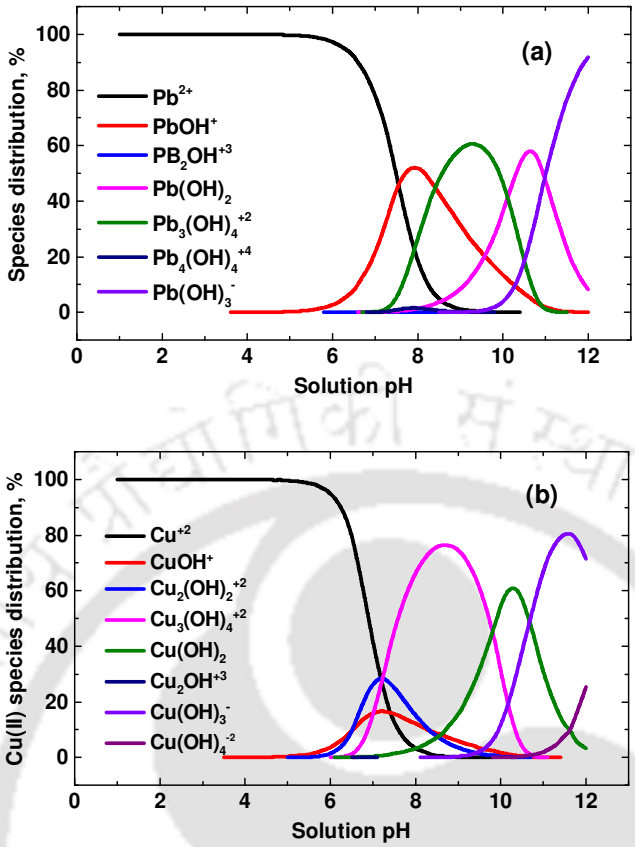

Figure 3.11: Speciation of (a) Pb(II) and, (b) Cu(II) determined using MINTEQ 3.0 software [Pb(II) or Cu(II) 32 mg/L (0.157 mM), temperature 30°C].

Pb(II) and Cu(II) precipitation tests were carried out by elevating the solution pH and the results are shown in Fig. 3.12. It can be seen that no precipitation of either metal was noted at pH<5.0. Likewise, the optimum pH was taken to be 5.0. Therefore, all further experiments were carried out at pH 5.0.

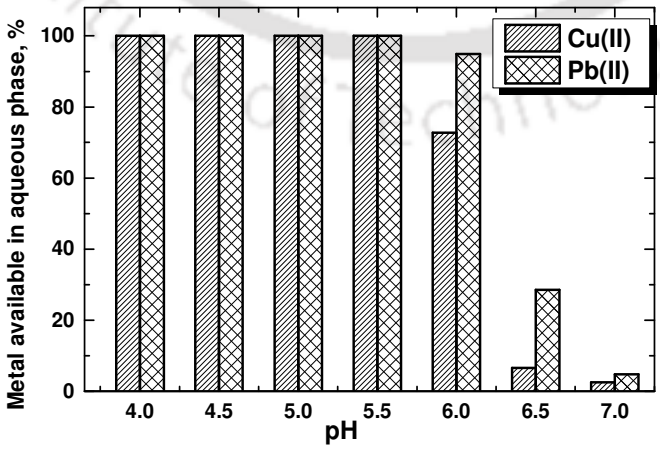

Figure 3.12: Availability of Pb(II) and Cu(II) in aqueous state at different pH.

The results of FFA and IR120 performance in Pb(II) and Cu(II) removal at various metal concentrations are presented in Figs. 3.13 and 3.14 respectively. It was observed that the removal efficiency was decreased; whereas the adsorption capacity was increased with the increase in metal concentration. FFA was equally efficient in the removal both Pb(II) and Cu(II) at a lower metal concentration (≤0.3 mM) but IR120 outperformed at a higher metal concentration. The highest adsorption capacity of FFA for Pb(II) and Cu(II) was 0.95 and 0.39 mM/g with 2.5 mM initial concentration. It was 1.8 and 1.5 mM/g for IR120 at the concentrations.

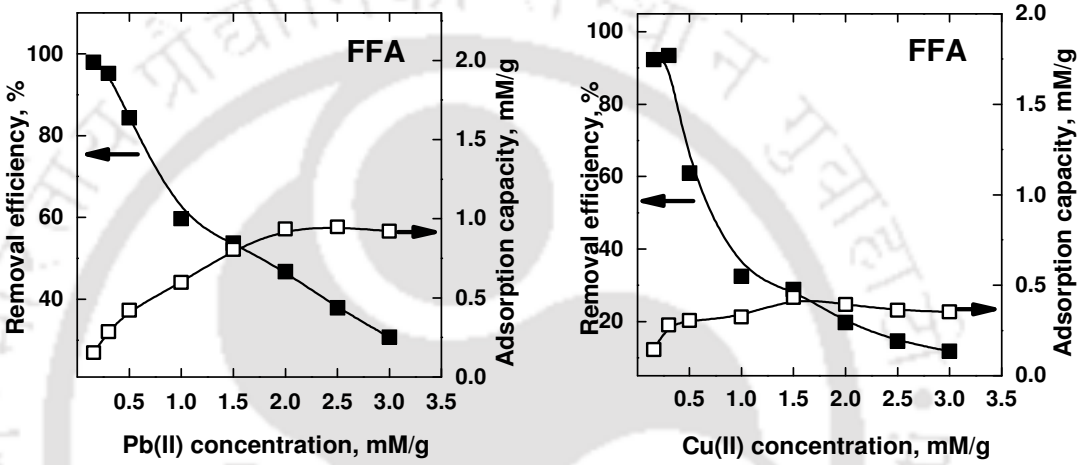

Figure 3.13: Performance of FFA in removal of Pb(II) and Cu(II) at different concentrations [Cu(II) or Pb(II) 0.157-3 mM, adsorbent dose 1 g/L, pH 5.0, temperature 30°C, and 180 rpm].

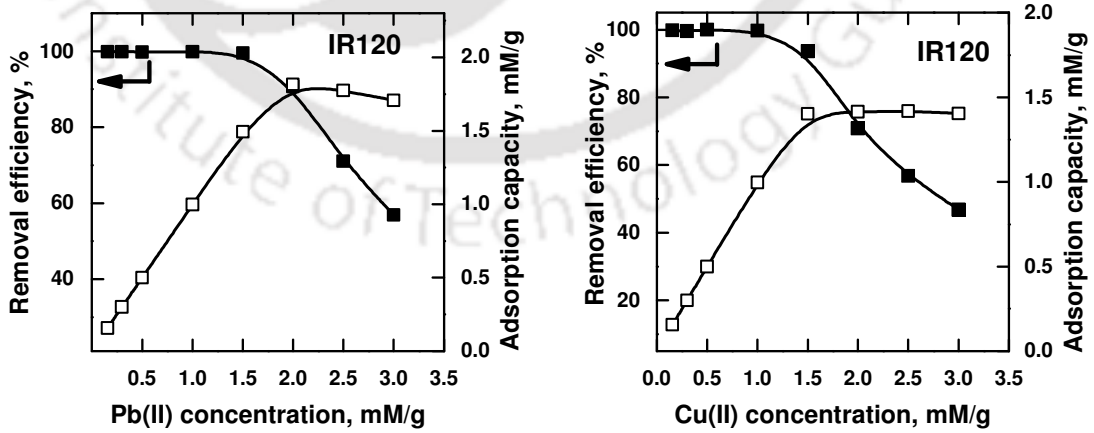

Figure 3.14: Performance of IR120 in removal of Pb(II) and Cu(II) at different concentrations [Cu(II) or Pb(II) 0.157-3 mM, adsorbent dose 1 g/L, pH 5.0, temperature 30°C, and 180 rpm].

3.2.3.2 Kinetics of Pb(II) and Cu(II) uptake

Figs. 3.15 and 3.16 shows the kinetics of Pb(II) and Cu(II) removal respectively, in the mono metal system. It was observed that IR120, IRC50, FFA showed metal uptake capacities of 0.156, 0.023, 0.155 and 0.153, 0.035, 0.145 mM/g for Pb(II) and Cu(II), respectively. The removal trend of both the metals by FFA and resins showed three distinct phases. Where, the first removal stage was the fastest and contributed the highest percentage of metal removal in 15 min of contact time. This phase is referred to the availability of most of the metal sorption sites. In this stage, FFA outperformed IR120 showing the higher affinity for Cu(II) adsorption. The better performance of FFA over IR120 was attributed to the presence of carboxylic as well as sulfonic groups on FFA. The second stage of metal uptake between 0.25 and 2 h was slower. The reduction in removal rate was due to the decrease in a number of available sites. The decrease in metal removal rate was higher in the case of FFA compared to IR120. After 2 h of contact, pH of the solution was reduced to 3.0±0.1. It increased the competitive adsorption of a proton over the metal ions and eventually removal became a plateau. The equilibrium time was 3 h for both resins, whereas it was 5 h for FFA. The third phase was observed from 2−3 and 2−5 h for IR120 and FFA, respectively.

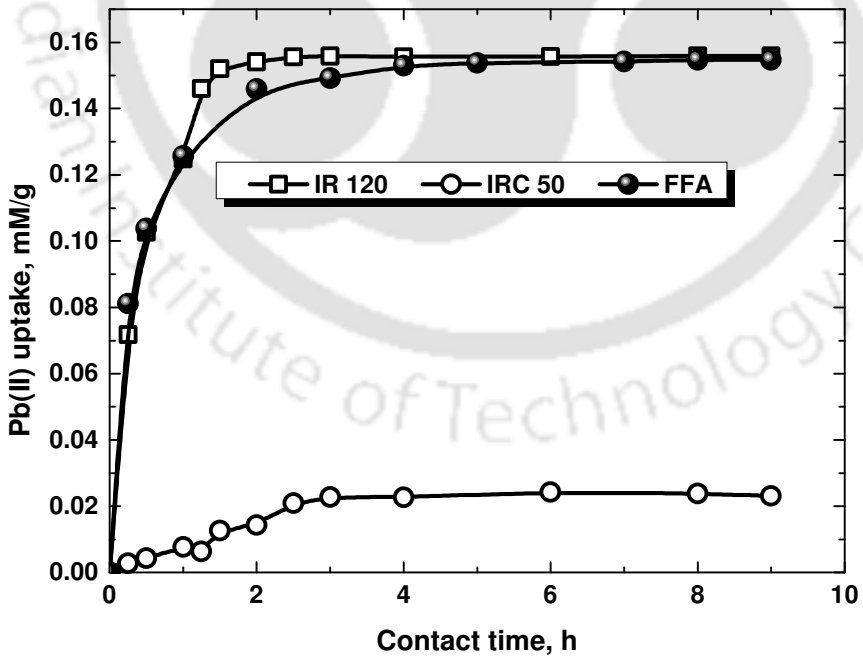

Figure 3.15: Pb(II) uptake as a function of contact time [Pb(II) 0.157 mM, adsorbent dose 1 g/L, pH 5.0, temperature 30°C, 180 rpm].

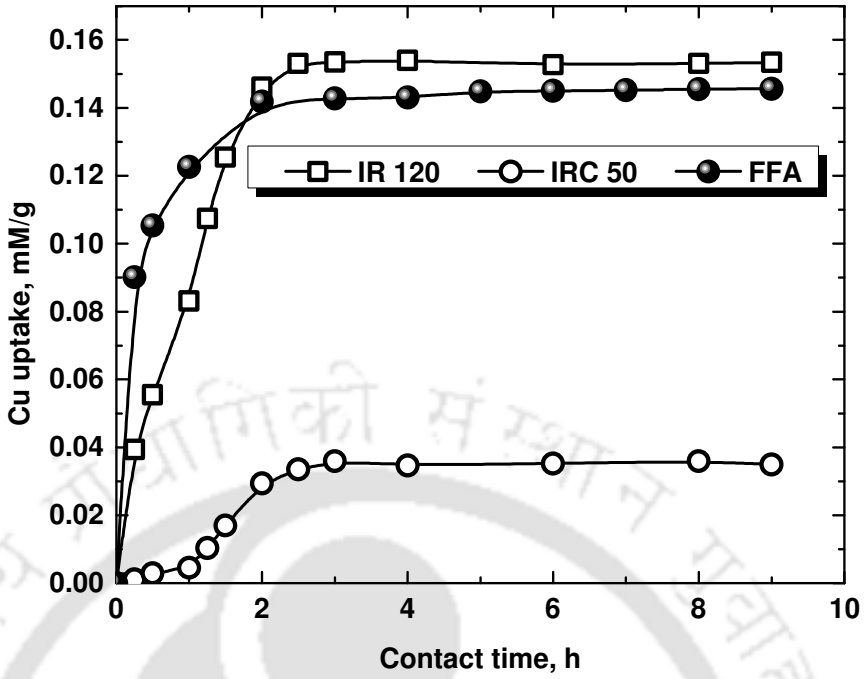

Figure 3.16: Cu(II) uptake as a function of contact time [Cu(II) 0.157 mM, adsorbent dose 1 g/L, pH 5.0, temperature 30°C, 180 rpm].

The kinetic data of the Pb(II) removal was analyzed using two sorption kinetic models viz. pseudo-first order and Pseudo-second-order. The theory of sorption kinetic models is described below.

***Pseudo first order kinetic model*:** The Lagergren first-order rate expression [267] is generally expressed as follows (Eq. 3.1).

$$\frac{dq}{dt} = k_1 (q_e - q) \tag{3.1}$$

Integrating this equation (Eq. 3.1) with the boundary conditions ($t = 0$, $q = 0$, and at $t = t$, $q = q_t$), Eq. 3.2 is obtained.

$$q_t = q_e\left(1 - e^{-k_1 \times t}\right) \tag{3.2}$$

This can be presented in linear form as in Eq. 3.3.

$$\ln(q_e - q_t) = \ln q_e - k_1 \times t \tag{3.3}$$

Where, q_t (mg/g) is uptake of FFA at time 't', q_e (mg/g) is equilibrium uptake, k_1 (1/min) is first order rate constant and 't' is time (min).

***Pseudo-second-order kinetic model*:** The pseudo second order model [268] can be expressed as in Eq. 3.4.

$$\frac{dq}{dt} = k_2 (q_e - q)^2 \tag{3.4}$$

Integrating Eq. 3.4 with the boundary conditions ($t = 0$, $q = 0$, and at $t = t$, $q = q_t$), Eq. 3.5 is obtained.

$$q_t = \frac{k_2 q_e^2 t}{1 + k_2 q_e t} \tag{3.5}$$

Where, q_t (mg/g) is the metal uptake of FFA at time 't', q_e (mg/g) is the equilibrium uptake, k_2 is the second order rate constant (g/mg.min), and t is time (min).

The Pb(II) uptake behavior was studied through kinetic models viz. pseudo first order (Eq. 3.3) and pseudo second order (Eq. 3.5) and is presented in Fig. 3.17. It can be seen that the pseudo second order model well predicted the equilibrium uptake capacity (correlation coefficient 0.99). It implies that chemical sorption to be the rate limiting step for the adsorption of Pb(II) onto FFA [269].

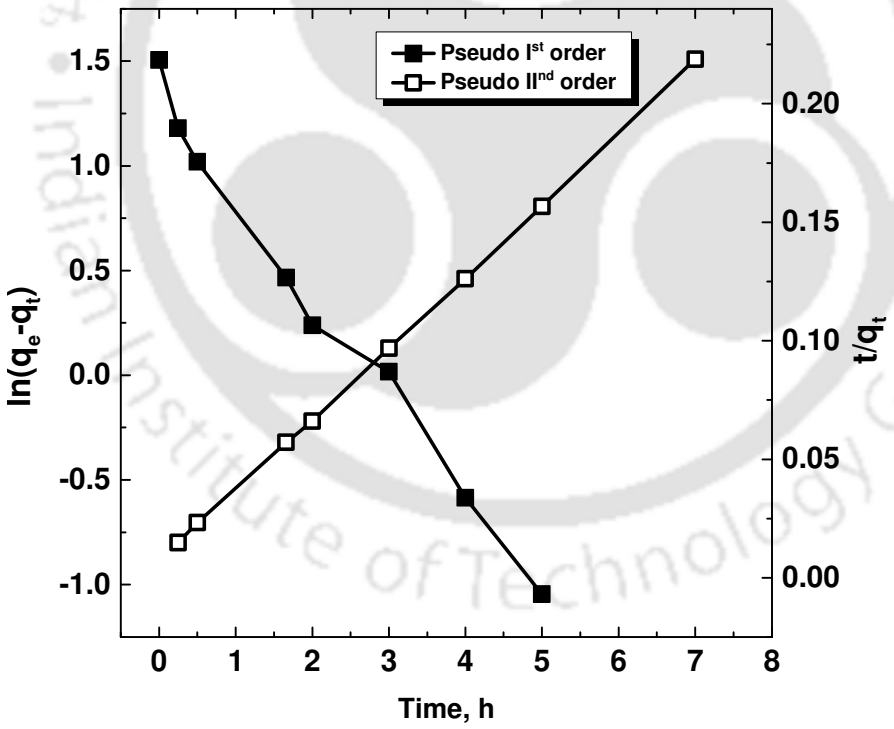

Figure 3.17: Goodness of fit of sorption kinetic models for Pb(II) uptake by FFA [Pb(II) 32 mg/L (0.157 mM), FFA dose 1 g/L, pH 5.0, temperature 30°C, 180 rpm].

3.2.3.3 Equilibrium isotherm study

The results of equilibrium isotherm study at varying IR120 and FFA dosages on Pb(II) and Cu(II) removals are shown in Fig. 3.18(a) and (b), respectively. It can be observed that the removal efficiency was increased with the increase in adsorbent or resin dose. Pb(II) removal efficiency was 42 and 57% at 0.2 g/L of IR120 and FFA, respectively. However, the complete removal of Pb(II) was observed at a dosage of 1.4 g/L of either adsorbent or resin. Cu(II) removal efficiency was 51 and 53% at 0.2 g/L of IR120 and FFA, respectively. Complete removal of Cu(II) was observed at 1.8 g/L of IR120 as well as at a dosage of 2.0 g/L of FFA. It shows that at low dosage (0.2 g/L) of IR120, efficiency on Cu(II) removal (51%) was far better than Pb(II) removal (42%). However, metals removal efficiency differed only by 4% at the lowest dose of 0.2 g/L of FFA. Furthermore, complete removal of both the metals could be achieved using IR120 or FFA at a dosage below 2.0 g/L. It is obvious to observe the improvement in removal efficiency at higher dose, due to the increasing number of available metal sorption sites.

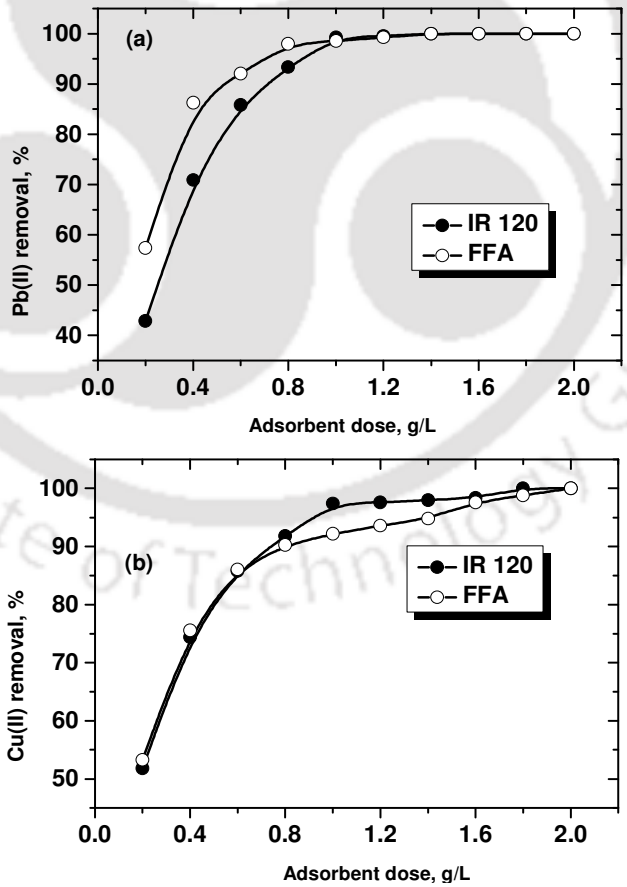

Figure 3.18: Effect of adsorbent dose on (a) Pb(II) and (b) Cu(II) removal efficiency [Pb(II) or Cu(II) 0.157 mM, contact time 5 h, pH 5.0, temperature 30°C, 180 rpm].

Among various adsorption isotherms, the experimental data were fitted well to Langmuir and/or Freundlich isotherms. Brief introduction and linear forms of Langmuir and Freundlich isotherm models are presented below.

The Langmuir isotherm is expressed as in Eq. 3.6.

$$q_e = \frac{bq_m C_e}{1+bC_e} \quad \text{(Non-linear form)} \tag{3.6}$$

Where, b (l/mg) is the Langmuir isotherm constant, C_e (mg/L) is the equilibrium metal concentration, and q_m is the maximum monolayer metal uptake. Eq. 3.7 shows the linearized form of Eq. 3.6. The Langmuir constants, q_m and b were determined from the slope and intercept of the best fit plot (Eq. 3.7) of the experimental data.

$$\frac{1}{q_e} = \frac{1}{q_m} + \frac{1}{q_m bC_e} \tag{3.7}$$

Freundlich isotherm is derived to model the multilayer sorption on heterogeneous surfaces and is formulated as show in Eq. 3.8.

$$q_e = K_f C_e^{1/n} \text{ (Non-linear form)} \tag{3.8}$$

Where, q_e (mg/g) is the adsorption capacity, C_e (mg/L) is the equilibrium solute concentration, and K_f and 1/n are the measure of adsorption capacity and adsorption intensity. The values of the empirical constants, i.e. 1/n and K_f were found out from the slope and intercept of the best fit line (Eq. 3.9) of the experimental data.

$$\ln q_e = \frac{1}{n}\ln C_e + \ln K_f \tag{3.9}$$

It can be seen that Cu(II) removal by IR120 and FFA fitted well to both Freundlich as well as Langmuir isotherms. However, Pb(II) removal data fitted better to the Freundlich isotherm. The maximum adsorption capacity was estimated through Langmuir isotherm, which is practical limiting capacity of the adsorbent. The goodness of the fitting is illustrated in Fig. 3.19 and, the values of isotherm constants are given in Table 3.3. It can be seen that FFA showed little higher adsorption capacity (q_m) for Cu(II) over IR120. However, it was 1.41 times that of IR120 for Pb(II). Both IR120 and FFA showed higher adsorption capacity for Cu(II) than Pb(II) as per its electronegativity character [Cu(1.8) > Pb(1.6)] [270]. The Freundlich constant 'n' was higher in Pb(II) removal than that of Cu(II)

for both FFA and IR120 indicating greater affinity and stronger bond of Pb(II) with adsorbent/resin [271].

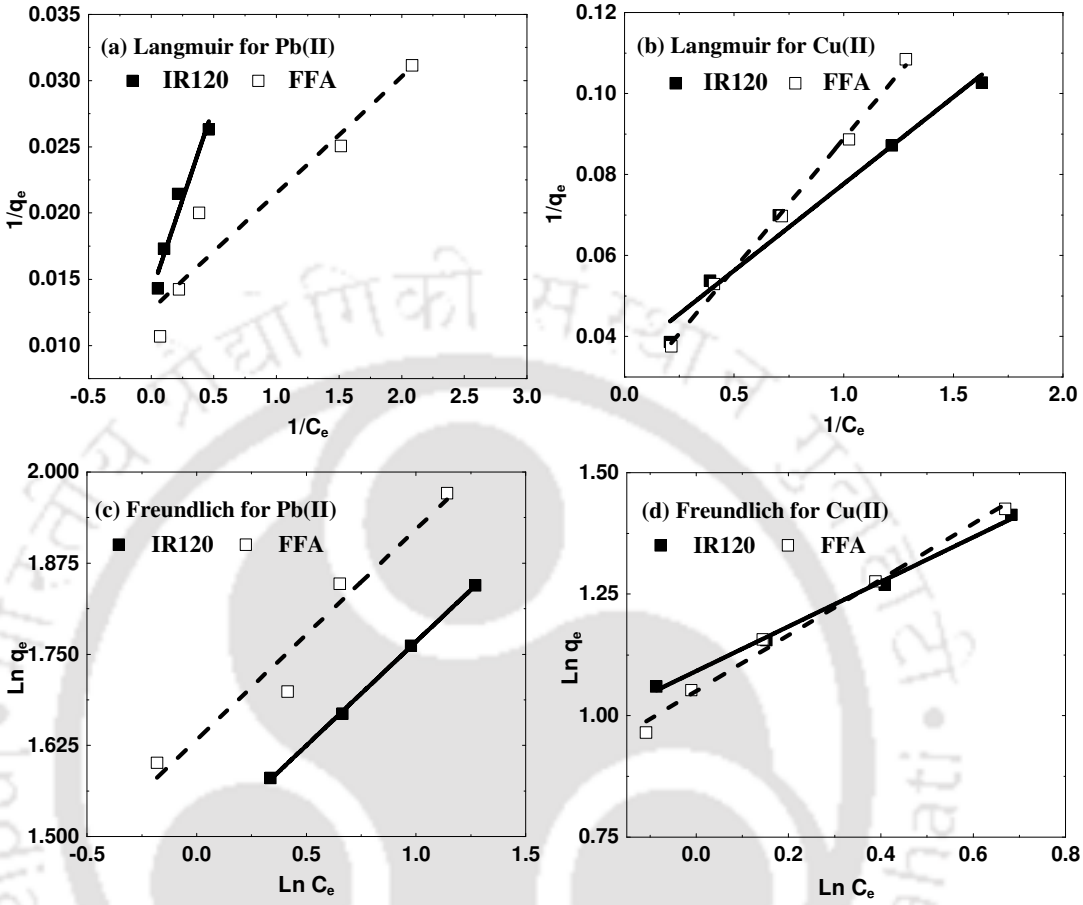

Figure 3.19: Isotherm fitting of Pb(II) and Cu(II) removal by FFA and IR120 (a) Langmuir for Pb(II) (b), Langmuir for Cu(II), (c) Freundlich for Pb(II) and, (d) Freundlich for Cu(II) [Pb(II) or Cu(II) 0.157 mM, equilibrium time 5 h, resin/adsorbent dose 0.2–2 g/L, pH 5.0, temperature 30°C, 180 rpm].

Table 3.3: Langmuir and Freundlich isotherm constants for Pb(II) and Cu(II) uptake in the mono metal system [Pb(II) or Cu(II) 0.157 mM, equilibrium time 5 h, adsorbent dose 0.2–2 g/L, pH 5.0, temperature 30°C, 180 rpm].

Metal	Adsorbent	Langmuir parameters			Freundlich parameters		
		b, L/mM	q_m, mM/g	R^2	K_f	n	R^2
Pb(II)	IR120	31.1	0.346	0.92	30.37	3.51	0.99
	FFA	91.4	0.38	0.88	42.95	3.46	0.92
Cu(II)	IR120	167	0.452	0.97	12.34	2.17	0.99
	FFA	79.2	0.64	0.99	11.23	1.74	0.98

It also can be seen that the adsorption capacity of FFA was comparable to other commercial resins and low-cost adsorbents with similar experimental condition (Table 3.4). The BET surface area of PSDC resin and the total concentration of –COOH and –OH were 21.43 m^2/g and 1.06 mM/g which showed the uptake capacity of 1.87, 1.57, and 1.46 mM/g (Table 3.4) for Pb(II), Cu(II), and Ni(II), respectively [272]. PSED resin [152], silkworm chitosan [6], and peanut husk [136] contain –COOH groups in common and, the ion exchange is to be the sole or one of the metal removal mechanisms. In comparison, FFA showed a comparable adsorption capacity of 0.95 and 0.39 mM/g for Pb(II) and Cu(II), respectively.

Table 3.4: Comparison of adsorption capacities of various commercial resins and low-cost adsorbents with FFA.

Adsorbent or Resin	**Metal studied**	**Mechanism of adsorption**	**Dose, g/L**	**Adsorption capacity, mM/g**	**Source**
Amberlite IR 120	Cr(III)	Ion exchange	5	1.3	[273]
Amberlite IR 120	Cu(II)	Ion exchange	5	0.34	[274]
	Pb(II)	Ion exchange		0.90	
Amberlite IR 120	Pb(II)	Ion exchange	5	0.01	[262]
Dolomite	Pb(II)	chemisorption		0.21	
Amberlite IR 120	Cu(II)	Ion exchange	10	1.66	[275]
Synthesized PSDC resin	Pb(II)	Physical and chemical adsorption	1	1.87	[272]
	Cu(II)			1.57	
	Ni(II)			1.46	
Polystyrene-supported ethylenediaminediaceti c acid resin (PSED)	Cu(II)	Chemisorption	4	3.85	[152]
	Ni(II)			3.76	
	Zn(II)			3.6	
	Pb(II)			0.96	
Silkwarm chitosan	Pb(II)	NA	1	0.41	[6]
	Cu(II)			1.13	
IDA-chelating resin	Cu(II)	Chemical interaction	1	2.27	[270]
	Pb(II)			1.27	
	Cd(II)			0.65	
Sawdust	Pb(II)	NA	1	0.10	[136]
	Cu(II)			0.10	
Modified peanut husk	Pb(II)	NA	1	0.14	
	Cu(II)			0.16	
FFA	Pb(II)	Ion exchange	1	0.95	Present study
	Cu(II)			0.39	
IR 120	Pb(II)	Ion exchange	1	1.8	
	Cu(II)			1.5	

3.2.3.4 Influence of EDTA and co-occurring ions on metal uptake

EDTA is a multidentate ligand having two nitrogen groups, which can form the complex with the divalent metal ions. A divalent metal ion can be bonded with a maximum of three EDTA molecules, which makes metal complexes more stable. The studies on Pb(II) and Cu(II) removal by FFA in the presence of EDTA were carried out as outlined earlier and, the results are shown in Fig. 3.20.

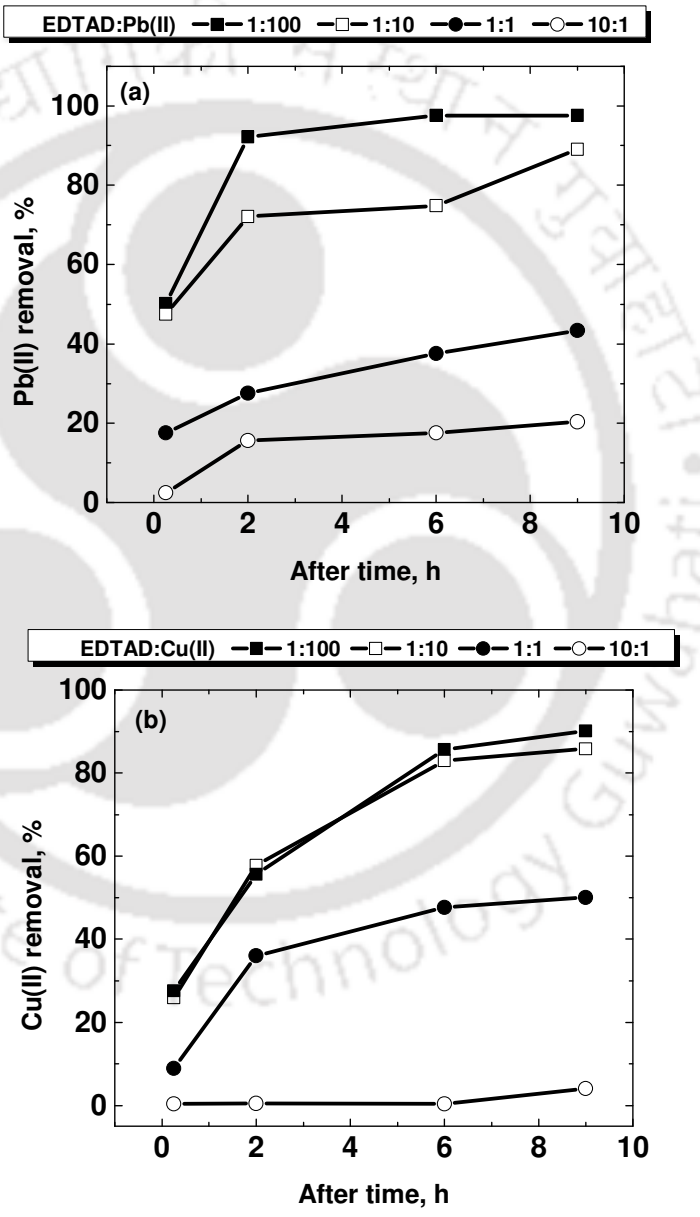

Figure 3.20: (a) Pb(II) and (b) Cu(II) removal efficiency at different concentrations of EDTA [Pb(II) or Cu(II) 0.157 mM, adsorbent dose 1 g/L, contact time 5 h, pH 5.0, temperature 30°C, 180 rpm].

It can be seen that the removal of Pb(II) and Cu(II) by FFA remained unaffected at EDTA: metal ratio of 1:100, the reason for that was an abundance of free metal ions with such a low EDTA concentration, also acidic sites on FFA were able to adsorb metal ions. Pb(II) removal reduced a little with the increase in EDTA concentration. Further increase in molar ratio resulted in lower Pb(II) removal efficiency and only 43 and 20% removal was achieved in molar ratios of 1:1 and 10:1. However, it was only 50 and 4% for Cu(II). The reason can be explained on the basis of speciation of Pb(II) and Cu(II) and their tendency to form complexes with EDTA. Furthermore, the metal with a lower atomic number forms more stable complex with EDTA than the metal with a higher atomic number [264], hence Cu(II) removal got affected much. The removal efficiency of Pb(II) was higher than that of Cu(II) in all the binary system experiments. It was also because of ionic properties of Pb(II) and Cu(II) (Table 3.5) as outlined in the study of binary system. Similar results for metal removal by Amberlite IR120 are also reported elsewhere [276].

Table 3.5: Ionic properties of Pb(II) and Cu(II) [277, 278].

Parameter	**Cu(II)**	**Pb(II)**
Ionic radius, A°	0.73	1.19
Hydrated radius, A°	4.19	4.01
Hydration energy, kJ/mol	2100	1481
Electronegativity[a]	1.9	2.33

[a] Pauling electronegativity

The speciation of Pb(II) and Cu(II) in the presence of EDTA with different molar ratios was studied using the MINTEQ software, and the results are presented in Fig. 3.21. Fig. 3.21a shows that Pb^{2+} species was abundant, precisely 99.71, 98.7 and 89.7% when the molar ratio of EDTA: Pb(II) was 0:1, 1:100 and 1:10, respectively. Other species such as $PbOH^{+}$, $PbEDTA^{2-}$ and $PbHEDTA^{-}$ were less than 1% of the former. However, the concentration of $PbEDTA^{2-}$was increased to 10% lowering Pb^{2+}at the latter case. The further increase of EDTA concentration in molar ratios 1:1 and 10:1 completely reduced the available Pb^{2+} species and, but 99% of $PbEDTA^{2-}$ was present. Similarly, the speciation of Cu(II) shown in Fig. 3.21b shows that 99.6, 98 and 89% Cu^{2+} was present in 0:1, 1:100 and 1:10 molar ratios and, $CuEDTA^{2-}$ species was abundant in 1:1 and 10:1 molar ratios with no availability of Cu^{2+}.

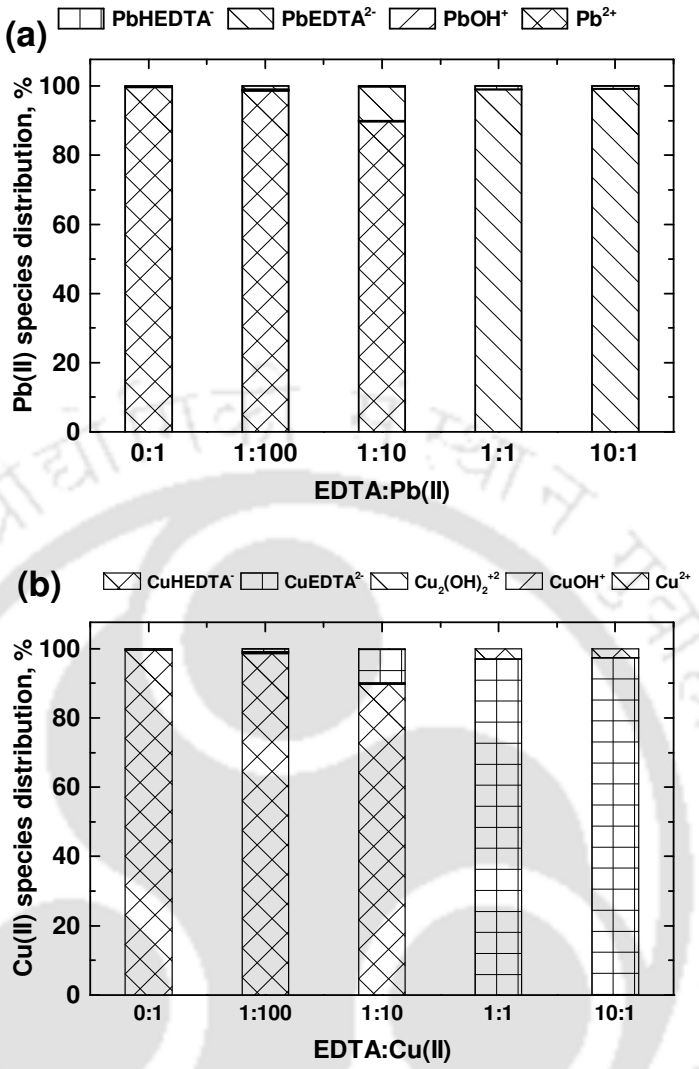

Figure 3.21: Speciation of (a) Pb(II) and (b) Cu(II) at different EDTA: metal molar ratios [Cu(II) or Pb(II) 0.157 mM, pH 5.0 and temperature 30°C].

The effects of co-occurring cations on the removal of metals by FFA and IR120 were studied, and results are presented in Fig. 3.22. The Cu(II) removal efficiency was affected much when compared with Pb(II) in the presence of Ca^{2+} and Na^{+}. Pb(II) removal remained unaffected for both FFA and IR120 having a higher affinity of adsorption. Cu(II) removal efficiency was reduced by 13, 4% and 21, 10% in presence of Ca^{2+}, Na^{+} using FFA and IR120, respectively.

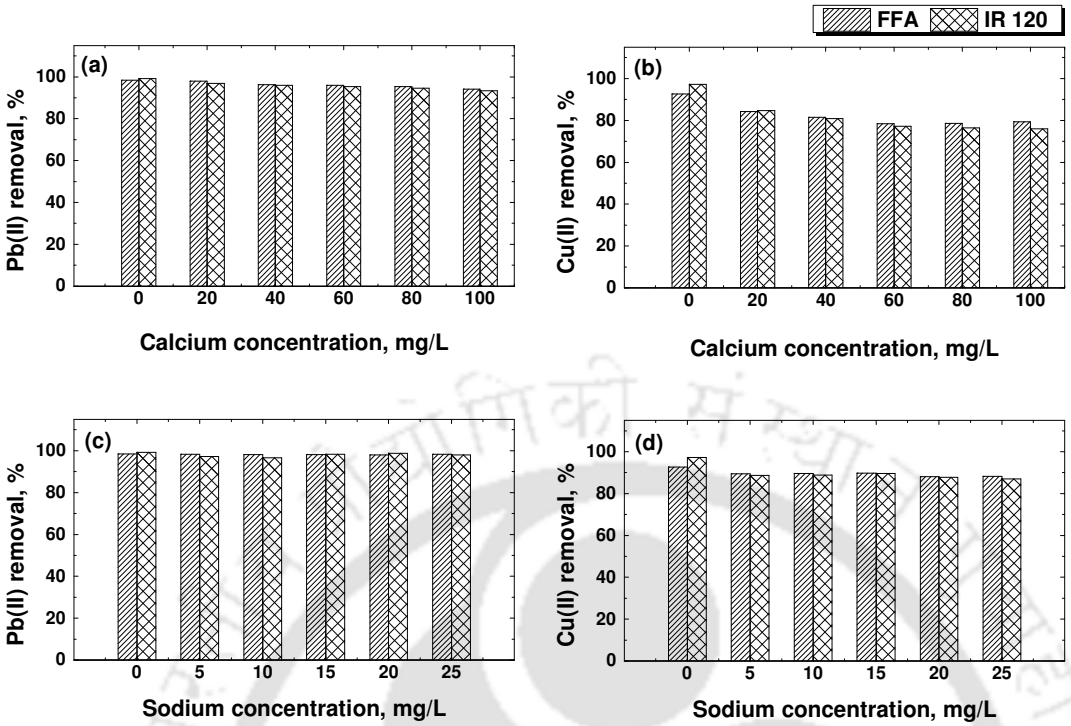

Figure 3.22: Effects of Ca^{2+} (a and b) and Na^{+} (c and d) ions on metal removal efficiency by FFA and IR 120 [Pb(II) or Cu(II) 0.157 mM, corresponding anion concentration Cl^{-} 0–177 mg/L, NO_3^{-} 0–67.5 mg/L, adsorbent dose 1 g/L, pH 5.0, temperature 30°C, 180 rpm].

3.2.3.5 Pb(II) and Cu(II) removal in binary metal system

In the binary metal system, an equimolar (0.0785 mM) solution of Pb(II) and Cu(II) was employed to study the influence of co-existing metal cations on their removal efficiencies. The results are shown in Figs. 3.23a and 3.23b. Both IR120 and FFA exhibited higher affinity for Pb(II) than Cu(II). Pb(II) removal of more than 99% was found in both the cases. Cu(II) removal efficiency was 97 and 92% in the mono metal system which reduced to 86 and 88% in the binary system, respectively by IR120 and FFA. Hence, the overall metal removal efficiency was lesser when compared to mono metal.

In the binary system, each metal competes for the same site, which is also dependent on its ionic properties such as hydration energy, hydrated radius, and electronegativity. Hydration energy plays an important role in metal ion hydrolysis. During metal ion hydration, water ligands present in the inner coordination sphere of a metal ion are replaced by hydroxogroup, so, the metal ion having lesser hydration energy can be preferentially removed [245]. Hydration energy of Pb(II) is lower than Cu(II). Also, the ionic radius of

Pb(II) is greater than that of Cu(II), and it could lose the outer hydration sphere and, could have greater accessibility to the surface of certain adsorption sites than Cu(II). The ionic properties are given in Table 3.5. Pb(II) has a smaller hydrated radius and can be attached to these functional groups easily [277-279]. These ionic properties resulted in a preferential removal of Pb(II) over Cu(II) in the binary system. In the binary system, the removal efficiency, as well as the rate of Pb(II) removal was observed to be higher than that of Cu(II). The higher affinity of Pb(II) can also be explained on the basis of hard and soft acids and bases theory.

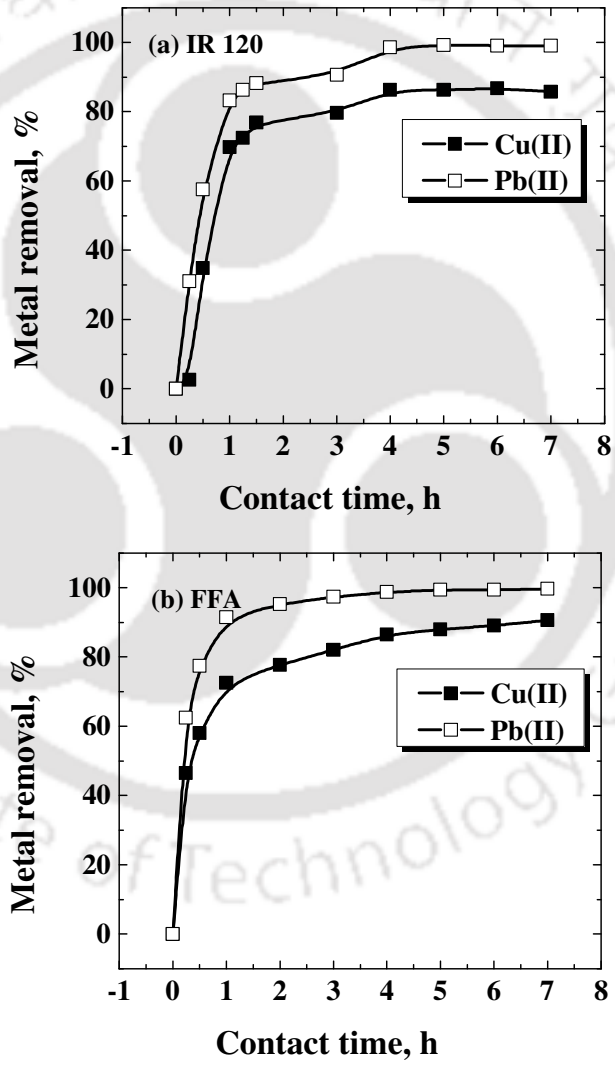

Figure 3.23: Metal removal efficiency of (a) IR120 and (b) FFA in binary system [Pb(II) and Cu(II) 0.0785 mM each, adsorbent dose 1 g/L, pH 5.0, temperature 30°C, 180 rpm].

Table 3.6: The selectivity factors for Pb(II) over other metal ions.

M(II)	D_{Pb}		D_M		α_M^{Pb}	
	FFA	**IR120**	**FFA**	**IR120**	**FFA**	**IR120**
Cu(II)	26.33	29.68	2.62	2.84	10.03	10.42
Mg(II)	23.64	541.17	0.82	2.59	28.64	208.70
Zn(II)	17.48	649.60	1.14	204.35	15.28	3.17
Cd(II)	31.85	405.63	3.04	219.58	10.45	1.84
Mn(II)	08.91	153.90	1.85	358.79	04.81	0.42
Fe(II)	16.67	649.60	1.00	122.83	16.55	5.28
Co(II)	15.76	812.26	0.95	230.57	16.51	3.52
Ni(II)	11.75	324.30	0.37	91.15	31.44	3.55
Hg(II)	44.18	80.32	7.28	2.78	06.06	28.88

The carboxylic and sulfonic groups are hard Lewis bases, and Pb(II) is borderline hard Lewis acid, whereas Cu(II), is soft Lewis acid. Hence, being a hard acid, Pb(II) showed a greater attraction than Cu(II) towards the hard basic functional groups [272]. It was also found that FFA was highly selective (Eq. 2.9) towards Pb(II) removal irrespective to the other metal ions (M(II)) present in the solution (Table 3.6). However, IR120 exhibited a higher selectivity for Pb(II) uptake only in the case of Mg(II) and Hg(II) binary systems.

3.2.4 Performance of FFA and CAC in Pb(II) removal

In order to compare the performance of FFA and CAC, the Pb(II) uptake capacities were determined, and the results are shown in Fig. 3.24. It was observed that FFA showed higher uptake capacity at the elevated initial concentration due to stronger driving force between the bulk solution and active sites on FFA. In case of CAC, the uptake capacity was improved when the initial concentration of Pb(II) was increased. However, beyond 125 mg/L, the increment was insignificant, indicating the exhaustion of CAC. Whereas, the uptake capacity of FFA was increased almost linearly untill the highest initial concentration of 200 mg/L. Pb(II) uptake of 92 mg/g FFA was increased by 31% by increasing the initial concentration from 125 to 200 mg/L. The uptake capacities of FFA and CAC with 200 mg/L initial concentration of Pb(II) were 118.66 and 56.79 mg/g, respectively. The results of this study imply fairly high capacity and significant superiority of FFA over CAC in Pb(II) removal.

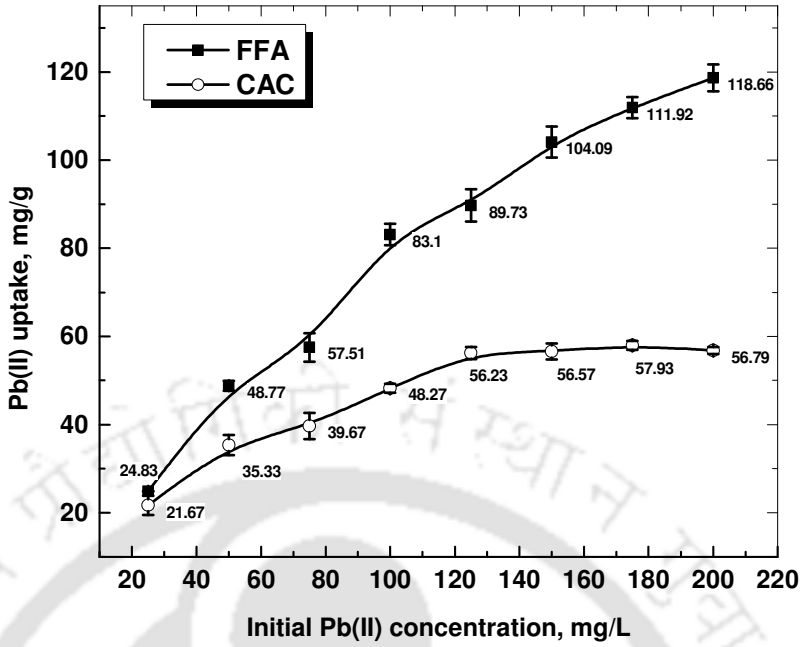

Figure 3.24: Maximum Pb(II) uptake capacities at different initial concentrations [initial Pb(II) concentration 25 to 200 mg/L, adsorbent dosage 1 g/L, agitation speed 180 rpm, temperature 30°C, contact/ equilibrium time 5 h].

3.2.5 FFA exhaustion and regeneration

The exhaustion study using FFA in the removal of Pb(II) from synthetic solution was performed and, the results are shown in Fig. 3.25.

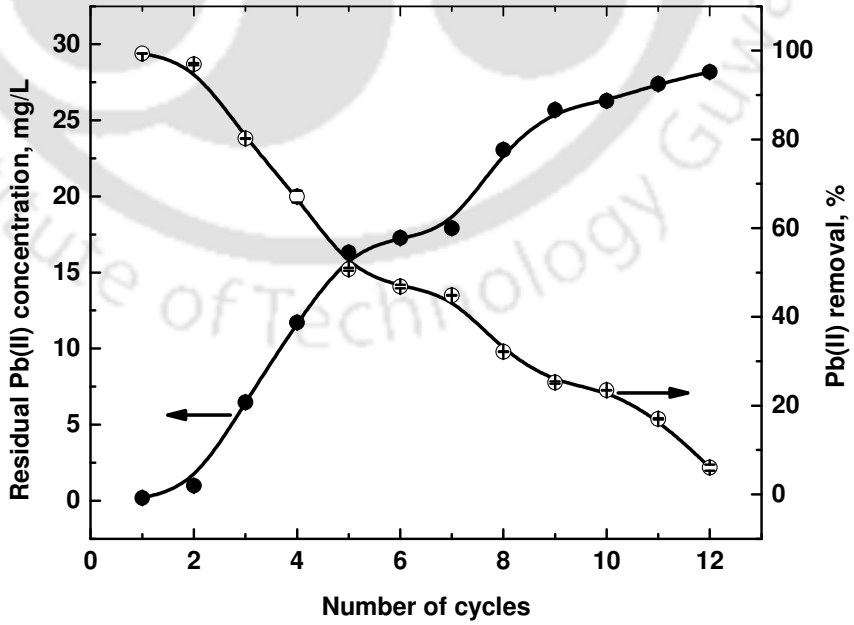

Figure 3.25: Removal of Pb(II) in cyclic batch adsorption study by FFA [Pb(II) 32 mg/L (0.157 mM), FFA dose 1 g/L, temperature 30°,C and agitation speed 180 rpm].

It can be seen that in first adsorption cycle almost 100% Pb(II) was removed from an initial concentration of 32 mg/L (0.157 mM). The Pb(II) removal continued in the second cycle also, with little decrease wherein removal of 97% was achieved. Second cycle onwards, after every cycle, gradual decrease in Pb(II) removal was observed. Removal of Pb(II) became insignificant after 12 cycles. This capacity of FFA rendered its applicability especially in a continuous mode of operation for ground applications [280]. Almost the whole amount of FFA used in the adsorption study was recoverable. So the mass loss due to repeated washing and drying was found to be insignificant (< 1 % in 12 cycles).

The desorption efficiency of Pb(II) from the spent FFA using 0.1 N H_2SO_4, HCl and HNO_3 was determined and the results are shown Fig. 3.26a.

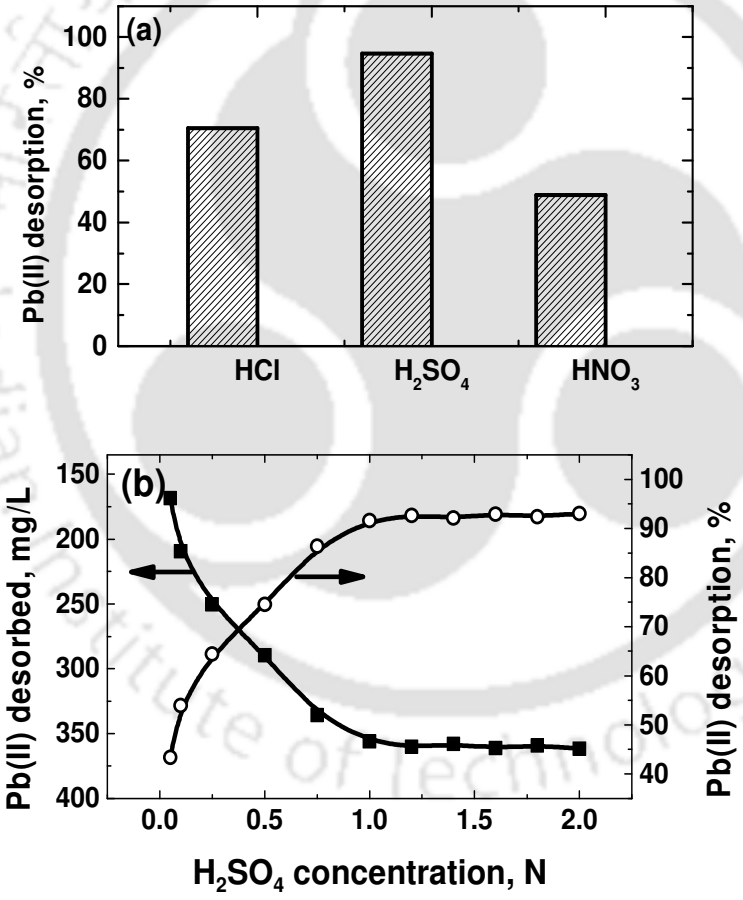

Figure 3.26: Regeneration of (a) spent FFA collected after 1st cycle using 0.1 N acid solution [initial metal loading 32 mg/g spent FFA, FFA dose 2 g/L, desorption time 30 min, temperature 30°C, 180 rpm] and (b) exhausted FFA collected after 12th cycle using H_2SO_4 at different concentration [initial metal loading 194.5 mg/g exhaust FFA, FFA dose 2 g/L, desorption time 30 min, temperature 30°C, 180 rpm].

It can be seen that H_2SO_4 outperformed HCl and HNO_3 for FFA regeneration and, Pb(II) desorption efficiency was 95, 70 and 49%, respectively, from an initial Pb(II) loading of 32 mg/g spent FFA. Henceforth, H_2SO_4 was further used for the regeneration of exhaust FFA with an initial Pb(II) loading of 194.5 mg/g collected after the 12th cycle of cyclic adsorption studies using the same FFA. H_2SO_4 concentration was varied from 0.05 to 2 N and, the results are presented in Fig. 3.26b. The desorption efficiency of Pb(II) was increased from 43 to 92% with the increase in the concentration of H_2SO_4 from 0.05 to 1 N within 30 min., i.e., at a higher proton concentration [275]. It can be seen that a concentration of 0.1 N H_2SO_4 could regenerate 54% active sites, which were 71% more for the exhaust FFA compared to the spent FFA. However, only 8% of the active sites could not be regenerated even at >1 N H_2SO_4.

3.2.6 Proton sorption model and Pb(II) binding

3.2.6.1 Development of dual-site proton adsorption (DSPA) model

FFA predominantly contains two acidic sites i.e. carboxylic and sulfonic groups (as outlined in sections 3.1.3 & 3.6). The dissociation reaction of carboxylic acid can be written as in Eq. 3.10 [219].

$$\equiv \mathrm{COOH} \leftrightarrow \equiv \mathrm{COO^-} + \mathrm{H^+} \tag{3.10}$$

Where, the symbol "≡" indicates the surface of the adsorbent to which the functional groups are attached, $\equiv \mathrm{COOH}$ and $\equiv \mathrm{COO^-}$ are protonated and dissociated carboxylic acid at equilibrium.

The acid dissociation constant K_1 (M) can be expressed as in Eq. 3.11.

$$K_1 = \frac{[\equiv \mathrm{COO^-}][\mathrm{H^+}]}{[\equiv \mathrm{COOH}]} \tag{3.11}$$

The total concentration of carboxylic sites (N_1, M) at any point of time can be given as (Eq. 3.12):

$$N_1 = [\equiv \mathrm{COOH}] + [\equiv \mathrm{COO^-}] \tag{3.12}$$

The equilibrium protonated carboxylic site concentration can be expressed as in Eq. 3.13 by rearranging Eq. 3.11 and 3.12.

$$[\equiv \mathrm{COOH}] = N_1 \left[\frac{[\mathrm{H^+}]}{[\mathrm{H^+}]+K_1}\right] \tag{3.13}$$

Similarly, for protonated sulfonic site as is in Eq. 3.14.

$$[\equiv SO_3H] = N_2\left[\frac{[H^+]}{[H^+]+K_2}\right] \quad (3.14)$$

Hence, the total pronated acidic site concentration ($N_{P,total}$, mol/g) is given by Eq. 3.15.

$$N_{P,total} = N_1\left[\frac{[H^+]}{[H^+]+K_1}\right] + N_2\left[\frac{[H^+]}{[H^+]+K_2}\right] \quad (3.15)$$

The equilibrium metal (M^{2+}) adsorption in solution can be described as

$$\equiv COO^- + M^{2+} \leftrightarrow \equiv COOM^+ \quad (3.16)$$

The metal binding constant, K_{M1} can be written as (Eq.3.17)

$$K_{M1} = \frac{[\equiv COOM^+]}{[\equiv COO^-][M^{2+}]} \quad (3.17)$$

Further, the concentration carboxylic group in presence of M^{2+} (with M^{2+} binding) can be expressed as in Eq. 3.18

$$N_1 = [\equiv COOH] + [\equiv COO^-] + [COOM^+] \quad (3.18)$$

Eq. 3.19 can be obtained by substituting $[\equiv COOH]$ and $[\equiv COO^-]$ from Eq. 3.13 and 3.17

$$N_1 = [COOM^+]\left[\frac{K_1K_{M1}[M^{2+}]+[H^+]+K_1}{K_1K_{M1}[M^{2+}]}\right] \quad (3.19)$$

Similarly for sulfonic site and total metal attached to both the sites q_e, (mol/g) can be expressed as Eq. 3.20

$$q_e = \left[\frac{N_1K_1K_{M1}[M^{2+}]}{K_1K_{M1}[M^{2+}]+[H^+]+K_1}\right] + \left[\frac{N_2K_2K_{M2}[M^{2+}]}{K_2K_{M2}[M^{2+}]+[H^+]+K_2}\right] \quad (3.20)$$

3.2.6.2 Evaluation of DSPA model in Pb(II) binding

Protonation characteristics of FFA were obtained from the difference between the bulk proton concentration with and without FFA. The experimental details on potentiometric titrations of FFA are provided in Section 2.4.3.4 (Chapter 2). FFA usually stabilizes the solution pH around 3.2. The different equilibrium pH (Figs. 3.27 and 3.28)

was adjusted through repeated addition of either 6 N H_2SO_4 or NaOH. The related results with the potentiometric titration of FFA and RH are also provided in Section 3.2.1.4 of this Chapter. The acidic sites concentration was determined using DSPA model given by Eq. 3.15. K_1, K_2 and N_1, N_2 refer to dissociation constants and total number (mol/g) of each functional group. The model constants were estimated by fitting the results obtained in potentiometric titration using GRG nonlinear regression analysis (solver tool of Microsoft Office Excel 2013). The experimental and model fitted (R-squired value of 0.98) values of N_p (mol/g) are presented in Fig. 3.27. The model showed an excellent agreement with the experimental data. The FFA was containing two major functional groups with pK_{a1} and pK_{a2} values of 3.21 and 1.62, respectively, corresponding to strongly acidic groups [254]. The surface functional groups possess the same pK_a values as of their organic acids and; pK_{a1} and pK_{a2} could be assigned to carboxylic and sulfonic groups, respectively [254, 281]. The total concentration of carboxylic groups was 25% lesser than that of sulfonic groups and it was calculated to be 1.53×10^{-3} and 2×10^{-3} mol/g. Availability of a particular acidic site for metal adsorption is dependent upon protonation and deprotonation which in turn is a function of pH. Percentage distribution of protonated sites at various solution pH is shown in Fig. 3.28. With rise in pH, protonation of sulfonic sites decreased and that of carboxyl sites increased. Weakly acidic carboxylic group (pK_{a1} 3.21) were available partially (protonated 40-50%) for Pb(II) binding below pH 3.2 from synthetic solution. Whereas rise in pH above 3.21 enriched protonated site concentration and thereby increasing available Pb(II) sorptive sites. Availability of carboxylic sites for Pb(II) binding was higher than sulfonic sites at pH > 1.2. Sulfonic sites were available partially for Pb(II) removal, particularly at higher proton concentration (Fig. 3.28). Similar results for contribution of sulfonate groups to heavy metal biosorption are reported [126]. They found that the contribution of sulfonate groups in heavy metal removal was little but could be significant at higher proton concentration.

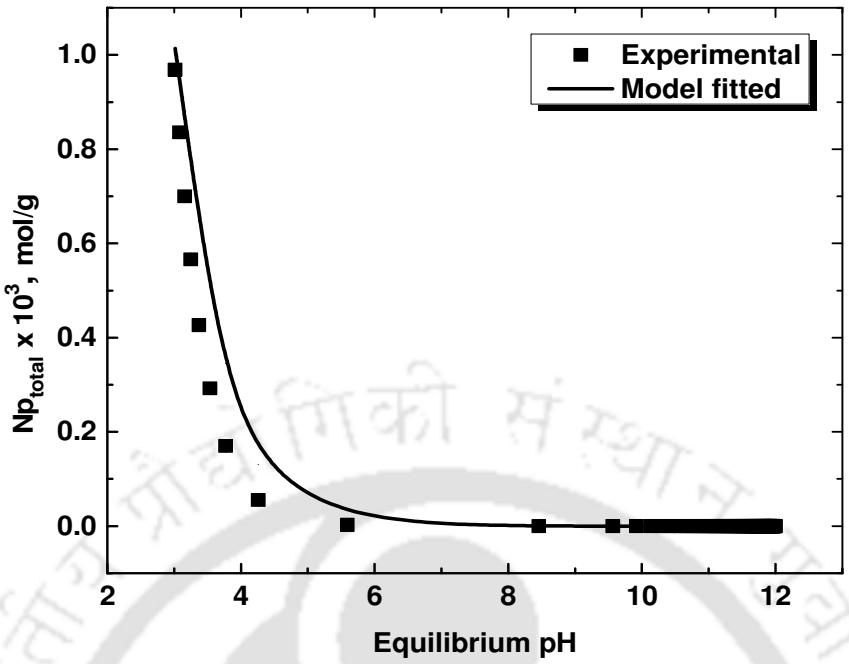

Figure 3.27: Determination of acid dissociation constants using DSPA model (Eq. 3.15) in absence of Pb(II) [FFA dosage 1 g/L, 180 rpm, 30°C) from potentiometric titration and model fitting (RMSE 6.01×10^{-5}, SD 3.61×10^{-9}, SSE 2.56×10^{-7}].

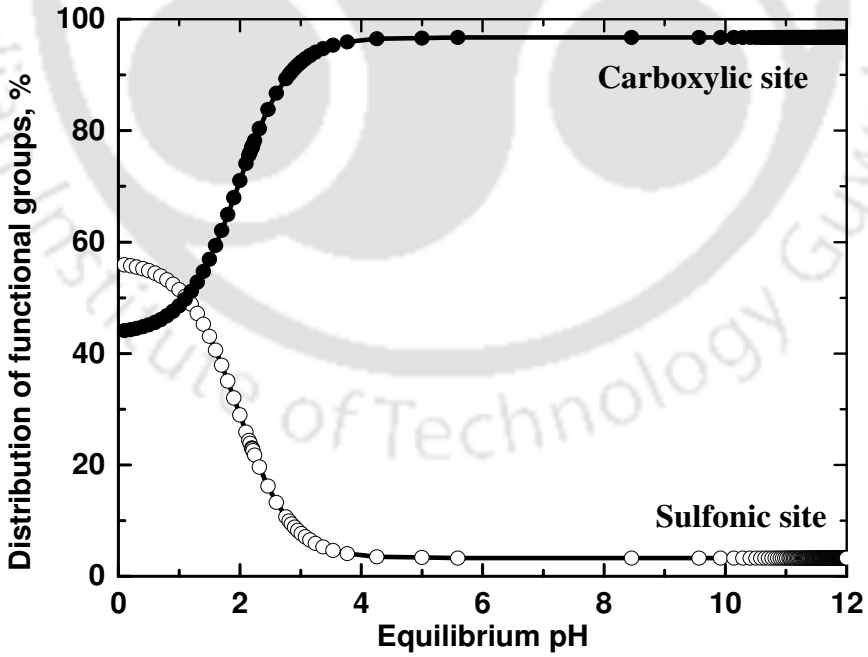

Figure 3.28: Percentage distribution of protonated carboxylic and sulfonic sites in titrated pH range obtained from Fig. 3.27.

Equilibrium binding model (Eq. 3.20) was employed to reveal the binding nature of Pb(II) with functional sites. Pb(II) removal data at different equilibrium pH was fitted to find out Pb(II) binding constants of K_{M1} and K_{M2} for carboxylic and sulfonic sites, respectively. The model exhibited great agreement with the experimental results (Fig. 3.29). K_{M1} and K_{M2} were found to be 5.20×10^{6} and 28.11 L/mol, respectively. Fig. 3.30 shows contribution of carboxylic and sulfonic group for Pb(II) binding. It can be observed that at all pH values carboxylic group was mostly involved in Pb(II) binding and sulfonate group exhibited negligible Pb(II) uptake. Removal of Pb(II) was because of its strong affinity towards carboxylic group. Sulfonic groups gave only an uptake of 6.4 mg/g (0.031 mM/g) of FFA at pH 2 indicating that little Pb(II) removal could be possible at lower pH. The similar results for sulfonate groups of raw and modified biomass of *Sargassum fluitansare* are reported in literature [126]. They investigated both qualitative and quantitative contribution of carboxylic and sulfonic functional groups for uptake of Cd(II) and Pb(II) by selective esterification method. Plette and coworkers also showed predominant Cd(II) bounding to carboxylic sites than phosphatic of a gram-positive soil bacterium [282].

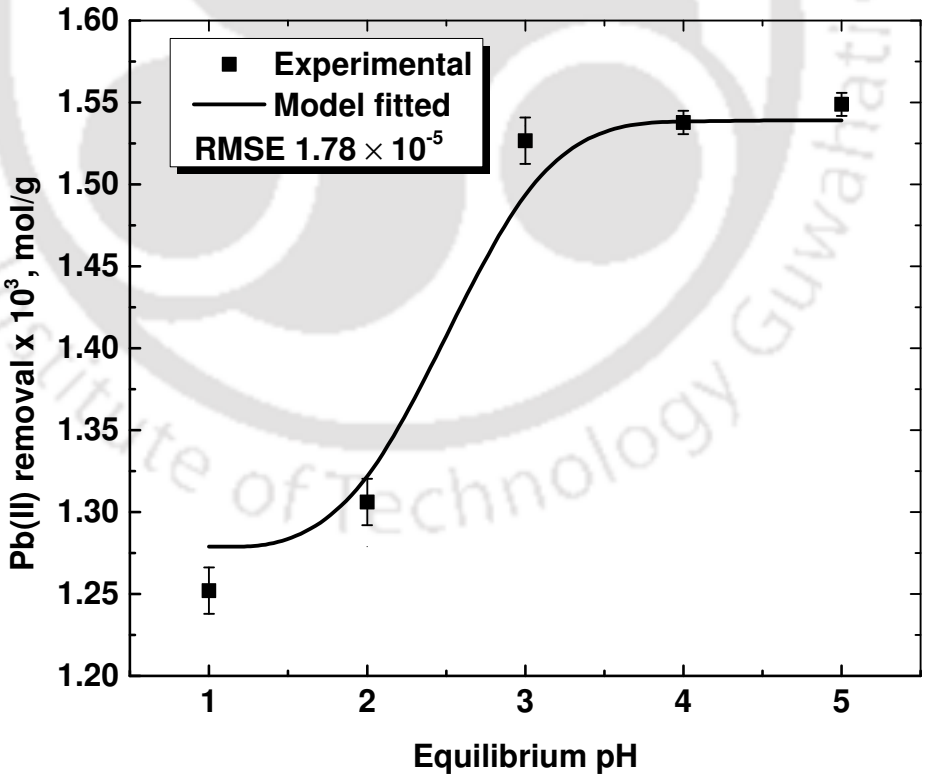

Figure 3.29: Equilibrium Pb(II) removal at different pH: Experimental vs. model fitted (Eq. 3.20). [FFA dosage 1 g/L, agitation speed 180 rpm, temperature 30°C].

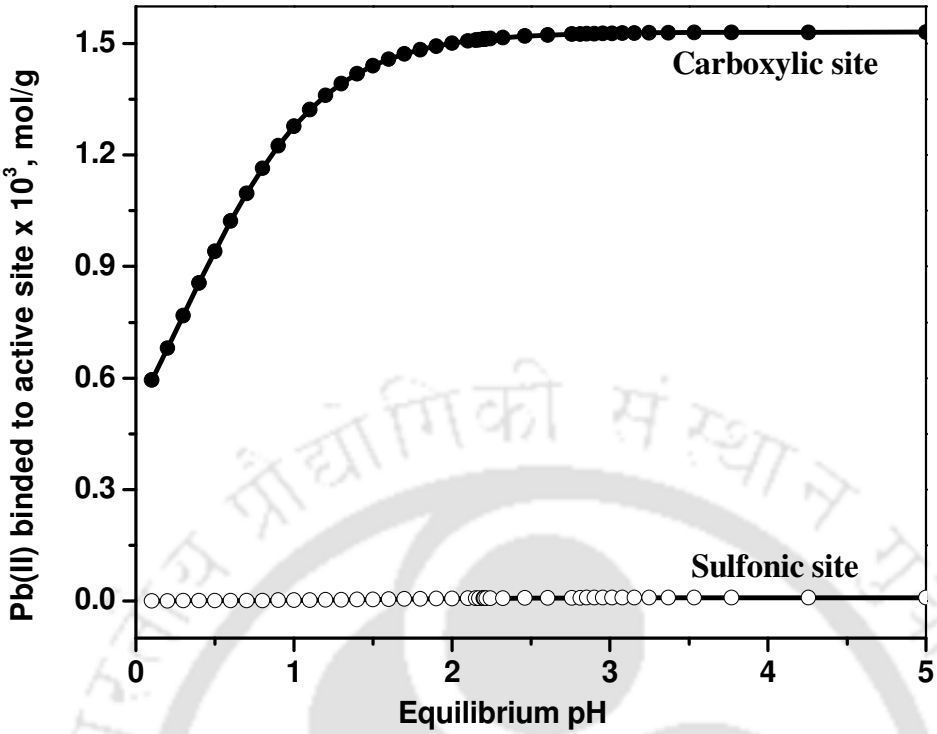

Figure 3.30: Contribution of each functional group in Pb(II) binding [FFA dosage 1 g/L, agitation speed 180 rpm, temperature 30°C].

3.2.7 Performance of FFA for the treatment of LABW

pH and conductivity of LABW were 1.13±0.02 and 248±23 mmho. Such high values could be a result of using of H_2SO_4 in lead-acid batteries. The initial concentration of Mg, Mn, Pb, Cu, Fe, Ni and Cd in LABW was found as 12.58±0.62 (0.517±0.026), 1.03±0.02 (0.018±0.0), 9.85±0.16 (0.047±0.001), 0.25±0.05 (0.004±0.001), 59.51±0.75 (1.064±0.013), 0.67±0.02 (0.011±0.0) and 3.25±1.14 (0.029±0.002) mg/L (mM), respectively. Thus, the total metal concentration in LABW was 1.7 mM, which was 10.8 times the concentration of Pb(II) and/or Cu(II) [0.157 mM] in synthetic wastewater in the mono and binary metal systems. The LABW was highly contaminated with Pb along with Cd and Fe with concentrations above the allowable discharge limits. The metals concentrations in LABW are higher when compared to those reported in the literature [27, 89, 283]. The efficiency of the uptake of these metals was studied at various dosages of FFA. The results are presented in Fig. 3.31.

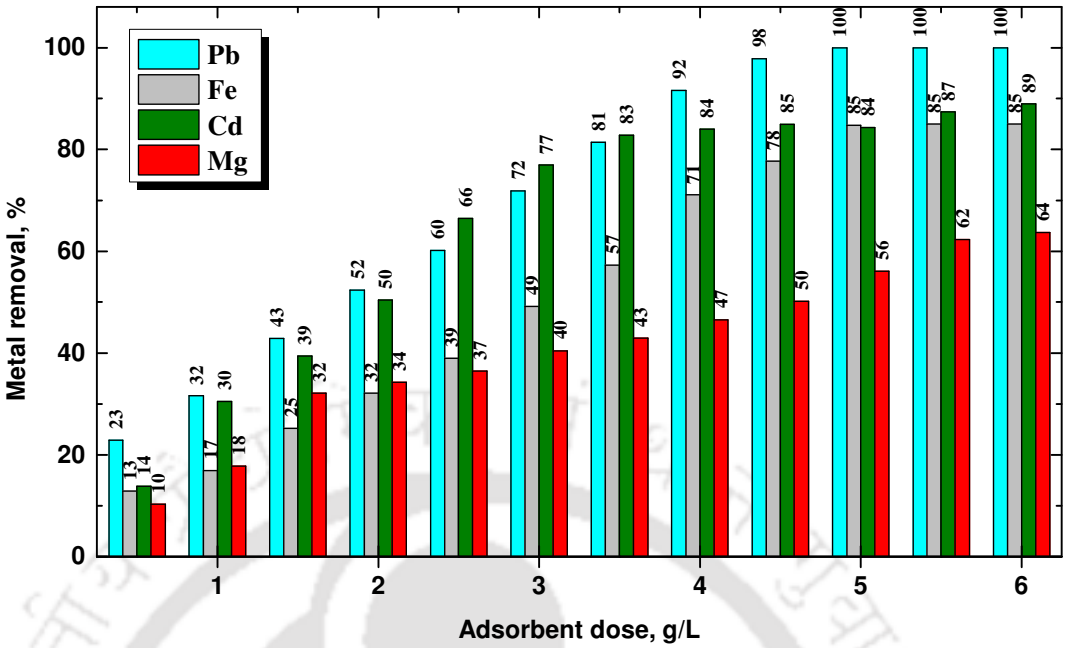

Figure 3.31: Effect of adsorbent dose on the removal of Pb(II) from battery industry wastewater [pH 4.0, contact time 9 h, temperature 30°C, 180 rpm].

Around 32% Pb was removed at a dosage of 1 g/L. Although the complete removal of Pb(II) from synthetic wastewater (initial 0.157 mM / 32 mg/L) was achieved using 1.4 g/L of FFA, however, LABW required 5 g/L dose to achieve the same. The need for a higher dose of FFA for complete Pb removal could be due to competitive adsorption of Fe, Mg, Cd, Ni, and Mn as well as organic contaminants [217]. Cd, Fe, and Mg were uptaken with removal efficiencies of 85, 84 and 63.7%, respectively, at 5 g/L FFA. It implies that FFA successfully managed to bring down Pb and Cd concentration below the allowable discharge limit adopted in India. These experimental observations indeed rope the feasibility of FFA for the removal of metals from industrial wastewater.

3.2.8 Cost analysis

The cost analysis of the FFA preparation was performed according to the procedure mentioned elsewhere [284]. The detailed analysis is included in the Annexure II with final cost of Rs. 110/kg of FFA. The FFA can be produced cheaply in comparison with market rate of activated carbon (Rs. 200 to 1000 per kg) and is as effective as activated carbon (Section 3.2.4).

3.3 Major findings

- This study uncovers a potential route of inducing new (sulfonic) and exposing parental (carboxylic) functional groups on arecanut husk through sulphuric acid treatment.
- The dissociation constant (pKa) of carboxylic and sulfonic groups were 3.21 and 1.62 determined from DSPA model and their concentrations estimated to be 1.53×10^{-3}, 2×10^{-3} mol/g.
- The synthesised FFA showed buffering capacity of 1.88×10^{-2} mol/g at a dosage of 1 g/L and the Pb(II) binding constants (K_M) were found to be 5.2×10^{6} and 28.11 L/mol for carboxylic and sulfonic sites, respectively with an overall binding constant of 1.46×10^{8} L/mol.
- Highly acidic pH was found to be indigent for Pb(II) removal, however, almost 100% removal was achieved at pH 5 in mono metal system, and preferential removal of Pb(II) over Cu(II) was observed in binary metal system.
- The presence of equimolar concentration of EDTA as that of metal hampered the metal removal by 50% for both FFA and IR120.
- FFA outperformed commercial mono-functional cation exchange resins viz. IR120 (sulfonic) and IRC50 (carboxylic) exhibiting clear superiority in terms of Langmuir capacities of 1.1 and 1.41 times for Pb(II) and Cu(II), respectively and it was about 3.4 times higher than the commercial activated carbon.
- The adsorbent could be used, as many as 12 times, and the exhaustion capacity was found to be 194.94 mg/g at pH 5, for which the contribution of carboxylic groups was much higher.
- In treatment of LABW, FFA removed Pb completely and the removal efficiencies of Fe, Cd, and Mg were 85, 84 and 56%, respectively, at 5 g/L FFA. On the other hand, 92% of the active sites of the exhaust FFA can be regenerated using only 1 N H_2SO_4.

CHAPTER 4

Synthesis and Characterization of Carboxylic Cation Exchange Bio-resin for LAB and Synthetic Wastewater Treatment

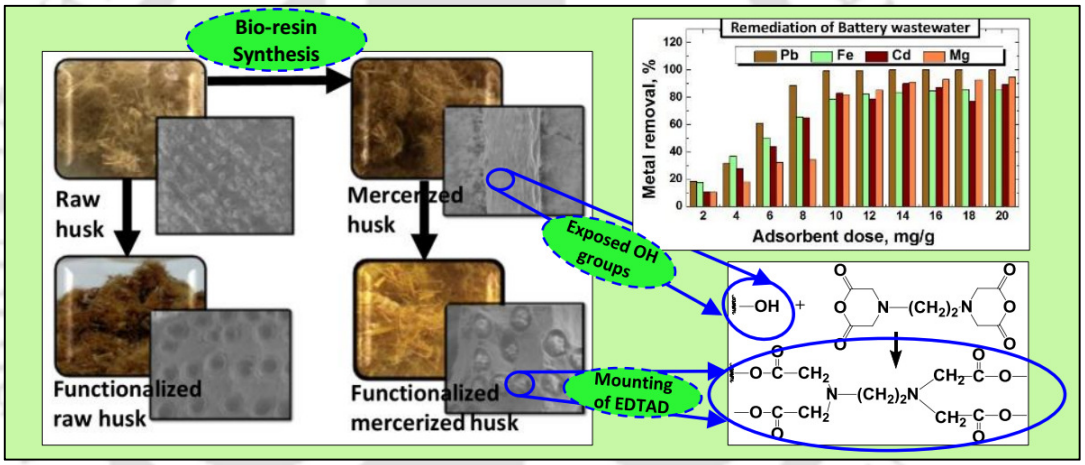

4.1 Specific background

The potential use of bio-based adsorbents in heavy metal remediation is studied by many researchers (Section 1.10, Chapter 1). However, their application is limited due to leaching of lignin, pectin, and tannin during treatment [9, 285]. Chemical modifications such as crosslinking, grafting and/or functionalization in favorable experimental conditions can improve leaching resistance, swelling properties as well as thermal stability and, induce new functional groups on biomaterials which could make it more efficient and selective towards a target pollutant [9]. The reactive groups of biomaterials are tightly packed within the lignocellulosic mass, and they are usually inaccessible under ordinary conditions. Nevertheless, boiling water or pretreatment with acid or alkali could expose them [129]. Alkali pretreatment solubilizes a part of cellulose, degrades lignin, and hydrolyzes ether

bond forming water soluble phenolic compounds [286]. It exposes the -OH groups, which could react with cyclic anhydrides to arouse functional sites, effective for heavy metal binding [129, 138]. Ethylenediaminetetraacetic dianhydride (EDTAD) containing two anhydride groups could induce chelating groups such as ethylenediamine-*N,N´*-diacetic acid (EDDA), carboxylic, amine, and/or iminodiacetic (IDA) on biomaterials to improve the uptake capacity [149]. The literature is evident enough and the explorations of crosslinking, grafting, and/or functionalization of biomaterials are copious. Modification of baker's yeast biomass by acylation reaction induced 3 of 4 carboxylic groups to the ionized biomass. The modified biomass showed adsorption capacities up to 10 and 14 times for Pb(II) and Cu(II), respectively, than that of the unmodified biomass [149]. Removal of cationic dyes by EDTAD modified sugarcane bagasse showed about 4.2 and 6.7 folds increase in adsorption capacity over the unmodified biomass [150, 287]. Mercerized sugarcane bagasse showed Cu(II) adsorptive capacity of 92.6 mg/g against 66.7 mg/g for raw biomass [147]. Despite of numerous biomaterials tested for modification, the potential of arecanut husk remains unexplored (Section 3.1, Chapter 3). Further, the fundamental insights such as the accessibility of the impregnated -COOH groups for metal binding from the theoretical considerations are not yet studied. Moreover, there is an imperative need for its validation from experimental studies.

Hence, this chapter is designed to achieve the first primary objective 'Heavy metal removal using functionalized adsorbent and bio-resin' using arecanut husk through mercerization and EDTAD functionalization. A cation exchange bio-resin was synthesized from arecanut husk using EDTAD as a carboxylating reagent. Two-stage synthesis method for the conversion of arecanut husk into a cation exchange was proposed. The synthesized bio-resin was characterized using elemental analysis, TGA, FESEM, EDX, XRD, and FTIR spectroscopy. Furthermore, the concentration of -COOH groups impregnated was determined by the potentiometric titration using a modified proton adsorption model (PAM) and, validated from gravimetric analysis (based on N-content). The synthesized cation exchange bio-resin was successfully applied for the removal of Pb and Cd from a battery industry wastewater. The possible chemical regeneration of spent bio-resin was explored to investigate the practical implication for industrial wastewater treatment.

4.2 Results and discussions

This part of Chapter 4 provides judicious discussion on the optimization of bio-resin, i.e., functionalized mercerized husk (FMH) synthesis parameters such as NaOH strength, reaction time, reaction temperature, and EDTA. The assortment of bio-resins was rendered on the basis of crystallinity index (CI), mass percent loss/gain (mpl/g), and concentration of carboxylic groups impregnated on arecanut husk. The FMH thus synthesized at optimized parameters was characterized through various physicochemical and spectroscopic techniques. It was applied for Pb(II) removal from synthetic wastewater, and the modified proton adsorption model was applied to understand the mechanism of Pb(II) uptake by the functional groups of FMH. Further, application of FMH for Pb(II) removal from LABW was experimented. Finally, the regeneration potential of exhausted FMH was evaluated using various eluting agents.

4.2.1 Bio-resin characterizations

4.2.1.1 mpg/mpl and CI of mercerized husks

The extent of mercerization was assessed in terms of mpl and CI. The X-ray diffractograms (Fig. 4.1) of husks mercerized (MHs) at different NaOH concentration, mercerization time, and temperature were used for the determination of CI. It can be seen from Fig. 4.2 that the mpl was increased from 16 to 40% and CI (estimated using Eq. 2.7, Chapter 2) was decreased from 49 to 27% with the increase in NaOH concentration from 10 to 20%. The mpl was increased only by 2% and, the CI was decreased by 1% with 30% NaOH concentration. So, NaOH concentration of 20% was chosen for further studies which is in line with a typical NaOH concentration for successful mercerization carried out preferably at a lower temperature [147, 150, 151, 226, 288]. It was found that the effect of reaction time beyond 24 h on mpl (only 5% increase) and CI was marginal (Fig. 4.2). CI was 43, 27, and 26% for the reaction times of 8, 24, and 40 h. Though mercerization at elevated temperatures increased the mpl but the CI was increased by 11% between 25 and 75°C as it could inhibit the exposure of hydroxyl groups [147, 151, 288]. Hence, the optimal condition for the mercerization was selected as 20% NaOH at 25°C with a reaction time of 24 h. The mpg of functionalized raw husk (FRH), functionalized mercerized husk (FMH), and functionalized double mercerized husk (FMMH) after EDTAD ridging was estimated using Eq. 2.6 (Chapter 2). FRH showed only 3% of mpg when compared to 40 and 33% for FMH and FMMH. The FTIR spectra of FRH showed the absence of characteristic peaks of

either ester or carboxylic groups (Fig. 4.3), indicating no penetration of EDTAD in RH. However, the double mercerization of RH resulted neither in improving swelling and structural behavior nor in a fruitful increment in mpg, but it was affected adversely as the first alkali treatment caused the maximum swelling. The structure of crystalline part of the alkali-cellulose formed in the case of FMH was so stable that further alkali treatment didn't make any difference at all in swelling and crystal arrangements [222]. The double mercerization resulted in a lesser mpg (33% for FMMH) when compared with FMH (40%) [222]. However, the double mercerization of cellulose and bagasse reported a higher mpg [147].

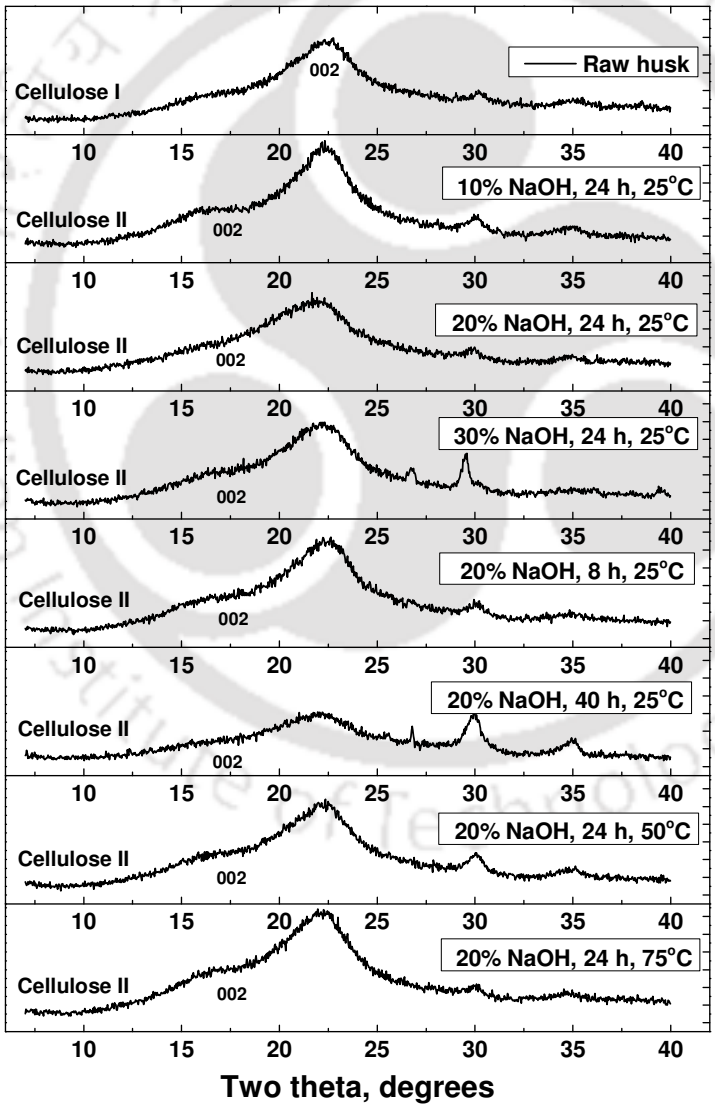

Figure 4.1: XRD plots of MHs at varying NaOH concentration, mercerization time, and temperature.

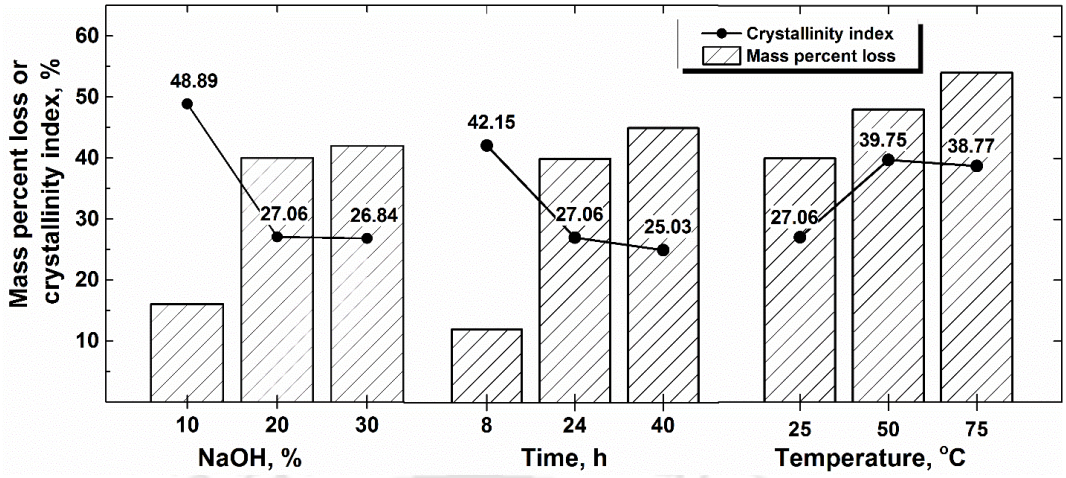

Figure 4.2: Mass percent loss and crystallinity index of MHs at different NaOH strength, reaction time, and reaction temperature.

4.2.1.2 FTIR spectra of bio-resins

The treatment of RH, MH, and MMH in anhydrous DMF provoked the acylation reaction of anhydride functions of EDTAD with hydroxyl groups of lignocellulosic materials [147]. This reaction resulted in the introduction of carboxylic groups on FMH through ester linkage [151]. The FTIR spectra of RH, MH, FMH, FMMH, and FRH (Fig. 4.3) were acquired. RH showed typical spectra for lignocellulosic materials. However, peaks appearing at 3648, 1445, 1306, 1065, and 973 1/cm in FTIR spectra of RH shifted to 3622, 1443, 1332, 1063, and 987 1/cm, respectively in MH spectra. The intense and broad band stretch ranging from 3450-3650 1/cm for the characteristic bond of alcohol with -OH free hydroxyl group appeared in this region [289]. The adsorption bands at 2965 and 1770 1/cm can be attributed to stretching vibrations of -C-H and stretching vibrations of hemicellulose of -C=O [287]. The peaks at 1505, 1445, and 1065 1/cm in RH depicts an aromatic skeleton ring vibration due to lignin, symmetric bending vibrations of $-CH_2$, and stretching vibrations of -C-OH, respectively [287]. A characteristic peak of lignin at 1505 1/cm disappeared for MH, confirming its removal due to mercerization. The FTIR spectra of FMH and FMMH showed a peak at 1738 1/cm, which could be attributed to the introduction of carbonyl functions of ester and carboxylate groups [147]. The presence of such a peak was not detected in the case of FRH. The peaks at 1435 and 1280 1/cm for FMH can be assigned to -OH bends and -C-O stretch of the carboxylic functional group. The presence of ester and carboxylic groups on FMH when compared to RH indicates EDTAD ridging through ester linkage, following the release of the carboxylic functional group [151].

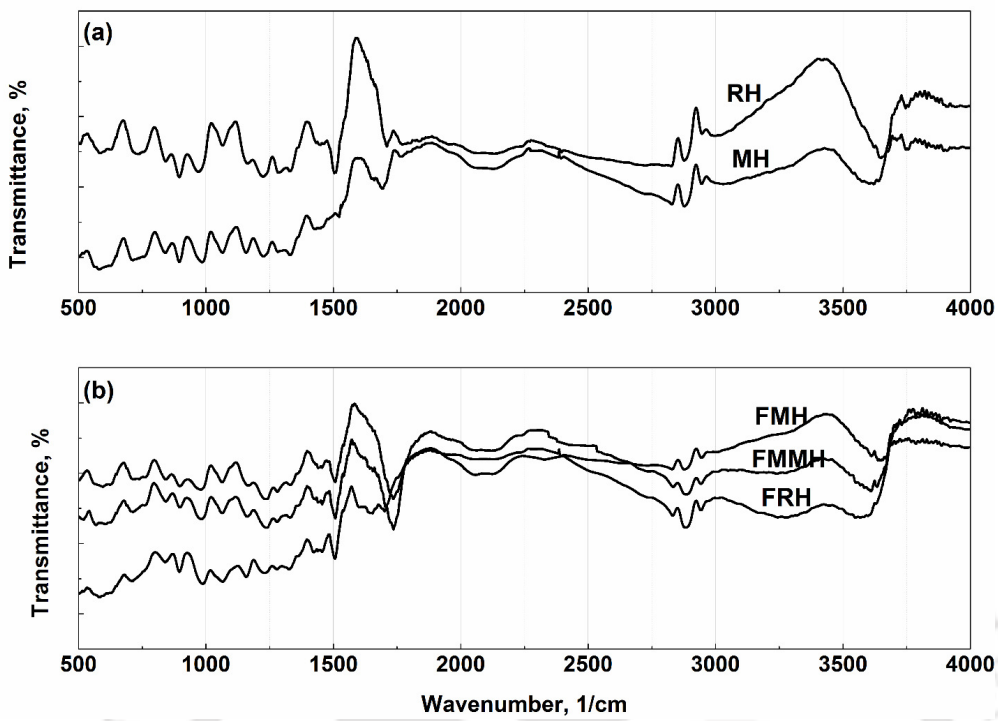

Figure 4.3: FTIR spectra of (a) RH, MH, and (b) FMH, FMMH, and FRH.

4.2.1.3 Optimization of EDTAD dose and reaction time

In bio-resin synthesis, the reaction time (5-25 h) and mass of EDTAD added (5-25 g) were chosen on the basis of EDTA moiety (C_{EDTA}) impregnated which was calculated by elemental analysis of RH, MH, FRH, FMH, and FMMH as shown in Table 4.1.

Table 4.1: Elemental analyses and concentration of EDTAD introduced in bio-resins.

Sample	EDTAD Used, g	Reflux time, h	Elemental composition, %				C_{EDTA}, mM/g
			C	*H*	*N*	*S*	
RH	0	0	49.640	5.915	0.432	44.013	0.1543
MH	0	0	45.830	6.005	0.319	47.846	0.1139
FMH	5	5	45.61	6.018	1.016	47.356	0.3629
	5	10	46.366	6.016	1.275	46.343	0.4554
	5	15	46.814	6.21	1.405	45.571	0.5018
	5	20	47.019	6.301	1.569	45.111	0.5604
	5	25	46.974	6.293	1.54	45.193	0.5500
	10	20	46.802	6.061	1.704	45.433	0.6086
	15	20	45.829	5.887	1.919	46.365	0.6854
	20	20	47.664	6.018	2.058	44.26	0.7350
	25	20	47.679	6.154	2.078	44.089	0.7421
FMMH	20	20	49.894	6.842	0.874	42.39	0.3121
FRH	20	20	48.611	5.942	0.520	44.927	0.1857

With the progress of reaction time, C_{EDTA} increased until 20 h and; it did not change afterward. The dose of EDTAD was increased in the range of 5 to 25 g, which elevated the C_{EDTA} from 0.36 to 0.56 mM/g of FMH with EDTAD mass of 20 g. The elemental analysis showed that RH had high contents of C, H, and O; it also revealed that mercerization diminished the proportion of C, N, and H. The decrease of C content indicated the extraction of lignin due to mercerization, as lignin polymer hold high C and H content. Functionalization increased N-content of bio-resins and, it was the highest for FMH owing to the maximum amount of EDTAD ridged. The N-content of FMH was also higher than that of FRH due to mercerization. The increase in N and O content and the decrease in its C content also signified EDTAD ridging through acylation reaction [149]. The mechanism of the reaction is given in Fig. 4.4. The MH reacts with EDTAD through an acylation reaction [147, 149, 151]. The chelate rings having the lone electron pair on the oxygen atom were opened through a protonation reaction followed by a nucleophilic attack. Only one carbonyl group molecule out of four of an EDTAD molecule reacted with the hydroxyl group of MH resulting in the formation of the ionized groups. These molecular groups are capable of forming stable complexes with metal ions [149]. The quantity of EDTAD introduced in FMH was higher than that of FMMH due to shrinkage caused by double mercerization (Table 4.1).

The physicochemical properties of bio-resin were compared with a commercial cation exchange resin, IR 120, as a reference. The cation exchange capacity (CEC) of synthesized bio-resins estimated using Eq. 2.4 (Chapter 2) was found to be 2.01 meq/g for FMH and 4.64 meq/g for IR120. The typical working pH range of IR120 is 1 to 5. FMH was also found to be effective within this pH range with a maximum capacity at pH 5. The surface area of the FMH was found to be low (11 m^2/g), but it was higher than that of IR120 (4 m^2/g). The parameters such as particle size, drying loss, morphology, and ionic form are also summarized in Table 4.2 for comparison.

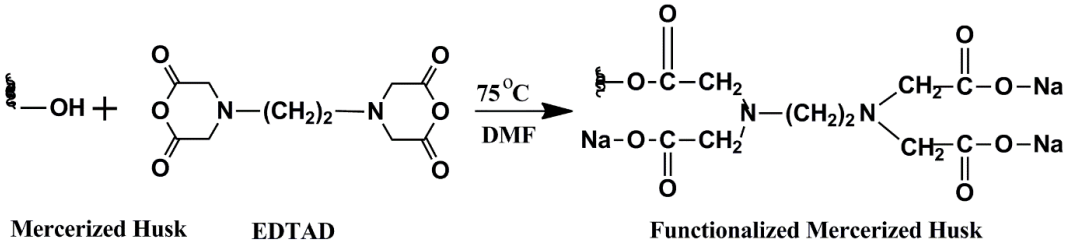

Figure 4.4: Mechanism of EDTAD ridging onto MH through acylation reaction by formation of the ester linkage.

Table 4.2: Comparison of synthesized bio-resins with commercial cation exchange resin.

Resin	Particle size, mm	Ionic form	CEC, meq/g	Drying loss, %	BET surface area, m^2/g	Morphology
FRH	2-5	NA	0.2	Max 15	01	Fibrous
FMH	2-5	H^+	2.01	Max 12	11	Fibrous
FMMH	2-5	H^+	1.03	Max 12	17	Fibrous
IR120	0.3-0.9	H^+	4.64	Max 50	04	Spherical

4.2.1.4 Modified proton adsorption model (PAM) and potentiometric titrations

The FMH contained only carboxylic group as depicted by FTIR studies unlike FFA. Hence, the already-developed PAM (Section 3.2.6.1, Chapter 3) was modified for FMH. The dissociation reaction of the carboxylic group impregnated onto FMH can be written as in Eq. 4.1 [220].

$$\equiv \mathrm{COOH} \leftrightarrow \equiv \mathrm{COO^-} + \mathrm{H^+} \quad (4.1)$$

Where "≡" indicates the FMH surface, $\equiv \mathrm{COOH}$ and $\equiv \mathrm{COO^-}$ are protonated and dissociated carboxylic groups.

The equilibrium constant (K_a) for this reaction can be expressed as in Eq. 4.2.

$$K_a = \frac{[\equiv \mathrm{COO^-}][\mathrm{H^+}]}{[\equiv \mathrm{COOH}]} \quad (4.2)$$

So, the total concentration of carboxylic groups (N_T) present on FMH can be estimated by Eq. 4.3.

$$N_T = [\equiv \mathrm{COOH}] + [\equiv \mathrm{COO^-}] \quad (4.3)$$

The concentration of protonated carboxylic groups (N_p) at equilibrium can be expressed by rearranging Eq. 4.2 and 4.3 as in Eq. 4.4

$$Np = N_T \left[\frac{[\mathrm{H^+}]}{[\mathrm{H^+}]+K_a}\right] \quad (4.4)$$

Eq. 4.4 was used to estimate the concentration of protonated carboxylic groups present on FMH by measuring the proton concentration difference in the presence and in the absence of FMH during potentiometric titrations [219].

The equilibrium metal (M^{2+}) adsorption by the carboxylic groups of FMH can be described as in Eq. 4.5 [220].

$$\equiv COO^- + M^{2+} \leftrightarrow \equiv COOM^+ \quad (4.5)$$

The metal binding constant, K_θ for this reaction can be determined as in Eq. 4.6.

$$K_\theta = \frac{[\equiv COOM^+]}{[\equiv COO^-][M^{2+}]} \quad (4.6)$$

Further, the concentration of the carboxylic groups in the presence of M^{2+} (with M^{2+} binding) can be expressed as in Eq. 4.7.

$$N_T = [\equiv COOH] + [\equiv COO^-] + [COOM^+] \quad (4.7)$$

Substituting $[\equiv COOH]$ and $[\equiv COO^-]$ from Eqs. 4.4 and 4.6, Eq. 4.8 is obtained.

$$N_T = [COOM^+]\left[\frac{K\,K_M[M^{2+}]+[H^+]+K}{K\,K_M[M^{2+}]}\right] \quad (4.8)$$

Hence, the total amount (q_e, mol/g) of metal attached to the carboxylic sites can be represented as in Eq. 4.9.

$$q_e = N_T\left[\frac{K\,K_M[M^{2+}]}{K\,K_M[M^{2+}]+[H^+]+K}\right] \quad (4.9)$$

The cumulative volume of 0.5 N NaOH added vs. equilibrium pH during potentiometric titrations with and without FMH is shown in Fig. 4.5a. As depicted, the shift of the titration curve towards the right side was observed for FMH due to the release of protons from the carboxylic groups. It gave the buffering capacity of 2.4×10^{-4} mol/g estimated in the pH range 1.6 to 3 [129]. Such shift of the titration curve was not noticed in the case of RH. Similar results for dead biomass of *B. subtillis* are reported with a buffering capacity of 2.8×10^{-4} mol/g, at the dose of 75-150 g/L [255]. The FMH showed comparable buffering capacity at a comparatively low dose level, which projected its potentially high proton adsorptive capacity. It was assumed that change in solution pH was solely due to the release of the proton by FMH. The results obtained in potentiometric titration of FMH were fitted with the modified PAM (Eq. 4.4) using GRG Nonlinear regression analysis (solver tool of Microsoft Office Excel 2016). The modified PAM displayed an excellent agreement with experimental results as shown in Fig. 4.5b.

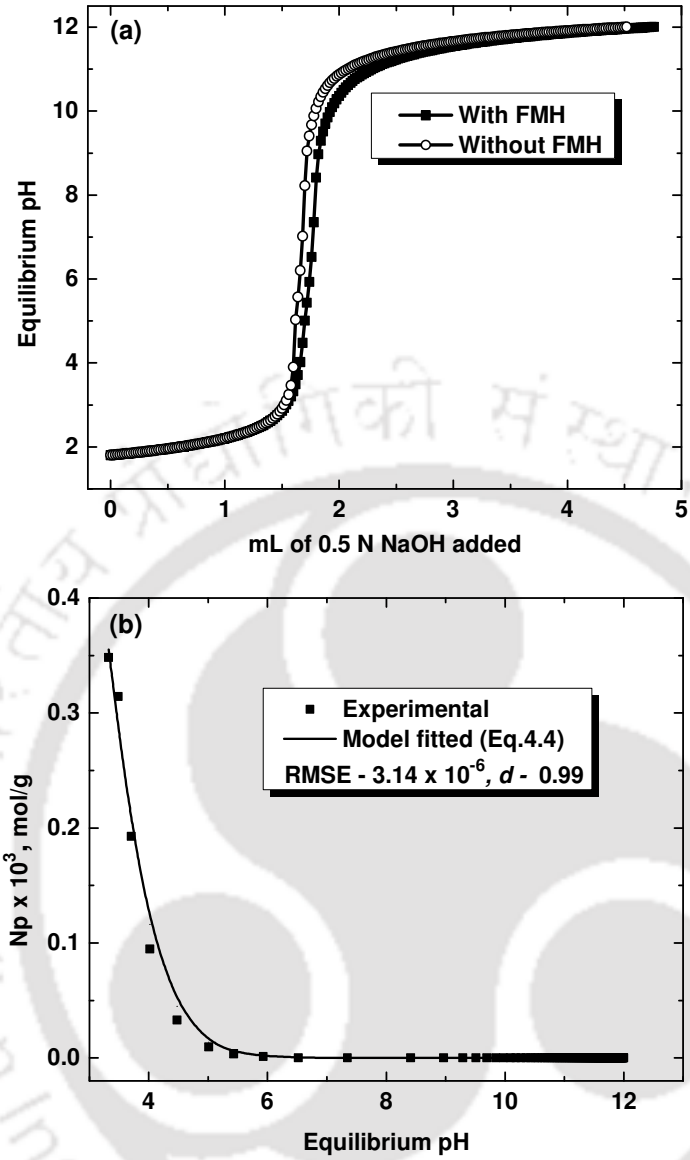

Figure 4.5: (a) Titration curve for 0.1 N $NaNO_3$ solution with and without FMH, and (b) Plot of experimental and PAM fitted number of protonated sites for the estimation of the acid dissociation constant [FMH dose 5 g/L, agitation speed 180 rpm, and temperature 30°C].

The predicted data was validated using the index of agreement (*d*) determined using Eq. 4.10. The value of '*d*' ranged from $0 \leq d \leq 1$, where 1 indicates the ideal agreement between the experimental and modeled values and, 0 indicates no agreement [290].

$$d = \frac{\Sigma(q_e - q_m)^2}{\Sigma\{|q_e - \bar{q_e}| + |q_e - \bar{q_e}|\}^2} \quad (4.10)$$

Where, q_e and q_m represent the experimental and model fitted Pb(II) uptake, whereas the bar over the notation denotes the mean value. The pKa value of 3.29 (estimated

from modified PAM) was assigned to the carboxylic groups, which is also well supported by the previous studies [254, 281, 291]. The concentration of carboxylic groups (N_T) was found to be 0.741 mM/g of FMH against 0.735 mM/g based on N-content determined by the elemental analysis.

4.2.1.5 Thermal stability of bio-resins

TGA and DTG curves for bio-resins are presented in Fig. 4.6. The thermal decomposition profile for RH, FMH, and FMMH was obtained using an isothermal ramping program. It showed significant weight losses in RH, FMH, and FMMH in the range of 300–350, 215–360 and 215–350°C, respectively (Fig. 4.6a).It can be observed that Cellulose and hemicellulose started decomposing at around 206 and 315°C, while lignin started decomposing over the temperature of 330°C [215]. RH showed resistance to thermal degradation up to 300°C due to its stable structure consolidated by lignin, whereas FMH and FMMH started degrading at a comparatively lower temperature of 215°C due to the loss of lignin during mercerization. It can also be observed from TGA curves that the overall weight loss was higher in RH whereas it was least in FMH followed by FMMH. A groove at 330°C in the DTG curve of RH referred to the loss of lignin (Fig. 4.6b). This characteristic groove was not detected in DTG profile of FMH and FMMH indicating the absence of lignin.

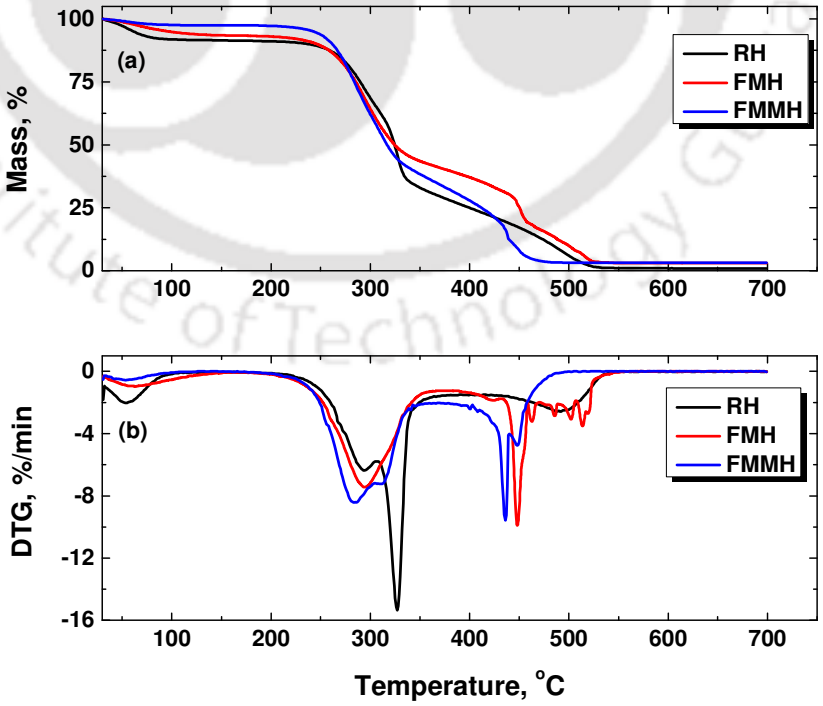

Figure 4.6: (a) TGA analysis, and (b) DTG profile of RH, FMH, and FMMH.

4.2.1.6 FESEM micrographs of bio-resins

The FESEM micrographs of RH, MH, FRH, and FMH are shown in Fig. 4.7. The micrograph of RH at 0.5 K magnification showed vesicles those longitudinally run along the length of fiber with parallel orientations (Fig. 4.7a1). In magnification with 1 K, vesicles appeared to be occupied and closely spaced (Fig. 4.7a2). However, the vesicles were filled with organic cell materials having undulations, as evident from a higher magnification image (Fig. 4.7a3). The effect of mercerization can be seen from Figs. 4.7b1, 4.7b2 and 4.7b3. It showed the disruption of the lignocellulosic fiber with cracks and swelled vesicles (Figs. 4.7b1 and 4.7b2). A closer view at 3.5 K magnification illustrates the removal of organic cell materials from the vesicles due to mercerization (Fig. 4.7b3). The micrograph of FRH and FMH are shown in Figs. 4.7c1, 4.7c2, 4.7c3 and 4.7d1, 4.7d2, 4.7d3, respectively.

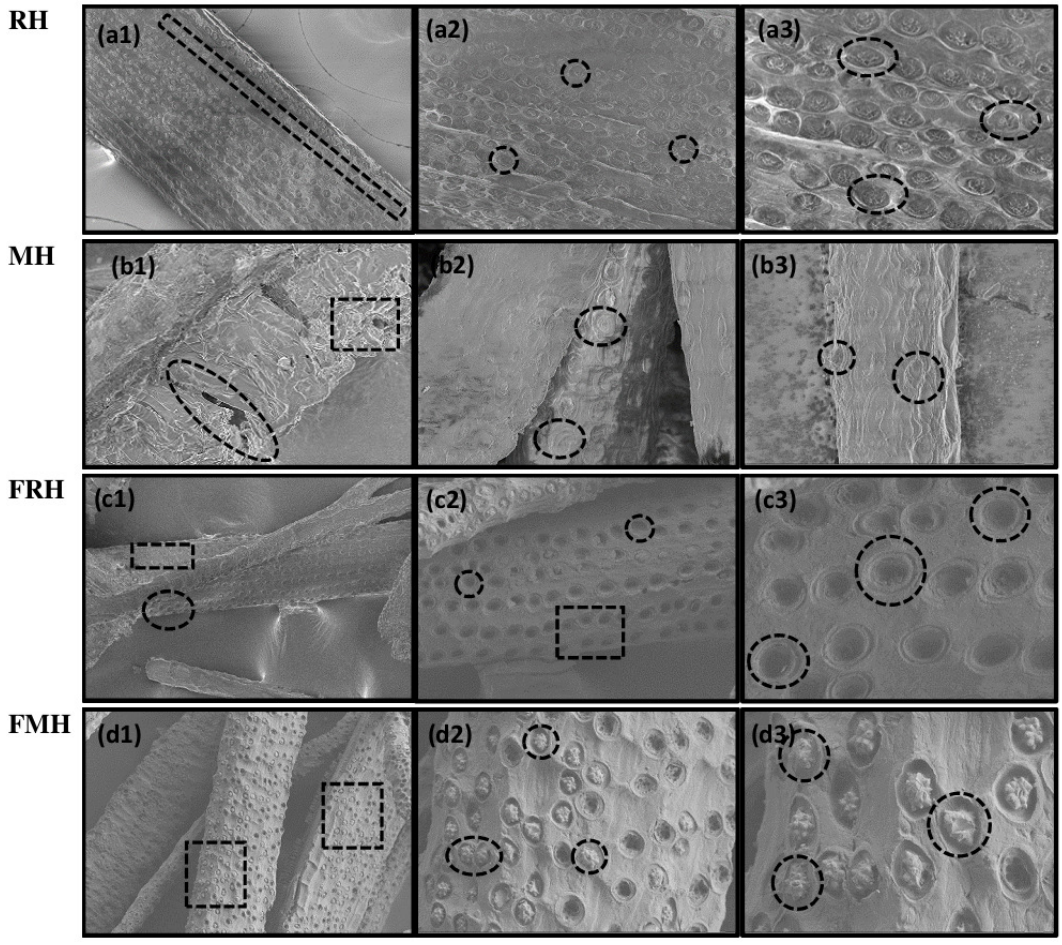

Figure 4.7: FESEM micrographs of bio-resins showing changes at every modification stage in different magnification scales: RH [a1, a2 and a3], MH [b1, b2 and b3], FRH [c1, c2 and c3], and FMH [d1, d2 and d3].

For FRH, 0.5 K magnification showed morphological changes, but 1 K magnification evinced a coating of a layer over the surface as a result of EDTAD modification. EDTAD was stranded on the cell material, but the vesicles remained empty (Fig. 4.7c3). In the case of FMH, as can be seen that the fiber surface and vesicles were coated with EDTAD (Fig. 4.7d1). EDTAD bounding to most of the vesicles and surface can be seen at 2 K magnification. A higher magnification at 4 K revealed that vesicles were filled with EDTAD, forming a chain of ridges and were oriented spiking outwards (Fig. 4.7d3).

4.2.2 Application of FMH for Pb(II) removal from synthetic wastewater

FMH was first applied for Pb(II) removal from synthetic wastewater prior to LABW treatment for the selection of suitable bio-resin. The results are shown in Figs. 4.8 and 4.9.

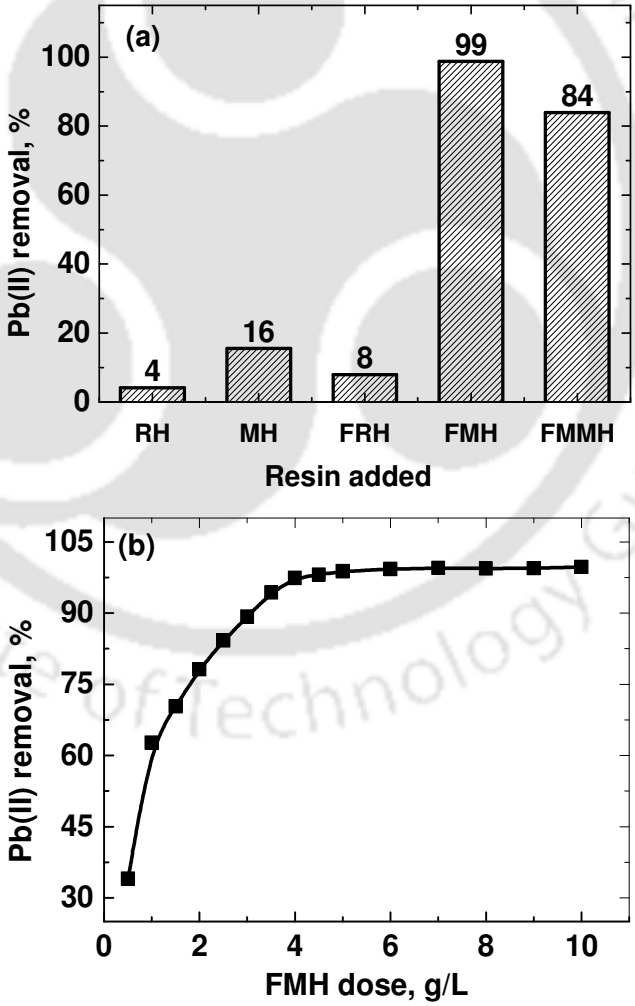

Figure 4.8: (a) Performance of bio-resins in Pb(II) removal, and (b) Effect of FMH dose on Pb(II) removal.

FMH removed 99% Pb(II) from an initial concentration of 32 mg/L (0.157 mM) over a period of 8 h. Pb(II) removal was 4, 18, 8, 99, and 84% with RH, MH, FRH, FMH, and FMMH, respectively, at an equal dosage of 10 g/L. So, Pb(II) uptake of FMH was 23.84, 6.36, 12.47, and 1.17 times than that of RH, MH, FRH, and FMMH. MH showed little Pb(II) removal (15.5%) as alkali treatment had destroyed lignocellulosic binding [129, 222]. The poor performance of FMMH in Pb(II) removal was due to less number of -COOH sites (Table 4.1). Thus, further experimentation was carried out with FMH. The effect of FMH dose on Pb(II) removal is shown in Fig. 4.8b. With the increase in FMH dose from 0.5 to 5 g/L, the removal efficiency was improved from 34 to 99% in 8 h.

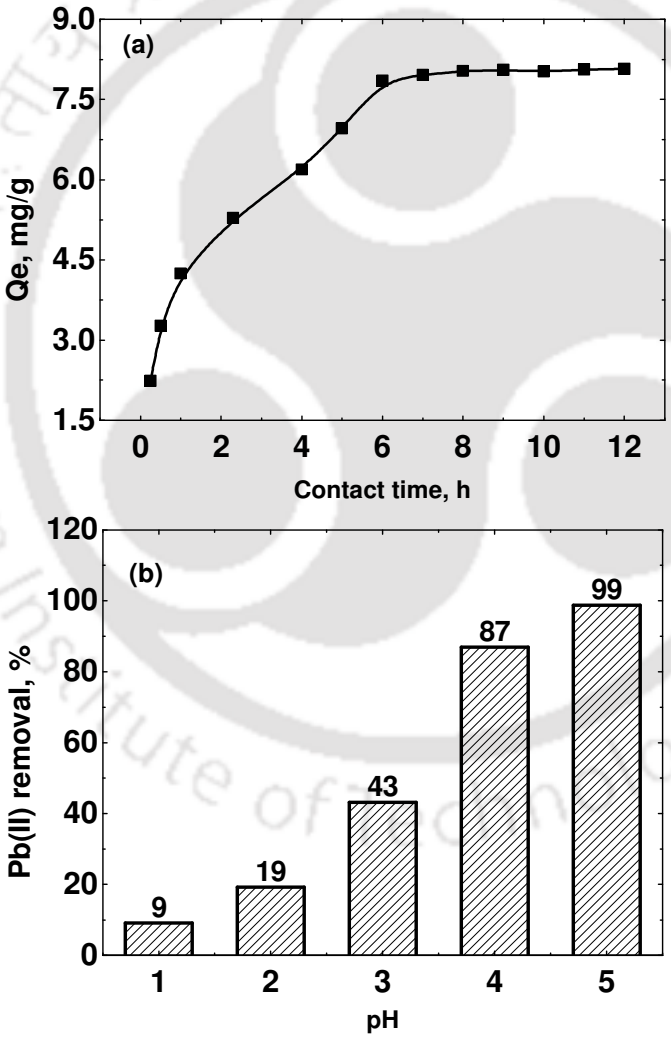

Figure 4.9: (a) Effect of contact time on Pb(II) removal by FMH, and (b) Performance of FMH in Pb(II) removal at different pH.

The kinetics of Pb(II) removal ascertained the equilibrium time of 8 h (Fig. 4.9a). The effects of pH on Pb(II) removal are presented in Fig. 4.9b. Pb(II) removal was unfavorable in acidic pH and, it increased with the elevation of pH. There was only 9% removal at pH 1 and, it increased to 99% at pH 5 in 8 h treatment. Pb(II) abundance is ~100% at pH 1. So, the competitive adsorption of protons at a lower pH gave lower metal uptake efficiency. Therefore, the pH variation beyond 5 was not compared to eliminate the effect of Pb(II) precipitation [129].

4.2.3 Pb(II) removal and modified PAM for Pb(II) uptake

The nature of equilibrium Pb(II) binding with carboxylic sites on FMH was examined using the modified PAM for Pb(II) uptake (Eq. 4.9). The concentration of carboxylic groups (0.741 mM/g) and pKa (3.29) determined (Fig. 4.10), were used to estimate the Pb(II) binding constant (K_θ). The best-fitted results are presented in Fig. 4.10.

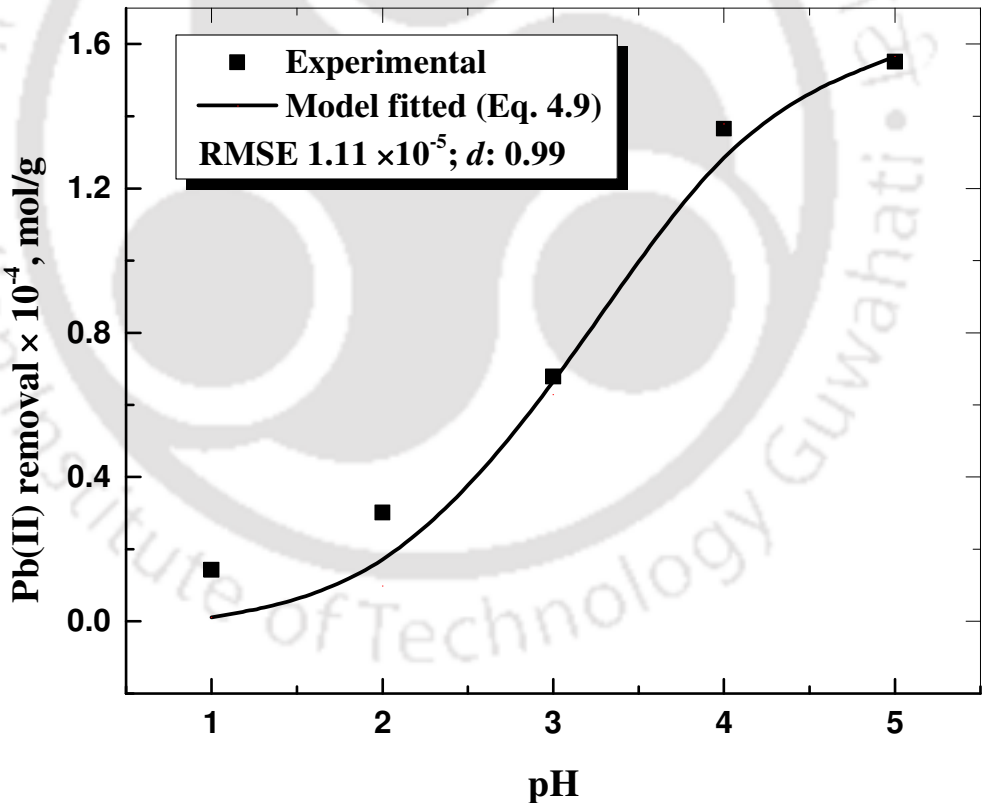

Figure 4.10: Experimental vs. model fitted (Eq. 4.9) equilibrium Pb(II) uptake at different pH [Pb(II) 32 mg/L (0.157 mM), FMH dose 5 g/L, temperature 30C, and agitation speed 180 rpm].

The value of '*d*' was found to be 0.99 with the metal binding constant, K_θ, of 1.73 × 10^3 L/mol. Pb(II) removal was only 9 and 19 % at pH 1 and 2, respectively and, the model notably underestimated Pb(II) removal below pH 3 (Fig. 4.10). In the case of FFA, (Section 3.2.6.2, Chapter 3) the carboxylic group concentration was 25% lesser than the sulphonic groups, but Pb(II) was mostly uptaken by the carboxylic groups for acid treated biomass adsorbent with K_θ of 5.2 × 10^6 L/mol [129]. The K_θ of 80.9 L/mol was reported for Cr(III) binding with the carboxylic groups of *Spirulina platensis* biomass [219].

4.2.4 Application of FMH for Pb(II) removal from LABW

pH and conductivity of LABW were 1.13±0.02 and 248±23 m.mho. Low pH of LABW was due to the use of H_2SO_4 in the battery manufacturing process. LABW was found to contain several metals, such as Mg, Mn, Pb, Cu, Fe, Ni and Cd with the concentration of 12 (0.518), 1 (0.019), 10 (0.048), 0.25 (0.004), 60 (1.064), 0.67 (0.012), and 4 (0.03) mg/L (mM) respectively. So, Pb, Fe and Cd were exceeding the allowable discharge limits of 0.1, 3, and 2 mg/L, provided by the Central Pollution Control Board, India [292].

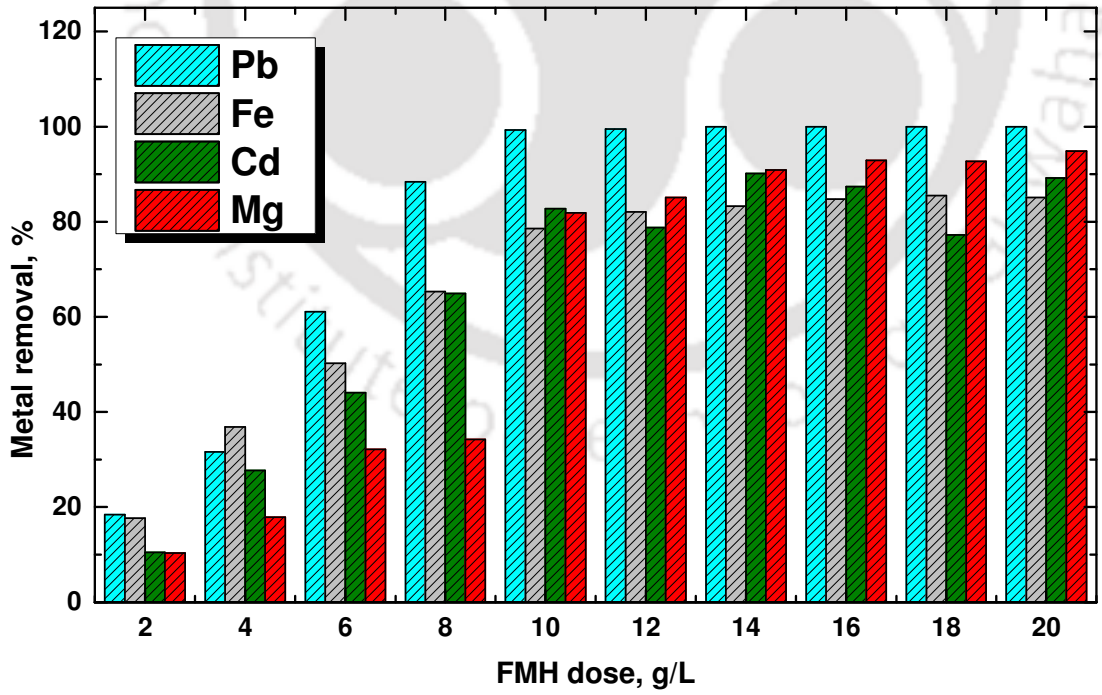

Figure 4.11: Effect of FMH dose on the removal of Pb, Fe, Cd, and Mg from LABW [FMH dose 10 g/L, pH 5, temperature 30°C, and agitation speed 180 rpm].

The dose of FMH was varied from 2-20 g/L, and the results are shown in Fig. 4.11. Pb removal was only 18% at a dose of 2 g/L. Though FMH exhibited 99% of Pb(II) removal from synthetic wastewater at a dose of 5 g/L but LABW took a higher dose of 10 g/L to achieve the same as the cumulative concentration of all metals was higher by about 10 times [86, 217]. Fe, Cd and Mg uptake efficiencies were 79, 83, and 82%, respectively.

4.2.5 Exhaustion and regeneration of FMH

From the exhaustion study, it can be seen that FMH could be utilized for the maximum of 5 cycles for Pb(II) removal (Fig. 4.12a).

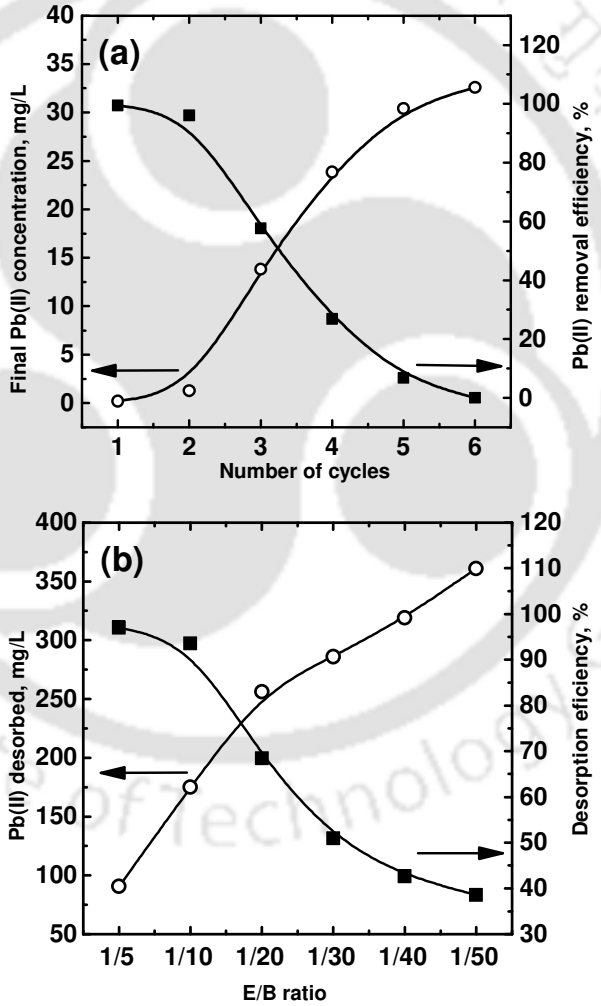

Figure 4.12: (a) Removal of Pb(II) in exhaustion study of FMH [Pb(II) 32.6 mg/L, FMH dose 5 g/L, temperature 30°C, and agitation speed 180 rpm], and (b) Regeneration of FMH using 0.1 N HCl at various E/B ratios [initial metal loading 18.7 mg/g, desorption time 30 min, temperature 30°C, and 180 rpm].

FMH removed 99% of Pb(II) from synthetic wastewater in the first cycle and, it was unaffected in the second cycle. From 3rd cycle onwards, the removal efficiency reduced considerably to 57%. However, after 5 cycles, Pb(II) uptake was completely withdrawn. The cumulative Pb(II) uptake until FMH exhaustion was found to be 18.7 mg/g of FMH (Eq. 2.8, Chapter 2). The regeneration of exhausted FMH at an eluent/bio-resin (E/B) ratio of 1/5, gave 72, 97 and 13% desorption efficiency using 0.1 N EDTA, HCl, and absolute ethanol, respectively. A higher desorption efficiency was resulted from the exchange between protons and Pb(II) (Eq. 4.11). So, further desorption experiments were carried out with different volumes of HCl and, the results are shown in Fig. 4.12b. It was noticed that the desorption efficiency was reduced with a decreasing E/B ratio from 1/5 to 1/50. It was 97, 93, 68, 51, 43, and 39% at E/B ratios of 1/5, 1/10, 1/20, 1/30, 1/40, and 1/50, respectively. The reduction in desorption efficiency was due to a lesser volume of HCl used.

$$\equiv \mathrm{COOM^{+}} + \mathrm{H^{+}} \leftrightarrow \equiv \mathrm{COOH} + \mathrm{M^{2+}} \qquad (4.11)$$

4.3 Major findings

- The study in Chapter 4 successfully demonstrated a new approach for the synthesis of carboxylic bio-resin from arecanut husk using a two-stage protocol i.e., mercerization followed by EDTAD carboxylation involving the formation of ester linkage by an acylation reaction.
- The concentration of carboxylic functional groups estimated by gravimetric analysis (based on N content) and modified PAM model (based on potentiometric titrations) closely matched.
- The synthesized bio-resin achieved 99% Pb(II) removal efficiency from an initial concentration of 32 mg/L at a dosage of 5 g/L of bio-resin for which Pb(II) binding constant was found to be 1.73×10^{3} mol/L with a pKa of 3.29 and carboxylic group concentration of 0.741 mM/g.
- The bio-resin showed CEC of 2.01 meq/g and a buffering capacity of 2.4×10^{-4} mol/g within the pH range of 1.6 to 3.
- The bio-resin showed promising results for the removal of Pb and Cd from LABW well below the permissible discharge limits along with significant reduction of Fe and Mg.
- The bio-resin was capable of Pb(II) uptake up to 5 cycles with an exhaustion capacity of 18.7 mg/g and, 97% adsorption/exchange sites could be regenerated using 0.1 N HCl.

Chapter 5

Characterization and Implication of LABS for the Production of Clay Bricks for Effective Heavy Metal Fixation

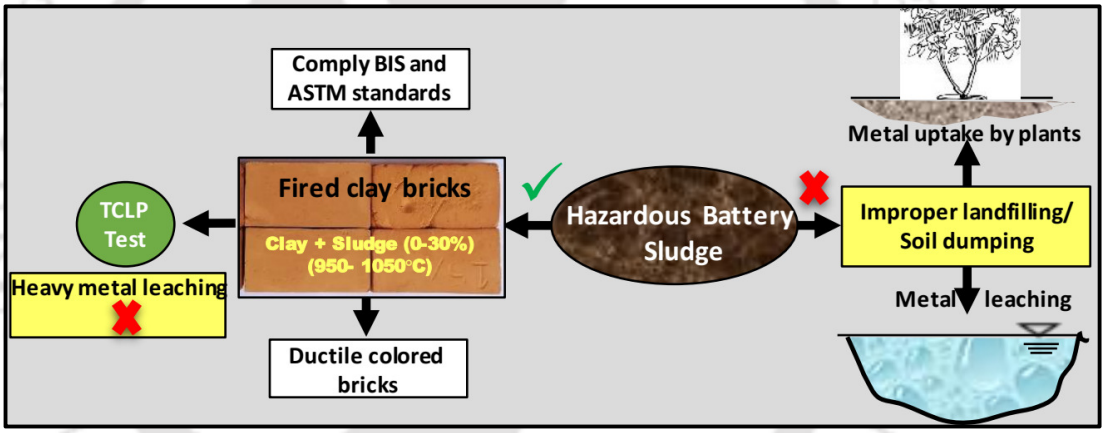

5.1 Specific background

Industrial sludge arising from alkali treatment of metal plating, electroplating, metal smelting, and lead-acid battery (LAB) manufacturing wastewater is a complex mixture of numerous contaminants including valuable metals. The current disposal practices for such sludge include incineration, landfilling, ocean dumping, stabilization/solidification, using as construction material, and lagooning [38, 174, 293]. However, none of these are healthy and sustainable in all aspects and possess own merits and demerits. Incineration of sludge causes the release of toxic gases, its improper landfilling and/or solidification may allow heavy metals to leach out in due course of time [293]. Further, the selection of an appropriate disposal technique is solely dependent upon the sludge characteristics, which differs from industry to industry, depends on manufacturing process and the type of raw material used. Although there are studies on characterization of sludges arising from

various industries [11, 38], it is mostly neglected for lead-acid battery sludge (LABS). A sustainable option of LABS disposal could be its utilization in agricultural or nonagricultural lands by minimizing the metal loading along with the recovery of heavy metals [294]. The characterization of LABS in terms of heavy metal content along with its speciation in various forms such as exchangeable (F1), reducible (F2), oxidizable (F3), and residual (F4) could determine its relative toxicity. Nevertheless, the recovery of valuable metals from such sludge enriches its value. However, such studies for LABS are scanty. Furthermore, physical distribution of heavy metals in different size fractions of LABS particles is scarce. Adding to it, an ecological risk assessment of LABS could be useful in deciding disposal options, posing recovery potential and/or its use in construction [217, 293, 295]. The state of the art in sludge disposal area has already pointed out it's utilized in clay soil stabilization. A study reported improved the compressive strength of soft clay when stabilized with recycled basanite [14]. Several studies reported potential of various sludges as a construction material for partial replacement of sand/fly ash/ cement [170, 193, 203]. There are multiple attempts to incorporate sludge in construction work as bricking material (cemented or fired), binder (partial or full replacement), and admixture [158, 296]. Hence, solidification using an appropriate binder with heavy metal fixation is practiced for several industries [174, 204, 297]. The investigations in the utilization of LABS for such purposes are imperatively low in number. Henceforth, this chapter is designed to achieve the second major objective of the thesis "Toxicity assessment and valorization potential of heavy metallic sludge". The critical analyses of LABS through FESEM, EDX, XRD, TGA, and XRF were carried out to understand its mineralogy and chemical composition. The heavy metal analysis was carried out in multiple directions, including total metal content of LABS, heavy metal speciation of LABS, and their concentration in various particles sizes of LABS. The toxicity of LABS was assessed through TCLP and DTPA tests as well as using risk assessment indices. The progressive acidification LABS using five different acids was carried out in order to explore potential of metal recovery and subsequent valorization. Further, based on the characterization results of LABS, a potential of its utilizations as a partial replacement of fertile clay in fired brick manufacturing was thoroughly investigated. The negative-valued LABS was used as a partial replacement for fertile clay that is used for fired brick production to provide a clean and effective solution for LABS disposal and heavy metal fixation. In first place composition of pulverized clay soil (PCS) and pulverized LABS (PBS) was investigated. Secondly, the firing temperature as well as clay-brick proportion was optimized to manufacture bricks complying the Bureau of Indian Standards (BIS) and ASTM International. The fired bricks were tested for

compressive strength, cold water absorption test, linear shrinkage, and TCLP. The mechanics of brick failure patterns were studied as a function of firing temperature. The spectroscopic and mineralogical analysis of the samples was systematically carried out as a function of firing temperature and percentage of PBS addition to understand microscopic arrangements and strength developing compounds generated during firing of bricks.

5.2 Results and discussions

The LABS was characterized thorough physicochemical techniques, heavy metal analysis, chemical leaching tests, and sequential extraction; its valorization potential studied by recovering heavy metals through progressive acidification is presented here. The hazardous nature of LABS is evaluated by the TCLP test and the extent of toxicity through risk assessment indices. The results of LABS tests in production of fired clay brick as a viable solution for the disposal of hazardous heavy metallic sludge and conjoint heavy metal fixation are presented and discussed. Further, the results of bricks assessment parameters such as linear shrinkage behavior, the volume of open pores, apparent porosity, bulk density, and loss on ignition were estimated. The brick quality criterions viz. water absorption and compressive strength were determined to investigate compliance of manufactured bricks to Indian Standards and ASTM International.

5.2.1 LABS characterization

5.2.1.1 Physicochemical, spectroscopic and thermogravimetric characteristics

LABS collected was moist, ash black in color and appeared fine particulate with touch. The outer layer of sludge turned red gray upon exposure to the atmospheric air. This observation gave a preliminary impression of the presence of Fe in sludge, which might have oxidized upon atmospheric exposure. LABS was alkaline (pH~8) due to the addition of lime during treatment and possessed a very high conductivity (3000±0 mmho/cm) as a result of sulphuric acid usage in the manufacturing process. The proximate analysis of LABS revealed that moisture content (MC) was low (43.33±2.6%) as LABS was collected from the drying beds. The volatile solids (VS) content was less (4.85±0.53%), and ash content (52.46±1.53%) was very high due to high metal content. The cation exchange capacity (CEC) of the sludge was found to be 1.75±0.32 meq/100g. A comparison between the characteristic of LABS and other industrial sludge was performed and presented in Table 5.1. The abundance of Pb and Mg in LABS used in this study was notably higher than its concentration in sludge generated from electroplating and metal processing industries.

Table 5.1: Characteristics of battery industry sludge used in present study and comparison with various metal bearing industrial sludge.

Parameter **Reference**	**Battery** Present study	**Battery** [298]	**Battery** [11]	**Electroplating** [299]	**Metal process** [11]	**Industrial Plant** [300]
Pb	08322	ND	005	00967.6	68.2	71.9
Fe	15721	NA	NA	008642	NA	NA
Cu	00175	000237	266	00554.2	196.1	NA
Cd	01215	112,500	10.3	00153.4	15.3	42.1
Ni	00155	018,135	316	176000	655.3	64.8
Mg	04324	NA	NA	NA	NA	NA
Mn	00300	NA	NA	000643	NA	NA
Al	04800	NA	NA	NA	NA	NA
Co	00425	NA	NA	001174	NA	NA
Ca	65712	NA	NA	NA	NA	NA
Zn	00310	001700	NA	048780	NA	NA
Cr	ND	000031	005	036300	15.1	4.92
pH	~ 8	000011	5.98	0009.02	6.93	7.33
Moisture content, %	43.33	98.2	77.3	NA	78.8	NA

ND: Not detected, NA: Not available, Metal concentration is presented in mg/kg

The XRD pattern of LABS showed a predominance (56%) of basanite ($CaSO_4 \cdot 0.5(H_2O)$) mineral in raw LABS (Fig. 5.1a). Presence of gypsum and ettringite are expected in sludge as a result of lime [$Ca(OH)_2$] addition to high sulphate wastewater, but it was not detected in XRD. Due to drying of LABS at 105°C, gypsum ($CaSO_4 \cdot H_2O$) could have converted to bassanite mineral. This could also be due to rapid neutralization of sulphate bearing wastewater and formation of precipitates of gypsum and ettringite with poor crystallinity, making it difficult to detect in XRD [38]. The next significant minerals present were manitobaite ($Na_{16}Mn_{25}^{2+}Al_8(PO_4))_{30}$, $Fe(PO_4)$, calcite ($CaCO_3$), and $Mn(MoO_4)$ in 9, 8, 6, and 5%. These minerals are soluble either in water or in mildly acidic conditions, which contribute to the exchangeable metal fraction. Other trace minerals of metal oxides such as periclase (MgO), hercynite ($FeAl_2O_4$), FeO, MnO, brucite (MgH_2O_2), NiO, and ZnO were present. Even with the crystalline forms of minerals, there could be amorphous mineral compositions too, because many compounds present in LABS are isostructural and possess similar lattice parameters causing overlapping of the XRD peaks. LABS contained irregular and angular particles as a result of micro-aggregated metals precipitation. The crystals of calcite were also observed all over the LABS (Fig. 5.1b). Further, the EDX image mapping showed high concentrations of Fe, Pb, Ca, and Cd along with traces of Cu and Zn (Fig. 5.1c). Oxygen (O) was uniformly distributed over the LABS having the oxide forms of metals.

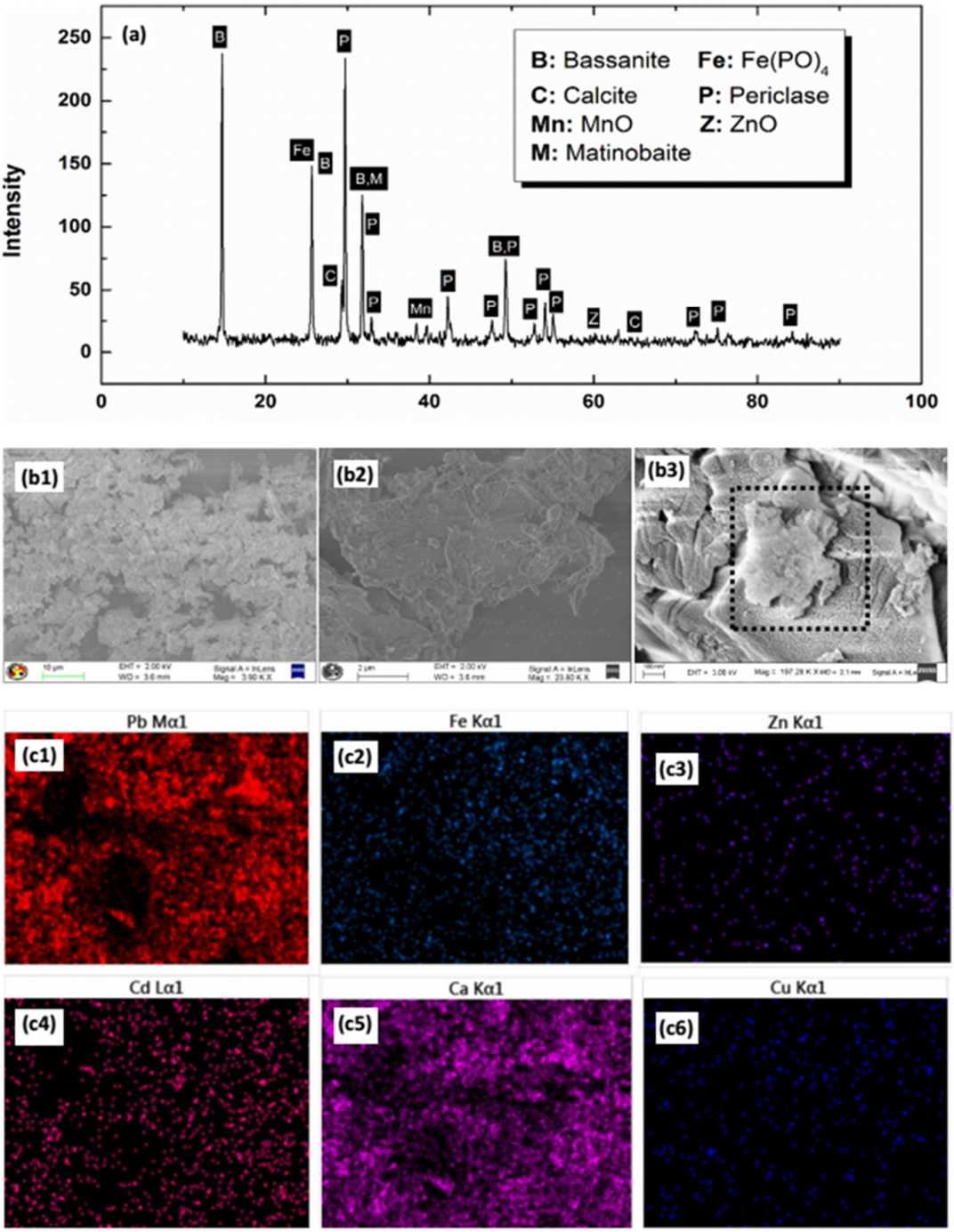

Figure 5.1: (a) XRD pattern of LABS showing mineralogical composition, (b1-b3) FESEM micrographs of LABS, and (c1-c6) Elemental image mapping of LABS using EDX.

The TGA curve for LABS showed five distinct phases of thermal decomposition in the temperature ranges of 30–145, 146–270, 271–620, 621–820, and 821-900°C, respectively (Fig. 5.2). The major weight loss was observed in the first phase (17.87%) corresponding to removal of adsorbed water and combustion of basanite ($2CaSO_4.H_2O$).

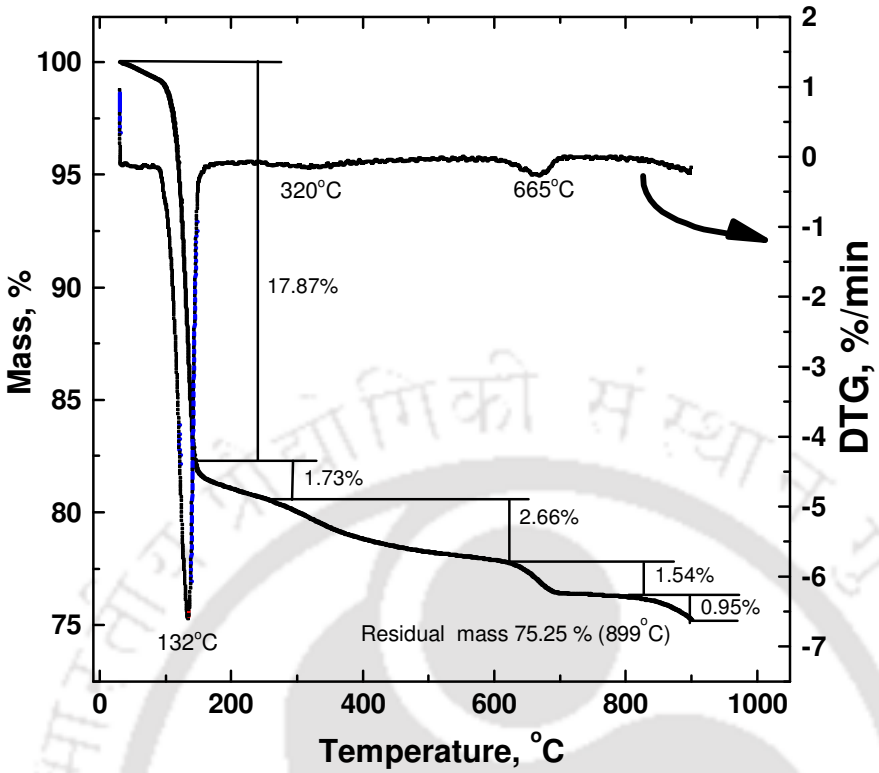

Figure 5.2: TGA and DTG curve through thermogravimetric analysis of LABS.

In second phase, the anhydride basanite formed was combusted. The differential thermogravimetric (DTG) curve shows a major groove corresponding to this combustion, centered at 132°C. Similar thermal decomposition profile for calamine processing waste is reported in literature [196]. The third phase corresponds to combustion of organics and dehydroxylation of amorphous ferrous hydroxides present. The weight loss in the fourth phase was attributed to the combustion of calcium and magnesium carbonates with the release of CO_2 [197, 301]. The second deepest groove centered at 665°C was observed in the DTG curve, corresponding to this mass loss. Further weight loss in the fifth phase was due to more persistent compounds and intermediate products of LABS.

The chemical composition of the pulverized LABS (PBS) was analyzed through X-ray fluorescence (XRF) analysis. It was found that the PBS was dominated by the presence of calcium oxide (73%) as a result of unreacted lime after wastewater treatment, followed by silica and aluminium oxides. The content of fluxing agents was only 2.2% excluding CaO. Basanite was predominantly present in the LABS as evident from the XRD pattern (Fig. 5.1). A high content of CaO oxide and basanite was due to lime addition to high sulphate wastewater.

5.2.1.2 Heavy metal analysis

It can be seen that the LABS contained a large number of metals in high concentrations (Table 5.2). The concentration of Pb, Fe, Cu, Cd, Ni, Mg, Mn, Al, Co, Ca, and Zn were 8322, 15721, 175, 1215, 155, 4324, 300, 4800, 425, 65712, and 310 mg/kg of LABS. The cumulative concentration of all heavy metals in LABS was 101.5±0.56 g/kg equivalent to 712.4 mM/kg of LABS. The heavy metals present in various industrial sludge is well documented (Table 5.1), but information on its contributory sources is missing [10, 11, 302]. In the case of LABS, a higher Pb content was due to use of Pb in battery manufacturing, whereas the high concentration of Fe was the result of using mild steel pipes, conduits, and channels for carrying sulphuric acid or acidic water in the manufacturing process. Higher concentrations of Ca and Al were results of lime addition for precipitation, and the presence of traces of elements such as Cu, Ni, Mn, Co, and Zn could be out of impurities in lead precursor as well as in lime used for wastewater treatment. The source of high Mg and Cd in sludge remained unknown as no manufacturing process is supposed to contribute towards Mg and Cd. It can be observed from Table 5.2, that Pb concentration in sludge was not complying with the standards for the use of sludge for land application. The LABS was also containing a huge amount of Fe and Ca.

Table 5.2: Total metal, DTPA, and TCLP concentrations in LABS and standards.

Element	Disposal on soil limit[a], mg/kg	LABS, mg/kg	TCLP limit[b], mg/L	TCLP of LABS, mg/L	DTPA of LABS, mg/L
Pb	500	8322	5	20.4	6.71
Fe	[c]	15721	[c]	16.5	8.69
Cu	400	175	[c]	0.11	3.21
Cd	[c]	1215	1	3.78	1.86
Ni	200	155	5	1.52	3.74
Mg	[c]	4324	[c]	8.65	6.23
Mn	[c]	300	[c]	0.82	0.56
Cr	300-400	ND	5	ND	ND
Al	[c]	4800	[c]	13.2	17.1
Co	[c]	425	[c]	1.26	1.23
Ca	[c]	65712	c	36.7	69.3
As	[c]	ND	5	ND	ND
Zn	500	310	5	1.16	0.36

[a] National Standard of the People's Republic of China GB 15618–1995: Environmental quality standard for soils

[b] Maximum allowable concentration for TCLP by USEPA: 40 CFR 261, Appendix II, 1993 ed.

[c] Element not enlisted, ND: Not detected.

5.2.1.3 Particle size distribution and metal content

LABS was heterogeneous in nature with 1-100 µm sized particles (Fig. 5.3a). Two major fractions were from 1-10 and 10-100 µm. The earlier one was about 55% and, the rest comprised 45% of LABS. Precisely, about 6, 31, 55, 69, 77, and 95% were passing through 1, 5, 10, 15, 20 and 50 µm sieves, respectively. Similar results for blast furnace slag with high metal content are reported. The slag had two major size fractions, 90% of the particles being below 50 µm size and, most of the metals were concentrated in the fine fractions [42, 303]. The histogram for LABS was plotted to represent the individual percentage of each sized particle (Fig. 5.3b). Most of the particles (>75%) were in the range of 5 to 50 µm with an average particle size of 15 µm.

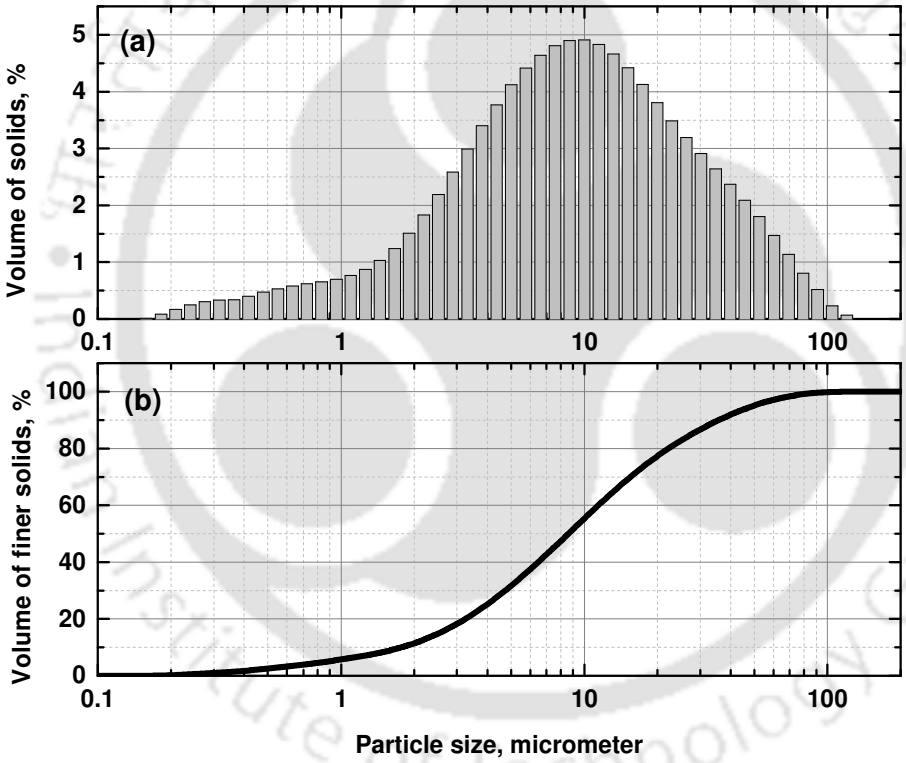

Figure 5.3: (a) Particle size distribution curve of LABS, and (b) size band histogram.

LABS was separated into different size fractions following the methodology explained in Section 2.6.1.4 of Chapter 2. It was analyzed for total heavy metals content, and the results are shown in Fig. 5.4. It was observed that all the metals were concentrated in particle size smaller than 10 µm. Pb, Cd, Fe, and Ni were of 53, 45, 59, and 53% of total metal in this fraction. The fine fractions in sludge was mostly a chemical compound

containing metal sulphates, oxides, and carbonates further confirmed by spectroscopic studies [295]. The coarse fraction (>75 µm) contained inorganics and soil particles with a little amount (<5%) of heavy metals. Similar results for anaerobically digested sludge and blast furnace slags are reported [232, 303]. Therefore, the physical segregation before treatment could benefit adopting an appropriate treatment according to the metal content in fine and coarse fractions. The metal abundance was 51-76% only with <10 µm particles. Valorization through chemical leaching could be beneficial for the most concentrated fraction whereas, it would be worthy to decontaminate the bulk sludge having a lesser metal concentration

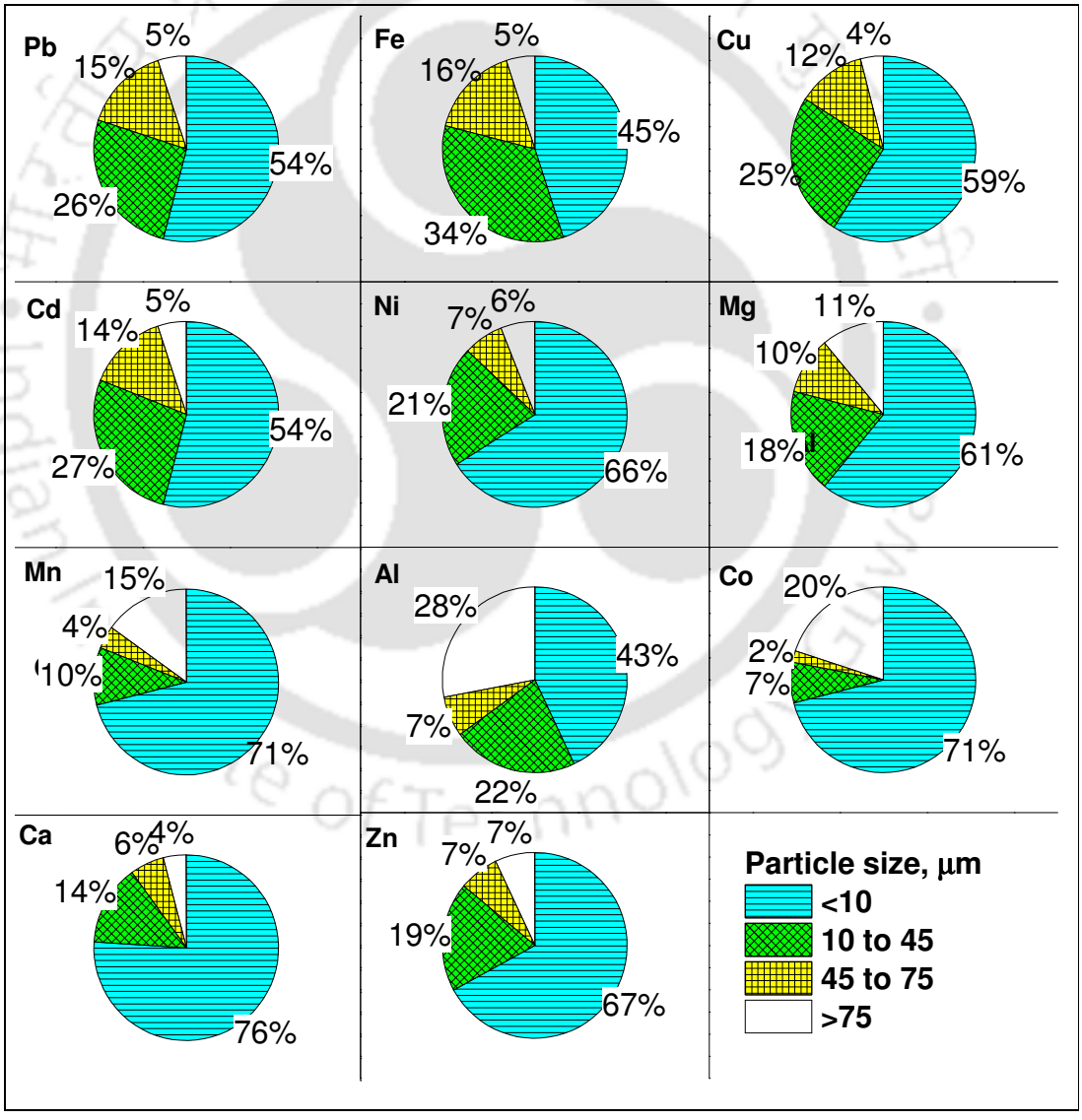

Figure 5.4: Percentage distribution of individual in different size fractions of LABS.

.

5.2.1.4 TCLP and DTPA tests on LABS

Results of the TCLP tests conducted on LABS for various metals leaching are given in Table 5.2. It was observed that leaching of Ni and Zn was within TCLP standards but Pb and Cd exceeded the limit, making the LABS hazardous in nature. The Pb and Cd in leachate were 5 and 4 times higher than that of the respective standards. The leachability of the metals followed the order as Ca>Pb>Fe>Al>Mg>Cd>Ni>Co>Zn>Mn>Cu. The DTPA test was carried out to estimate the mobile fractions and, the results are presented in Table 5.2. The mobile fractions were in the order as Ca>Al>Fe>Pb>Mg>Ni>Cu>Cd>Co>Mn>Zn. The DTPA test doesn't dissolve carbonates, but only exchangeable fractions, whereas TCLP test dissolves carbonates as well as oxides to some extent [299]. Hence, the concentrations of the DTPA tests were lower than that of TCLP. Higher DTPA concentrations of Cu, Ca, Al, and Ni than that of TCLP indicated that these metals were higher in mobile fractions than that of the other fractions. Higher concentrations of TCLP for Pb, Fe, Cd, Mg, Mn, Zn, and Co indicate that these metals were present mostly in the oxide forms.

5.2.1.5 Sequential extraction

The BCR sequential extraction uses destructive solutions and leaches out heavy metals categorizing them in exchangeable, reducible, oxidizable, and residual fractions to provide insight of metal association in solid, crystalline or amorphous phases [230, 295, 299]. The heavy metals mobility is highly sensitive to pH changes, which often occurs in the environment. Therefore, sequential extraction was carried out for LABS, percentage of heavy metals in each size fraction was plotted individually in Fig. 5.5, and explained below.

Exchangeable fraction (F1)

Metals in this fraction are usually associated with sulphates and carbonates without metals in organic and Fe/Mn bound matrix. Though LABS contained high concentrations of sulphates and carbonates, only Ca, Ni, Zn, and Mn were prominently found in F1 fraction. In this fraction, the order of metal prominence was as Al>Ca>Cu>Ni >Zn>Mn>Mg>Co>Pb>Cd>Fe. LABS being a lime treated sludge. Al and Ca are supposed to be associated with sulphates, carbonates, and oxides [295], which is loosely attached and leached as F1 fraction. In LABS, calcium sulphate was present in crystalline forms of basanite, gypsum, calcite, and ettringite [158], which gets dissolved in mildly acidic conditions contributing to F1 fraction of Ca and Al. Out of the total, 75 and 57% of Al and Ca was present in this fraction. Trace metals such as Cu, Ni, Zn, and Co were in 36, 32, 29,

and 14% in F1 form. The F1 fraction of Pb and Cd was only 19 and 7% but found to be higher than the allowable limits for disposal [233] due to high toxicity levels [304]. Though Fe content in sludge was second highest, only 4% of Fe existed in F1 form. It suggests that the direct disposal of LABS on the land will make the metal in F1 bioavailable to plants in accordance with their prominence [305].

Reducible fraction (F2)

The metals bound to Fe/Mn oxides are generally released when exposed to reducible conditions. These oxides are abundant in soil; hence, this step brings possible leaching of metals in reducing conditions. The highest leaching of metals from LABS was 55, 49, 45, and 42% for Mn, Fe, Zn, and Mg, respectively. These metals are usually present in amorphous oxides, but over the years with dissolving atmospheric CO_2, and it forms crystalline Fe oxides. Similar results for Acid Mine Drainage neutralized metallic sludge are reported, where, Fe, Mn, Mg, and Al were present predominantly in F2 fraction [295]. Mn was found to be primarily in amorphous forms contributing to F2 fraction. Other metals viz. Ni, Ca, Pb, Cd, Co, Al, and Cu were 27, 13, 10, 9, 8, and 4%, respectively. Ca extracted in F2 forms was present in calcite and fluorite forms, as further confirmed by spectroscopic studies. It indicates that the disposal of LABS in an acidic environment could lead to significant metal leaching present in F2 [235].

Oxidizable fraction (F3)

The metals bound to organics are leached out in this fraction. The metals in this fraction are bonded in stable humic structures. Pb and Cu showed higher affinity for an organic fraction with 67 and 55% abundance. The results were in line with studies carried out for Acid Mine Drainage treated sludge [295]. The other metals viz. Co, Mg, Ni, Cd, Ca, Al, Zn, Mn, and Fe were in 35, 23, 23, 20, 18, 13, 11, 9, and 5%, respectively. Low pH (<1) could solubilize crystalline aluminum oxide present and, Al was extracted in F3 fraction [295]. Therefore, the metals in F3 needs a strong oxidizing environment to be leached out upon its disposal [235].

Residual fraction (F4)

Mg, Cu, and Zn were present in 62, 42, and 41% in F4. The order of metals in this fraction was as Mg>Zn>Cu>Cd>Ni>Fe>Ca>Mn>Pb>Co>Al. F4 fraction is the most stable form, and metals are in the mineral crystal lattice and/or crystal oxides. This form is not available for plants uptake, hence possess least or no risk [299].

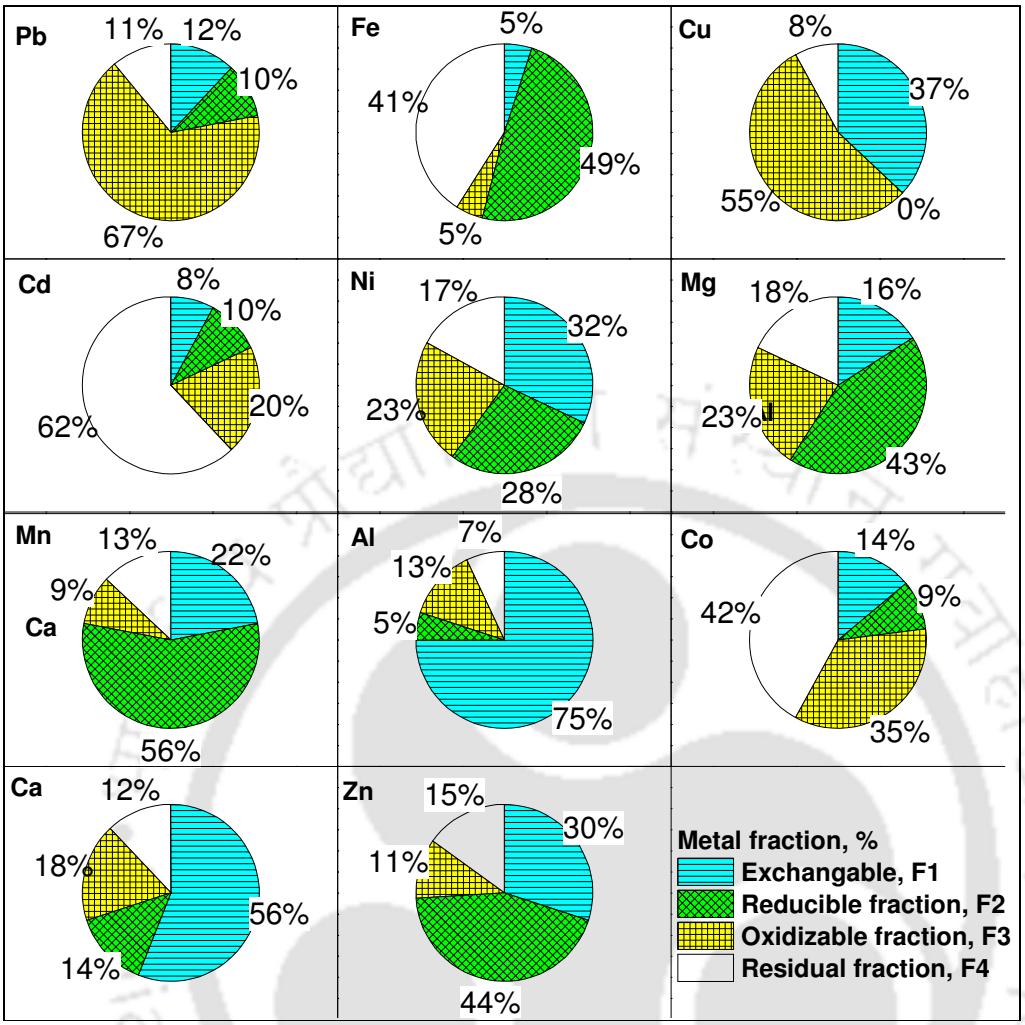

Figure 5.5: Speciation of individual metals in LABS as per BCR extraction scheme.

5.2.1.6 Risk assessment indices

The hazardous nature of LABS was confirmed from the TCLP tests. However, the extent of possible risk was assessed by well-established risk assessment codes and indices [238, 306]. The results of risk assessment are shown in Table 5.3. It was observed that Pb and Cd possessed the highest risk for LABS and, the contamination factor (C_f) was 16 and 14, respectively, indicating a very high risk followed by Ni, Cu, and Zn, which possessed a low risk to the environment [307]. The contamination degree (C_d) of LABS was found to be 32, falling into a very high-risk potential zone, if disposed on the land [295]. PLI for the LABS was found to be 1.38, PLI=0 indicates no risk, PLI from 0 to 1 indicates an allowable risk and, PLI>1 indicates a progressive risk [238]. The PER index for individual metals also suggested a very high risk of Pb and a considerable risk for Cd followed by a low risk for Zn, Ni, and Cu. The cumulative PER for LABS was 435 making LABS very risky in the case of unsafe land disposals.

Table 5.3: Various risk assessment indices in LABS and their decisive limits.

Risk Index	Estimation of risk levels	Metal of interest				
		Pb	Cd	Ni	Cu	Zn
Contamination factor (C_f)[a]	Low (<1); moderate (1-3); considerable (3-6); very high (>6)	16	14	0.7	0.4	0.06
Contamination degree (C_d)[b]	Low (<5); moderate (5-10); considerable (10-20); very high (>20)	15.58				
Pollution load index (PLI)[b]	No risk (0); baseline (1); progressive deterioration (>1)	1.38				
Individual environment risk (E_r^i)[a]	Low (<40); moderate (40-80); considerable (80-160); high (160-320); very high (>320)	83	429	4	2	0.06
Potential environment risk (PER)[b]	Low (<65); moderate (65-130); considerable (130-260); very high (>260)	435				

[a] risk index estimated for individual metal
[b] risk index estimated for LABS

5.2.2 Valorization through progressive acidification

LABS contained huge amounts of metals of economic interest such as Pb, Zn, and Cu. About 70% of the Pb used in battery manufacturing industry is derived from recycled used lead acid batteries (ULABs) [155]. However, the recovery of Pb from sludge was less explored due to the limitation of selective metal recovery [232]. The progressive acidification of LABS for metal recovery was carried out and, the results are shown in Fig. 5.6. It was observed that the citric acid (at pH 2) was effective in leaching most of the heavy metals over oxalic acid at the same pH. The leaching efficiency using citric acid was 47, 77, 60, 19, 58, 59, 67, 41, and 51 for Pb, Fe, Cu, Cd, Ni, Mn, Al, Co, and Zn; whereas, it was 47, 41, 32, 4, 12, 41, 34, 41, and 35% when oxalic acid was used for leaching. The higher efficiency of citric acid was due to the presence of three carboxylic groups in citric acid; whereas, oxalic acid contains two carboxylic groups. Another reason could be the presence of calcium which forms calcium oxalate precipitate with oxalic acid, inhibiting metal extraction [232]. All inorganic acids used in this study showed significant extraction potential. However, H_3PO_4 found to be the best among all (Fig. 5.6). The metals bound to organics were the most difficult to extract and is the simplest exchangeable ones. The citric acid showed the best metal recovery from all fractions. Therefore, the effect of contact time on metal recovery was studied using citric acid, H_3PO_4, and HCl acids due to higher metal recovery (Fig. 5.6), and the results are presented in Fig. 5.7.

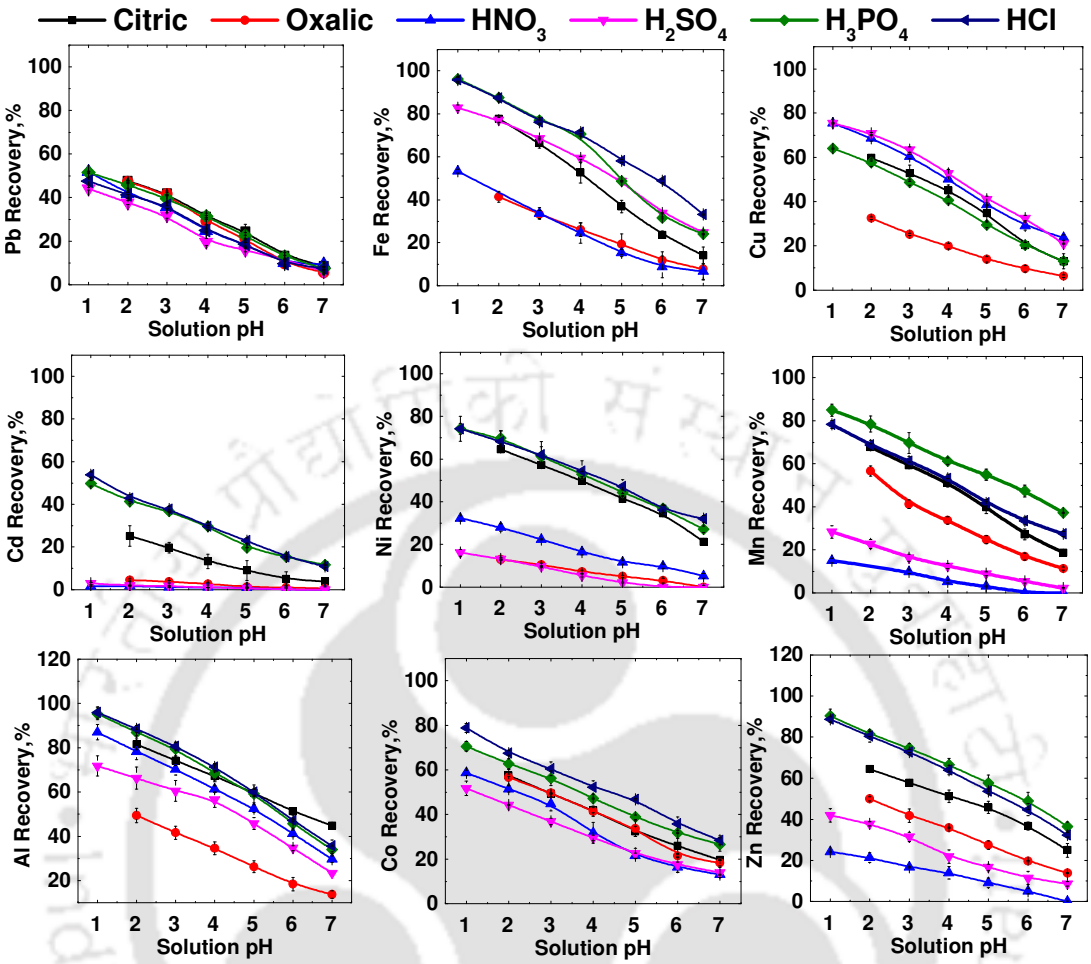

Figure 5.6: Progressive acidification of LABS for heavy metal recovery using organic and inorganic acids.

It can be observed from Fig. 5.7 that Pb, Fe, Cu, Cd, Ni, Mn, Co, and Zn recoveries with citric acid were improved from 31, 49, 28, 12, 35, 40, 25, and 32% to 67, 83, 75, 28, 64, 65, 46, and 63% at the end of 24 h of contact time. But, H_3PO_4 and HCl acids didn't show much improvement in the metal recovery with prolonged leaching duration.

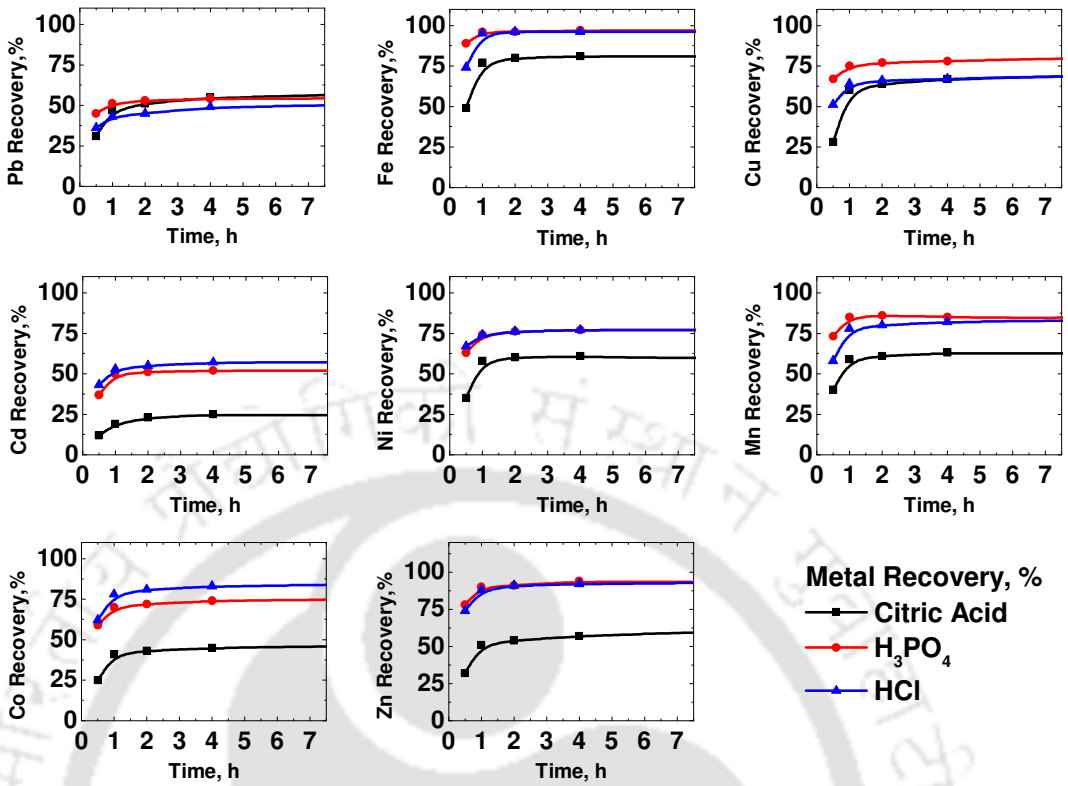

Figure 5.7: Effect of contact time on metal recovery using citric acid, H_3PO_4, and HCl.

The lower ionization of citric acid (1.3 to 2.1%) resulted in slow penetrability into sludge particles [308] in comparison with H_3PO_4 and HCl acids [232]. Percentage enhancement in metal recovery was the highest for Pb (169%) and Cu (267%), as these metals were mostly present in the oxidizable form. The effect of H_2O_2 addition on metal recovery was also studied. H_2O_2 addition accelerated the metal recovery, especially from the organic bound fraction (Fig. 5.8). H_2O_2 (E^0= 1.763 V vs. standard hydrogen electrode, SHE) itself acts as an oxidizing agent along with the formation of highly reactive hydroxyl radicals (HO•, E^0=2.80 V vs. SHE) through Fenton reaction facilitating the metal recovery by oxidizing organic matters [232, 309-311]. The Pb recovery was 42, 39, and 36% with citric acid (pH 3), which upon the introduction of H_2O_2 (highest dose of 7.6 ml/L) was increased to 80, 79, and 72%. Similarly, Fe recovery was increased by 24, 18, and 14% using citric, H_3PO_4, and HCl acids, respectively.

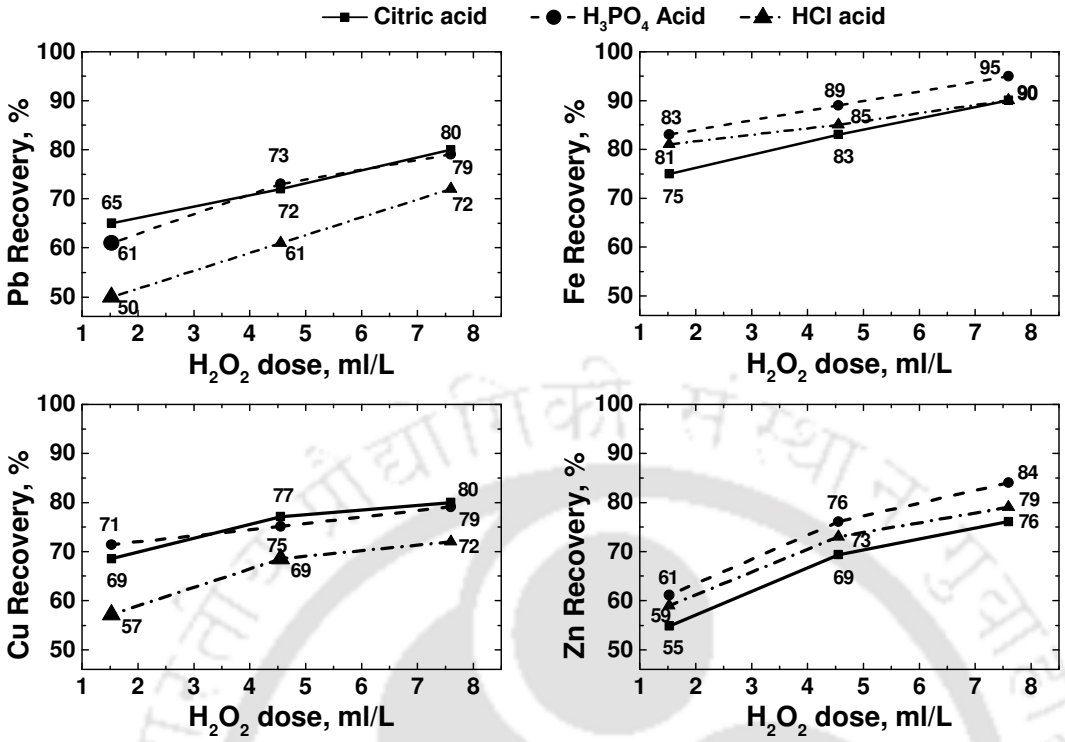

Figure 5.8: Effect of H_2O_2 addition on metal recovery from LABS using citric acid, H_3PO_4, and HCl at pH 3.

The acidic leachate was containing multiple metals and high impurities, which doesn't match any market reuse specifications. To account for the metal recovery from waste streams or multi-metal solutions, the use of different synthetic/biomass selective resins/adsorbents and selective precipitation has been extensively reported [149, 156, 269, 312]. The successful application of such metal recovery especially Pb, from battery manufacturing sludge, may pose a big profit margin to companies and reuse of environmental resources, heading towards economic and cleaner battery production.

5.2.3 Brick manufacturing and testing

This part of Chapter 5 investigates on the characterization of bricking clay and properties of bricks with respect to firing temperature and its environmental aspects such as heavy metal leaching. Finally, the manufactured bricks were tested against standard criterions viz. compressive strength and water absorption to review its compliance with Indian Standards and ASTM International.

5.2.3.1 Characterization of bricking clay

The quality of a fired brick depends greatly on the physicochemical properties of raw materials. Hence, the TGA analysis of PCS was carried out, and the results are shown in Fig. 5.9. The mass loss against temperature and DTG were obtained using the inbuilt software with an instantaneous recording system. The DTG plot is of much importance in TGA as it provides even small changes in mass loss, which are easier to be identified in the form of DTG peaks. The PCS showed a typical TGA profile of Asian sepiolite [313] (Fig. 5.9). The TGA curve didn't show either endothermic or exothermic peaks. However, the curve was divided into four segments as per thermal behavior of clay. The DTG profile identified small changes and showed endothermic as well as exothermic peaks. The characteristic endothermic reactions were due to dehydration, loss of crystal structure and exothermic reactions for the formation of new phases at elevated temperatures. The weight loss in the temperature range of 25–250°C was 3.14% and referred to a loss of adsorbed water with endothermic peak appearing at 95°C in the DTG curve [197]. The major mass loss of 5.76% was observed in the temperature range of 251–500°C and attributed to combustion of organics. The corresponding exothermic peak was observed in DTG curves at 400°C. The dehydroxylation of silicates was observed in the temperature range of 450–630°C with endothermic peak at 470°C in the DTG curve [301]. The mass loss in the temperature range of 500–700°C was 3.99% and attributed to dehydration of kaolinite and halloysite [313]. Further, the weight loss and peaks in the DTG curve were due to the formation/transformation into new compounds such as crystalline quartz and/or illite. The chemical composition of PCS through XRF was analyzed. The PCS exhibited a typical clay composition dominated by the presence of silica followed by aluminum and ferrous oxides. The durability of the bricks is dependent upon the percentage of the silica oxide present in clay. The content of alkaline and alkaline earth metal oxides was 21%, which acts as fluxing agent during firing and promotes vitrification of bricks [314]. The XRD pattern for PCS (Fig. 5.10) also showed an intense peak of SiO_2. The amount of Fe_2O_3 was significant which imparts reddish color to the bricks upon firing. The K_i index, a ratio of SiO_2/Al_2O_3 was significantly high (2.8) representing kaolinitic clay [315]. However, the TGA profile suggested that the clay was a combination of all the minerals as the mass loss was almost at an angle of 45° to the baseline. The XRD diffractogram showed the peaks for the presence of minerals such as albite (22.7%), kaolinite (13.2%), lintisite (7.5%), wonesite (6.1%), and magnesite (5.4%) along with traces of potassium aluminate silicate hydroxide, tsaregorodtsevite, richetite, and alabandite.

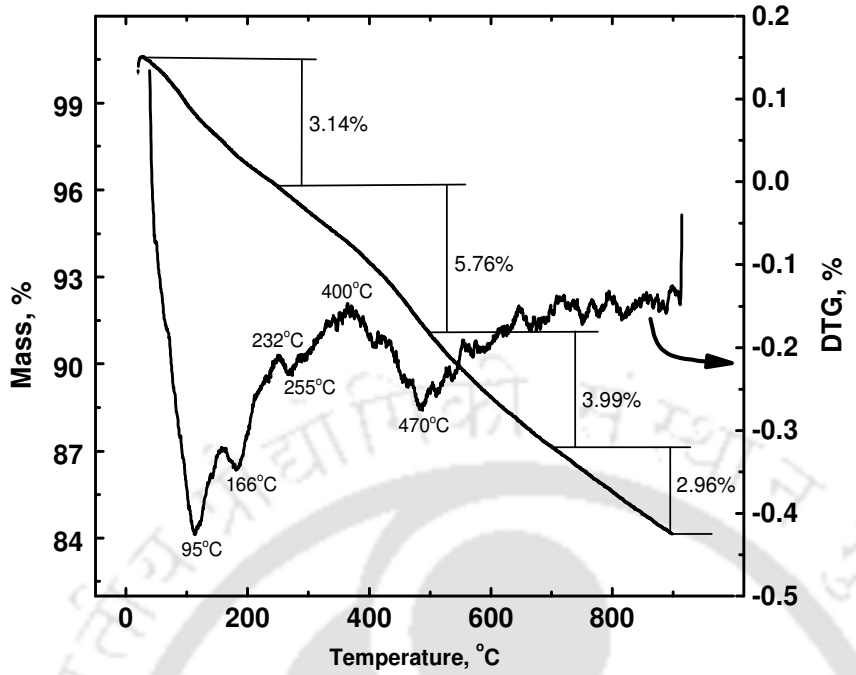

Figure 5.9: TGA and DTG curve through thermogravimetric analysis of PCS.

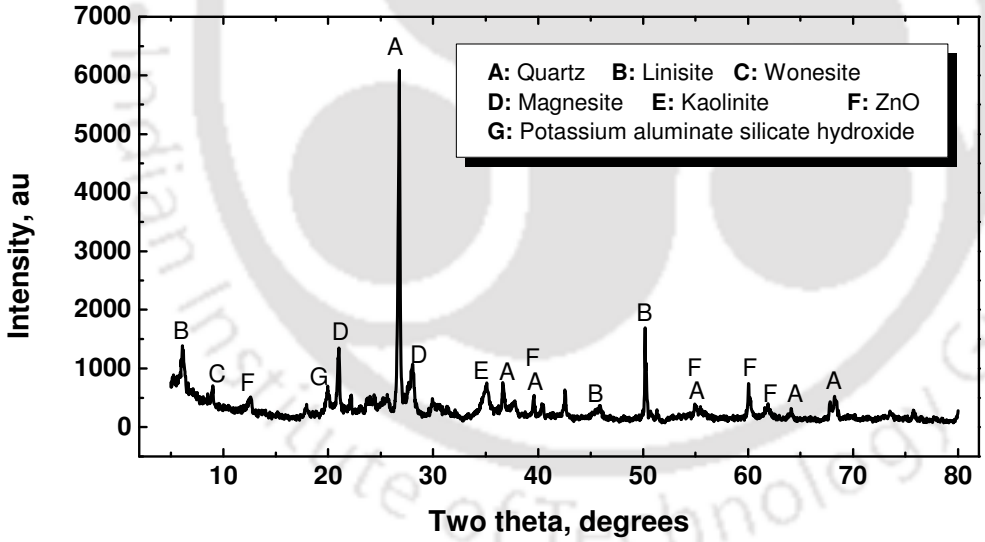

Figure 5.10: XRD pattern of pulverized clay soil (PCS).

5.2.3.2 Effect of firing temperature on pure clay bricks

The firing temperature is an important parameter for manufacturing of desired quality bricks. However, studies focusing on the effects of firing temperature on brick properties are limited. The increase in firing temperature increased the compressive strength of B0 bricks up to 950°C through partial vitrification of clay minerals [313].

However, at firing temperatures ≥1000°C, B0 bricks showed the convex deformation. Further, the increase in firing temperature caused complete dissolution of clay minerals and soil started boiling. The trapping of high-pressure gases caused the highest pore volume expansion at 1250°C. This was resulted in bulking of brick, and losing its shape.

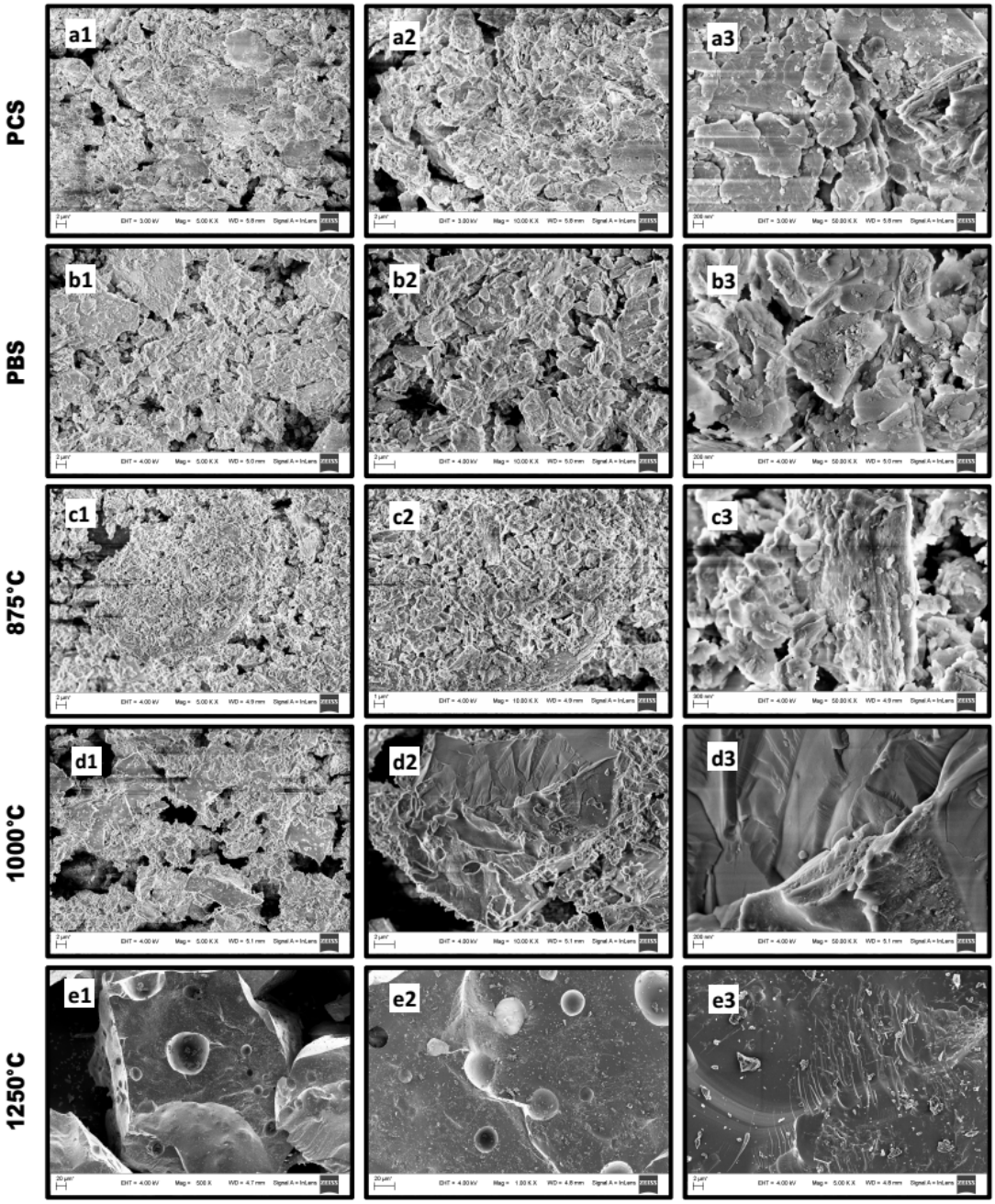

Figure 5.11: FESEM images of (a) PCS, (b) PBS, (c) B0 bricks at 875°C, (d) B0 bricks at 1000°C, and (e) B0 bricks at 1250°C.

Figs. 5.11a and 5.11b show the FESEM micrographs of PCS and PBS. The FESEM micrographs of brick B0 surface at different firing temperature are shown in Figs. 5.11c to 5.11e. The expansion in length, width, and thickness of brick was 5, 7, and 50%, respectively. The highest thickness expansion was due to capillary pressure built by entrapped gases and faster cooling rates. Similar observations for distortion and crack development in brick manufacturing using urban river sediment are reported in literature [197]. The B0 bricks fired at 1250°C showed a negligible water absorption (0.2%) and a low compressive strength (1.76 N/mm^2). The surface appeared to be glassy in nature (Fig. 5.11e). Measurement of open pore volume, apparent porosity, and bulk density was not done due to a distorted shape of brick. The PBS added in B5−B50 bricks acted as an impurity and bricks showed no cracks and distortion, even at higher temperatures up to 1050°C.

5.2.3.3 Parametric variations of brick properties

The bricks with a varying percentage of PBS were cast and fired at different firing temperatures. The optimum firing temperature obtained in manufacturing of B0 bricks was treated as a reference with the variation of ±50°C. Hence, the B5−B50 bricks were fired at three temperatures 950, 1000, and 1050°C. The properties of bricks such as bulk density, linear shrinkage, porosity, loss on ignition, compressive strength, open pore volume, and water absorption were measured.

The effect of firing temperature and sludge content on loss on ignition (LOI) is presented in Fig 5.12. The LOI was increased by 383, 367, and 366% with the increase in sludge content from 0 to 50% at the firing temperature of 950, 1000, and 1050°C, respectively. This might be for the intensification of decomposition reaction at an elevated firing temperature. The higher LOI was attributed to combustion of basanite, iron hydroxides and carbonate minerals and anhydrite, organic matter, and oxidation-reduction of iron (Eq. 5.1) [316]. On increased PBS content, the LOI increased. The results were in line with TGA analysis of bricking materials [314]. The LOI implies formation of pores and subsequently increasing porosity.

$$6FeO + 1.5O_2 \rightarrow 2Fe_3O_4 + 0.5O_2 \quad (5.1)$$

The higher firing temperature caused partial liquefaction of clay minerals that increased surface tension of liquid phase. This resulted in the increase of capillary pressure and densification through conversion of open porosity into a closed one.

Water absorption is one of the important parameters in brick characterization. It is also recognized as the indicator of durability and porosity. Low water absorption exhibits high density, resistance to the weathering conditions, and an acceptable permeability of bricks [198, 301]. The results of water absorption at different firing temperature as a function of PBS content are presented in Fig. 5.13. Water absorption was increased with the increase in PBS content; these results can be correlated with higher LOI values at increased PBS addition. On firing, basanite and other compounds are decomposed, increasing porosity of bricks hence increasing water absorption. On the other hand, despite of higher LOI, the water absorption was decreased with the increase in the firing temperature, and it was 17, 8, and 2% for brick B0. The water absorption reduced by 89, 91, 67, 34, 30, 23, 19, and 31% for bricks B0, B5, B10, B15, B20, B30, B40, and B50, when the firing temperature was increased from 950 to 1050°C. This could be due to melting of clay minerals at a higher firing temperature and formation of a new dense and impervious/glassy surface which reduced water absorption [317].

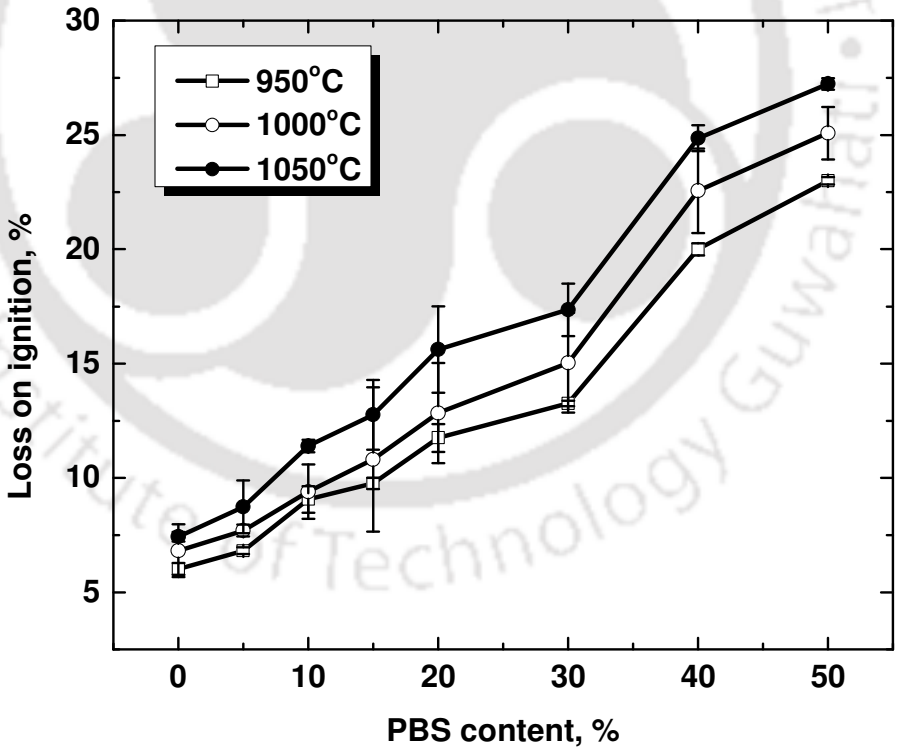

Figure 5.12: Loss on ignition of bricks (B0–B50) at different firing temperature.

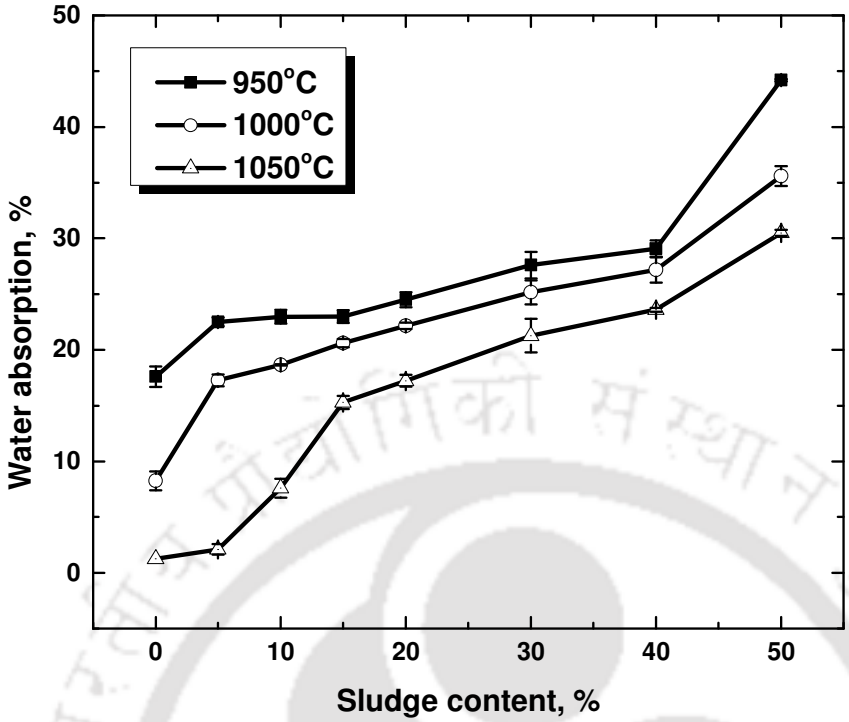

Figure 5.13: Water absorption of bricks (B0–B50) at different firing temperature.

Furthermore, bulk density, apparent porosity, and volume of open pores of bricks fired were estimated at different temperature (Fig. 5.14a), and the effects of the firing temperature of 950, 1000, and 1050°C are illustrated in Figs. 5.14b to 5.14c. It was observed that the apparent porosity and volume of open pores were decreased and bulk density was increased from 35 to 4%, 11 to 1%, and 1.51 to 1.98 g/cc respectively, with the increase in firing temperature from 500 to 1050°C (Fig. 5.14a). With the increase in PBS content, the apparent porosity and volume of open pores were increased and, the bulk density of bricks was decreased at all firing temperatures. These results support the earlier finding that thermal treatment combusted basanite, iron hydroxides, carbonates, and anhydrite. The combustion leads to emission of high pressure gases which get trapped into pores leading to expansion of pores i.e. bloating [316]. High porous bricks are beneficial as they are lighter in weight and may offer good thermal resistance provided water absorption is within the limit [317].

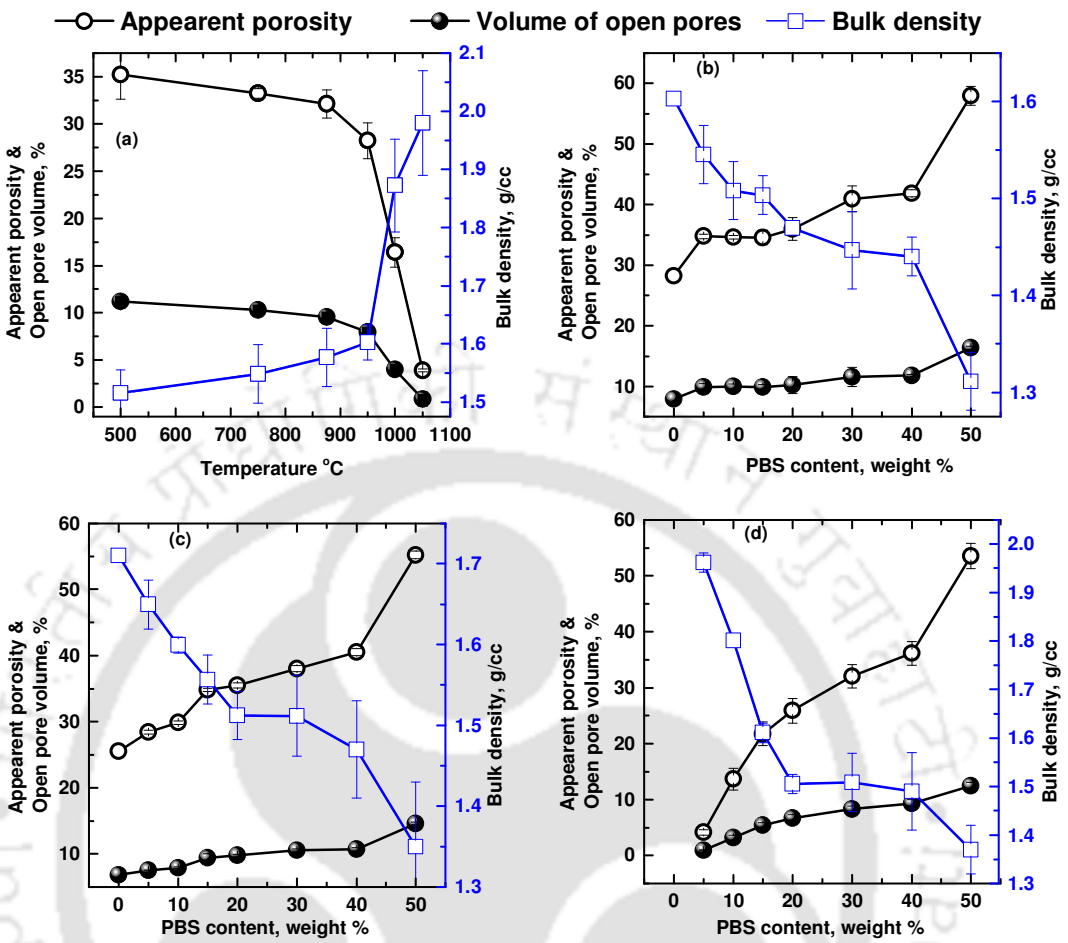

Figure 5.14: Apparent porosity, volume of open pores, and bulk densities of bricks (B0–B50) (a) as a function of firing temperature and at temperature of (b) 950°C, (c) 1000°C, and (d) 1050°C.

5.2.3.4 Linear shrinkage, modulus of elasticity, and stress-stress curve of bricks

Higher shrinkage of bricks may cause tension in the bricks leading to crack development during firing [301]. The linear shrinkage of the bricks B0–B50 was estimated and reported in Table 5.4. It was observed that the linear shrinkage was increased with the increase in firing temperature. The reason could be an enhanced densification through partial liquid phase generation [197]. The addition of PBS reduced linear shrinkage due to combustive content in PBS. A few studies also reported negative linear shrinkage for the addition of organic matter rich waste materials [197, 301].

Table 5.4: Linear shrinkage and modulus of elasticity of PBS added bricks.

PBS, %	Linear shrinkage, %			Modulus of elasticity (E), GPa		
	950°C	1000°C	1050°C	950°C	1000°C	1050°C
0%	4.2±0.8	7.4±0.9	13.2±0.5	0.33±0.15	NA	NA
5%	2.3±0.2	3.7±0.2	11.6±0.9	0.45±0.26	1.04±0.14	0.553±0.47
10%	1.9±0.6	3.1±0.3	9.0±0.5	0.41±0.05	0.999±0.21	0.63±0.18
15%	1.7±0.3	2.6±0.5	6.1±0.4	0.56±0.21	0.71±0.17	0.457±0.24
20%	1.7±0.5	2.5±0.3	5.5±0.8	0.68±0.16	0.743±0.28	0.527±0.32
30%	1.6±0.2	2.7±0.5	4.6±0.1	0.68±0.25	0.653±0.21	0.546±0.18
40%	1.4±0.2	2.5±0.6	3.2±0.3	0.52±0.24	0.520±0.17	0.567±0.36

NA: not applicable

The modulus of elasticity is a measure of brick stiffness; the stiff bricks fail by rupture on loading rather than crushing failure. The modulus of elasticity of bricks may not be the correct measure for the bricks, as the brick loading tends to be perfectly nonlinear. However, it was measured for the portion up to which it behaves linearly. The modulus of elasticity was observed to have increased with the increase in firing temperature and decreased with the addition of PBS (Table 5.4). The failure patterns of bricks were further investigated with the stress-strain curve obtained during compressive testing of the bricks (Fig. 5.15). It can be seen that at the lower firing temperatures (500–875°C) brick B0 presented plastic failure pattern with low compressive strength (Fig. 5.15a). Whereas, the elevated firing temperature (950–1000°C) showed an improved compressive strength and sudden or brittle failure. The sudden failure is indicative of lack of ductility and a high stiffness of the brick imparted by a higher firing temperature, fortified by modulus of elasticity of bricks (Table 5.4). The stiffness of bricks with a low PBS content prevented any plastic deformation to occur before failure. In building masonry units, the structural integrity is often lost due to brittle failure of building elements. The brittle failure in masonry units usually leads to initiation of crack that propagates rapidly through the material leading to catastrophic failure of the system, as there is a short period between initiation of failure and complete rupture. In contrast, the bricks with the PBS addition showed significant compressive strength to comply with standards along with plastic failure (Figs. 5.15b and 5.15c). The stress-strain curves of brick B20 and B30 at 1000 and 1050°C firing temperatures, showed plastic failure pattern when compared to bricks B5, B10, and B15. This indicates that the addition of PBS was resulted in increased ductility of the bricks as an added advantage.

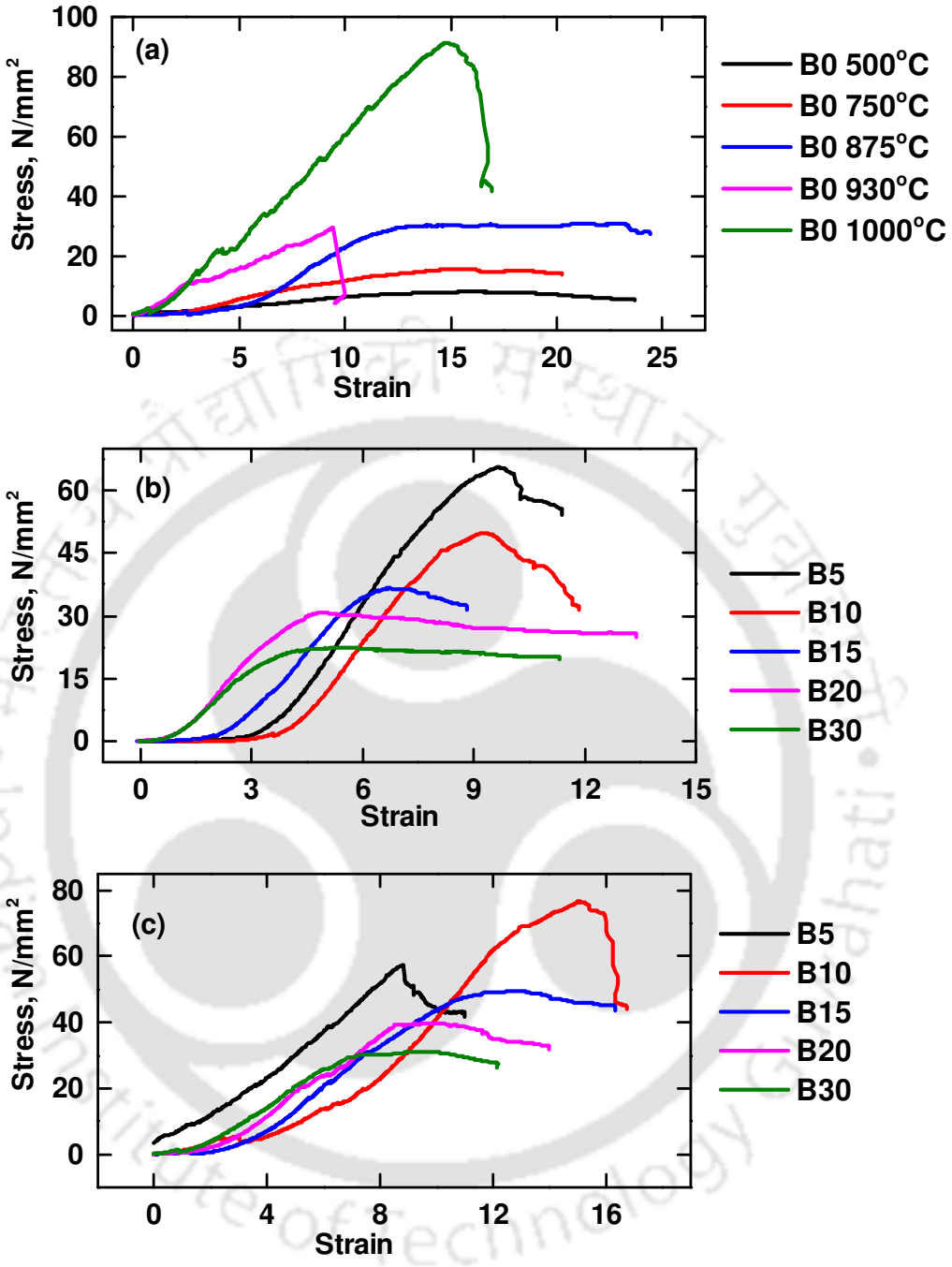

Figure 5.15: Stress-strain curves for bricks (a) for brick B0 at different firing temperatures, (b) for bricks B5–B30 at 1000°C firing temperature, and (c) for bricks B5–B30 at 1050°C firing temperature.

5.2.3.5 Color changes in bricks as a function of firing temperature

The fired bricks have a characteristic uniform red color, which is an indicator of bricks quality. However, the color of the brick is essentially controlled by the firing temperature, chemical composition of raw materials, firing atmosphere, and cooling rate [318]. As it can be seen from Fig. 5.16, the color of unfired bricks was dark gray, and became red on firing due to conversion of Fe_2O_3 to Fe_3O_4 [316]. The red color darkened at an elevated firing temperature. However, at a firing temperature ≥1000°C, the bricks were blackened albeit. This could be due to reducing condition in the muffle furnace [318]. The color of bricks added with PBS was light red, and faded with an increasing PBS amount when fired until 1000°C. At firing temperature of 1050°C, the bricks became yellow due to a higher content of CaO. The mass ratio, the lowest of Fe_2O_3/Ale_2O_3 or Fe_2O_3/CaO decides the final color of the bricks [196]. Iron oxide is the prime colorant of the brick, imparting a red color. Whereas, CaO content imparts yellow and beige to light brown color to bricks [319]. This coloring property can be used for the manufacturing of bricks for decorative work. The white or yellow bricks are usually expensive than that of the red bricks [318]. Hence, the PBS added brick manufacturing could be profitable for industries.

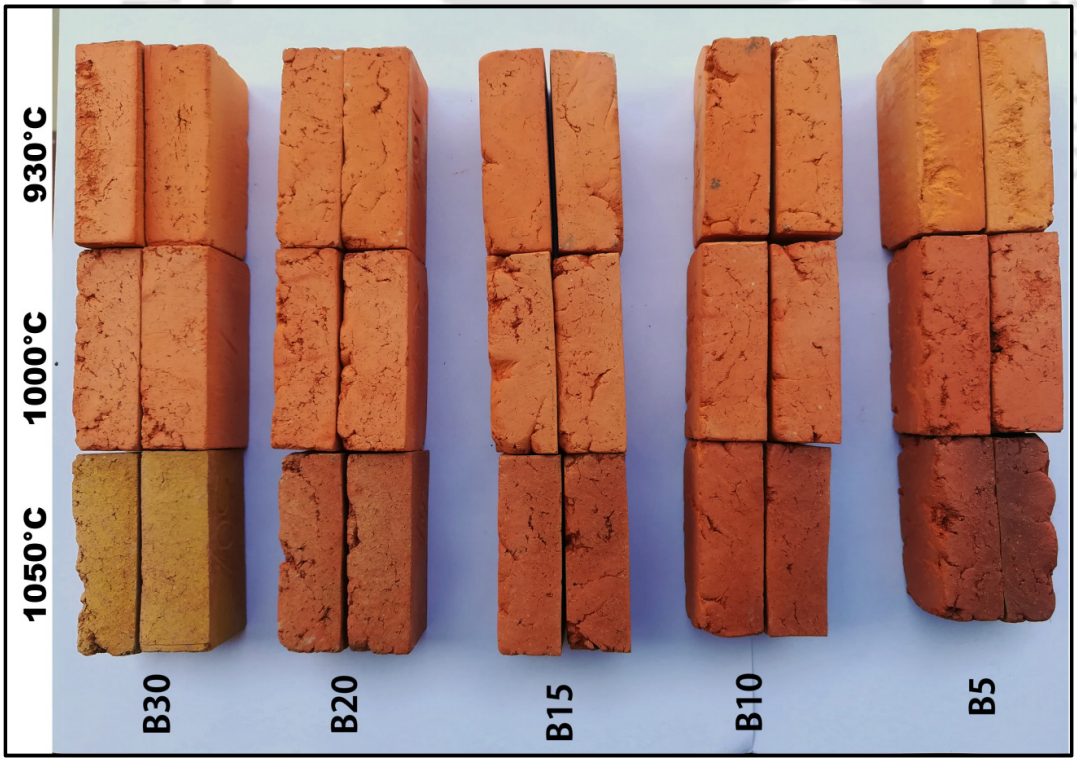

Figure 5.16: Color developments in bricks B5–B30 at firing temperatures of 950, 1000, and 1050°C.

5.2.3.6 Compressive strength of manufactured bricks

Compressive strength is the most important parameter for building materials, imparted by the formation of new crystalline phases and minerals e.g., moganite, hematite, and mullite during the firing of the clay bricks [316]. The results of compressive strength development in B0 bricks are presented in Fig. 5.17. The obvious trend of increased compressive strength with increased firing temperature was observed. The compressive strength was improved from 7.3 to 54.8 N/mm^2 when the firing temperature was increased from 500 to 1000°C. The increment was 50% when the temperature was increased from 950 to 1000°C. However, the addition of PBS hampered compressive strength development and it was 65 and 74 N/mm^2 with brick B5 at firing temperature 1000 and 1050°C, which reduced to 17 and 21 N/mm^2 with B40 bricks, respectively (Fig. 5.17a). Though PBS addition showed a detrimental trend in strength development, it helped sustaining higher firing temperatures. The compressive strength of B5 bricks at 1000 and 1050°C was 1.2 and 1.36 times to that of B0 bricks fired at 1000°C. The higher strength of PBS added bricks was possibly due to a higher elasticity of these bricks compared to B0 [191]. This suggests that the addition of PBS not only retained B0 brick strength, but also it was improved at higher firing temperatures. Fig. 5.17b shows the effect of the PBS addition on compressive strength development at different firing temperatures.

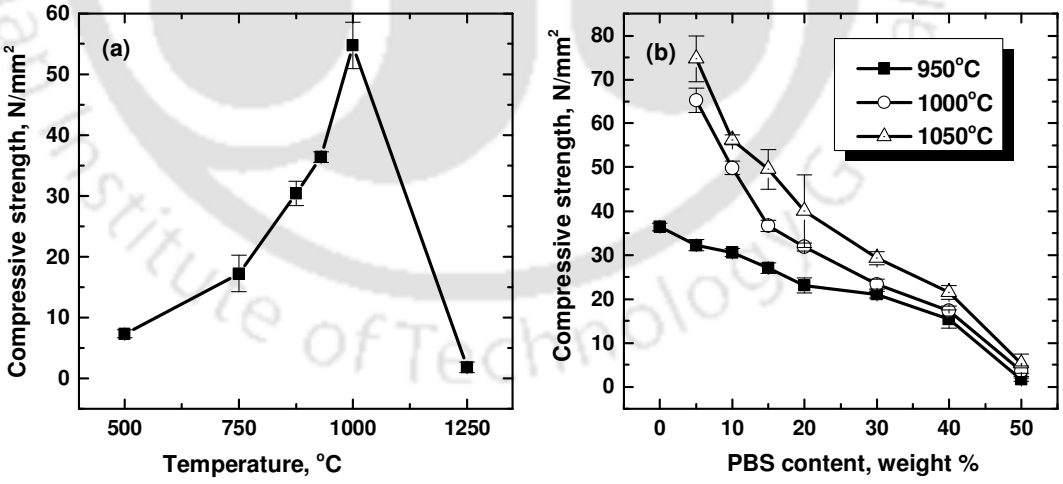

Figure 5.17: (a) Compressive strength of B0 bricks at different firing temperature, and (b) compressive strength of bricks B5–B50 at different firing temperature**.**

5.2.3.7 Environmental considerations

Heavy metal leaching from PBS is the prime environmental concern. Hence, the raw materials as well as fired bricks added with PBS were tested for heavy metal leaching through the TCLP test (USEPA method #1311). The results are presented in Table 5.5 along with the maximum allowable TCLP limit of different heavy metals. It can be seen that PCS didn't leached any metal. However, for PBS, the concentration of Pb and Cd exceeded the prescribed limit of 5 and 1 mg/L, respectively. The test on fired bricks revealed that the leaching concentration of Pb and Cd was well within the prescribed limits. In fact, insignificant leaching of heavy metals was obtained. The reason could be that thermal treatments have changed the metals from the exchangeable fraction to oxidizable/reducible/residual fraction [197].

5.2.4 Brick compliance with Indian and international standards

The physical requirement of fired bricks in most of the standards including BIS and ASTM international are compressive strength, water absorption, and effloresces (Table 5.6). The ASTMC62 (2017) specifies the minimum compressive strength of 10.3 N/mm^2 for negligible weathering conditions with no limit for water absorption. However, the IS:1077 (1992) specifies the minimum compressive strength of 3.5–35 N/mm^2 for the different classes of bricks with water absorption not more than 20% up to class 12.5 and 15% for higher classes. The bricks B0–B40 at all temperatures complied with the compressive strength requirements. However, water absorption was higher than 20% at 950°C. The bricks fired at 1050°C with the addition of maximum 15 and 20% PBS complied the class 35 and class 12.5 [205]. Whereas, to achieve the same at a lower temperature of 1000°C, the PBS content needs to be reduced to a maximum of 10 and 15%.

Table 5.5: TCLP concentrations of heavy metals in raw bricking materials, fired brick samples, and TCLP limits.

Sample	950°C				1000°C				1050°C			
	Pb	**Cd**	**Ni**	**Zn**	**Pb**	**Cd**	**Ni**	**Zn**	**Pb**	**Cd**	**Ni**	**Zn**
B0	ND	ND	ND	ND	ND	ND	ND	ND	ND	ND	ND	ND
B5	0.41	ND	ND	ND	0.38	ND	ND	ND	ND	ND	ND	ND
B10	0.87	0.06	ND	ND	0.65	ND	ND	ND	ND	ND	ND	ND
B15	0.84±0.2	0.11±0.	0.05±0	0.56±0.1	0.72±0.2	0.06±0.0	0.08±0.0	0.48±0.1	0.52±0.1	0.08±0.0	ND	0.32±0.2
B20	0.93±0.1	0.17±0	0.13±0	0.81±0.2	1.21±0.2	0.12±0.1	0.15±0.0	0.76±0.1	0.76±0.5	0.12±0.0	0.06±0.0	0.48±0.1
B30	1.26±0.2	0.23±0.1	0.14±0	0.96±0.3	0.98±0.3	0.16±0.1	0.18±0.0	0.81±0.3	0.81±0.3	0.16±0.0	ND	0.65±0.2
B40	1.52±0.8	0.31±0.1	0.21±0.1	1.06±0.1	1.38±0.5	0.21±0.1	0.32±0.1	1.08±0.5	0.89±0.3	0.2±0.0	ND	0.72±0.2
PCS	ND	ND	ND	ND			TCLP Limits		5	1	5	5
PBS	20.42±0.1	3.78±1	1.5±0.8	1.16±0.2								

All metal concentrations are in mg/L
ND: Not detected

Table 5.6: Specifications and classification of bricks as per IS:1077 (1992) and ASTMC62 (2017).

Standard	**Brick**	**Minimum compressive strength, N/mm²**		**Maximum Water Absorption, % (24 h cold water immersion)**	
Type	**designation**	**Average of 5**	**Individual**	**Average of 5**	**Individual**
BIS	35	NA	35	NA	Water absorption shall not be more than 20 % by weight up to class 12.5 and 15 % by weight for higher classes.
	30	NA	30	NA	
	25	NA	25	NA	
	20	NA	20	NA	
	17.5	NA	17.5	NA	
	15	NA	15	NA	
	12.5	NA	12.5	NA	
	10	NA	10	NA	
	7.5	NA	7.5	NA	
	5	NA	5	NA	
	3.5	3.5	3.5		
	Grade SW	20.7	17.2	17	20
ASTM	Grade MW	17.2	15.2	22	25
International	Grade NW	10.3	8.6	No limit	No limit

5.3 Major findings

- The LABS was found to be highly contaminated with not only Pb but also many other metals in concentrations of 8322 (Pb), 15721 (Fe), 175 (Cu), 1215 (Cd), 155 (Ni), 4324 (Mg), 300 (Mn), 4800 (Al), 425 (Co), 65712 (Ca), and 310 (Zn).
- LABS was found to be a potential building material for construction, fortified by spectroscopic studies
- BCR sequential chemical extraction studies revealed that the Al and Ca were prominent in exchangeable, Fe, Mn, and Zn reducible, Pb (67%) and Cu (55%) in oxidizable and, Mg and Cd were mostly in the residual fraction
- The TCLP test and toxicity indices categorized LABS as hazardous waste for the land disposal, physical segregation of LABS showed heavy metals to be concentrated in the finer fractions and, only 5% in coarse fraction
- Valorization of LABS through progressive acidification was highest using citric acid, however, use of H_2O_2 along with acids further mobilized metals from organic fractions enriching metal recovery potential
- Studies on partial replacement of clay by LABS in fired brick manufacturing revealed that the highest compressive strength was found to be 74 N/mm^2 against the water absorption of 2.1% achieved by B5 (5% LABS) bricks at a firing temperature of 1050°C
- The study achieved effective fixation heavy metal in LABS by utilizing in manufacturing of fired clay bricks complying IS:1077:1992 class 12.5.
- PCS-PBS bricks showed a higher porosity compared to PCS bricks that restrained deformation and distortion of bricks during firing. The addition of PBS improved ductile behavior of bricks that could avoid catastrophic failure and imparted a yellow coloration due to high CaO content.
- The TCLP test confirmed an effective fixation of Pb, Cd, Ni, and Zn in PCS-PBS bricks and, its concentration in leachate was well within the USEPA permissible limits

.

CHAPTER 6

Conclusions, limitations and future scopes of the study

The present project work aims at preparation of new adsorbents and resins from an agricultural waste product and their application on removal of lead from LABW, and valorization of LABS as a potential building material. Towards this goal, two functionalized sorbents, namely, FFA and bio-resin were synthesized using arecanut husk, a locally abundant agricultural waste, for the treatment of LABW. The potential hazard and risk associated with heavy metallic LABS were studied, and valuable heavy metals were recovered by the progressive acidification. Further, the utilization of LABS in the manufacturing of LABS-clay bricks was investigated. The overall conclusions reflecting the key findings of the dissertation along with limitations and future scopes of study are presented in this chapter.

6.1 Overall conclusion

- The study demonstrated synthesis of high metal uptake capacity FFA (194 mg/g) through a simple sulphuric acid treatment that showed 99% Pb(II) removal at a dosage of 1 g/L from an initial 32 mg/L Pb(II) concentration.
- A proton adsorption model (PAM) was developed, and it was further modified for Pb(II) uptake on the basis of proton exchange mechanism. FFA was laden with carboxylic and sulfonic groups which was identified by FTIR spectra and further confirmed by PAM. pK_a values and concentration of carboxylic and sulfonic groups were of 3.21 and 1.62, and 1.53×10^{-3}, 2×10^{-3} mol/g, respectively. Pb(II) binding constants (K_M) were estimated as 5.2×10^{6} and 28.11 L/mol for carboxylic and sulfonic sites, respectively, with an overall binding constant of 1.46×10^{8} L/ mol.

- FFA was found to be superior in terms of Langmuir capacity that was 1.1 and 3.4 times higher than commercial IR120 resin and commercial activated carbon, respectively, and the effect of Ca^{+}, Na^{2+}, Mg^{2+} and EDTA on Pb(II) removal was insignificant at a lower concentration (< 2.5 M).
- Application of FFA to LABW removed Pb completely, and the removal efficiencies of Fe, Cd, and Mg were 85, 84, and 56% complying discharge standards in India.
- In synthesis of bio-resin, mercerization followed by EDTAD carboxylation induced a high concentration of carboxylic groups (0.735 mM/g) as a result of the formation of an ester linkage through an acylation reaction.
- The bio-resin showed 99% efficiency in Pb(II) removal from synthetic wastewater (initial 32 mg/L or 0.157 mM), for which the Pb(II) binding constant was determined as 1.73×10^3 L/mol from the PAM with an exhaustion capacity of 18.7 mg/g.
- Desorption efficiency of Pb(II) from the exhausted bio-resin was found to be about 97% with 0.1 N HCl, and the bio-resin simultaneously removed Pb and Cd from LABW well below detection limit along with a significant removal of Fe, Mg, Ni, and Co ions.
- Heavy metal present in LABS was mostly concentrated in the finer sizes. Fe, Mn, and Zn were abundant in the reducible fraction. Mobility of Al was the highest, and that of Fe was the lowest among the metals present. Pb (67%) and Cu (55%) showed the highest percentage in the oxidizable fraction, and Cd was mostly present in the residual form. The TCLP tests as well as the toxicity indices categorized LABS as a hazardous waste. The mineralogical study of LABS explored its potentiality as a construction material.
- Valorization of LABS through the progressive acidification suggested citric acid as the best eluent. However, use of H_2O_2 along with acids further mobilized metals from organic fraction, enriching metal recovery potential.
- The potential application of LABS for fired brick production as a substitute of fertile clay up to 20% remained successful along with an effective heavy metal fixation, and the bricks manufactured with 5% LABS showed the highest compressive strength of 74 N/mm^2 against the water absorption of 2.1% complying Indian Standards as well as ASTM International.
- LABS modified clay bricks showed increased porosity and a higher sustainable firing temperature that restrained bricks deformation, distortion, and/or cracks development during firing. It also improved ductility behavior of bricks avoiding catastrophic failure and imparted a yellow coloration.

6.2 Limitations of the present work

- Both FFA and bio-resin were synthesized in laboratory using a small amount of arecanut husk (150 g arecanut husk) collected from a specific source. The quality and performance of FFA and bio-resin may vary with the variation of biomass precursor quality and also in a scaled up process.
- The synthesized FFA was (micro) fibrous in nature making it difficult to maintain uniform particle size that may have a significant effect on its consistent performance in metal removal.
- The FFA was tested for the removal of Pb along with the accompanying metal ions from synthetic and LAB wastewater in the batch mode of operation (250 mL) with an electrically driven shaker. The probability of lower frequency of collision between the FFA/bio-resin and contaminants (heavy metal/organics/inorganic) is higher in a continuous operation. Therefore, the performance and uptake capacity of FFA/bio-resin may fall down from what is reported in batch studies. The efficiency of FFA may differ from present study due to presence of chelating contaminants in industrial wastewater and could permanently kill the functionalized sites.
- LABS-clay bricks were manufactured in a scaled down size. Hence, its qualities and properties may differ from what are reported here.
- LABS-clay bricks were manufactured in the controlled laboratory condition. The bricks manufacturing in a real industrial kiln also could influence its quality.
- The release of toxic gases, including the heavy metal(s) vapor could be a serious limitation of the utilization of LABS for fired clay manufacturing.

6.3 Recommendations for the future work

- Performance of synthesized functionalized sorbents was investigated in a batch mode having a higher contact time. Studies on the understanding in a continuous mode of operation and design of an adsorption process using these sorbents may be taken up for further studies.
- Synthesized sorbents were only tested for LABW treatment. Studies on the performance of these materials for the treatment of heavy metallic wastewater laden with organic/inorganic contaminants will further explore the spectrum for common/general wastewater treatment.

- Studies for the safe disposal of spent adsorbents and resins should be considered with an equal priority to take care of secondary water and soil pollution. Use of spent adsorbents in brick manufacturing may alleviate the disposal issue of spent adsorbents with energy recovery from biomass burning.
- Due to limited supply of LABS, manufacturing of (LABS) bricks were performed with a scaled down size under controlled laboratory condition. Therefore, bricks manufacturing in a real kiln with normal size and geometry need to be studied.
- Bricks testing were done following the standard laboratory procedures. However, its testing as a construction element such as in real paving and wall fencing are open for future studies.
- Release of toxic gases (e.g. NOx, SOx etc.), if any, from the decomposition of LABS during bricks manufacturing could trigger (hazardous) air pollution. Therefore, the studies in this direction are imperative.

Annexure I

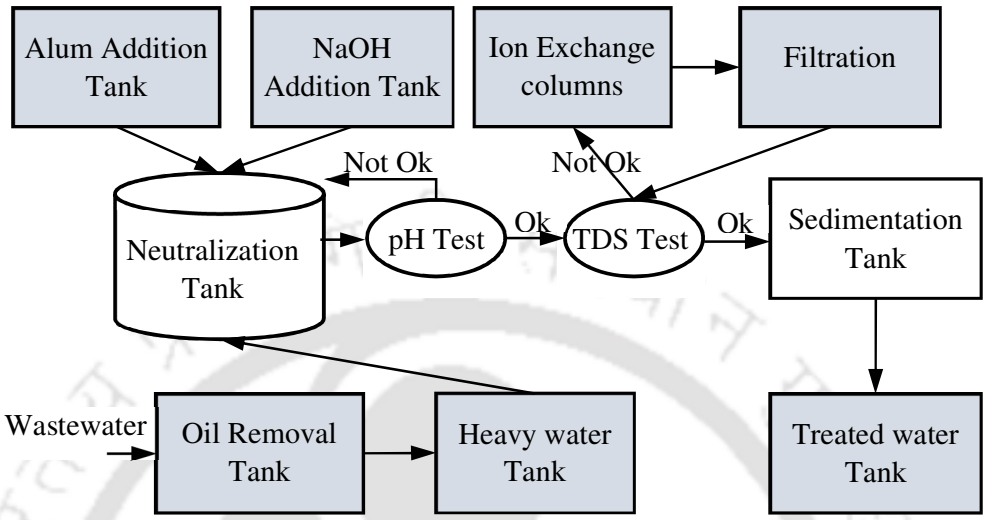

Figure A1: Block diagram for treatment of LAB manufacturing wastewater [88].

Annexure II

Cost analysis of FFA

The preliminary cost for the synthesis of FFA was estimated for FFA produced using concentrated H_2SO_4 (Section 2.4.2.1). In the synthesis experiment, an amount of 150 g of dried RH was mixed with 300 mL concentrated H_2SO_4 (98 %) that produced 125 g of FFA. Hence, the production of 1 kg FFA needs 2.4 L of concentrated H_2SO_4 (98 %). The cost of preliminary treatments such as washing and husk cutting is minimal and can be considered as Rs 10 per kg of FFA.

Cost of raw material and preliminary treatment per kg of FFA = Rs. 10

Cost of concentrated H_2SO_4 (98 %) ≈ Rs. 30/L

Cost of concentrated H_2SO_4 (98 %) per kg of FFA = 2.4 ×30

= Rs. 72/-

Cost of drying comes to be Rs. 5 per kWh [284] and the hot air oven consumes 4 kWh in 24 h, at temperature 105 °C (ICT Kolkata).

Total drying/heating time of the adsorbent = 5+2+12 h

= 19 h

Power consumed in drying/heating = 19 × 0.166 kWh

= 3.66 kWh

Cost of drying/heating (Rs) = 5 × 3.66

= 18.3

Hence, the net cost of FFA/kg (Rs.) = 10 + 72 + 18.3

= 100.3/ kg of FFA

Additional 10% can be added to take care of miscellaneous charges such as washing water cost and labor cost.

Hence, the final cost of FFA/kg (Rs.) = 100.3 + 10.03

≈ 110/kg of FFA

This preliminary cost calculation doesn't consider the reuse of spent H_2SO_4 acid. Therefore, further reduction in the synthesis cost of FFA is possible with careful optimization and design of synthesis process.

References

[1] Dahodwalla, H. and S. Herat, *Cleaner production options for lead-acid battery manufacturing industry.* Journal of Cleaner Production, 2000. **8**(2): p. 133-142.

[2] TEAM, *Tackling a global crisis: International Year of Sanitation.*, W.S.S.C. Council, Editor. 2008: United Nations.

[3] Trivedi, V., *Hazardous waste recycling: A case study analysis of lead acid battery*, in *Environment and Sustainable Development*. 2017, Tata Institute of Social Sciences, Guwahati, India: Guwahati.

[4] Kulkarni, V.V., A.K. Golder, and P.K. Ghosh, *Critical analysis and valorization potential of battery industry sludge: Speciation, risk assessment and metal recovery.* Journal of Cleaner Production, 2017.

[5] Rao, S.M. and G.C. Raju, *Comparison of alkaline treatment of lead contaminated wastewater using lime and sodium hydroxide* Journal of Water Resource Protection, 2010. **2**(3): p. 282-290.

[6] Paulino, A.T., L.B. Santos, and J. Nozaki, *Removal of Pb^{2+}, Cu^{2+}, and Fe^{3+} from battery manufacture wastewater by chitosan produced from silkworm chrysalides as a low-cost adsorbent.* Reactive and Functional Polymers, 2008. **68**(2): p. 634-642.

[7] Chauhan, D. and N. Sankararamakrishnan, *Highly enhanced adsorption for decontamination of lead ions from battery wastewaters using chitosan functionalized with xanthate.* Bioresource Technology, 2008. **99**(18): p. 9021-9024.

[8] Bai, R.S. and T.E. Abraham, *Studies on enhancement of Cr(VI) biosorption by chemically modified biomass of Rhizopus nigricans.* Water Research, 2002. **36**(5): p. 1224-1236.

[9] Xiao, B., X.F. Sun, and R. Sun, *The chemical modification of lignins with succinic anhydride in aqueous systems.* Polymer Degradation and Stability, 2001. **71**(2): p. 223-231.

[10] Wu, Q., et al., *Effective removal of heavy metals from industrial sludge with the aid of a biodegradable chelating ligand GLDA.* Journal of Hazardous Materials, 2015. **283**(0): p. 748-754.

[11] Islam, M.S., et al., *Heavy metals in the industrial sludge and their ecological risk: A case study for a developing country.* Journal of Geochemical Exploration, 2017. **172**: p. 41-49.

[12] Sikka, R. and V.K. Nayyar, *Monitoring of lead (pb) pollution in soils and plants irrigated with untreated sewage water in some industrialized cities of Punjab, India.* Bulletin of Environmental Contamination and Toxicology, 2016. **96**(4): p. 443-448.

[13] Chibuike, G.U. and S.C. Obiora, *Heavy metal polluted soils: Effect on plants and bioremediation methods.* Applied and Environmental Soil Science, 2014. **2014**: p. 12.

[14] Ahmed, A., *Compressive strength and microstructure of soft clay soil stabilized with recycled bassanite.* Applied Clay Science, 2015. **104**(Supplement C): p. 27-35.

[15] Duruibe, J.O., M.O.C. Ogwuegbu, and J.N. Egwurugwu, *Heavy metal pollution and human biotoxic effects.* International Journal of Physical Sciences, 2007. **2**(5): p. 112-118.

[16] Goyer, R., *Issue paper on the human health effects of metals* 2004, U.S. Environmental Protection Agency Risk Assessment Forum Lexington, USA.

[17] *Toxicity and Carcinogenicity of Chromium Compounds in Humans.* Critical Reviews in Toxicology, 2006. **36**(2): p. 155-163.

[18] Fosmire, G.J., *Zinc Toxicity.* The American Journal of Clinical Nutrition, 1990. **51**(225): p. 7.

[19] Mahmood, Q., et al., *Current Status of Toxic Metals Addition to Environment and Its Consequences*, in *The Plant Family Brassicaceae: Contribution Towards Phytoremediation*, A.N. Anjum, et al., Editors. 2012, Springer Netherlands: Dordrecht. p. 35-69.

[20] Abdel -Aty, A.M., et al., *Biosorption of cadmium and lead from aqueous solution by fresh water alga Anabaena sphaerica biomass.* Journal of Advanced Research, 2013. **4**(4): p. 367-374.

[21] Mushak, P., *Chapter 15 - The Nephrotoxicity of Lead in Human Populations*, in *Trace Metals and other Contaminants in the Environment*. 2011, Elsevier. p. 567-595.

[22] A.Wuana, R. and F.E. Okieimen, *Heavy metals in contaminated soils: A review of sources, chemistry, risks and best available strategies for remediation.* ISRN Ecology, 2011. **2011**: p. 20.

[23] Scragg, A.H., *Environmental biotechnology*. 1999: Longman.

[24] Sörme, L. and R. Lagerkvist, *Sources of heavy metals in urban wastewater in Stockholm.* Science of The Total Environment, 2002. **298**(1–3): p. 131-145.

[25] Godin, P.M., M.H. Feinberg, and C.J. Ducauze, *Modelling of soil contamination by airborne lead and cadmium around several emission sources.* Environmental Pollution Series B, Chemical and Physical, 1985. **10**(2): p. 97-114.

[26] A.Moura, R.C., et al., *Study of chromium removal by the electrodialysis of tannery andmetal-finishing effluents.* International Journal of Chemical Engineering, 2012.

[27] Bahadir, T., et al., *The investigation of lead removal by biosorption: An application at storage battery industry wastewaters.* Enzyme and Microbial Technology, 2007. **41**(1–2): p. 98-102.

[28] Kazemipour, M., et al., *Removal of lead, cadmium, zinc, and copper from industrial wastewater by carbon developed from walnut, hazelnut, almond, pistachio shell, and apricot stone.* Journal of Hazardous Materials, 2008. **150**(2): p. 322-327.

[29] Basha, C., et al., *Heavy metal removal from copper smelting effluent using electrochemical cylindrical flow reactor.* Journal of Hazardous Materials, 2008. **152**(1): p. 71-78.

[30] Espinoza, E., R. Escudero, and F.J. Tavera, *Waste Water Treatment by Precipitating Copper, Lead and Nickel species.* Research Journal of Recent Sciences, 2012. **1**(10): p. 1-6.

[31] Hsu, M.J., K. Selvaraj, and G. Agoramoorthy, *Taiwan's industrial heavy metal pollution threatens terrestrial biota.* Environmental Pollution, 2006. **143**(2): p. 327-334.

[32] Agarwal, S.K., *Heavy Metal Pollution*. 2009: APH Publishing Corporation.

[33] Herrera S, P., et al., *Acid mine drainage treatment through a two-step neutralization ferrite-formation process in northern Japan: Physical and chemical characterization of the sludge.* Minerals Engineering, 2007. **20**(14): p. 1309-1314.

[34] Srivastava, N.K. and C.B. Majumder, *Novel biofiltration methods for the treatment of heavy metals from industrial wastewater.* Journal of Hazardous Materials, 2008. **151**(1): p. 1-8.

[35] Kumar Sharma, R., M. Agrawal, and F. Marshall, *Heavy metal contamination of soil and vegetables in suburban areas of Varanasi, India.* Ecotoxicology and Environmental Safety, 2007. **66**(2): p. 258-266.

[36] Sharma, R.K., M. Agrawal, and F. Marshall, *Heavy metal contamination in vegetables grown in wastewater irrigated areas of Varanasi, India.* Bulletin of Environmental Contamination and Toxicology, 2006. **77**(2): p. 312-318.

[37] Sharma, R.K., M. Agrawal, and F.M. Marshall, *Heavy metals in vegetables collected from production and market sites of a tropical urban area of India.* Food and Chemical Toxicology, 2009. **47**(3): p. 583-591.

[38] Macias, F., et al., *Management strategies and valorization for waste sludge from active treatment of extremely metal-polluted acid mine drainage: A contribution for sustainable mining.* Journal of Cleaner Production, 2017. **141**: p. 1057-1066.

[39] Nocete, F., et al., *An archaeological approach to regional environmental pollution in the south-western Iberian Peninsula related to Third millennium BC mining and metallurgy.* Journal of Archaeological Science, 2005. **32**(10): p. 1566-1576.

[40] Bhatia, S.C., *Handbook of Industrial Pollution and Control Volume 2*. Vol. Volume 2. 2002, New Delhi: CBS publishers. 577.

[41] Duffy, G.J., R.D. Lanauze, and J.W. Kable, *Reducing the environmental impact of coal-washing practice in Australia.* Minerals and the Environment, 1981. **3**(4): p. 103-110.

[42] Veres, J., et al., *Characterization of blast furnace sludge and removal of zinc by microwave assisted extraction.* Hydrometallurgy, 2012. **129–130**(0): p. 67-73.

[43] Veres, J., S. Jakabsky, and M. Lovas, *Zinc recovery from iron and steel making wastes by conventional and microwave assisted leaching.* Acta Montanistica Slovaca, 2011. **16**(3): p. 185-191.

[44] Eckenfelder, W.W., *Industrial water pollution control*. 2000: McGraw-Hill.

[45] Patwardhan, A.D., *Industrial Waste Water Treatment*. 2008: PHI Learning.

[46] Kuan, Y.-C., I.H. Lee, and J.-M. Chern, *Heavy metal extraction from PCB wastewater treatment sludge by sulfuric acid.* Journal of Hazardous Materials, 2010. **177**(1): p. 881-886.

[47] Kabdasli, I., et al., *Complexing agent and heavy metal removals from metal plating effluent by electrocoagulation with stainless steel electrodes.* Journal of Hazardous Materials, 2009. **165**(1–3): p. 838-845.

[48] Akbal, F. and S. Camci, *Copper, chromium and nickel removal from metal plating wastewater by electrocoagulation.* Desalination, 2011. **269**(1–3): p. 214-222.

[49] Balde, C.P., et al., *The global e-waste monitor – 2014*. 2015, United Nations University, IAS – SCYCLE: Bonn, Germany. p. 1-41.

[50] Kiddee, P., R. Naidu, and M.H. Wong, *Electronic waste management approaches: An overview.* Waste Management, 2013. **33**(5): p. 1237-1250.

[51] Olafisoye, O.B., T. Adefioye, and O.A. Osibote, *Heavy metals contamination of water, soil, and plants around an electronic waste dumpsite.* Polish Journal of Environmental Studies 2013. **22**(5): p. 1431-1439.

[52] Govil, P.K., et al., *Soil contamination of heavy metals in the Katedan Industrial Development Area, Hyderabad, India.* Environmental Monitoring and Assessment, 2008. **140**(1): p. 313-323.

[53] Tiwari, M.K., et al., *Assessment of heavy metal concentrations in surface water sources in an industrial region of central India.* Karbala International Journal of Modern Science, 2015. **1**(1): p. 9-14.

[54] Jose, J., et al., *Heavy metal pollution exerts reduction/adaptation in the diversity and enzyme expression profile of heterotrophic bacteria in Cochin estuary, India.* Environmental Pollution, 2011. **159**(10): p. 2775-2780.

[55] Singh, M.P., et al., *Status of trace and toxic metals in Indian rivers*. 2014, Central Water Comission, Government of India: New Delhi. p. 58-59.

[56] Banerjee, U.S. and S. Gupta, *Impact of industrial waste effluents on river Damodar adjacent to Durgapur industrial complex, West Bengal, India.* Environmental Monitoring and Assessment, 2013. **185**(3): p. 2083-2094.

[57] Bhattacharya, A., et al., *Assessment of Yamuna and associated drains used for irrigation in rural and peri-urban settings of Delhi NCR.* Environmental Monitoring and Assessment, 2014. **187**(1): p. 4146.

[58] Sikka, R., V. Nayyar, and S.S. Sidhu, *Monitoring of Cd pollution in soils and plants irrigated with untreated sewage water in some industrialized cities of Punjab, India.* Environmental Monitoring and Assessment, 2009. **154**(1): p. 53-64.

[59] Singh, N.K., et al., *Arsenic and other heavy metal accumulation in plants and algae growing naturally in contaminated area of West Bengal, India.* Ecotoxicology and Environmental Safety, 2016. **130**(Supplement C): p. 224-233.

[60] Thornton, I., R. Rautiu, and S. Brush, *Lead: the facts*. 2001, Surrey, UK: IC Consultants Ltd.

[61] Gupt, Y., *Economic instruments and the efficient recycling of batteries in Delhi and the National Capital Region of India.* Environment and Development Economics, 2015. **20**(2): p. 236-258.

[62] Zhang, W., et al., *A critical review on secondary lead recycling technology and its prospect.* Renewable and Sustainable Energy Reviews, 2016. **61**(Supplement C): p. 108-122.

[63] USEPA. *Land, Waste, and Cleanup Topics*. 2009; Available from: https://www.epa.gov/environmental-topics/land-waste-and-cleanup-topics.

[64] Tian, X., et al., *The lead-acid battery industry in China: outlook for production and recycling.* Waste Management & Research, 2015. **33**(11): p. 986-994.

[65] Mao, J., Z. Lu, and Z. Yang, *The eco-efficiency of lead in China's lead-acid battery system.* Journal of Industrial Ecology, 2006. **10**(1-2): p. 185-197.

[66] Cao, S., et al., *Health risk assessment of various metal(loid)s via multiple exposure pathways on children living near a typical lead-acid battery plant, China.* Environmental Pollution, 2015. **200**(Supplement C): p. 16-23.

[67] Gottesfeld, P. and A. Pokhrel, *Review: lead exposure in battery manufacturing and recycling in developing countries and among children in nearby communities.* Journal of Occupational and Environmental Hygiene, 2011. **8**.

[68] Rieuwerts, J.S., M. Farago, and V. Bencko, *Topsoil and housedust metal concentrations in the vicinity of a lead battery manufacturing plant.* Environmental Monitoring and Assessment, 1999. **59**(1): p. 1-13.

[69] Liu, W., et al., *Temporal and spatial characteristics of lead emissions from the lead-acid battery manufacturing industry in China.* Environmental Pollution, 2017. **220**(Part A): p. 696-703.

[70] Rajagopalan, V., *Recent indian policy initiatives in lead battery scrap management and their impact on the domestic demand-supply gap of lead*. 2001, Ministry of Environment & Forests, India: New Delhi.

[71] Dasgupta, N., *Greening small recycling firms: the case of leadsmelting units in Calcutta*. Environment and Urbanization, 1997. **9**(2): p. 289-306.

[72] van der Kuijp, T.J., L. Huang, and C.R. Cherry, *Health hazards of China's lead-acid battery industry: a review of its market drivers, production processes, and health impacts.* Environmental Health, 2013. **12**(1): p. 61.

[73] Zhang, Q., *The current status on the recycling of lead-acid batteries in China.* International Journal of Electrochemical Science, 2013. **8**(5): p. 6457 - 6466.

[74] Haefliger, P., et al., *Mass lead intoxication from informal used lead-acid battery recycling in Dakar, Senegal.* Environ Health Perspect, 2009. **117**.

[75] Kaewsomboon, W., M. Mahidon, and M.M.K.S.m.l. Sapphayākṇsāt, *Removal of Lead from Battery Manufacturing Wastewater by Egg Shell*. 2006.

[76] Trigune, M.B., *Waste management in Exide industry, Ahmadnagar, India*, V.V. Kulkarni, Editor. 2014.

[77] Li, L., et al., *Preparation and characterization of nano-structured lead oxide from spent lead acid battery paste.* Journal of Hazardous Materials, 2012. **203-204**(Supplement C): p. 274-282.

[78] Ghosh, P., A.N. Samanta, and S. Ray, *Reduction of COD and removal of Zn(II) from rayon industry wastewater by combined electro-Fenton treatment and chemical precipitation.* Desalination, 2011. **266**(1–3): p. 213-217.

[79] Baltpurvins, K.A., et al., *Effect of electrolyte composition on zinc hydroxide precipitation by lime.* Water Research, 1997. **31**(5): p. 973-980.

[80] Avena, M.J., C.E. Giacomelli, and C.P. De Pauli, *Formation of Cr(III) hydroxides from chrome alum solutions: 1. Precipitation of active chromium hydroxide.* Journal of Colloid and Interface Science, 1996. **180**(2): p. 428-435.

[81] Mahmoud, A. and A.F.A. Hoadley, *An evaluation of a hybrid ion exchange electrodialysis process in the recovery of heavy metals from simulated dilute industrial wastewater.* Water Research, 2012. **46**(10): p. 3364-3376.

[82] Lu, S. and S.W. Gibb, *Copper removal from wastewater using spent-grain as biosorbent.* Bioresource Technology, 2008. **99**(6): p. 1509-1517.

[83] Standeker, S., et al., *Silica aerogels modified with mercapto functional groups used for Cu(II) and Hg(II) removal from aqueous solutions.* Desalination, 2011. **269**(1-3): p. 223-230.

[84] Radha, K.V., V. Sridevi, and K. Kalaivani, *Electrochemical oxidation for the treatment of textile industry wastewater.* Bioresource Technology, 2009. **100**(2): p. 987-990.

[85] Ghosh, P.K., *Hexavalent chromium [Cr(VI)] removal by acid modified waste activated carbons.* Journal of Hazardous Materials, 2009. **171**(1-3): p. 116-122.

[86] Barakat, M.A., *New trends in removing heavy metals from industrial wastewater.* Arabian Journal of Chemistry, 2011. **4**(4): p. 361-377.

[87] Fu, F. and Q. Wang, *Removal of heavy metal ions from wastewaters: A review.* Journal of Environmental Management, 2011. **92**(3): p. 407-418.

[88] Uddin, M.J., et al., *An Approach to Reduce Waste in Lead Acid Battery Industries.* Global Journal of Researches in Engineering, 2013. **13**(2).

[89] Macchi, G., et al., *A bench study on lead removal from battery manufacturing wastewater by carbonate precipitation.* Water Research, 1996. **30**(12): p. 3032-3036.

[90] Charerntanyarak, L., *Heavy metals removal by chemical coagulation and precipitation.* Water Science and Technology, 1999. **39**(10–11): p. 135-138.

[91] Chen, Q., et al., *Precipitation of heavy metals from wastewater using simulated flue gas: Sequent additions of fly ash, lime and carbon dioxide.* Water Research, 2009. **43**(10): p. 2605-2614.

[92] Tunay, O. and N.I. Kabdaşli, *Hydroxide precipitation of complexed metals.* Water Research, 1994. **28**(10): p. 2117-2124.

[93] Alvarez, M.T., C. Crespo, and B. Mattiasson, *Precipitation of Zn(II), Cu(II) and Pb(II) at bench-scale using biogenic hydrogen sulfide from the utilization of volatile fatty acids.* Chemosphere, 2007. **66**(9): p. 1677-1683.

[94] Guo, Z.-R., et al., *Enhanced chromium recovery from tanning wastewater.* Journal of Cleaner Production, 2006. **14**(1): p. 75-79.

[95] Zongo, I., et al., *Removal of hexavalent chromium from industrial wastewater by electrocoagulation: A comprehensive comparison of aluminium and iron electrodes.* Separation and Purification Technology, 2009. **66**(1): p. 159-166.

[96] Wang, L.K., et al., *Heavy Metals in the Environment*. 2009: Taylor & Francis.

[97] Aksu, Z., Y. Sag, and T. Kutsal, *The biosorpnon of copperod by C. vulgaris and Z. ramigera.* Environmental Technology, 1992. **13**(6): p. 579-586.

[98] Das, N., R. Vimla, and P. Karthika, *Biosorption of heavy metals – An overview* Indian Journal of Biotechnology, 2008. **7**: p. 159-169.

[99] Han, R., et al., *Biosorption of copper(II) and lead(II) from aqueous solution by chaff in a fixed-bed column.* Journal of Hazardous Materials, 2006. **133**(1–3): p. 262-268.

[100] Wilde, E.W., et al., *Bioremediation of aqueous pollutants using biomass embedded in hydrophilic foam. Final report*, in *Other Information: DN: TTP No. SR-16-PL-42; PBD: [1996]*. 1996. p. Medium: ED; Size: 261 p.

[101] Gupta, V.K., et al., *Biosorption of copper(II) from aqueous solutions by Spirogyra species.* Journal of Colloid and Interface Science, 2006. **296**(1): p. 59-63.

[102] Gupta, V.K. and A. Rastogi, *Biosorption of lead from aqueous solutions by green algae Spirogyra species: Kinetics and equilibrium studies.* Journal of Hazardous Materials, 2008. **152**(1): p. 407-414.

[103] Sari, A. and M. Tuzen, *Biosorption of Pb(II) and Cd(II) from aqueous solution using green alga (Ulva lactuca) biomass.* Journal of Hazardous Materials, 2008. **152**(1): p. 302-308.

[104] Ahluwalia, S.S. and D. Goyal, *Microbial and plant derived biomass for removal of heavy metals from wastewater.* Bioresource Technology, 2007. **98**(12): p. 2243-2257.

[105] Peavy, H.S., D.R. Rowe, and G. Tchobanoglous, *Environmental Engineering*. 1985: McGraw-Hill Higher Education.

[106] Metcalf, Eddy, and G. Tchobanoglous, *Wastewater engineering: treatment disposal reuse*. 1979: McGraw-Hill.

[107] Tripathi, A. and M.R. Ranjan, *Heavy metal removal from wastewater using low cost adsorbents.* Journal of Bioremediation & Biodegradation, 2015. **6**(6): p. 2155-6199.

[108] Jusoh, A., et al., *A simulation study of the removal efficiency of granular activated carbon on cadmium and lead.* Desalination, 2007. **206**(1–3): p. 9-16.

[109] Kang, K.C., et al., *Sorption of Cu^{2+} and Cd^{2+} onto acid- and base-pretreated granular activated carbon and activated carbon fiber samples.* Journal of Industrial and Engineering Chemistry, 2008. **14**(1): p. 131-135.

[110] Kurniawan, T.A., *A research study on Cr(VI) removal from contaminated wastewater using chemically modified low cost adsorbents and commercial activated carbon*, in *Environmental Technology Program*. 2003, Thammasat University. p. 129.

[111] Anandkumar, J., *Synyhesis and application of novel adsorbents for wastewater treatment*, in *Department of Civil Engineering*. 2012, Indian Institute of Technology Guwahati: Guwahati. p. 319.

[112] Largitte, L. and R. Pasquier, *A review of the kinetics adsorption models and their application to the adsorption of lead by an activated carbon.* Chemical Engineering Research and Design, 2016. **109**(Supplement C): p. 495-504.

[113] Hua, M., et al., *Heavy metal removal from water/wastewater by nanosized metal oxides: A review.* Journal of Hazardous Materials, 2012. **211-212**(Supplement C): p. 317-331.

[114] Freeman, J.J., *Active carbon* Journal of Chemical Technology & Biotechnology, 1990. **48**(2): p. 240-241.

[115] Kobya, M., et al., *Adsorption of heavy metal ions from aqueous solutions by activated carbon prepared from apricot stone.* Bioresource Technology, 2005. **96**(13): p. 1518-1521.

[116] Demirbas, E., et al., *Removal of Ni(II) from aqueous solution by adsorption onto hazelnut shell activated carbon: equilibrium studies.* Bioresource Technology, 2002. **84**(3): p. 291-293.

[117] Acharya, J., et al., *Removal of lead(II) from wastewater by activated carbon developed from Tamarind wood by zinc chloride activation.* Chemical Engineering Journal, 2009. **149**(1): p. 249-262.

[118] González, J.F., et al., *Porosity development in activated carbons prepared from walnut shells by carbon dioxide or steam activation.* Industrial & Engineering Chemistry Research, 2009. **48**(16): p. 7474-7481.

[119] Namasivayam, C. and K. Kadirvelu, *Activated carbons prepared from coir pith by physical and chemical activation methods.* Bioresource Technology, 1997. **62**(3): p. 123-127.

[120] Namasivayam, C. and K. Kadirvelu, *Agricultural solid wastes for the removal of heavy metals: Adsorption of Cu(II) by coirpith carbon.* Chemosphere, 1997. **34**(2): p. 377-399.

[121] Hasar, H., *Adsorption of nickel(II) from aqueous solution onto activated carbon prepared from almond husk.* Journal of Hazardous Materials, 2003. **97**(1): p. 49-57.

[122] Altundogan, H.S., et al., *The use of sulphuric acid-carbonization products of sugar beet pulp in Cr(VI) removal.* Journal of Hazardous Materials, 2007. **144**(1–2): p. 255-264.

[123] Thangalazhy-Gopakumar, S., et al., *Utilization of palm oil sludge through pyrolysis for bio-oil and bio-char production.* Bioresource Technology, 2015. **178**(Supplement C): p. 65-69.

[124] Selvi, K., S. Pattabhi, and K. Kadirvelu, *Removal of Cr(VI) from aqueous solution by adsorption onto activated carbon.* Bioresource Technology, 2001. **80**(1): p. 87-89.

[125] Kadirvelu, K., K. Thamaraiselvi, and C. Namasivayam, *Removal of heavy metals from industrial wastewaters by adsorption onto activated carbon prepared from an agricultural solid waste.* Bioresource Technology, 2001. **76**(1): p. 63-65.

[126] Fourest, E. and B. Volesky, *Contribution of sulfonate groups and alginate to heavy metal biosorption by the dry biomass of sargassum fluitans.* Environmental Science & Technology, 1995. **30**(1): p. 277-282.

[127] Suhas, P.J.M. Carrott, and M.M.L. Ribeiro Carrott, *Lignin – from natural adsorbent to activated carbon: A review.* Bioresource Technology, 2007. **98**(12): p. 2301-2312.

[128] Pagnanelli, F., et al., *Heavy metal removal by olive pomace: biosorbent characterisation and equilibrium modelling.* Chemical Engineering Science, 2003. **58**(20): p. 4709-4717.

[129] Kulkarni, V.V., A.K. Golder, and P.K. Ghosh, *Synthesis of a functionalized fibrous adsorbent of high uptake capacity: A study on Pb(II) uptake and simple acidic site model development.* RSC Advances, 2016. **6**(7): p. 5341-5349.

[130] Mosier, N., et al., *Features of promising technologies for pretreatment of lignocellulosic biomass.* Bioresource Technology, 2005. **96**(6): p. 673-686.

[131] Lasheen, M.R., N.S. Ammar, and H.S. Ibrahim, *Adsorption/desorption of Cd(II), Cu(II) and Pb(II) using chemically modified orange peel: Equilibrium and kinetic studies.* Solid State Sciences, 2012. **14**(2): p. 202-210.

[132] Abdel Salam, O.E., N.A. Reiad, and M.M. ElShafei, *A study of the removal characteristics of heavy metals from wastewater by low-cost adsorbents.* Journal of Advanced Research, 2011. **2**(4): p. 297-303.

[133] Leyva-Ramos, R., L.A. Bernal-Jacome, and I. Acosta-Rodriguez, *Adsorption of cadmium(II) from aqueous solution on natural and oxidized corncob.* Separation and Purification Technology, 2005. **45**(1): p. 41-49.

[134] Argun, M.E., et al., *Heavy metal adsorption by modified oak sawdust: Thermodynamics and kinetics.* Journal of Hazardous Materials, 2007. **141**(1): p. 77-85.

[135] Acar, F.N. and Z. Eren, *Removal of Cu(II) ions by activated poplar sawdust (Samsun Clone) from aqueous solutions.* Journal of Hazardous Materials, 2006. **137**(2): p. 909-914.

[136] Li, Q., et al., *Kinetic studies of adsorption of Pb(II), Cr(III) and Cu(II) from aqueous solution by sawdust and modified peanut husk.* Journal of Hazardous Materials, 2007. **141**(1): p. 163-167.

[137] Anandkumar, J. and B. Mandal, *Removal of Cr(VI) from aqueous solution using Bael fruit (Aegle marmelos correa) shell as an adsorbent.* Journal of Hazardous Materials, 2009. **168**(2–3): p. 633-640.

[138] Anirudhan, T.S. and P.G. Radhakrishnan, *Improved performance of a biomaterial-based cation exchanger for the adsorption of uranium(VI) from water and nuclear*

industry wastewater. Journal of Environmental Radioactivity, 2009. **100**(3): p. 250-257.

[139] Yasumasa, S., H. Yoichi, and K. Takehiro, *The removal of arsenate in waste water with an adsorbent prepared by binding hydrous Iron(III) oxide with polyacrylamide.* Bulletin of the Chemical Society of Japan, 1980. **53**(5): p. 1475-1476.

[140] Fanta, G.F., R.C. Burr, and W.M. Doane, *Graft polymerization of acrylonitrile onto wheat straw.* Journal of Applied Polymer Science, 1987. **33**(3): p. 899-906.

[141] Huang, Y., et al., *Graft copolymerization of methyl methacrylate on stone ground wood using the H_2O_2/Fe^{2+} method.* Journal of Applied Polymer Science, 1992. **45**(1): p. 71-77.

[142] Hwang, D.-C. and S. Damodaran, *Equilibrium swelling properties of a novel ethylenediaminetetraacetic dianhydride (EDTAD)-modified soy protein hydrogel.* Journal of Applied Polymer Science, 1996. **62**(8): p. 1285-1293.

[143] Raji, C. and T.S. Anirudhan, *Preparation and metal-adsorption properties of the polyacrylamide-grafted sawdust having carboxylate functional group.* Indian Journal of Chemical Technology, 1996. **3**(6): p. 345-350.

[144] Shubha, K.P., C. Raji, and T.S. Anirudhan, *Batch metal removal by modified hydrous titanium (IV) oxide gel: Kinetics and thermodynamics.* Indian Journal of Engineering and Management sciences, 1998. **5**(2): p. 65-71.

[145] Raji, C. and T.S. Anirudhan, *Batch Cr(VI) removal by polyacrylamide-grafted sawdust: Kinetics and thermodynamics.* Water Research, 1998. **32**(12): p. 3772-3780.

[146] Karnitz, O., et al., *Adsorption of heavy metal ion from aqueous single metal solution by chemically modified sugarcane bagasse.* Bioresource Technology, 2007. **98**(6): p. 1291-1297.

[147] Junior, O.K., et al., *Adsorption of Cu(II), Cd(II), and Pb(II) from aqueous single metal solutions by mercerized cellulose and mercerized sugarcane bagasse chemically modified with EDTA dianhydride (EDTAD).* Carbohydrate Polymers, 2009. **77**(3): p. 643-650.

[148] Gurgel, L.V.A., R.P.d. Freitas, and L.F. Gil, *Adsorption of Cu(II), Cd(II), and Pb(II) from aqueous single metal solutions by sugarcane bagasse and mercerized sugarcane bagasse chemically modified with succinic anhydride.* Carbohydrate Polymers, 2008. **74**(4): p. 922-929.

[149] Yu, J., et al., *Enhanced and selective adsorption of Pb(II) and Cu(II) by EDTAD-modified biomass of baker's yeast.* Bioresource Technology, 2008. **99**(7): p. 2588-2593.

[150] Xing, Y. and D. Deng, *Enhanced adsorption of Malachite Green by EDTAD-modified sugarcane bagasse.* Separation Science and Technology, 2009. **44**(9): p. 2117-2131.

[151] Pereira, F.V., L.V.A. Gurgel, and L.F. Gil, *Removal of Zn(II) from aqueous single metal solutions and electroplating wastewater with wood sawdust and sugarcane bagasse modified with EDTA dianhydride (EDTAD).* Journal of Hazardous Materials, 2010. **176**(1–3): p. 856-863.

[152] Charef, N., et al., *Preparation of a new polystyrene supported-ethylenediaminediacetic acid resin and its sorption behavior toward divalent metal ions.* Solvent Extraction and Ion Exchange, 2012. **30**(1): p. 101-112.

[153] Mejia Likosova, E., et al., *A novel electrochemical process for the recovery and recycling of ferric chloride from precipitation sludge.* Water Research, 2014. **51**: p. 96-103.

[154] Li, R., et al., *Heavy metal removal and speciation transformation through the calcination treatment of phosphorus-enriched sewage sludge ash.* Journal of Hazardous Materials, 2015. **283**(Supplement C): p. 423-431.

[155] Maruthamuthu, S., et al., *Elecrokinetic separation of sulphate and lead from sludge of spent lead acid battery.* Journal of Hazardous Materials, 2011. **193**: p. 188-193.

[156] Sethurajan, M., et al., *Leaching and selective zinc recovery from acidic leachates of zinc metallurgical leach residues.* Journal of Hazardous Materials, 2017. **324, Part A**: p. 71-82.

[157] Ye, M., et al., *Bioleaching combined brine leaching of heavy metals from lead-zinc mine tailings: Transformations during the leaching process.* Chemosphere, 2017. **168**(Supplement C): p. 1115-1125.

[158] Garcia-Mate, M., et al., *Tailored setting times with high compressive strengths in bassanite calcium sulfoaluminate eco-cements.* Cement and Concrete Composites, 2016. **72**: p. 39-47.

[159] Li, Y.-C., et al., *Co-treatment of gypsum sludge and Pb/Zn smelting slag for the solidification of sludge containing arsenic and heavy metals.* Journal of Environmental Management, 2016. **181**: p. 756-761.

[160] Kadir, A.A., M.R.A. Jalil, and M.M.A.B. Abdullah, *Properties of steel mill sludge waste incorporated in fired clay brick.* Materials Science Forum, 2016. **857**: p. 358-362.

[161] Munoz Velasco, P., et al., *Fired clay bricks manufactured by adding wastes as sustainable construction material – A review.* Construction and Building Materials, 2014. **63**(Supplement C): p. 97-107.

[162] Cherifi, M., S. Hazourli, and M. Ziati, *Initial water content and temperature effects on electrokinetic removal of aluminium in drinking water sludge.* Physics Procedia, 2009. **2**(3): p. 1021-1030.

[163] Ferri, V., et al., *Electrokinetic extraction of surfactants and heavy metals from sewage sludge.* Electrochimica Acta, 2009. **54**(7): p. 2108-2118.

[164] Ghosh, P., S. Balagurunathan, and C. Basha, *Electrokinetic Migration of Nickel [Ni(II)] in Contaminated Sludge.* Journal of Hazardous, Toxic, and Radioactive Waste, 2012. **16**(3): p. 201-206.

[165] Virkutyte, J., M. Sillanpää, and P. Lens, *Electrokinetic copper and iron migration in anaerobic granular sludge.* Water, Air, and Soil Pollution, 2006. **177**(1-4): p. 147-168.

[166] Turer, D. and A. Genc, *Assessing effect of electrode configuration on the efficiency of electrokinetic remediation by sequential extraction analysis.* Journal of Hazardous Materials, 2005. **119**(1–3): p. 167-174.

[167] Wang, J.-Y., et al., *Evaluation of electrokinetic removal of heavy metals from sewage sludge.* Journal of Hazardous Materials, 2005. **124**(1–3): p. 139-146.

[168] Zhang, L., *Production of bricks from waste materials – A review.* Construction and Building Materials, 2013. **47**(Supplement C): p. 643-655.

[169] Bories, C., et al., *Development of eco-friendly porous fired clay bricks using pore-forming agents: A review.* Journal of Environmental Management, 2014. **143**(Supplement C): p. 186-196.

[170] Fungaro, D.A. and M.V.D.S. Silva, *Utilization of water treatment plant sludge and coal fly ash in brick manufacturing.* American Journal of Environmental Protection, 2014. **2**(5): p. 83-88.

[171] Islam, M.M., et al., *Strength behavior of mortar using slag as partial replacement of cement.* MIST Journal: GALAXY (DHAKA), 2011. **3**.

[172] Garcia-Mate, M., et al., *Effect of calcium sulfate source on the hydration of calcium sulfoaluminate eco-cement.* Cement and Concrete Composites, 2015. **55**(Supplement C): p. 53-61.

[173] Asavapisit, S., G. Fowler, and C.R. Cheeseman, *Solution chemistry during cement hydration in the presence of metal hydroxide wastes.* Cement and Concrete Research, 1997. **27**(8): p. 1249-1260.

[174] Chen, Q.Y., et al., *Immobilisation of heavy metal in cement-based solidification/stabilisation: A review.* Waste Management, 2009. **29**(1): p. 390-403.

[175] Malhotra, S.K. and S.P. Tehri, *Development of bricks from granulated blast furnace slag.* Construction and Building Materials, 1996. **10**(3): p. 191-193.

[176] Kumar, S., *A perspective study on fly ash–lime–gypsum bricks and hollow blocks for low cost housing development.* Construction and Building Materials, 2002. **16**(8): p. 519-525.

[177] Binici, H., O. Aksogan, and T. Shah, *Investigation of fibre reinforced mud brick as a building material.* Construction and Building Materials, 2005. **19**(4): p. 313-318.

[178] Cicek, T. and M. Tanrıverdi, *Lime based steam autoclaved fly ash bricks.* Construction and Building Materials, 2007. **21**(6): p. 1295-1300.

[179] Turgut, P. and H. Murat Algin, *Limestone dust and wood sawdust as brick material.* Building and Environment, 2007. **42**(9): p. 3399-3403.

[180] Algin, H.M. and P. Turgut, *Cotton and limestone powder wastes as brick material.* Construction and Building Materials, 2008. **22**(6): p. 1074-1080.

[181] Turgut, P. and B. Yesilata, *Physico-mechanical and thermal performances of newly developed rubber-added bricks.* Energy and Buildings, 2008. **40**(5): p. 679-688.

[182] Zhao, F.-Q., J. Zhao, and H.-j. Liu, *Autoclaved brick from low-silicon tailings.* Construction and Building Materials, 2009. **23**(1): p. 538-541.

[183] Liu, Z., et al., *Utilization of the sludge derived from dyestuff-making wastewater coagulation for unfired bricks.* Construction and Building Materials, 2011. **25**(4): p. 1699-1706.

[184] Raut, S.P., et al., *Reuse of recycle paper mill waste in energy absorbing light weight bricks.* Construction and Building Materials, 2012. **27**(1): p. 247-251.

[185] Zhao, Y., et al., *Preparation of high strength autoclaved bricks from hematite tailings.* Construction and Building Materials, 2012. **28**(1): p. 450-455.

[186] Zhou, J., et al., *Utilization of waste phosphogypsum to prepare non-fired bricks by a novel Hydration–Recrystallization process.* Construction and Building Materials, 2012. **34**(Supplement C): p. 114-119.

[187] Vinai, R., et al., *Coal combustion residues valorisation: Research and development on compressed brick production.* Construction and Building Materials, 2013. **40**(Supplement C): p. 1088-1096.

[188] Shakir, A.A., S. Naganathan, and K.N. Mustapha, *Properties of bricks made using fly ash, quarry dust and billet scale.* Construction and Building Materials, 2013. **41**(Supplement C): p. 131-138.

[189] Kamyotra, J.S., *Brick kilns in india. Roadmap for brick kiln sector: Challenges and opportunities*. 2016, Centre for Science and Environment (CSE): New Delhi.

[190] Coletti, C., et al., *How to face the new industrial challenge of compatible, sustainable brick production: Study of various types of commercially available bricks.* Applied Clay Science, 2016. **124-125**(Supplement C): p. 219-226.

[191] Goel, G. and A.S. Kalamdhad, *An investigation on use of paper mill sludge in brick manufacturing.* Construction and Building Materials, 2017. **148**(Supplement C): p. 334-343.

[192] Demir, I., *An investigation on the production of construction brick with processed waste tea.* Building and Environment, 2006. **41**(9): p. 1274-1278.

[193] Herek, L.C.S., et al., *Characterization of ceramic bricks incorporated with textile laundry sludge.* Ceramics International, 2012. **38**(2): p. 951-959.

[194] Goel, G. and A.S. Kalamdhad, *Degraded municipal solid waste as partial substitute for manufacturing fired bricks.* Construction and Building Materials, 2017. **155**(Supplement C): p. 259-266.

[195] Hassan, K.M., et al., *Effects of using arsenic–iron sludge wastes in brick making.* Waste Management, 2014. **34**(6): p. 1072-1078.

[196] Taha, Y., et al., *Natural clay substitution by calamine processing wastes to manufacture fired bricks.* Journal of Cleaner Production, 2016. **135**(Supplement C): p. 847-858.

[197] Xu, Y., et al., *The use of urban river sediments as a primary raw material in the production of highly insulating brick.* Ceramics International, 2014. **40**(6): p. 8833-8840.

[198] Aouba, L., et al., *Properties of fired clay bricks with incorporated biomasses: Cases of olive stone flour and wheat straw residues.* Construction and Building Materials, 2016. **102**(Part 1): p. 7-13.

[199] Sutcu, M. and S. Akkurt, *The use of recycled paper processing residues in making porous brick with reduced thermal conductivity.* Ceramics International, 2009. **35**(7): p. 2625-2631.

[200] Weng, C.-H., D.-F. Lin, and P.-C. Chiang, *Utilization of sludge as brick materials.* Advances in Environmental Research, 2003. **7**(3): p. 679-685.

[201] Sengupta, P., N. Saikia, and P.C. Borthakur, *Bricks from petroleum effluent treatment plant sludge: Properties and environmental characteristics.* Journal of Environmental Engineering, 2002. **128**(11): p. 1090-1094.

[202] Viana, C.E., et al., *The use of submerged-arc welding flux slag as raw material for the fabrication of multiple-use mortars and bricks.* Soldagem & Inspeção, 2009. **14**: p. 257-262.

[203] Arsenovic, M., Z. Radojevic, and S. Stankovic, *Removal of toxic metals from industrial sludge by fixing in brick structure.* Construction and Building Materials, 2012. **37**: p. 7-14.

[204] Shih, P.-H., Z.-Z. Wu, and H.-L. Chiang, *Characteristics of bricks made from waste steel slag.* Waste Management, 2004. **24**(10): p. 1043-1047.

[205] IS:1077, *Common Burnt Clay Building Bricks - Specification*. 1992, Bureau of Indian Standards: New Delhi.

[206] Ramappa, B.T., *Economics of areca nut cultivation in Karnataka, a case study of Shivamogga district.* IOSR Journal of Agriculture and Veterinary Science, 2013. **3**(1): p. 50-59.

[207] Raghupathy, R., R. Viswanathan, and C.T. Devadas, *Quality of paper boards from arecanut leaf sheath.* Bioresource Technology, 2002. **82**(1): p. 99-100.

[208] Available from: https://www.canstockphoto.com/vector-clipart/areca-nut.html.

[209] Yussop, M. *A private nature park developed by Syarikat Lanskap Kambatik based on the principles of ecological diversity, oil palm integrated agro-forestry practices and Kambatik landscape design philosophy and aesthetics (accessed on 17 Jan 2014).* 2013; Available from: http://kambatikpark.blogspot.in/2013/11/the-betel-nut-palm.html.

[210] Raghavan, V. and H.K. Baruah, *Arecanut: India's popular masticatory —history, chemistry and utilization.* Economic Botany, 1958. **12**(4): p. 315-345.

[211] Rajan, A., J.G. Kurup, and T.E. Abraham, *Biosoftening of arecanut fiber for value added products.* Biochemical Engineering Journal, 2005. **25**(3): p. 237-242.

[212] Premaja, P. and P.K. Malathy, *Area and production statistics of arecanut and spices*. 2008, Directorate of Arecanut and Spices Development: Calicut , Kerala, India.

[213] Huang, H.-J., et al., *Process modeling and analysis of pulp mill-based integrated biorefinery with hemicellulose pre-extraction for ethanol production: A comparative study*. Bioresource Technology, 2010. **101**(2): p. 624-631.

[214] Chaturvedi, V. and P. Verma, *An overview of key pretreatment processes employed for bioconversion of lignocellulosic biomass into biofuels and value added products.* 3 Biotech, 2013. **3**(5): p. 415-431.

[215] Sasmal, S., V.V. Goud, and K. Mohanty, *Characterization of biomasses available in the region of North-East India for production of biofuels.* Biomass and Bioenergy, 2012. **45**(0): p. 212-220.

[216] Li, X.-m., et al., *Removal of Pb (II) from aqueous solutions by adsorption onto modified areca waste: Kinetic and thermodynamic studies.* Desalination, 2010. **258**(1–3): p. 148-153.

[217] Alvarez, P., C. Blanco, and M. Granda, *The adsorption of chromium (VI) from industrial wastewater by acid and base-activated lignocellulosic residues.* Journal of Hazardous Materials, 2007. **144**(1–2): p. 400-405.

[218] Sivakumar, D., *Hexavalent chromium removal in a tannery industry wastewater using rice husk silica.* Global Journal of Environmental Science and Management, 2015. **1**(1): p. 27-40.

[219] Gagrai, M.K., C. Das, and A.K. Golder, *Non-ideal metal binding model for Cr(III) sorption using Spirulina platensis biomass: Experimental and theoretical approach.* The Canadian Journal of Chemical Engineering, 2013. **91**(12): p. 1904-1912.

[220] Gagrai, M.K., C. Das, and A.K. Golder, *Reduction of Cr(VI) into Cr(III) by Spirulina dead biomass in aqueous solution: Kinetic studies.* Chemosphere, 2013. **93**(7): p. 1366-1371.

[221] Fisher, S. and R. Kunin, *Routine exchange capacity determinations of ion exchange resins.* Analytical Chemistry, 1955. **27**(7): p. 1191-1194.

[222] Stepanova, G.A., et al., *The swelling of alkali cellulose in sodium hydroxide solutions.* Fibre Chemistry, 1982. **13**(6): p. 405-407.

[223] Segal, L., et al., *An empirical method for estimating the degree of crystallinity of native cellulose using the X-ray diffractometer.* Textile Research Journal, 1959. **29**(10): p. 786-794.

[224] Xu, D., et al., *Removal of Pb(II) from aqueous solution by oxidized multiwalled carbon nanotubes.* Journal of Hazardous Materials, 2008. **154**(1–3): p. 407-416.

[225] Ben-Ali, S., et al., *Characterization and adsorption capacity of raw pomegranate peel biosorbent for copper removal.* Journal of Cleaner Production.

[226] Yang, H., et al., *Preparation and characterization of EDTAD-modified magnetic-Fe_3O_4 chitosan composite: application of comparative adsorption of dye wastewater with magnetic chitosan.* Water Science and Technology, 2013. **68**(1): p. 209.

[227] IS:3495, *Methods of Tests of Burnt Clay Building Bricks*. 1992, Bureau of Indian Standards: New Delhi.

[228] Reganold, J.P. and J.B. Harsh, *Expressing cation exchange capacity in milliequivalents per 100 grams and in SI units.* Journal of Agronomic Education, 1985. **14**(2): p. 84-90.

[229] Singh, J. and A.S. Kalamdhad, *Assessment of bioavailability and leachability of heavy metals during rotary drum composting of green waste (Water hyacinth).* Ecol. Eng., 2013. **52**(0): p. 59-69.

[230] Ure, A.M., et al., *Speciation of heavy metals in soils and sediments. An account of the improvement and harmonization of extraction techniques undertaken under the auspices of the BCR of the commission of the european communities.* International Journal of Environmental Analytical Chemistry, 1993. **51**(1-4): p. 135-151.

[231] Okoro, H.K., et al., *A review of sequential extraction procedures for heavy metals speciation in soil and sediments.* Open Access Scientific Reports, 2012. **1**(181): p. 2-9.

[232] Marchioretto, M.M., *Heavy metals removal from anaerobically digested sludge* in *Environmental Technology*. 2003, Wageningen University, Wageningen: Netherlands. p. 152.

[233] USEPA, *Test Methods for Evaluating Solid Waste*, in *Physical/Chemical Methods*. 2008, Office of Solid Waste and Emergency Response: Washington DC.

[234] Lindsay, W.L. and W.A. Norvell, *Development of a DTPA Soil Test for Zinc, Iron, Manganese, and Copper.* Soil Science Society of America Journal, 1978. **42**(3): p. 421-428.

[235] Veeken, A.H.M. and H.V.M. Hamelers, *Removal of heavy metals from sewage sludge by extraction with organic acids.* Water Science and Technology, 1999. **40**(1): p. 129-136.

[236] Marchioretto, M.M., et al., *Heavy metals extraction from anaerobically digested sludge.* Water Science and Technology, 2002. **46**(10): p. 1-8.

[237] Luo, W., et al., *Effects of land use on concentrations of metals in surface soils and ecological risk around Guanting Reservoir, China.* Environmental geochemistry and health, 2007. **29**(6): p. 459-471.

[238] Hakanson, L., *An ecological risk index for aquatic pollution control: A sedimentological approach.* Water Research, 1980. **14**(8): p. 975-1001.

[239] IS:2117, *Guide for manufacture of hand-made common burnt-clay building bricks*. 1991, Bureau of Indian Standards: New Delhi.

[240] Chen, Y., et al., *Preparation of eco-friendly construction bricks from hematite tailings.* Construction and Building Materials, 2011. **25**(4): p. 2107-2111.

[241] ASTMC326-09, *Standard Test Method for Drying and Firing Shrinkages of Ceramic Whiteware Clays*. 2000, ASTM International: West Conshohocken, United States.

[242] ASTMC20, *Standard Test Methods for Apparent Porosity, Water Absorption, Apparent Specific, Gravity, and Bulk Density of Burned Refractory Brick and Shapes by Boiling Water*. 2000, ASTM International, : West Conshohocken, USA.

[243] Taffarel, S.R. and J. Rubio, *Removal of Mn^{2+} from aqueous solution by manganese oxide coated zeolite.* Minerals Engineering, 2010. **23**(14): p. 1131-1138.

[244] Hsu, G.Y., et al., *Washing characteristics of copper-containing clay sludge cake.* Water Research, 1999. **33**(1): p. 248-256.

[245] Ricordel, S., et al., *Heavy metals removal by adsorption onto peanut husks carbon: Characterization, kinetic study and modeling.* Separation and Purification Technology, 2001. **24**(3): p. 389-401.

[246] Yu, B., et al., *The removal of heavy metals from aqueous solutions by sawdust adsorption — removal of lead and comparison of its adsorption with copper.* Journal of Hazardous Materials, 2001. **84**(1): p. 83-94.

[247] Babel, S. and T.A. Kurniawan, *Low-cost adsorbents for heavy metals uptake from contaminated water: a review.* Journal of Hazardous Materials, 2003. **97**(1): p. 219-243.

[248] Kolodynska, D., H. Hubicka, and Z. Hubicki, *Sorption of heavy metal ions from aqueous solutions in the presence of EDTA on monodisperse anion exchangers.* Desalination, 2008. **227**(1–3): p. 150-166.

[249] Oviedo, C. and J. Rodríguez, *EDTA: the chelating agent under environmental scrutiny.* Química Nova, 2003. **26**: p. 901-905.

[250] Umamaheswaran, K. and V.S. Batra, *Physico-chemical characterisation of Indian biomass ashes.* Fuel, 2008. **87**(6): p. 628-638.

[251] Xu, F., Y.-C. Shi, and D. Wang, *Towards understanding structural changes of photoperiod-sensitive sorghum biomass during sulfuric acid pretreatment.* Bioresource Technology, 2013. **135**(0): p. 704-709.

[252] Tan, I.A.W., A.L. Ahmad, and B.H. Hameed, *Adsorption of basic dye on high-surface-area activated carbon prepared from coconut husk: Equilibrium, kinetic and thermodynamic studies.* Journal of Hazardous Materials, 2008. **154**(1–3): p. 337-346.

[253] Sanna, G., et al., *Determination of conditional stability constants of metal-trichoderma viride complexes by the potentiometric titration method.* Fresenius Environmental Bulletin, 2002. **1**(9b): p. 636-641.

[254] Joao Paulo de, M., B.M. Patricia, and G. Honoria de Fatima, *Characterization of copper adsorption on oxidized activated carbon.* Journal of the Brazilian Chemical Society, 2006. **17**(6): p. 1133-1143.

[255] Seders, L.A. and J.B. Fein, *Proton binding of bacterial exudates determined through potentiometric titrations.* Chemical Geology, 2011. **285**(1–4): p. 115-123.

[256] Nwabanne, J.T. and P.K. Igbokwe, *Comparative study of lead (II) removal from aqueous solution using different adsorbents.* International Journal of Engineering Research and Applications (IJERA), 2012. **2**(4): p. 1830-1838.

[257] Fanou, D., et al., *Heavy metals removal in aqueous solution by two delta-diketones.* Journal of Applied Sciences, 2007. **7**(2): p. 310-313.

[258] Anirudhan, T.S. and P.G. Radhakrishnan, *Chromium(III) removal from water and wastewater using a carboxylate-functionalized cation exchanger prepared from a lignocellulosic residue.* Journal of Colloid and Interface Science, 2007. **316**(2): p. 268-276.

[259] Wong, K.K., et al., *Removal of Cu and Pb from electroplating wastewater using tartaric acid modified rice husk.* Process Biochemistry, 2003. **39**(4): p. 437-445.

[260] Ozer, A., D. Ozer, and A. Ozer, *The adsorption of copper(II) ions on to dehydrated wheat bran (DWB): determination of the equilibrium and thermodynamic parameters.* Process Biochemistry, 2004. **39**(12): p. 2183-2191.

[261] Low, K.S., C.K. Lee, and A.C. Leo, *Removal of metals from electroplating wastes using banana pith.* Bioresource Technology, 1995. **51**(2–3): p. 227-231.

[262] Kocaoba, S., *Comparison of Amberlite IR120 and dolomite's performances for removal of heavy metals.* Journal of Hazardous Materials, 2007. **147**(1–2): p. 488-496.

[263] Riveros, P.A., *The extraction of Fe(III) using cation-exchange carboxylic resins.* Hydrometallurgy, 2004. **72**(3–4): p. 279-290.

[264] Tamura, H., M. Kudo, and R. Furuichi, *Polyfunctionality of carboxyl sites on IRC-50, an MR-type ion-exchange resin, evaluated by modeling with the Frumkin isotherm.* Reactive and Functional Polymers, 1998. **38**(2–3): p. 177-181.

[265] Roy, K., et al., *Incorporation of thiosemicarbazide in Amberlite IRC-50 for separation of astatine from α-irradiated bismuth oxide.* Applied Radiation and Isotopes, 2004. **60**(6): p. 793-799.

[266] Mustafa, S., et al., *Chromium (III) removal by weak acid exchanger Amberlite IRC-50 (Na).* Journal of Hazardous Materials, 2008. **160**(1): p. 1-5.

[267] Lagergren, S., *About the theory of so-called adsorption of soluble substances.* Kungliga Svenska Vetenskapsakademiens Handlingar, 1898. **24**(4): p. 1-39.

[268] Largitte, L. and R. Pasquier, *A review of the kinetics adsorption models and their application to the adsorption of lead by an activated carbon.* Chemical Engineering Research and Design, 2016. **109**: p. 495-504.

[269] Hosseini-Bandegharaei, A., et al., *Use of a selective extractant-impregnated resin for removal of Pb(II) ion from waters and wastewaters: Kinetics, equilibrium and thermodynamic study.* Chemical Engineering Research and Design, 2014. **92**(3): p. 581-591.

[270] Li, L., et al., *Displacement mechanism of binary competitive adsorption for aqueous divalent metal ions onto a novel IDA-chelating resin: Isotherm and kinetic modeling.* Water Research, 2011. **45**(3): p. 1177-1188.

[271] Okeola, F.O. and E.O. Odebunmi, *Comparison of Freundlich and Langmuir isotherms for adsorption of methylene blue by agrowaste derived activated carbon* Advances in Environmental Biology, 2010. **4**(3): p. 329-335.

[272] Jing, X., et al., *Adsorption performances and mechanisms of the newly synthesized N,N'-di (carboxymethyl) dithiocarbamate chelating resin toward divalent heavy metal ions from aqueous media.* Journal of Hazardous Materials, 2009. **167**(1–3): p. 589-596.

[273] Alguacil, F.J., M. Alonso, and L.J. Lozano, *Chromium (III) recovery from waste acid solution by ion exchange processing using Amberlite IR-120 resin: batch and continuous ion exchange modelling.* Chemosphere, 2004. **57**(8): p. 789-793.

[274] Demirbas, A., et al., *Adsorption of Cu(II), Zn(II), Ni(II), Pb(II), and Cd(II) from aqueous solution on Amberlite IR-120 synthetic resin.* Journal of Colloid and Interface Science, 2005. **282**(1): p. 20-25.

[275] Jha, M.K., et al., *Adsorption of copper from the sulphate solution of low copper contents using the cationic resin Amberlite IR120.* Journal of Hazardous Materials, 2009. **164**(2–3): p. 948-953.

[276] Juang, R.-S., S.-H. Lin, and T.-Y. Wang, *Removal of metal ions from the complexed solutions in fixed bed using a strong-acid ion exchange resin.* Chemosphere, 2003. **53**(10): p. 1221-1228.

[277] Nightingale, E.R., *Phenomenological theory of ion solvation. Effective radii of hydrated Ions.* The Journal of Physical Chemistry, 1959. **63**(9): p. 1381-1387.

[278] Padilla-Ortega, E., R. Leyva-Ramos, and J.V. Flores-Cano, *Binary adsorption of heavy metals from aqueous solution onto natural clays.* Chemical Engineering Journal, 2013. **225**(0): p. 535-546.

[279] Chip., A. and M. Lena., *Concentration, pH, and surface charge effects on cadmium and lead sorption in three tropical soils.* Journal of Environmental Quality, 2002. **31**(2): p. 581-9.

[280] Benefield, L.D., J.F. Judkins, and B.L. Weand, *Process chemistry for water and wastewater treatment*. 1982: Prentice-Hall.

[281] Martinez, R.E., et al., *Determination of intrinsic bacterial surface acidity constants using a Donnan shell model and a continuous pKa distribution method.* Journal of Colloid and Interface Science, 2002. **253**(1): p. 130-139.

[282] Plette, A.C.C., M.F. Benedetti, and W.H. van Riemsdijk, *Competitive binding of protons, calcium, cadmium, and zinc to isolated cell walls of a gram-positive soil bacterium.* Environmental Science & Technology, 1996. **30**(6): p. 1902-1910.

[283] Macchi, G., et al., *Battery industry wastewater: Pb removal and produced sludge.* Water Research, 1993. **27**(10): p. 1511-1518.

[284] Gupta, S., *Theoretical and Experimental Investigations for Removal of Pollutants using Adsorption*, in *Chemical Engineering*. 2008, Birla Institute of Technology and Science: Pilani. p. 140-148.

[285] Shibi, I.G. and T.S. Anirudhan, *Adsorption of Co(II) by a carboxylate-functionalized polyacrylamide grafted lignocellulosics.* Chemosphere, 2005. **58**(8): p. 1117-1126.

[286] Ubaidullaev, B.K., A.M. Kudratov, and Z.S. Salimov, *Preparation and ion-exchange properties of P-containing cellulose derivatives from certain plant species.* Chemistry of Natural Compounds, 2004. **40**(4): p. 410-411.

[287] Xing, Y., D. Liu, and L.-P. Zhang, *Enhanced adsorption of Methylene Blue by EDTAD-modified sugarcane bagasse and photocatalytic regeneration of the adsorbent.* Desalination, 2010. **259**(1–3): p. 187-191.

[288] Kontturi, E., T. Tammelin, and M. Osterberg, *Cellulose-model films and the fundamental approach.* Chemical Society Reviews, 2006. **35**(12): p. 1287-1304.

[289] Abdolali, A., et al., *A breakthrough biosorbent in removing heavy metals: Equilibrium, kinetic, thermodynamic and mechanism analyses in a lab-scale study.* Science of The Total Environment, 2016. **542, Part A**: p. 603-611.

[290] Singh, N.P. and S. Gokhale, *A method to estimate spatiotemporal air quality in an urban traffic corridor.* Science of The Total Environment, 2015. **538**: p. 458-467.

[291] Grive, M., et al., *A quantitative speciation model for the adsorption of organic pollutants on activated carbon.* Water Science and Technology, 2013. **68**(6): p. 1370-1376.

[292] CPCB, *Pollution control acts, rules and notifications issued therunder*, in *Standards for emission or discharge of environmental pollutants*. 2010, CPCB, Ministry of Environment and Forests, Government of India: New Delhi.

[293] Babel, S. and D. del Mundo Dacera, *Heavy metal removal from contaminated sludge for land application: A review.* Waste Management, 2006. **26**(9): p. 988-1004.

[294] Singh, R.P. and M. Agrawal, *Potential benefits and risks of land application of sewage sludge.* Waste Management, 2008. **28**(2): p. 347-358.

[295] Gomes, A.F.S., D.L. Lopez, and A.C.Q. Ladeira, *Characterization and assessment of chemical modifications of metal-bearing sludges arising from unsuitable disposal.* Journal of Hazardous Materials, 2012. **199–200**(0): p. 418-425.

[296] Napia, C., et al., *Leaching of heavy metals from solidified waste using Portland cement and zeolite as a binder.* Waste Management, 2012. **32**(7): p. 1459-1467.

[297] Sengupta, B., *Recycling and reuse of hazardous and other wastes as per hazardous and other wastes (management and transboundary movement) rules*. 2016, Centre for Environment Education: Ahmedabad, India.

[298] Wu, Q., et al., *Removal of heavy metal species from industrial sludge with the aid of biodegradable iminodisuccinic acid as the chelating ligand.* Environmental Science and Pollution Research, 2015. **22**(2): p. 1144-1150.

[299] Nair, A., A.A. Juwarkar, and S. Devotta, *Study of speciation of metals in an industrial sludge and evaluation of metal chelators for their removal.* Journal of Hazardous Materials, 2008. **152**(2): p. 545-553.

[300] Kazi, T.G., et al., *Evaluating the mobility of toxic metals in untreated industrial wastewater sludge using a BCR sequential extraction procedure and a leaching test.* Analytical and Bioanalytical Chemistry, 2005. **383**(2): p. 297-304.

[301] Eliche-Quesada, D., et al., *The use of different forms of waste in the manufacture of ceramic bricks.* Applied Clay Science, 2011. **52**(3): p. 270-276.

[302] Chen, C.-S., Y.-J. Huang, and Y.-H. Huang, *Treatment of lead frame nickel-plating wastewater with newly designed electrodeposition reactor.* Sustain. Environ. Res, 2011. **21**(6): p. 341-345.

[303] Veres, J., V. Sepelak, and S. Hredzak, *Chemical, mineralogical and morphological characterisation of basic oxygen furnace dust.* Miner Process Extr Metall., 2015. **124**(1): p. 1-8.

[304] Mushak, P., *Chapter 11 - Lead toxicity in humans: A brief historical perspective and public health context*, in *Trace Metals and other Contaminants in the Environment*. 2011, Elsevier. p. 401-437.

[305] Bose, S. and A.K. Bhattacharyya, *Heavy metal accumulation in wheat plant grown in soil amended with industrial sludge.* Chemosphere, 2008. **70**(7): p. 1264-1272.

[306] Suresh, G., et al., *Assessment of spatial distribution and potential ecological risk of the heavy metals in relation to granulometric contents of Veeranam lake sediments, India.* Ecotoxicology and Environmental Safety, 2012. **84**: p. 117-124.

[307] Bhuiyan, M.A.H., et al., *Heavy metal pollution of coal mine-affected agricultural soils in the northern part of Bangladesh.* Journal of Hazardous Materials, 2010. **173**(1–3): p. 384-392.

[308] Lee, I.H., Y.-J. Wang, and J.-M. Chern, *Extraction kinetics of heavy metal-containing sludge.* Journal of Hazardous Materials, 2005. **123**(1): p. 112-119.

[309] Giri, A.S. and A.K. Golder, *Decomposition of drug mixture in Fenton and photo-Fenton processes: Comparison to singly treatment, evolution of inorganic ions and toxicity assay.* Chemosphere, 2015. **127**: p. 254-261.

[310] Giri, A.S. and A.K. Golder, *Fenton, photo-fenton, H_2O_2 photolysis, and TiO_2 photocatalysis for dipyrone oxidation: Drug removal, mineralization, biodegradability, and degradation mechanism.* Industrial & Engineering Chemistry Research, 2014. **53**(4): p. 1351-1358.

[311] Giri, A.S. and A.K. Golder, *Chloramphenicol degradation in fenton and photo-fenton: Formation of Fe^{2+}-chloramphenicol chelate and reaction pathways.* Industrial & Engineering Chemistry Research, 2014. **53**(42): p. 16196-16203.

[312] Gharabaghi, M., M. Irannajad, and A.R. Azadmehr, *Selective sulphide precipitation of heavy metals from acidic polymetallic aqueous solution by thioacetamide.* Industrial Engineering and Chemical Research, 2012. **51**(2): p. 954-963.

[313] Grim, R.E., *Clay mineralogy*. 1953, New York: McGraw-Hill. 375.

[314] Manoharan, C., et al., *Analysis of temperature effect on ceramic brick production from alluvial deposits, Tamilnadu, India*. Vol. 54. 2011. 20-25.

[315] Koppi, A.J., et al., *Size and charge characteristics of kaolinitic soils in SE Queensland.* Journal of Soil Science, 1987. **38**(3): p. 395-404.

[316] Emrullahoglu Abi, C.B., *Effect of borogypsum on brick properties.* Construction and Building Materials, 2014. **59**(Supplement C): p. 195-203.

[317] García Ten, J., et al., *Thermal conductivity of traditional ceramics. Part I: Influence of bulk density and firing temperature*. Ceramics International, 2010. **36**(6): p. 1951-1959.

[318] Abdeen, H.H., *Properties of fired clay bricks mixed with waste glass*, in *Civil Engineering*. 2016, Islamic University of Gaza: Gaza. p. 71.

[319] Kreimeyer, R., *Some notes on the firing colour of clay bricks.* Applied Clay Science, 1987. **2**(2): p. 175-183.

Publications

International Journals

1) Kulkarni, V. V., Golder, A. K. and Ghosh, P. K. (2016). **Synthesis of a functionalized fibrous adsorbent of high uptake capacity: a study on Pb(II) uptake and simple acidic site model development**. RSC Advances 6(7), 5341-9.

2) Kulkarni, V. V., Golder, A. K. and Ghosh, P. K. (2017). **Synergistic effect using a functionalized dual-site adsorbent in Pb(II) and Cu(II) uptake and comparison with mono-site resins**. Journal of Water Process Engineering 18, 92-101.

3) Kulkarni, V. V., Golder, A. K. and Ghosh, P. K. (2018). **Synthesis and characterization of carboxylic cation exchange bio-resin for heavy metal remediation**. Journal of Hazardous Materials 341, 201-217.

4) Kulkarni, V. V., Golder, A. K. and Ghosh, P. K. (2018). **Critical analysis and valorization potential of battery industry sludge: Speciation, risk assessment and metal recovery**. Journal of Cleaner Production 171, 820-830.

5) Kulkarni, V. V., Golder, A. K. and Ghosh, P. K. **Production of composite clay bricks: A value-added solution to hazardous sludge through effective heavy metal fixation** Cement and Concrete Composites **(Under Review)**.

National/International Conferences

1. Kulkarni, V. V., Golder, A. K. and Ghosh, P. K. (2013) **Comparative Performance of Weak and Strong Acidic Cation-exchange Resins in Cu(II) Removal: Kinetic and Thermodynamic Studies.** Published paper in *Indian Chemical Engineering congress (**CHEMCON**)* at Institute of Chemical Technology, Mumbai, India, December 27-30.

2. Kulkarni, V. V., Golder, A. K. and Ghosh, P. K. (2014) **Removal Of Pb(II) by Weak And Strong Acidic Cation-Exchange Resins: Kinetic And Thermodynamic Studies.** Presented poster in *Indian Chemical Engineering congress (**CHEMCON**)* at University Institute of Chemical Technology, Punjab University, India, December 27-30.

3. Vihangraj V. Kulkarni, Animes Kumar Golder and Pranab Kumar Ghosh (2015) **Understanding the Potential Hazard and Nature of Battery Wastewater**

Sludge. Presented poster in *National Conference on Challenges in Environmental Research (**NCOCER**) at* Indian Institute of Technology Guwahati, India, June 4-6.

4. Kulkarni, V. V., Golder, A. K. and Ghosh, P. K. (2015) **Characterization and heavy metals speciation of Battery wastewater Sludge.** Presented poster in *Indian Chemical Engineering congress (**CHEMCON**)* at Indian Institute of Technology Guwahati, India, December 27-30.

5. Kulkarni, V. V., Golder, A. K. and Ghosh, P. K. (2015) **Effect of co-occurring ions on removal of Pb(II) by ion exchange resin.** Published a paper in *A National Conference on New Frontiers in Civil Engineering: Challenges and Opportunities in North-East India* at Royal School of Engineering & Technology Guwahati, India, November 5-6.

6. Kulkarni, V. V., Golder, A. K. and Ghosh, P. K. (2016) **Effect of sludge acidification on speciation behavior of heavy metals in battery wastewater sludge during electrochemical remediation.** Presented paper in *International Conference on Waste Management (**Recycle**)* at Indian Institute of Technology Guwahati, India, April 1-2.

7. Kulkarni, V. V., Golder, A. K. and Ghosh, P. K. (2016) **Sympathizing potential of functionalized arecanut husk for metal removal through its characterization.** Presented paper in *Reflux* at Indian Institute of Technology Guwahati, India, March 25-27.

8. Kulkarni, V. V., Kaushik Sarkar and Ghosh, P. K. (2018) **Synthesis and application of low cost adsorbent in Zn (II) removal by sulphuric acid treated arecanut husk**. Presented paper in an *International Conference on Waste Management (**Recycle**)* at Indian Institute of Technology Guwahati, India, Feb 22-24.